CRPP

CENTRE DE RECHERCHES EN PHYSIQUE DES PLASMAS
FACULTÉ DES SCIENCES DE BASE
ASSOCIATION EURATOM - CONFÉDÉRATION SUISSE

ÉCOLE POLYTECHNIQUE
FÉDÉRALE DE LAUSANNE

ANNUAL REPORT

2012

Table of contents

Préface

Cher Lecteur,

Nous vous présentons le Rapport Annuel 2012 du Centre de Recherches en Physique des Plasmas (CRPP). Il résume les activités de recherche, les résultats obtenus, ainsi que les activités d'enseignement et de sensibilisation de notre Centre. Nous avons pu atteindre nos buts grâce au dévouement de tous mes collègues, à qui j'exprime ma plus profonde reconnaissance.

L'énergie est – et continuera d'être – un défi important pour le monde de ce siècle. Nos chercheurs et toute notre équipe croient fermement que leur contribution scientifique et technologique à la quête de l'énergie de fusion aidera à atteindre l'objectif de fournir à l'humanité une source d'énergie sûre, bénigne pour l'environnement et durable pour chacun.

Nous avons été encouragés dans nos efforts par le soutien continu de nombreuses agences et institutions. Je saisis l'occasion de leur exprimer mes remerciements.

Prof. M.Q. Tran
Directeur Général

Foreword

Dear Reader,

The 2012 Annual Report of the Centre for Research in Plasma Physics (CRPP) is presented to your consideration. It summarizes the research activities, the results obtained, as well as the education and outreach activities of our Center. The achievement of our goals was made possible thanks to the dedication of all my colleagues to whom I express my deepest gratitude.

Energy is, and will continue, to be a major challenge for the world during this century. Our researchers, and our whole staff, firmly believe that their scientific and technological contribution to the quest for fusion energy will help achieving the goal of supplying mankind with safe, environmental friendly and sustainable energy for everyone.

We were encouraged in our effort by the continuous support of a large number of bodies and institutions. I would like to take this opportunity to express to them my thanks.

Prof. M.Q. Tran
General Director

Vorwort

Liebe Leserin, lieber Leser,

Hiermit präsentieren wir Ihnen den Jahresbericht 2012 des Forschungszentrums für Plasmaphysik (CRPP). In diesem Bericht sind die Forschungsaktivitäten und die dabei erzielten Ergebnisse zusammengefasst. Ausserdem berichten wir über die Tätigkeiten des Zentrums im Rahmen der Ausbildung und der Oeffentlichkeitsarbeit.

Dem unermüdlichen Einsatz von allen Kollegen und Mitarbeitern ist es zu verdanken, dass wir die gesetzten Ziele erreicht haben. Dafür möchte ich meine dankbare Anerkennung aussprechen.

Die Energieversorgung ist und bleibt eine grosse Herausforderung in diesem Jahrhundert. Unsere Wissenschaftler und das gesamte Personal sind davon überzeugt, dass unsere Beiträge in Forschung und Technologie die Entwicklung der kontrollierten Kernfusion weiter voran bringen werden und damit die Aussicht auf eine sichere, umweltfreundliche und dauerhafte Energieversorgung bieten

Prof. M. Q. Tran
Generaldirektor

Prefazione

Caro Lettore,

Le presentiamo il Rapporto Annuale 2012 del Centro di Ricerca in Fisica dei Plasmi (CRPP). Esso riassume le attività di ricerca, i risultati ottenuti e le attività d'insegnamento e d'informazione del nostro Centro. Questi traguardi sono stati raggiunti grazie all'impegno di tutti i miei colleghi, ai quali esprimo la mia più profonda riconoscenza.

L'energia è – e continuerà ad essere – una sfida importante per il mondo in questo secolo. I nostri ricercatori e il nostro intero gruppo credono fermamente che i loro contributi scientifici e tecnologici alla ricerca sull'energia da fusione aiuteranno a raggiungere l'obiettivo di fornire all'umanità una fonte d'energia sicura, rispettosa dell'ambiente e durevole.

Siamo stati incoraggiati nei nostri sforzi dal sostegno continuo di numerosi enti e istituzioni. Colgo l'occasione per esprimere loro i miei ringraziamenti.

Prof. M.Q. Tran
Direttore Generale

1 INTRODUCTION

1.1 The international frame and its relation to the Swiss programme

1.1.1 ITER

On the 9th of November 2012, the decree authorizing ITER as a nuclear installation was signed by the French Prime Minister. This event is a very important step for the project and shows that a fusion device also satisfies the very stringent safety requirements, which include the so-called "stress test". More specifically, with the signature of the decree, the ITER Organisation is authorized to create the "Installation nucléaire de base ITER" in the sense of the French nuclear legislation.

1.1.2 Euratom

The preparation of the fusion programme for the years 2014-2020 (part of the Euratom Horizon 2020 programme) continued in 2012. This year was marked by the preparation by the whole European Community of the roadmap towards the realisation of a fusion demonstration power plant also known as DEMO. DEMO is foreseen to start operation in the early 2040's and will produce net electricity to be injected into the grid at the level of a few hundred megawatts. It will be the only step between ITER and a first of kind commercial power plant.

The scientific content of the roadmap will be used to establish the workplan for the European Fusion Laboratories during the Horizon 2020. It is also foreseen that a new management structure will be put into place to implement this multi-annual workplan, making best use of the competencies in the working European laboratories.

Switzerland has decided to prolong its association with Euratom in 2012 and 2013, the last two years of the Framework Programme 7, pending a decision from the Parliament to allocate fund for the Swiss contribution for 2013. This decision will be taken in 2013. A decision for the participation in Euratom Horizon 2020 will also be taken during 2013.

1.2 A brief summary of the CRPP activities

Through the various chapters of the Annual Report, the readers will discover the many important results obtained in the fields of:

- tokamak physics
- theory and numerical simulation
- material science and technology
- superconductivity
- contribution to ITER construction
- participation to "Broader Approach"
- R&D on plasma processes for industrial application
- education

- public outreach

It is worth mentioning here that, in the field of tokamak physics, our work on a novel "divertor" structure, called a “snowflake”, was rewarded with the US "R&D 100 Innovation Reward".

The excellence of our work in the field of numerical simulation is highlighted by the fact that a CRPP team was selected as one of the first four in the world to run codes on the EU-Japan super computer HELIOS, in the frame of the "Lighthouse Project". Following this, CRPP got 111 millions CPU-hours on this computer, i.e. about 20% of the available resource.

Among other achievements, it is worth noting that the CRPP signed in 2012 with the ITER Organisation a 3-year contract with a value close to 9 millions Swiss Francs to test superconducting cables for ITER.

1. INTRODUCTION

1.1 La situation internationale en relation avec le programme Suisse

1.1.1 ITER

Le 9 novembre 2012, le décret autorisant ITER en tant qu'installation nucléaire a été signé par le premier ministre français. Cet événement représente un pas très important pour le projet et montre qu'une machine de fusion satisfait également les exigences de sécurités très contraignantes qui incluent les fameux «stress tests». Plus précisément, avec la signature de ce décret, l'organisation ITER est autorisée à créer une « Installation nucléaire de base » au sens de la législation française.

1.1.2 Euratom

La préparation du programme de fusion pour les années 2014-2020 (une partie du programme Euratom Horizon 2020) a continué en 2012. Cette annéle a été marquée par la préparation, par la communauté européenne, de la «feuille de route» pour la réalisation d'une centrale de fusion de démonstration, appelée DEMO. Il est prévu que DEMO soit mis en service au début des années 2040 et produise de l'électricité injectée dans le réseau à hauteur de quelques centaines de mégawatts. Ce sera la seule étape entre ITER et une centrale de production commerciale.

Le contenu scientifique de la feuille de route sera utilisé pour établir le plan de travail des laboratoires européens de fusion durant le programme Horizon 2020. Il est également prévu qu'une nouvelle structure de gestion soit mise en place pour implémenter ce plan multi annuel, en faisant le meilleur usage des compétences des laboratoires.

La Suisse a décidé de prolonger son association avec Euratom en 2012 et 2013, qui sont les deux dernières années du 7^{e} Programme Cadre, sous réserve d'une décision ultérieure du parlement d'allouer des fonds pour la contribution de la Suisse pour l'année 2013. Cette décision sera prise dans le courant de l'année.

1.2 Un bref résumé des activités du CRPP

Dans ces chapitres du rapport annuel, les lecteurs trouveront plusieurs résultats importants dans les domaines suivants:

- la physique du tokamak
- la théorie et la simulation numérique
- la science et la technologie des matériaus
- la supraconductivité
- la contribution à la construction d'ITER
- la participation à « l'Approche Elargie »
- les procédés plasmas pour applications industrielles

- l'enseignement
- la sensibilisation du public

Il vaut la peine de mentionner ici que, dans le domaine de la physique du tokamak, nos travaux sur une nouvelle structure du «divergeur», surnommée «flocon de neige» (snowflake), se sont vus couronnés du prix «US R&D 100 Innovation Reward».

D'autre part, l'excellence de nos travaux dans le domaine de la simulation numérique a été mise en évidence par le fait qu'une équipe du CRPP a été sélectionnée pour être une quatre des premières au monde à utiliser le super-ordinateur HELIOS, dédié à la recherche en fusion EU-Japon, dans le cadre du projet «LightHouse». Suite à cela, le CRPP a obtenu 111 millions d'heures de clacul sur cette plateforme, soit près de 20% de la resource totale disponible.

Parmi d'autres faits majeurs, mentionnons que le CRPP a signé en 2012 un contrat de 3 ans avec l'Organisation ITER, d'une valeur de près de 9 millions de francs suisses, pour tested les câbles supraconducteurs d'ITER.

1 EINLEITUNG

1.1 Das internationale Umfeld und dessen Einfluss auf das schweizerischen Forschungsprogramm

1.1.1 ITER

Am 9. November 2012 unterzeichnete der französische Ministerpräsident die Genehmigung für ITER als kerntechnische Anlage. Dieser Schritt ist von grosser Bedeutung für das Projekt, denn damit wird klar gestellt, dass die Kernfusionsanlage die strengen Sicherheitsvorschriften, insbesondere den sogenannten. „stress test", erfüllt. Genauer gesagt erhält die ITER Organisation damit die Berechtigung eine kerntechnische Anlage im Sinne der französischen Gesetzgebung zu erstellen und zu betreiben.

1.1.2 Euratom

Die Ausarbeitung des Programms zur Fusionsforschung für den Zeitraum 2014– 2020 (Teil des EURATOM-Programms Horizont 2020) lief im Jahr 2012 weiter. Ein wichtiger Bestandteil, der alle Partner in der europäischen Gemeinschaft betrifft, ist das sogenannte. Weissbuch („road map"), in dem der Weg zum Prototyp eines Fusionsreaktors (bekannt als DEMO) dargelegt wird. Der Reaktor DEMO soll kurz nach 2040 in Betrieb gehen und einige 100MW an elektrischer Energie ans Netz liefern. Damit soll die letzte Etappe zwischen ITER und einem kommerziellen Fusionskraftwerk erreicht werden.

Der wissenschaftliche Teil des Weissbuchs bildet bis zum Horizont 2020 die Grundlage für die Ausarbeitung des Arbeitsprogramms der europäischen Institute in der Fusionsforschung. Zur Verwirklichung dieses Programms soll eine neue organisatorische Struktur geschaffen werden die dafür sorgt, dass die Möglichkeiten und Fähigkeiten der verschiedenen europäischen Einrichtungen zur Fusionsforschung optimal genutzt werden.

Die schweizerische Eidgenossenschaft hat die bestehende Assoziation mit EURATOM für den Zeitraum 2012–2013, d.h. für die letzten Jahre des 7. europäischen Rahmenprogramms, verlängert. Diese Entscheidung stützt sich auf die Bewilligung der Mittel einer schweizerischen Beteiligung für die 2. Hälfte 2013 durch das Parlament. Im Lauf des Jahres 2013 wird auch über die Beteiligung am europäischen Programm Horizont 2020 entschieden.

1.2 Eine Zusammenfassung der Forschungs-ergebnisse des CRPP

Die Kapitel dieses Jahresberichts werden dem Leser einen Einblick in die wichtigsten Ergebnisse aus den verschiedenen Forschungsbereichen geben :

- physikalische Grundlagen des Tokamaks
- Theorie und numerische Simulationen des Plasmas
- Materialforschung und –technologie
- Supraleiter
- Beiträge zur Realisierung von ITER
- Beiträge zum erweiterten Programm der Fusionsforschung ("Broader approach")
- Forschung & Entwicklung in der Plasmaphysik für industrielle Anwendungen
- Ausbildung
- Oeffentlichkeitsarbeit

Wir sind stolz darauf zu erwähnen, dass im Bereich der Tokamakphysik, die Arbeit an einem neuartigen Divertor-Konzept («snowflake divertor»), in den U.S.A. mit dem Preis «R&D 100 Innovation Award» ausgezeichnet wurde.

Die hervorragenden Leistungen auf dem Gebiet der numerischen Simulation haben ihre Anerkennung darin gefunden dass die Gruppe des CRPP als eine der ersten im Rahmen des sogenannten «Light House» Projekts Zugang zum europäisch-japanischen Supercomputer HELIOS bekommen konnte, um aufwendige numerische Rechnungen durchzuführen. Dabei erhielt das CRPP über 110 Millionen Stunden CPU-Rechenzeit verfügen, was mehr als 20% der gesamten Rechnerkapazität entspricht.

Unterweiteren Errungenschaften ist insbesondere zu erwähnen, dass das CRPP im Jahr 2012 einen 3-Jahresvertrag über die Prüfung von supraleitenden Kabeln mit der ITER-Organisation abgeschlossen hat, der mit ca. 9 Millionen CHF dotiert ist.

1 INTRODUZIONE

1.1 La situazione internazionale e il suo rapporto con il programma svizzero.

1.1.1 ITER

Il 9 novembre 2012, il decreto che autorizza ITER in qualità di installazione nucleare è stato firmato dal Primo Ministro francese. Questo avvenimento rappresenta un passo importante per il progetto e mostra che un dispositivo a fusione soddisfa rigorosi requisiti di sicurezza, che comprendono anche il cosiddetto "stress test". Più precisamente, con la firma di questo decreto, l'organizzazione ITER è autorizzata a fondare un'"Installazione nucleare di base ITER" ai sensi della legislazione nucleare francese.

1.1.2 Euratom

La preparazione del programma di fusione per gli anni 2014-2020 (una parte del programme Euratom Orizzonte 2020) è continuata nel 2012. Quest'anno è stato caratterizzato dalla preparazione, per la comunità europea, della «Roadmap» (tabella di marcia) per la realizzazione di una centrale a fusione di dimostrazione, chiamata DEMO. È previsto che DEMO entri in funzione all'inizio degli anni 2040 e che fornisca alla rete energia dell'ordine di qualche centinaio di megawatt. Questa costituerà la sola tappa intermedia tra ITER e una centrale commerciale di produzione.

Il contenuto scientifico della Roadmap sarà utilizzato per stabilire il piano di lavoro dei laboratori europei di fusione durante il programma Orizzonte 2020. È inoltre previsto che una nuova struttura di gestione sia instaurata per implementare questo piano multiennale, facendo il miglior uso possibile delle competenze dei diversi laboratori.

La Svizzera ha deciso di prolungare il suo sodalizio con Euratom nel 2012 e nel 2013, gli ultimi due anni del programma "Framework Programme 7", in attesa della decisione del parlamento per lo stanziamento di fondi per il contributo svizzero per il 2013. Tale decisione verra' presa nel 2013. Sempre nel 2013 vera' presa la decione sulla partecipazione al programma "Euratom Horizon 2020".

1.2 Breve riassunto delle attività del CRPP

In questi capitoli del rapporto annuale, i lettori troveranno diversi risultati importanti nei settori seguenti :

- fisica del tokamak
- teoria e simulazioni numeriche
- scienza e tecnologia dei materiali
- superconduttività
- contributo alla costruzione di ITER
- partecipazione al «Broader Approach»
- processi al plasma per applicazioni industriali

- insegnamento
- sensibilizzazione del pubblico

Merita di essere detto che, nel campo della fisica del tokamak, il nostro lavoro su una nuova struttura di «divertore», soprannominata «fiocco di neve» (snowflake), ci ha meritato il premio` «US R&D 100 Innovation Reward».

D'altra parte, l'eccellenza del nostro lavoro nel campo della simulazione numerica è stato evidenziato dalla selezione di un gruppo del CRPP tra uno dei primi quattro al mondo ad utilizzare il supercomputer HELIOS, dedicato alla ricerca congiunta in fusione tra Europa e Giappone, nel quadro del progetto «LightHouse». In seguito a questa selezione, il CRPP ha ottenuto 111 millioni di ore di calcolo su questa piattaforma, ossia intorno al 20% delle risorse totali disponibili.

Tra gli altri eventi principali, menzioniamo che il CRPP ha firmato nel 2012 un contratto di 3 anni con l'Organizzazione ITER, per un valore di circa 9 millioni di franchi svizzeri, per testare i cavi superconduttori per ITER.

2 RESEARCH ACHIEVEMENTS OF THE CRPP IN 2012

2.1 The TCV tokamak

Experimentation on the Tokamak à Configuration Variable (TCV), the largest research facility on EPFL campus, continues to be the main effort of the CRPP Team. The TCV scientific programme is characterized by a high degree of flexibility, allowing it to respond quickly to new challenges from theory and to novel experimental proposals, which are accommodated alongside the longer-term campaign plan. The TCV programme involves a large proportion of external collaborators.

TCV is a conventional aspect ratio tokamak (major and minor radii 0.88 and 0.25m, respectively) with a vacuum toroidal magnetic field of 1.5T and an air-core transformer able to drive plasma currents up to 1MA. A highly elongated vacuum vessel accommodates plasmas of elongation up to 2.8. A set of 16 independently powered shaping and positioning coils – supplemented by two fast internal coils for vertical stabilization – are at the root of a unique shaping capability that encompasses negative triangularity, second-order X–points (as in the "snowflake" divertor configuration), highly up-down asymmetric plasmas, and – potentially - doublets. Auxiliary heating is provided by Electron Cyclotron Resonance Heating (ECRH), supplied by nine 0.5-MW gyrotrons (six at the 2nd (X2) and three at the 3rd (X3) harmonic, respectively 82.7 and 118.0GHz) to seven launchers with independent real-time steering capabilities. Fully non-inductive operation with Electron Cyclotron Current Drive (ECCD) is routinely performed up to a current of 210kA. A wide range of regimes is accessible, including internal transport barriers with reverse magnetic shear and quiescent ELM-free H–modes. The dominant electron heating is an effective simulator of aspects of ITER α-particle heating, while the overall flexibility encourages investigations of alternative paths to commercial fusion. Both approaches will be broadened further by planned upgrades, including additional ECRH sources and neutral beam injectors for direct ion heating.

TCV operation in 2012 resumed only in November, after an interruption that started in January, due to the need for flywheel generator maintenance, various machine and diagnostic refurbishments and upgrades. Meanwhile, the repair of the third X3 gyrotron was completed. The campaign starting at the end of 2012 will therefore benefit from the full TCV capabilities.

As the shutdown occupied most of the year, the 2012 scientific achievements reported here below stem from analyses of previously performed experiments. We note that in recent and present campaigns strong emphasis is placed on the development and demonstration of real-time control techniques, employing a new digital control system and affecting virtually every scientific theme.

2.1.1 Scenarios with internal transport barriers

Measurements of the toroidal and poloidal rotation speeds of carbon impurities were performed for the first time in discharges with electron internal transport barriers. From these measurements the radial electric field can be derived. It was found that there is no significant increase in the E×B velocity shear at the barrier formation, suggesting that the shearing rate does not play a major role in barrier physics. Furthermore, the value of the shearing rate is well below the theoretical growth rate of the trapped electron modes, which are believed to predominantly drive turbulent transport in this regime. Flow shear stabilization, by contrast, requires the shearing rate to exceed the growth rate of the modes.

2.1.2 H-mode physics

In 2012 analyses were pursued in the domain of L- to H-mode (L-H) transitions and ELM control. In the meantime, the third X3 gyrotron has been repaired and reconditioned, which will allow resuming the programme on H-mode discharges without ELMs.

Influence of the X-point location on the L-H transition

The present scaling law for the H-mode threshold power as a function of plasma and machine parameters does not include information on the divertor geometry or characteristics. Based on its unique plasma shaping capabilities, TCV is well positioned to shed light on this point, in particular to solve the apparently contradictory results obtained in JET and Alcator C-Mod.

ECH-X2 heating power was continuously varied during the plasma current flat-top in discharges located at different vertical positions in the vacuum vessel but otherwise very similar. Figure 2.1.1 shows the normalised threshold power as a function of the X-pt height. The L-H threshold power lies far above the predicted values in those discharges with the plasma located in the upper part of the vacuum vessel. This slightly decreases when the X-pt height is reduced down to about 10cm. A strong reduction is then observed during further lowering of the plasma. However it is difficult to single out the effect of the X-pt height for 2 reasons. First, experiments were performed at different dates, separated by several months, leaving the possibility of changes in the vacuum vessel conditioning. Second, experiments were done at densities close to the rollover in the threshold power, because of the ECH-X2 cut-off, leading to a high sensitivity of the threshold power on the plasma density. New experiments are planned for remedying these unwanted effects.

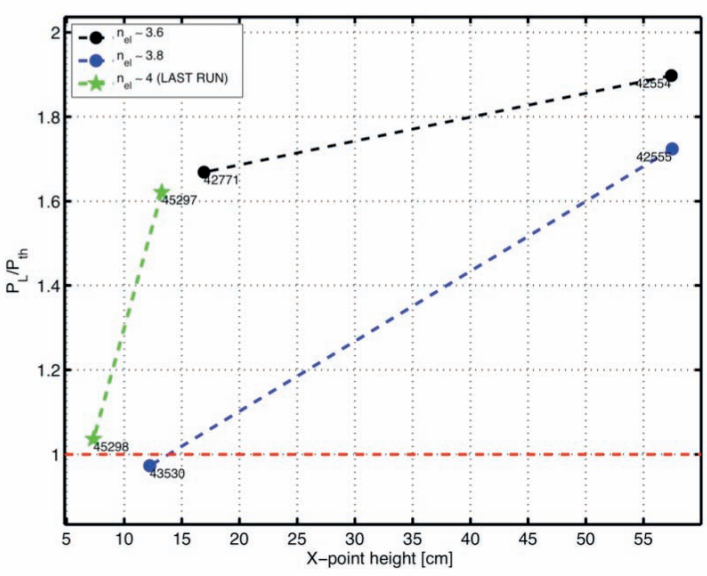

Fig. 2.1.1 *Power ratio needed to obtain the L- to H-mode transition in plasmas located at different vertical positions une the TCV vacuum vessel.*

ELM control with ECH power

Type I ELMs represent such a great concern for devices like ITER, such that their suppression or mitigation will be required. TCV explored several paths to mitigate them, in particular with edge heating using ECH X2.

Several experiments were performed. On one hand, real time controlled steps of ECH power were applied. ELMs were then destabilized right at the time at which the integrated power equalled the same amount as would be required with a constant injected power. On the other hand, straightforward modulation of the ECH X2 power led to ELM synchronisation only when the natural ELM frequency, corresponding to the averaged injected power, was equal to the modulation frequency.

Deeper analyses of these discharges have been performed. They confirmed the little effect that power modulation may have on the average ELM frequency. Indeed, Figure 2.1.2 only reflects the well-known, type I ELM dependence of the ELM frequency on the additional power, even in those cases where the power was modulated at a frequency that differs from the natural ELM frequency or where real time feedback was applied.

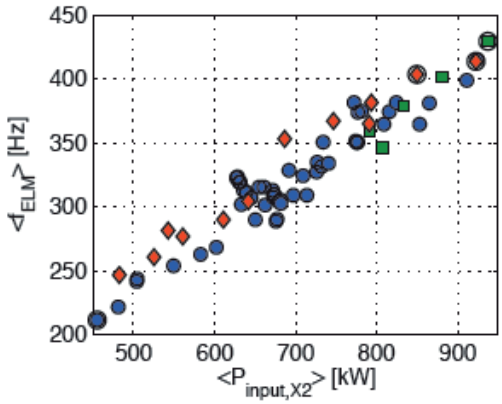

Fig. 2.1.2 *Measured ELM frequency as a function of additional power for different modulated power schemes.*

2.1.3 Plasma rotation

Measurement of Neoclassical Poloidal Rotation using inboard-outboard asymmetry of toroidal rotation.

A direct measurement of poloidal rotation in a tokamak is hindered by its relatively low magnitude (only a few km/s), which is close to the spectroscopic limit for optical diagnostics. Even obtaining statistically meaningful poloidal rotation measurements on TCV, with its relatively low power diagnostic neutral beam, requires plasma parameters to be held stable for at least 10ms. The poloidal rotation is, theoretically, limited to neoclassical values by strong damping resulting from the strong changes in the total magnetic field as particles follow field lines from the LFS to the HFS regions.

An alternative experimental spectroscopic measurement of poloidal plasma rotation in toroidally confined plasmas has proven effective in the TCV tokamak. The diagnostic neutral beam charge exchange diagnostic is used to measure the toroidal rotation profiles over a full mid-plane diameter to infer the complete bi-dimensional flow structure of the intrinsic C^{6+} impurity, which includes its poloidal component. For divergence free flows, the difference between the toroidal rotation frequency $f_t=u_t/R$ (u_t is the toroidal velocity and R the major plasma radius) at the inboard and outboard locations on the same flux surface is proportional to the poloidal rotation. This indirect measurement provides increased accuracy as the measured quantity $f_{t\text{-}in}\text{-}f_{t\text{-}out}\sim 4qu_p/R_{axis}$ (where q is the local safety factor) is larger than the intrinsic uncertainties of a direct spectroscopic measurement.

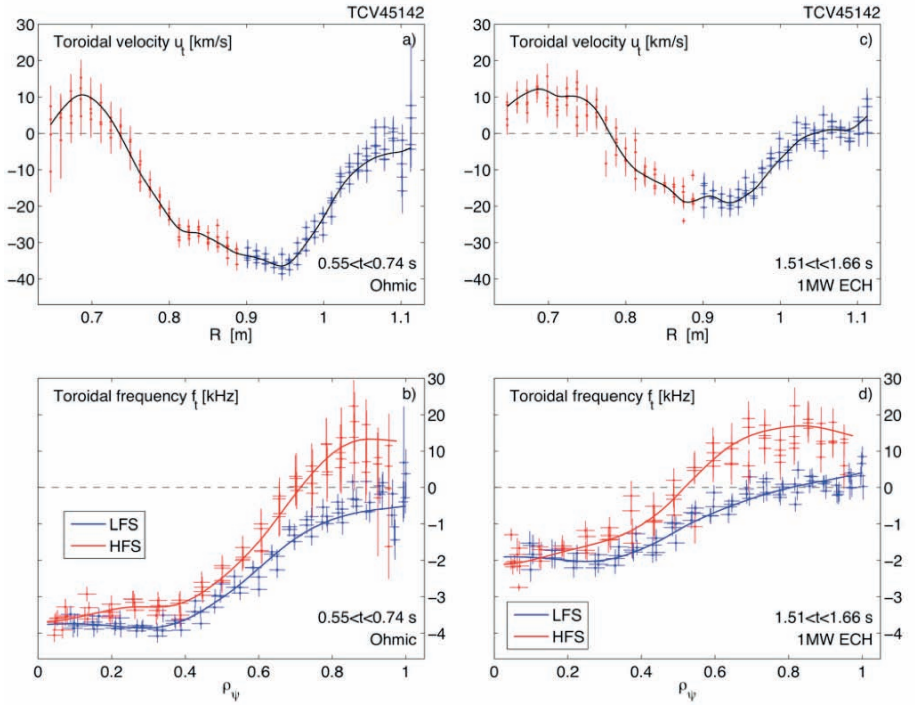

Fig 2.1.3 *Profiles of toroidal rotation velocity u_t measured during Ohmic (a) and ECH (c) phases of TCV 45142 plasma discharge, with the corresponding toroidal rotation frequency $f_t = u_t/R$, at the HFS and LFS, plotted as a function of the flux label ρ_ψ (b,d)*

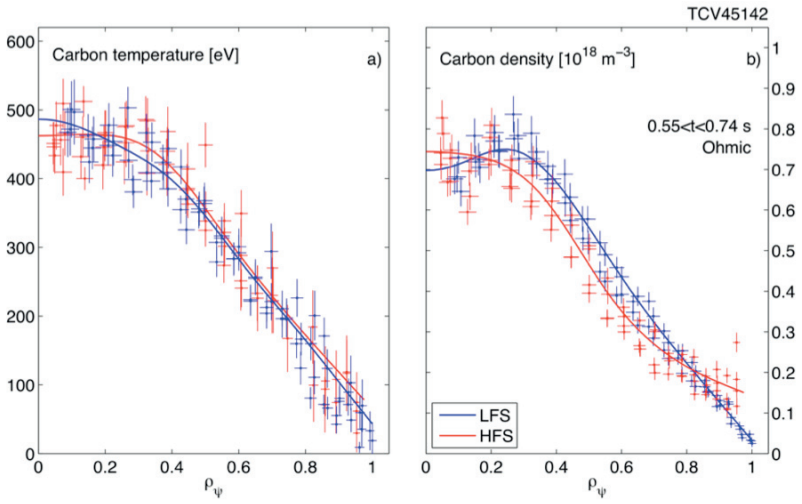

Fig 2.1.4 *Carbon temperature (a) and density (b) during the Ohmic phase of TCV discharge #45142. HFS and LHS measurements are presented as function of the normalised poloidal flux.*

As the diagnostic neutral beam (DNB) is strongly attenuated during its passage across the plasma from the outside towards the central column, the neutral density available for CXRS on the HFS can be problematic. A new, more sensitive, CCD camera will be available for this system in 2013, (see Section 3.3 on TCV Diagnostics).

This new method of indirect poloidal rotation measurement was first demonstrated, and tested, in a stable discharge with monotonic profiles where the deduced poloidal rotation is compared with a direct CXRS measurement (from the vertical CXRS camera) and neoclassical predictions.

Figure 2.1.3 shows the profiles of the toroidal velocities from the HFS and LFS camera in physical coordinates and mapped onto flux-label coordinates showing that the plasma is not simply rotating as a rigid body. Figure 2.1.4 shows the corresponding temperature and Carbon impurity densities again mapped to flux-label coordinates, showing that the gradients and absolute values agree well, despite the difference in toroidal rotation.

Since the indirect poloidal rotation technique requires the difference between two experimental measurements, each with their own uncertainties and measurement challenges, a complex statistical experiment was used to assess the overall uncertainty in the deduced poloidal velocity. All the experimental uncertainties were varied over their individual statistical ranges and the deduced poloidal velocity range used as a measure of the final uncertainty. The result of a comparison of the indirect, direct and neoclassical poloidal rotation values are shown in Fig. 2.1.5. Here shading indicates the variations of the uncertainty as a function of the flux coordinate. In comparison with the direct poloidal measurement, whose uncertainty made it often impossible to even determine the sign of the poloidal rotation, for these experiments, the indirect measurement is shown to agree, to within the evaluated overall uncertainty with the neoclassical predictions. Using this process as a justification of the technique, this procedure will be used in the 2013 campaigns and beyond to measure the poloidal rotation in situations where a discrepancy with the neoclassical predictions has been observed on TCV and elsewhere as a strong test of momentum transport behaviour in tokamaks.

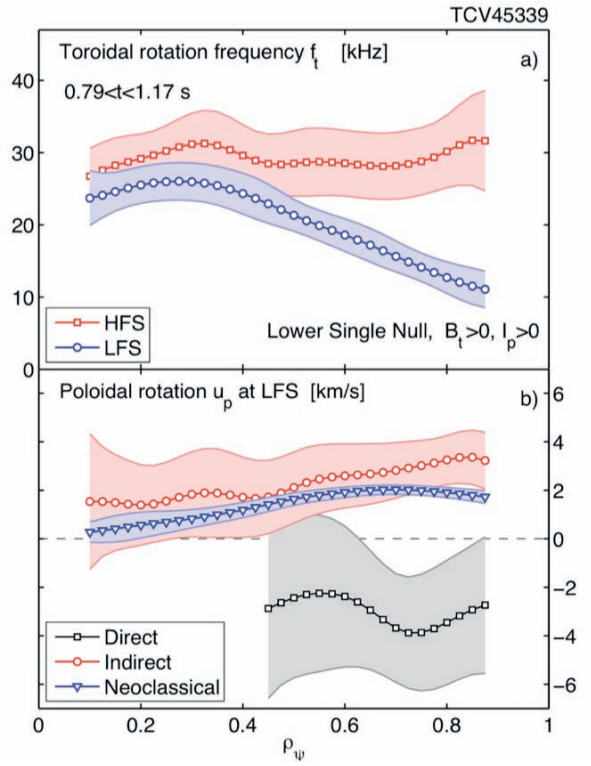

Fig. 2.1.5 *Toroidal rotation profiles (a) and indirect poloidal rotation measurement (b) for lower single null, co-current rotating discharge (TCV #45339).*

Rotation studies in electron Internal Transport Barriers on TCV

The formation and stabilisation of electron Internal Transport Barriers (eITBs) with simultaneous toroidal and poloidal rotation measurements was the main focus of recent experiments. Their aim was to demonstrate whether strong E×B shearing is essential for eITBs in TCV and determine the necessary magnitude. EITBs are formed using electron cyclotron heating and current drive (ECH/ECCD) to create hollow or flat current profiles. The present view at TCV is that the key ingredient in the formation and robustness of eITBs is the degree of reversed magnetic shear, with confinement improvements starting at shear levels smaller than 0.5. Other tokamaks have, in the past, concluded that either rational q or E×B shearing are the key. TCV thus plans to assess the role of rotation and E×B shearing rate, since the present CXRS cameras set up in standard and fast acquisition allow measurement of stationary and pre-barrier formation rotation profiles.

Two eITBS targets at a height of z=3cm were developed in parallel to study the effect of central EC power, total EC power and MHD activity on the barrier strength, rotation profiles, E_r and E×B shearing rate profiles. A central eITB target at z=3 cm with counter-ECCD (cnt-CD) applied on axis and co-ECCD off axis was first developed. TCV constraints allow an easier barrier formation for this configuration, although the achieved barrier is not as strong as with co-CD eITB plasma (only T_e barrier). A co-CD eITB was also formed by applying off-axis co-CD with central ECH to obtain a stronger and more off-axis barrier than for the first case. Development of this target proved to be extremely challenging due to unfavourable EC gyrotrons access angles and deposition regions around z=0 with the plasma density remaining often higher than that required to obtain strong barriers. Moreover, the CXRS and Thomson diagnostics were, at that time, not optimised for this second configuration, complicating the data analysis. For these reasons, the initial study focused on the central eITB target.

The effect of central EC power on the barrier strength and rotation profiles was examined by applying 730kW co-CD or counter-CD and then comparing with a similar Ohmic plasma discharge. All three cases are characterised by a counter-current rotation profile (v_φ>0, Fig. 2.1.6) and an inward E_r profile (E_r<0). The cnt-CD case featured a doubled central electron pressure, indicative of confinement improvement inside ρ_ψ=0.5 with 6keV

on-axis (Fig. 2.1.6, highlighted in magenta). From the p_e profiles a marked difference in the electron transport is deduced and a central barrier is observed in the cnt-CD case. Even though the E_r profile is slightly deeper for the co-CD case, the E×B shearing rate around ρ_ψ=0.3–0.5 remains similar for the cnt-CD (central barrier) and co-CD (no barrier) cases. This shows, experimentally for the first time, that the E×B shearing rate is not the cause of electron transport improvement in TCV. A quantitative comparison between the E×B shearing rate and the growth rate, γ, of TEM modes (the most instable in TCV eITB plasmas) shows that the former remains much smaller, consistent with the negligible effect of E×B shearing rate on TEM in TCV reverse shear. When the total ECH power is reduced, the toroidal rotation increases towards more cnt-current profiles and E_r strengthens in the inward direction. The development of an MHD mode is seen to destroy the barrier and causes a reversal of the toroidal rotation (co-current). The E_r profile is also strongly affected and tends to the outward direction in the core in the presence of significant MHD activity.

During this study, the poloidal rotation, determined using the indirect method based on the asymmetry of the toroidal rotation on a flux surface, were compared with the directly measured profiles, showing a good agreement. The E_r profile is found to be proportional to only two terms: the ion pressure gradient (diamagnetic term) and the ωRB_p term (determined from the HFS and LFS toroidal rotation on the same flux surface and more dominant for lower EC power). TCV is now able to obtain the poloidal rotation and the E_r profiles by from direct CXRS diagnostic measurement or using this indirect method described above.

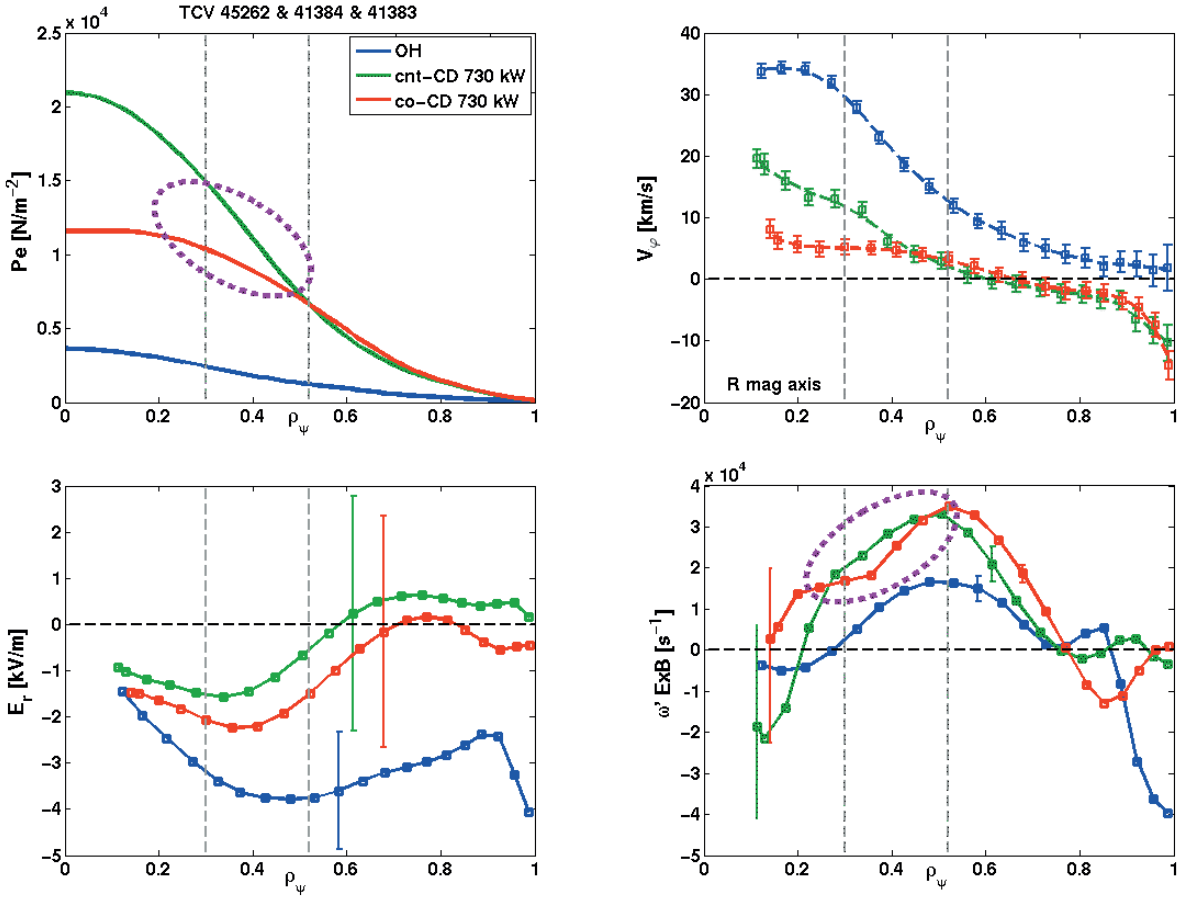

Fig 2.1.6 Electron pressure (p_e), toroidal velocity (v_φ), radial electric field (E_r) *and E×B shearing rate profiles for the cnt-CD, co-CD and OH cases*

2.1.4 Heat and particle transport

Electron transport in TCV high confinement mode plasmas was analyzed. It was observed that the electron density profile in these plasmas flatten when intense electron heating is applied, in contrast to observations on other machines where an increase of the profile peakedness was reported. We could show with quasi-linear gyrokinetic simulations that this effect, usually interpreted as an effect of collisionality, stems from the combined effect of many plasma parameters.

Significant activity was devoted to impurity transport. A multi-purpose gas injection system was developed, commissioned and calibrated. We could demonstrate that the system is capable of massive gas injections to provoke disruptions and of delivering small puffs of gaseous impurities for perturbative transport experiments. This flexible tool was exploited in a series of impurity transport experiments with argon and neon injections. The numerical techniques to extract transport coefficients from soft x-ray measurements have been developed and tested.

In the 2011 TCV experimental campaign a series of impurity transport experiments was conducted, resulting in an extensive dataset of argon and neon puff experiments. The numerical code STRAHL was used to solve the direct transport problem, i.e. to obtain the impurity density evolution given some transport coefficients. The expected radiation pattern of the injected impurities can be computed and compared to the experiments when the impurity density evolution is known.

The inverse problem of obtaining the transport coefficients from the observed radiation pattern is more difficult. Two numerical methods proposed recently for solving the inverse problem were implemented and applied to the impurity injection experiment dataset. The transport coefficients reconstructed from the soft x-ray radiation of argon and neon show a weaker variation as a function of the plasma parameters such as plasma current, shape etc. than it was previously reported. The solution of the inverse problem with different methods provides better insight into the nature and limitation of these transport investigations.

2.1.5 Advanced plasma profile and instability control

Very precise pacing of sawtooth oscillations was previously demonstrated in TCV by applying EC power just outside the q=1 surface, following the detection of each sawtooth crash, for a set duration. Since EC power stabilizes the underlying internal kink instability, a crash is then obtained immediately after the power is removed, providing a high degree of control over individual sawteeth. This experiment was extended by using a *destabilizing* agent instead, i.e., EC power well inside the q=1 surface, and reversing the strategy: the crash detection is followed by a power *cut* of set duration, after which the power is turned back up to trigger the next crash. In combination with steady-state power on the q=1 surface, this experiment successfully emulates the real-time destabilization strategy required for a fusion reactor, where sawteeth are expected to be stabilized by energetic fusion-born alpha particles.

An additional experiment was conducted to determine whether sawtooth period locking to a pre-determined power modulation frequency could also be achieved. It was shown that locking could indeed be achieved within a somewhat narrower range of periods than in the case of pacing, in accordance with theoretical predictions.

2.1.6 Exploration of new shapes and configurations

TCV continues to pursue the development and characterization of novel plasma configurations in order to improve the tokamak concept as reactor solution. The current activities focus on ways to decrease the anticipated high peak and steady-state power loads on plasma facing components (PFCs) in a reactor to tolerable levels.

Effect of negative triangularity on H-mode plasmas

Recent TCV experiments have shown that the plasma triangularity δ can be used to control the ELM size. It is well known that small changes of δ can have a significant effect on the ELM behaviour. TCV has developed a teardrop-shaped single-null diverted configuration that can be heated efficiently with both X2 and X3 ECRH throughout a scan of the upper triangularity δ_{top} from 0.2 to -0.2, while maintaining a type-I ELMy H-mode, Fig. 2.1.7. Such a large change of δ_{top} results in an increase of the ELM frequency by a factor of up to 3 and a corresponding decrease of the energy loss per ELM.

The reduction of the transient energy release per ELM comes at the price of a 20% reduction of the H-mode pedestal height as shown in Fig. 2.1.8.

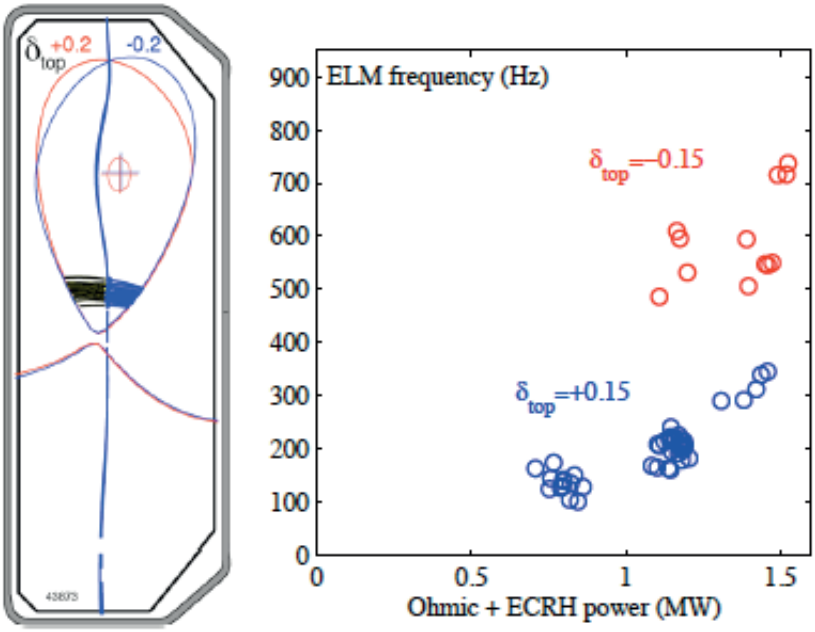

Fig. 2.1.7 *(Left) Separatrix contours with ray trajectories for edge-deposited X2 for positive and negative triangularity teardrop-shaped plasmas; (Right) Type-I ELM frequency vs. total input power for positive and negative triangularity.*

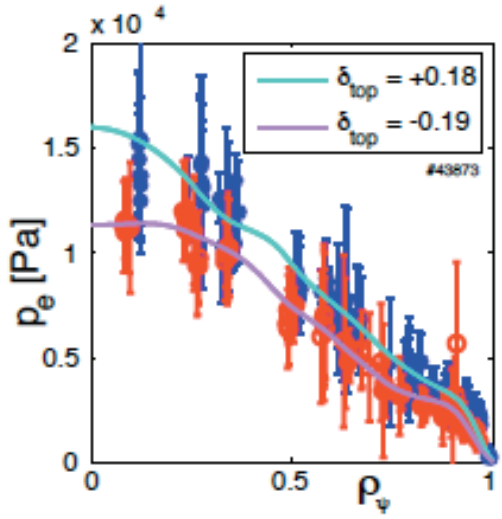

Fig. 2.1.8 *Time-averaged electron pressure profiles during H-mode with positive and negative upper triangularity as shown in Fig. 2.1.7.*

Characterisation of the snowflake divertor configuration

The Snowflake (SF) configuration has several properties that promise to reduce power flux densities on the divertor targets. The capability of TCV to document these advantageous properties has been increased by improving the control of the position of the secondary X-point when scanning the configuration from a conventional single null to a snowflake.

The analysis of the snowflake experiments focused on the potential of this novel configuration to decrease peak power fluxes onto the PFCs and is described in detail in the Section on edge physics.

Improved breakdown control for the development of the doublet configuration

The most promising path towards a doublet configuration in TCV is based on a simultaneous double breakdown and ramp up of two droplet plasmas. As a first step, the understanding and improving of the standard breakdown in TCV has been made subject of a recently started doctoral thesis project.

The analysis of the magnetic configuration at breakdown has confirmed the importance of the recently implemented feedback control of the currents in the Ohmic transformer and the poloidal field coils at the time of the breakdown. Further proposed improvements include an optimized magnetic configuration as well as a procedure to compensate for offsets that were identified in components of the plant control system.

2.1.7 Edge plasma physics

Reduction of peak wall power loads in L- and H-mode tokamak plasmas in TCV with the snowflake divertor

The investigation of the innovative snowflake configuration was continued with a detailed study of its power exhaust properties for both L- and H-mode. This was performed by

varying the proximity of the configuration to the ideal SF, whilst monitoring the exhaust properties with a range of radiation and edge diagnostics. Experimental SFs feature two X-points with finite separation, with the secondary one residing in the private flux region for the so-named SF+. The variation in the performed experiments, characterised by the parameter σ, defined as the separation between the two X-points normalized with respect to the minor radius was between a SF-like single null (σ=2.4) and a SF+ configuration (σ=0.4). H-mode was established by heating the core plasma with electron-cyclotron resonance heating (ECRH) at the 3rd harmonic (X3), and the edge, with ECRH at the 2nd harmonic (X2).

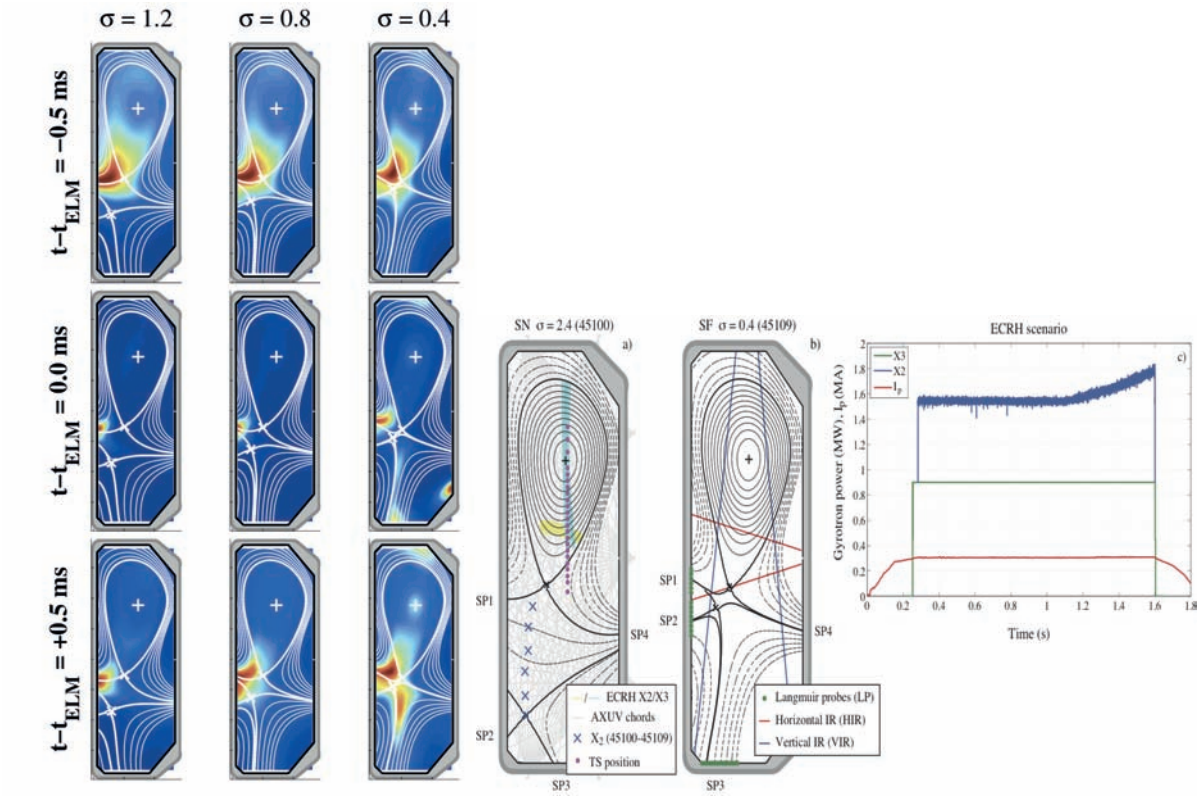

Fig. 2.1.9 *Left: Infrared radiation patterns in the poloidal plane for three values of σ (1.2, 0.8. 0.4) for three phases: 0.5ms before the ELM crash, at the crash, and 0.5 ms later. Right: Measurement set-up used for these experiments. (a) Location of X"; (b) AXUV sightlines and Thomson scattering measurement positions. (c) ECRH scenario.*

The middle panel fo Fig. 2.1.9 indicates the positions of the x2 and X3 beams, AXUV sightlines and Thomson scattering (TS) measurement points. The fields of view of the fast framing (15kfps) horizontal infrared (HIR) and vertical infrared (VIR) cameras and the locations of Langmuir probe (LP) arrays are also indicated. Typical discharge parameters are: I_p=300kA, B_t=1.45T, κ_{95}=1.7, δ_{95}=0.2, q_{95}=2.6, P_{X3}=900kW, P_{X2}=650kW, with the latter ramped to 900kW in the second half of the current flattop to identify the ELM type (right panel of Fig. 2.1.9).

The left panel of Fig. 2.1.9 shows the radiation patterns in the poloidal plane for three values of σ (1.2, 0.8. 0.4) for three phases: 0.5ms before the ELM crash, at the crash, and 0.5 ms later. These were determined from an inversion of AXUV bolometric camera data, coherently averaged over tens of ELMs. The plots use normalised (linear) colour scaling, so that they may be used to compare radiation patterns, but not absolute levels. From the figure a clear activation of the bottom secondary divertor leg during ELMs is seen at a value of σ between 0.8 and 0.4. Figure 2.1.10 shows that the radiated fraction

of the ELM energy loss is up to 60% higher in SF configuration than for the SN configuration that contributes to lowering the peak wall heat load.

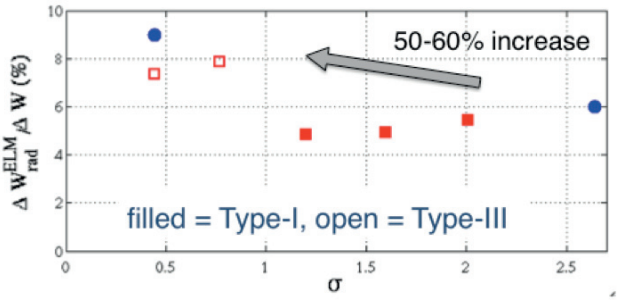

Fig. 2.1.10 *Radiated fraction of ELM energy loss as a function of the snowflake parameter σ.*

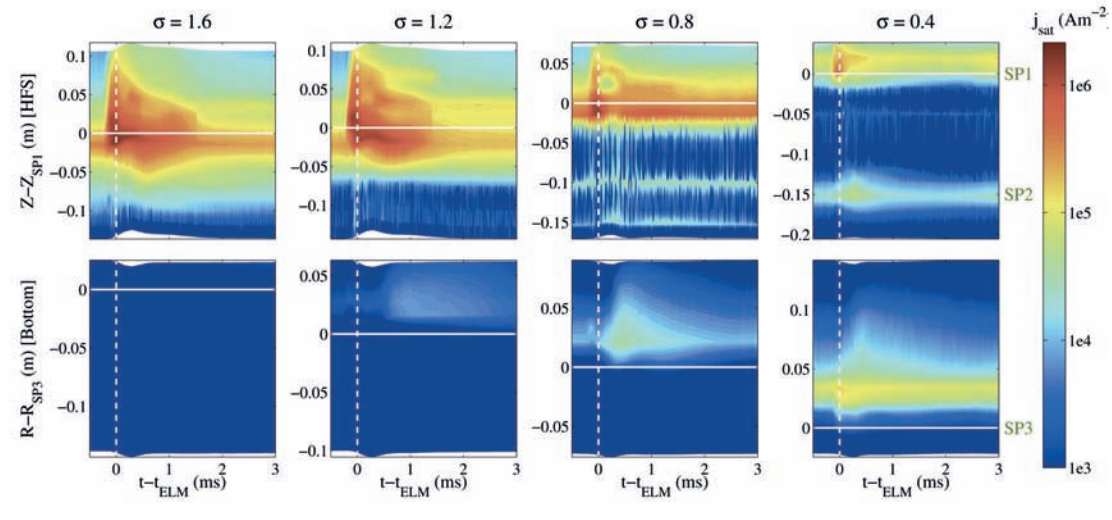

Fig. 2.1.11 *Spatio-temporal evolution of Langmuir probe saturation current signals for different values of the snowflake parameter σ.*

A similar picture arises from the edge measurements. Figure 2.1.11 shows the spatial and temporal profiles of the saturation current (i.e. particle flux density) during ELMs, measured with the Langmuir Probe (LP) arrays near the primary (SP1) and secondary (SP2, SP3) strike points for σ=0.4–1.6. Positions are shown relative to the strike point locations Z_{SP1} and R_{SP3}. SP2 is only diagnosed at σ=0.4. In the range σ=1.2–2.4, practically no plasma flux reaches the secondary strike point and the peak flux density at the primary strike point remains approximately constant. A clear reduction at SP1 and activation of the secondary strike points is observed for σ between 0.8 and 0.4.

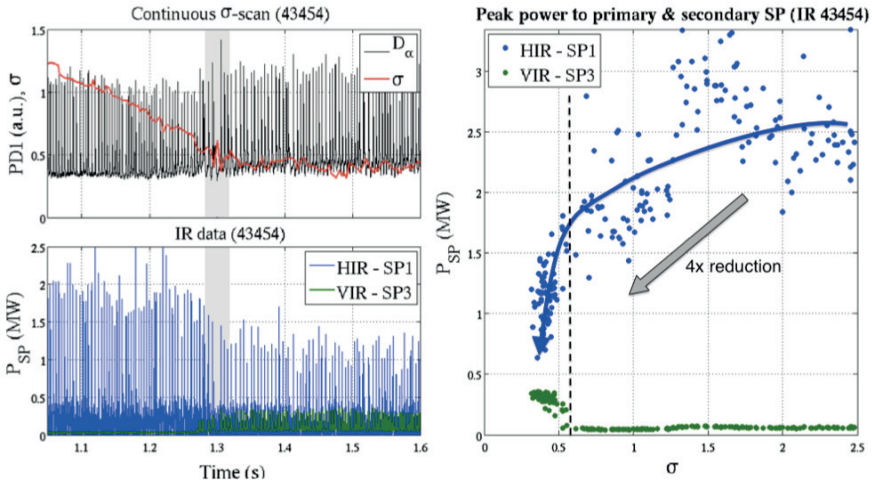

Fig. 2.1.12 *IR data taken during a continuous σ-scan.*

The strong decrease in j_{SP1} and increase in j_{SP3} with decreasing σ is seen more clearly in Fig. 2.1.12, which shows the IR data taken during a continuous σ-scan. The left column summarises the scenario with σ and D_α (top) and the spatial maxima of the heat flux profiles at SP1 (HIR) and SP3 (VIR) (bottom). The right column shows the peak powers to SP1, SP3 in blue-green respectively as a function of σ. The observed activation of SP3 at σ=0.6 is consistent with the LP results. The peak power to the primary SP1 is reduced by a factor of four as σ decreases from 2.4 to 0.4, with the majority of the reduction occurring for σ<0.6. Figure 2.1.13 shows that the heat flux at SP3 reaches 40% of the value at SP1 in H-mode at σ=0.4. In L-mode this fraction, inferred from the LP data, is significantly lower at this value of σ.

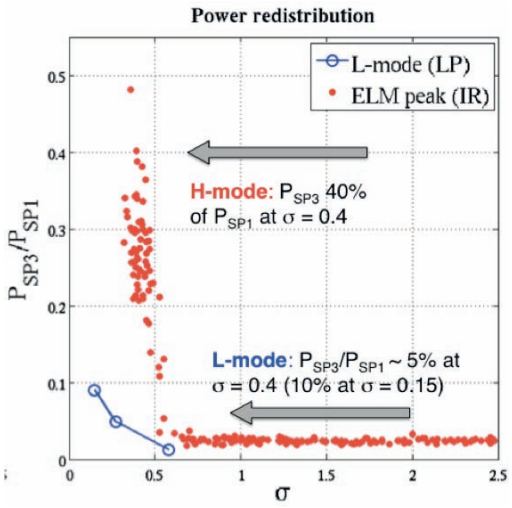

Fig. 2.1.13 *Ratio between heat flux at the two strike points SP3 and SP1 as a function of the snowflake parameter σ.*

The activation of the secondary strike point SP3 at the relatively large threshold value of σ=0.6 is qualitatively consistent with theory, and may explain the redistribution in non-ideal SFs by instability-driven convective transport across the null region. The threshold condition $\beta_p>1$ is satisfied in a sufficiently large region around the null point that is more easily satisfied with an increase in exhausted particles and heat entering the SOL during ELMs. A plasma pressure profile extending into the SOL was estimated by conditionally sampling all TS data points taken within 0.3ms of an ELM crash and fitting a spline, as

shown in Fig. 2.1.14a (n_e^{SOL}x10^{19}m^{-3}, T_e^{SOL}x200eV). The fitted p -profile was mapped onto the poloidal plane and used to estimate the local βp, as shown in Fig. 2.1.14b). These 2D profiles indicate that as σ decreases, the zone where β_p>>1 grows significantly. A second hint that such a transport may be in effect is given in Fig. 2.1.14c) which plots normalized spatial heat flux profiles during ELMs in flux-normalised coordinates at both SP1 and SP3. This shows that the spatial heat-profile at the secondary strike point is more symmetric than the usual asymmetric shape observed at the primary strike point. This is compatible with heat flowing into the secondary divertor leg from an approximately homogeneously filled upper region.

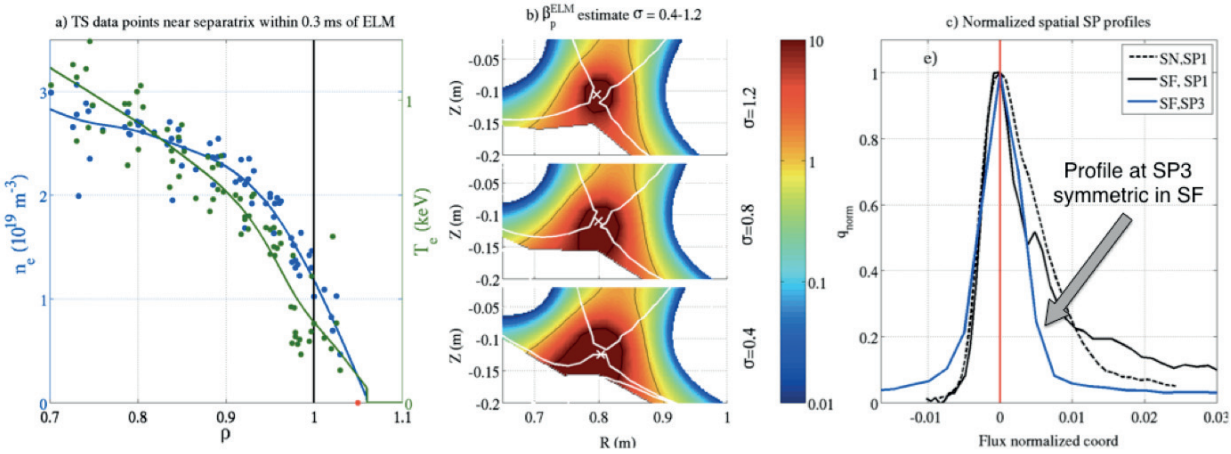

Fig. 2.1.14 *a) Conditionally sampled Thomson scattering data within 0.3ms of an ELM crash, extending into the SOL; b) estimated 2D β_p^{ELM} profiles in the null region for σ=1.2–0.4, with β=1, 10 contours in white; c) spatial heat flux profiles at SP1 and SP3 for the SN and SF during an ELM, normalized to the peak value and plotted against flux normalized coordinates.*

The significant power redistribution to the secondary strike points, and the corresponding reduction in peak heat load, observed well before the two X-points coalesce can have important implications for the applicability of the snowflake concept in large-scale fusion devices.

2.2 Theory and numerical simulation

2.2.1 Physics underlying anomalous transport

Global gyrokinetic simulations of trapped electron mode turbulence

Using the newly developed version of the global gyrokinetic ORB5 code, which includes particle collisions, several linear and nonlinear studies of Trapped Electron Mode (TEM) micro-instabilities and turbulence have been performed. A “hybrid” model was used for electrons, considering kinetic trapped electrons and assuming adiabatic passing electrons.

Particular attention has been paid to the numerical noise problem inherent to PIC delta-f codes such as ORB5. A new procedure to control noise, called “coarse graining”, has been carefully tested and verified against other algorithms based on the application of

Krook operators. Convergence with number of numerical particles and with the numerical electron mass has been demonstrated.

Finite size effects (ρ*) in the TEM regime have been investigated. Whereas there seems to be only a very weak ρ* effect on the linear TEM spectra, a robust finite ρ* effect was found in nonlinear simulations, which is comparable in magnitude to that of the ITG turbulence.

Electron-ion and electron-electron collisionality has been shown to have a stabilizing effect on TEM growth rates, and raises the electron temperature gradient threshold. In nonlinear TEM simulations, it was found that the turbulent heat flux reduction was even more important relatively to the collisionless TEM case. The effect of zonal flows on the TEM turbulent heat flux, on the other hand, appears to be very weak, contrary to the ITG situation.

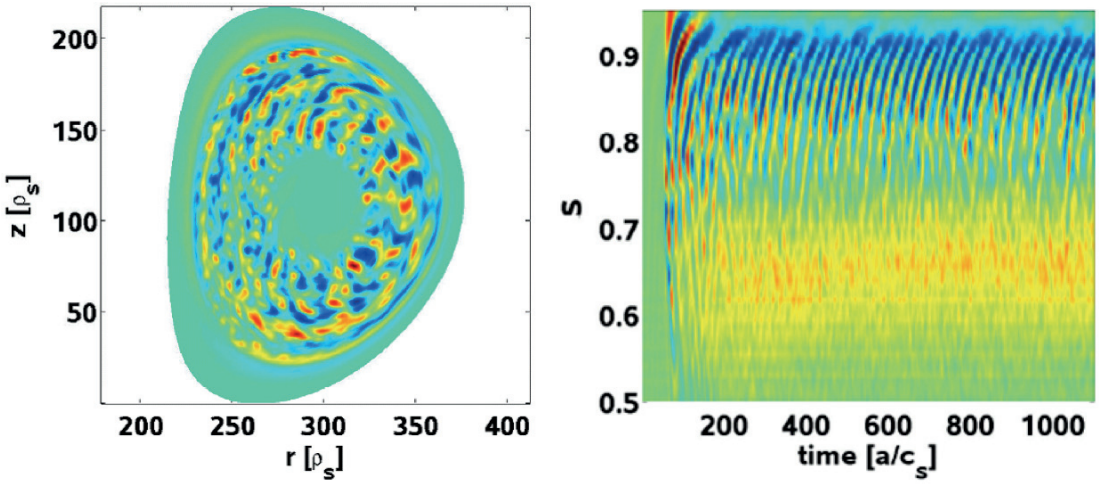

Fig. 2.2.1 *Left: contours of perturbed potential in a global TEM simulations of TCV shot #45353. Right: contours of zonal flow shearing rate versus time and radius.*

Global gyrokinetic simulations of microturbulence in TCV

As a first step towards the crucial point of validating gyrokinetic turbulence simulation codes, a reconstructed ideal MHD equilibrium from a specific TCV shot (#45353) and experimentally measured density and temperature profiles have been considered for global gyrokinetic simulations using the ORB5 code. The regime is clearly identified as TEM-dominated. The perturbations (Fig. 2.2.1, left) exhibit the typical "streamer"-like structures, partly broken up under the effect of zonal flow shearing. Interestingly, avalanches and geodesic acoustic mode (GAM) oscillations are predicted, especially in the outer half of the plasma radius (Fig. 2.2.1, right). These numerical results are being compared to experimental fluctuation measurements using Toroidal Phase Contrast Imaging (TPCI). Preliminary results indicate an excellent agreement for the frequencies and radial wavelength of these oscillations. These are among the first and few comparisons of direct numerical simulation of turbulence with detailed experiment measurements in the plasma core.

Global gyrokinetic simulations of ion temperature gradient turbulence in ITER

Global gyrokinetic simulations of Ion Temperature Gradient (ITG) driven turbulence in an ideal MHD ITER equilibrium plasma have been performed with the ORB5 code (Fig. 2.2.2).

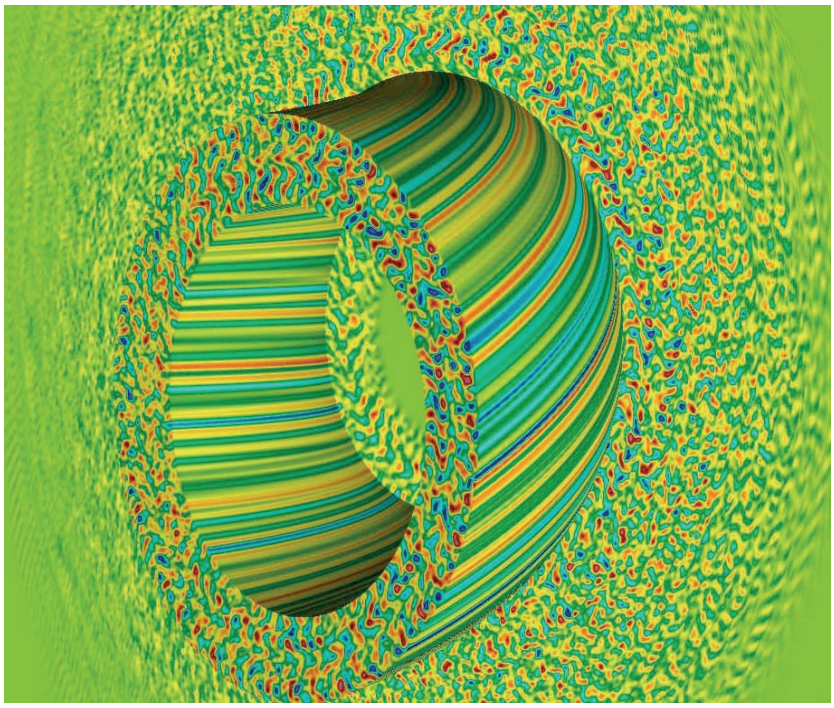

Fig. 2.2.2 *Contours of perturbed density in a global gyrokinetic ITG turbulence simulation of an ITER plasma with the ORB5 code.*

The noise control and field-aligned Fourier filtering procedures implemented in ORB5 have proven effective in obtaining numerically healthy results within a reasonable amount of computational effort: typical simulations require 10^9 grid points, 10^9 particles and, despite a particle per cell ratio of unity, achieve a signal to noise ratio larger than 50. As compared to a circular concentric configuration with otherwise similar parameters, the effective heat diffusivity is considerably reduced for the ITER MHD equilibrium. A self-organized radial structure appears (Fig. 2.2.3), with long-lived Zonal Flows (ZF), modulating turbulence heat transport and resulting in a corrugated temperature gradient profile. The ratio of long-lived ZF to fluctuating ZF (avalanches) is markedly higher for the ITER MHD equilibrium as compared to circular configurations, thereby producing a more effective ITG turbulence suppression, in spite of a higher linear growth rate. As a result, the nonlinear critical temperature gradient is about twice the linear critical temperature gradient. Moreover, the heat transport stiffness above the nonlinear threshold is considerably reduced as compared to circular cases. Plasma elongation is probably one of the essential causes of this behaviour: indeed, undamped ZF residual levels and Geodesic Acoustic Mode (GAM) damping are both increasing with elongation.

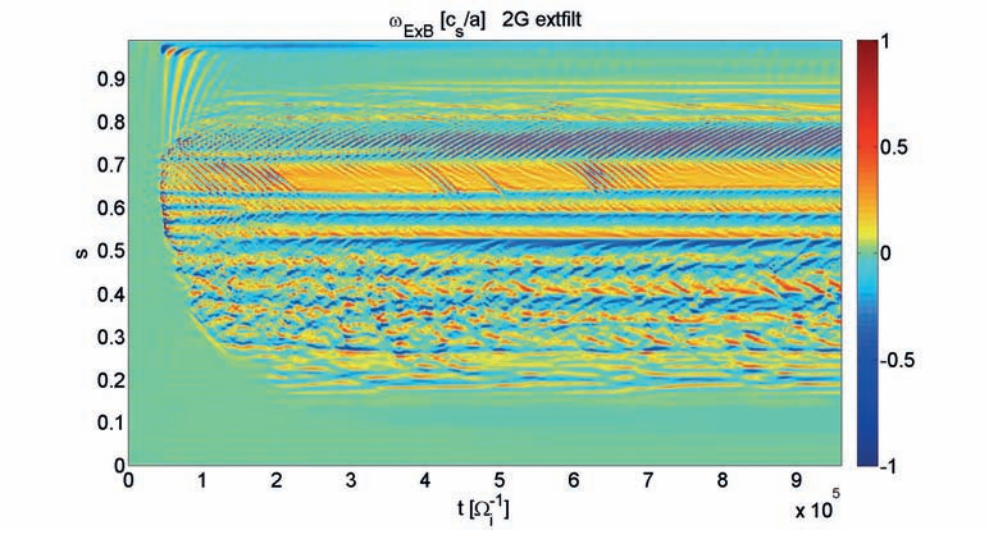

Fig. 2.2.3 *Contours of zonal flow shearing rate versus time and radius in a global gyrokinetic ITG turbulence simulation of an ITER plasma with the ORB5 code*

Benchmarking of gyrokinetic transport simulation codes

Linear simulations in the collisionless TEM regime have been validated through a successful benchmark between the global ORB5 and GENE codes. These comparisons have been made on a well defined parameter set known as the "Cyclone" case except for the ion temperature gradient which was lowered so that the most unstable modes are TEMs. The fully kinetic electron model has been used. The agreement between ORB5 and GENE results is excellent for the mode frequencies and growth rates in the long wavelength regime but some discrepancy appear in the short wavelength regime: this was to be expected due to the long wavelength approximation used in ORB5 but not on GENE.

Study of non-adiabatic kinetic electron response near mode rational surfaces

The non-adiabatic response of passing electrons near low order mode rational surfaces (MRSs) has been studied by carrying out GENE flux tube simulations. In the linear regime, radially fine structures centred at these MRSs appear on the envelope of ITG and TEM eigenmodes. The dependence on various essential parameters (safety factor, magnetic shear, ion/electron mass ratio, wavenumber) of the radial width of these fine structures has been systematically studied, showing very good agreement with theoretical estimates. Furthermore, the actual form of the linear eigenmodes' radial structure presents excellent agreement with a local dispersion relation model enabling to estimate the level of destabilization from the passing electrons. Nonlinear simulations were then carried out to investigate to what extent these structures survive in the saturated turbulent regime and affect the turbulent particle and heat transport levels. An evolution towards a self-organized step-like structure of the time-averaged density and temperature profiles has been observed, with flattening in the vicinity of the low order MRSs, reflecting increased transport in these radial intervals, and steepening in between. The amplitude of nonlinearly driven zonal flows are radially modulated, showing increased values of associated shearing rate between MRS's, thus providing stabilization of the steeper gradient regions.

Synthetic diagnostics for CECE and PCI

In order to enable closer comparisons between gyrokinetic simulations and experimental fluctuation measurements, synthetic diagnostics reproducing both Correlation Electron Cyclotron Emission (CECE) and Phase Contrast Imaging (PCI) as installed on the TCV tokamak have been implemented as post-processing analysis tools to the gyrokinetic codes. First comparisons with experimental results have been carried out using nonlinear GENE flux tube simulations under TCV relevant conditions,

Shaping effects on turbulent transport

A set of tokamak MHD equilibria with increasing geometrical complexity – starting from a simple equilibria with circular, concentric flux-surfaces to a Shafranov-shifted, elongated, triangular, diverted equilibria – have been suggested for carrying out benchmarks for gyrokinetic codes. This set of benchmark cases, considering fully kinetic ion and electron dynamics, have been considered for computing the linear spectra (presenting both ITG and TEM modes) using the flux-tube version of the GENE code. The GENE results were thoroughly compared to results from other flux-tube codes, in particular GS2 and GKW, showing excellent agreement. For the same set of equlibria, Rosenbluth-Hinton tests were carried out with GENE as well, thus extending the linear benchmarking results. Comparison with theoretical estimates including geometrical effects for the GAM frequency, damping rate and zonal flow residual is currently underway.

Locality properties of energy fluxes in gyrokinetic turbulence

Fundamental analysis of gyrokinetic turbulence has been carried out considering nonlinear GENE flux tube simulations in the ITG regime with adiabatic electron response. The purpose of this study was to investigate the locality in spectral k-space of nonlinear interactions, employing Kraichnan's infrared (IR) and ultraviolet (UV) locality functions. Due to the nontrivial dissipative nature of gyrokinetic turbulence (presence of damped modes throughout the whole k-spectrum), an asymptotic level for the locality exponents, indicative of a universal dynamical regime for gyrokinetics, was not recovered and an accentuated non-local behaviour of the IR interactions is found instead, in spite of the local energy cascade observed.

Parallel performance of gyrokinetic turbulence simulation codes

Continuing efforts have been made in order to improve the parallel scalability of the ORB5 code. Attention has focused in particular on the large system sizes requiring large grids for the field solver. The recent improvements to the parallelization scheme were crucial for the ITER simulations presented above. The code was ported to the HELIOS supercomputer, which is one of the most powerful HPC platforms in the world (1.5 PetaFlops/s peak, no.12 on the www.top500.org June 2012 list) and was run as one of four “LightHouse Projects” to which the machine was dedicated during the first three months of service. The good performance achieved with ORB5 allowed us to pursue with production projects, including particularly demanding collisional ITG and TEM simulations. The prospects are excellent for the near future: projects directed or co-directed by CRPP staff have been allocated 111 million cpu-hours on HELIOS for the period November 2012 – November 2013, in a very competitive call for proposals. This represents close to 20% of the total resources available on that platform.

2.2.2 RF waves

ICRF waves in 2D and 3D configurations

The SCENIC ICRH package has been applied to predictions of heating and stability properties in baseline scenarios in ITER. SCENIC is capable of self-consistently treating the interaction between the wave fields, fast ion heating and equilibrium. The code has been applied to He3 minority heating, in deuterium-tritium plasmas. These simulations have been applied to examining the stability of the resistive interchange modes in ITER, and in particular, to see what extent the ICRH ions can interact with these modes. In addition, the SCENIC code has made the first known integrated ICRH simulations in a 3D configuration (see Fig. 2.2.4). In particular, the power deposition, the fast ion deposition, and the equilibrium have been simulated for and ICRH system in a quasi-axisymmetric stellarator.

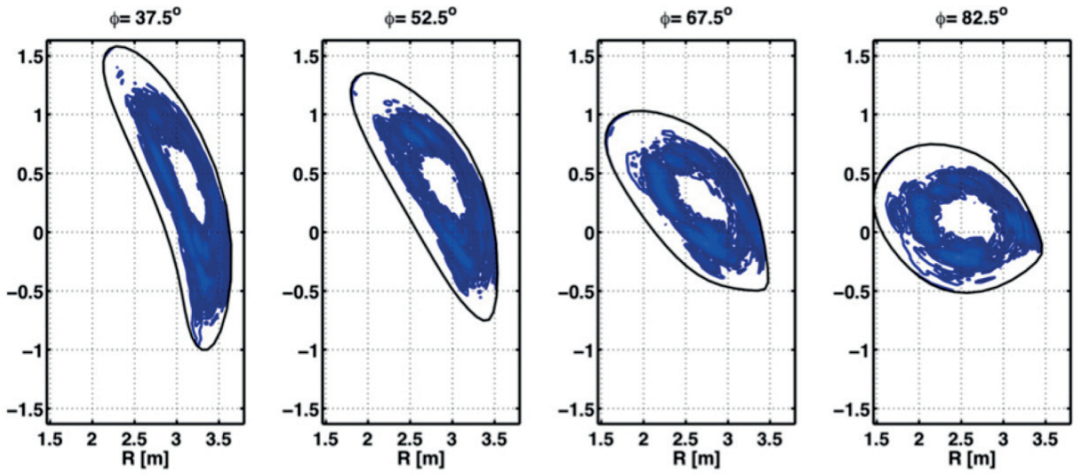

Fig. 2.2.4 *The power deposition of ICRH in a quasi-axisymmetric stellarator, plotted at various toroidal angles.*

2.2.3 Operational limitis

Effects of collisionless ions on MHD stability: Necessary conditions for stability

The formulation for the effects of energetic ions on MHD modes in tokamaks has been completed. Special attention has been given to Mercier modes, or interchange modes, since the stability threshold of these modes dictate a necessary condition for tokamak stability. Kinetic corrections in a collisionless plasma associated with parallel dynamics are treated by replacing the adiabatic equation of state with a moment equation obtained from the linearised collisionless drift kinetic equation. The work presented here seeks a new general treatment of the parallel dynamics associated with collisionless wave-particle interaction. The main known results in the literature on FLR and parallel kinetic effects are considered and challenged in the context of the more general results obtained here. This has been achieved through a solution to the drift kinetic equation that is simultaneously valid through the inner layer of a rational surface, and the outer region. At present it remains for growth rates and stability criteria to be obtained numerically. Finally, an important by-product of this work that has wider implications is the development of wave-particle interaction that takes into account a neoclassicaly resolved equilibrium distribution of superthermal particles.

MHD Stability Limits in Toroidally Rotating plasmas

Stability boundaries have been found against the external kink mode and the Kelvin Helmholz (KH) instability. These stability limits were established using analytic expansions of a rotating torus, and with the CASTOR-FLOW code using equilibria derived from the DIVA code. Recently we have used MHD theory for low-shear tokamak plasmas with large aspect ratio and sonic toroidal flows in order to improve the analytical understanding of this KH like instability. The analytic dispersion relation is exotic, and yields many roots (see Fig. 2.2.5). It is seen that instability of the principle KH mode can occur in these strongly rotation-sheared plasmas even when the value of q in the low-shear region is far from rational. Compared to a static plasma, the stabilising dependence of magnetic field line bending is weak, as is also the dependence of the static pressure.

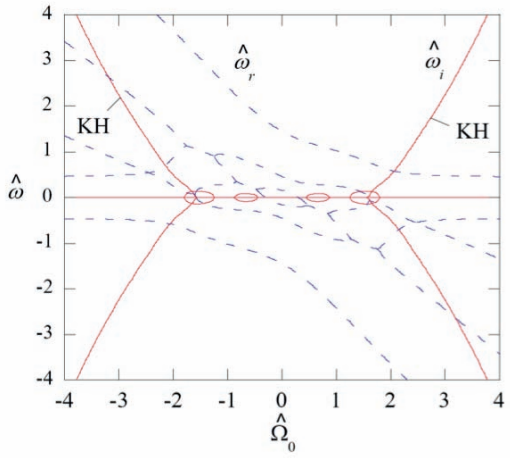

Fig. 2.2.5 *The exotic behaviour of the dispersion relation of Kelvin-Helmholz like instabilities in rotating tokamak equilibria. Plotted are the real and imaginary (growth rate) of modes plotted against the toroidal rotation frequency.*

2.2.4 Optimization of 3D configurations

Fast ion stabilization of global fluid MHD modes in heliotrons

A modified slowing-down distribution function that allows to model neutral beam ion injection from near normal to tangential has been completed and applied to high beta LHD discharges. The fluid MHD stability investigated with the TERPSICHORE code shows that the physical growth rates (a new feature implemented in the stability code) do not depend strongly with angle of injection. The maximum growth rates occur at beta ~ 2% and decrease significantly at beta ~ 4.5%. Stability at beta ~ 2.5% ensues for a sufficiently peaked hot particle pressure profile.

Energetic particle physics

The TAE mode benchmark comparison within the ITPA-EPP activities has been completed with respect to an n=6 mode. The simulations involve a large number of codes that included the VENUS fast particle distribution function solver. The VENUS applications in the zero Larmor radius limit compared very favorably with the other code predictions falling midway within the 15% error band with respect to the growth rate.

2.2.5 Integrated Tokamak Modelling (EFDA TF-ITM)

In the frame of the ITM EFDA project #IMP12, the codes CHEASE, CAXE and KINX have been updated to the most recent UAL version 4.10a. The CHEASE code is coupled to the two versions of the ETS solvers and these three codes are part of the MHD test taking part inside the IMP12 project.

The sawteeth and NTM modules have also been updated to 4.10a. The NTM module has been further developed to include three parts: checktearing, NTMmodule and D_{eff}. The first enables the initialization of an island at a given time, with a given size, mode numbers, frequency and phase. The second calculates the time evolution of the island width, frequency and phase. The third determines the effect of an island on the transport coefficients.

The safe integration of codes and various modules relies on a common understanding of the assumed coordinate convention. In order to uniquely define the equilibrium magnetic field used in various codes, and in particular in RF codes to calculate current drive components, it was found that there are at least 16 different possibilities. We have been able to develop a new index, the COCOS convention, which determines uniquely the assumed cylindrical coordinate (direction of φ), the assumed poloidal system (direction of θ), the sign of ψ and if the poloidal flux is divided by 2 or not.

Using this new definition, one can easily transform an equilibrium from one convention to another. Details can be found at http://crpp.epfl.ch/COCOS. The COCOS index is now part of all the EU-ITM CPOs and will be part of the ITER data model as well.

2.2.6 Tokamak simulations with 3D effects

Fast ion transport enhancement in 3D helical tokamaks

A collaboration with scientists at MAST was initiated to investigate the transport of fast ions in the presence of long-lived modes (LLM). Experimental measurements of neutron emissivity indicate that fast particles are ejected from the core region when these m=n=1 helical structures develop. By providing 3D ANIMEC equilibrium to VENUS-LEVIS orbit solver, slowing-down distributions were obtained and compared in both the axisymmetric and the helical core cases. Our simulations clearly show a depletion of hot particles in the core region of the plasma, as seen in Fig. 2.2.6; this depletion is proportional to the displacement of the helical axis. Our results are currently being verified and benchmarked for publication.

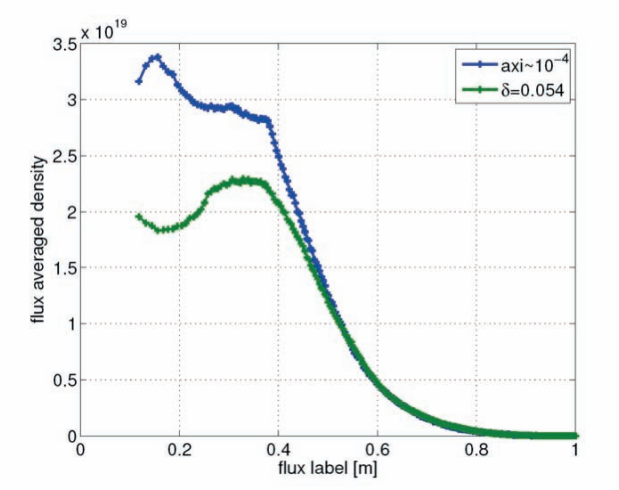

Fig. 2.2.6 *Comparison of neutral beam injection fast ion deposition from simulations using the VENUS-LEVIS guiding centre code: fast ion confinement is degraded in the core of tokamaks with a helical core.*

Linear and nonlinear MHD stability of hybrid equilibria

This work is devoted to the study of instabilities (both ideal and resistive) in hybrid tokamak scenarios. A numerical study of an ITER like hybrid scenario in the ideal MHD frame has been performed, showing that when $q_{min}>1$ equilibrium calculations almost agree with nonlinear simulations and analytic prediction, giving a saturated internal kinks like helical distortion. However for $q_{min}<1$ such helical distortion is not found by equilibrium calculation, in contrast with theory and nonlinear results. From the analytical point of view, the quasi-interchange mode model has been extended in order to include perpendicular viscosity, plasma diamagnetism and equilibrium E×B flows. Since the self adjointness of the MHD operator is lost, the equation describing the perturbed fluxes were derived directly from the equation of motion rather than performing delta-W minimization. Under an appropriate choice of the rotational transform, an exact analytic treatment of the magnetic perturbation has been possible. Three dispersion relations have been derived that treat diamagnetism, viscosity and equilibrium toroidal flows. Of particular interest is how these additional effects modify fast growing resistive modes close to the MHD stability boundary. The results are summarized in Fig. 2.2.8.

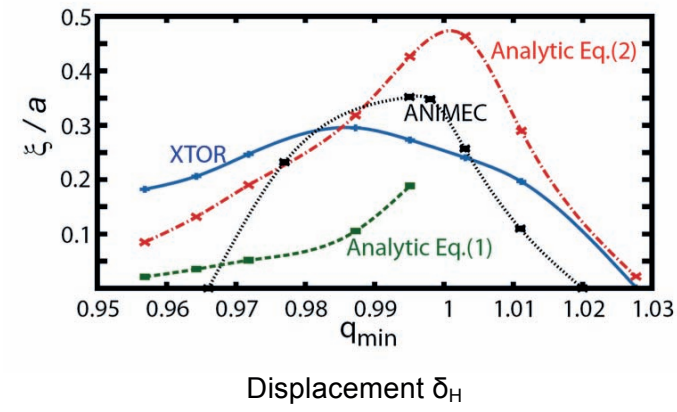

Fig. 2.2.8 *The amplitude of the displaced magnetic axis measuring the saturated helical core in simulations of the ITER hybrid scenario. Compared here is the displacement calculated with the ANIMEC 3D equilibrium code, the saturated state of XTOR-2F nonlinear initial value calculations, and analytic calculations*

Equilibria with external magnetic perturbations

The ANIMEC code has been applied to a MAST configuration with n=3 external perturbation coils. The modulation of the last closed magnetic flux surface at the outer midplane is predicted to reach 5cm (peak to trough) at maximum current (5.6kA). This is close to the experimentally measured variation.

Equilibrium states with helical core, magnetic ripple and resonant magnetic perturbations

Preliminary computations in which a helical core, magnetic ripple and external resonant magnetic perturbations are concurrently obtained in a single 3D MHD equilibrium simulation have been performed for the first time. The helical core deformation we calculate constitutes a reasonable and valid description of the Long-Lived Mode (LLM) in MAST. The extent of the helical core distortion is limited to the centre of the plasma and produces only a very weak modulation at the boundary, smaller than that of ripple, which has an amplitude of 0.7cm. The n=3 external coil perturbation alters the edge of the plasma significantly (a modulation of 4.5 cm peak to trough), but does not affect the central helical deformation. Simulations for DIII-D with helical core deformation in a hybrid scenario were undertaken with the ANIMEC code. The helical excursion of the magnetic axis when q_{min} is located near half-radius extends within a band of $0.94<q_{min}<1.02$ and reaches a maximum slightly over 40% of the minor radius, for q_{min} just below unity. A dedicated experiment on DIII-D was performed. The analysis of the discharges shows a dominant m=1, n=1 mode forming, but it is not clear yet whether this is a saturated ideal internal kink.

2.2.7 Edge Physics

Boundary conditions at the magnetic presheath and sheath physics

Any drift-reduced fluid model aiming at describing the dynamics of a magnetized plasma in an open magnetic field line configuration, as it is the case for GBS, requires boundary conditions at the magnetic presheath entrance, namely the region where the assumptions of the model are no longer satisfied (see Fig. 2.2.8). Boundary conditions determine the plasma losses at the vessel, thus strongly affecting the steady state profiles. A combined fluid and kinetic description of the plasma was used to derive an analytical set of boundary conditions for each quantities evolved by GBS (plasma density, temperature, potential, vorticity, and parallel ion and electron velocities) at the magnetic presheath entrance. Those boundary conditions were verified by performing particle simulations of the magnetized plasma-wall transition. This new set of boundary conditions was implemented in GBS. Simulations of the tokamak SOL region have been performed showing a smooth transition between the plasma bulk and the sheath dynamics.

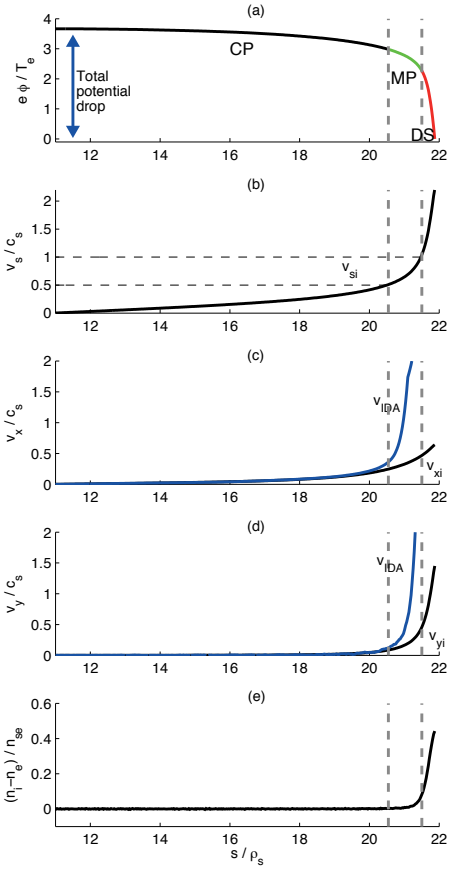

Fig. 2.2.8 *Time-averaged profiles in proximity of a solid wall, obtained from the PIC simulations performed with ODISEE. The magnetic field reaches the wall at an angle of 30 degrees. (a) electrostatic potential, (b) ion velocity in the direction perpendicular to the wall, (c) ion velocity in the x direction, perpendicular to the magnetic field and parallel to the wall (bottom, black) and the corresponding velocity as given by the ion-drift approximation, (d) ion velocity in the direction perpendicular to the magnetic field line and to x (bottom, black) and the corresponding ion-drift velocity, (e) charge imbalance normalized to the density at the Debye sheath entrance. Vertical dashed lines indicate the location of the magnetic presheath (MP) entrance and the Debye sheath (DS) entrance. Horizontal dashed lines indicate Mach numbers M=1 and M=0.5.*

Linear modes in the SOL

Focusing on the linear instability present in the SOL, we have provided a framework according to which, given a set of physical parameters that define the SOL, we can determine the dominant linear instability, i.e. the instability that has the fastest growth rate. In particular, we have considered five instabilities that are thought to dominate in the SOL dynamics: the resistive, inertial and ideal branches of the ballooning modes, and the resistive and inertial branches of the drift wave instabilities. The different regimes are sketched in Fig. 2.2.9. We have therefore developed a tool for the understanding of turbulence in the tokamak SOL, necessary to interpret the results of the nonlinear simulations.

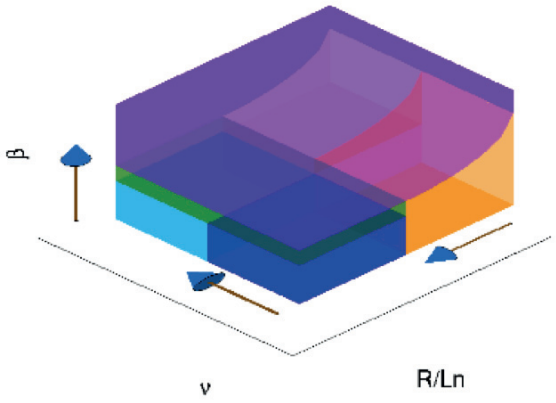

Fig. 2.2.9 *Sketch of the linear instability regimes in the parameter space. Different colors identify the parameter space of the different instabilities: resistive ballooning (pink), inertial ballooning (orange), resistive drift wave (light blue), inertial drift wave (dark blue), ideal ballooning (violet), and region of suppression of drift waves (green).*

Simulation of tokamak edge turbulence

The SOL nonlinear simulations carried out with GBS have considered a configuration with a toroidal limiter, focusing on the following six research avenues.

(i) The turbulence saturation mechanism has been analyzed and it has been shown that it is due to the gradient removal mechanism or to the Kelvin-Helmholtz instability, depending on the SOL parameters. The investigation of the turbulence saturation mechanism has led us to estimate the radial plasma flux and the plasma pressure scale length in the SOL.

(ii) We have analyzed the turbulence character as a function of the magnetic shear. In the case of negative shear, we observe a steepening of the pressure profile as compared to the shearless case. This is associated with the suppression of radial streamers and an overall decrease of the turbulent fluctuations. Instead, at positive values of the shear, we observe the development of elongated streamers in the radial direction that cause a large transport. Extensive analysis of the nonlinear data and additional comparisons with the linear calculations are ongoing.

(iii) Electromagnetic effects play a key role in tokamak edge turbulence. It has been suggested that the so-called density limit (which causes the termination of a tokamak discharge) may be due to the interplay between electromagnetic effects, diamagnetic flows and collisionality. In order to understand finite beta effects in steady-state global SOL turbulence, we have carried out GBS simulations within the high collisionality, high beta parameter range where density limit disruptions are observed. Our work has helped clarify certain aspects of the density limit; (a) GBS simulations with finite beta have so far shown that electromagnetic effects remain weak even at betas which are an order of magnitude larger than those observed in the experiment; (b) turbulent fluctuation magnitudes are consistent with the gradient removal mechanism, therefore showing that a previously suggested mechanism for the density limit cannot occur (electromagnetic suppresion of the Kelvin-Helmholtz instability); (c) collisionality effects are important in this parameter regime, and the plasma profiles become significantly flatter as the collision rate is increased. In order to investigate electromagnetic effects in the TORPEX device, electromagnetic GBS simulations have also been performed in this configuration, revealing the presence of electromagnetic fluctuations, whose amplitude scales linearly with beta. The same scaling is recovered from the linear theory. Comparison with experimental measurements of magnetic field fluctuations will be carried out.

(iv) The GBS code has been originally written in (s-α) geometry, i.e. assuming that the magnetic field is purely toroidal and constant while still retaining some curvature effects. In order to eliminate this inconsistency, the model equations have been rewrittten in a circular geometry retaining finite aspect ratio effects. First, the linear properties of the system have been investigated in this new geometry. Finite aspect ratio effects appear to be weak on drift waves, but they appear to be relatively more important for curvature-driven modes such as the resistive and the ideal ballooning modes. Second, this new geometry has been implemented in the GBS code, and the first GBS simulations with finite aspect ratio effects are ongoing.

(v) The GBS code is now being used to simulate blob motion in three dimensions. It is important to carry out this study in the view of recent results of 3D simulation work, where it is suggested that blobs can only travel a very short distance because they are vulnerable to secondary instability (drift waves). We are employing the GBS code to investigate these claims. Preliminary results show that blob motion is similar to what was previously found in 2D simulations, i.e. blobs can travel a long distance and therefore can reach plasma facing components.

(vi) Finally, we have started an investigation of the effects of plasma size upon scrape-off layer turbulence. This is an important and urgent issue for magnetic confinement fusion because it is necessary to understand the width of the scrape-off layer in order to design plasma facing components. There is currently no theoretical understanding of the width of the SOL as the plasma size increases,

while the experimental evidence is contradictory. Simulations are being carried out at the MonteRosa supercomputer thanks to a 3.2 million CPU hour allocation granted by CSCS specifically for this study. Simulation work is ongoing. Currently, our largest simulated SOL size is equivalent to that of the TCV tokamak.

Regarding the GBS development, we point out that several optimizations and improvements have been brought to the code. A parallel solver for the vorticity and Ampère's equation has been implemented, and the data is now stored using parallel I/O. A good scalability up to 2048 processors has been demonstrated on several computer architectures.

2.2.8 Kinetic simulations of Laser Plasma Interaction (CRPP-LLNL collaboration)[*]

Studies related to kinetic simulations of Laser Plasma Interaction (LPI) for inertial confinement-related conditions have been pursued in the frame of a collaboration with the Lawrence Livermore National Laboratory (LLNL) and UCLA.

Making use of the 1+1 dimensional Vlasov code SAPRISTI, the kinetic effects of electrons on the nonlinear evolution of Ion Acoustic Waves (IAWs) have been studied, in particular analyzing their effect on the nonlinear frequency shift. Such shifts play a critical role in disrupting frequency matching underlying parametric instabilities of the laser beam interacting with plasma waves, which may lead to significant light reflectivity and thus to a degradation of the drive. It has been systematically shown for the first time that the positive contribution to the shift from resonant electrons is dominant for large electron-ion tempreature ratios, $ZT_e/T_i>10$, while the negative ion contribution dominates for lower temperature ratios. Very good agreement of these frequency shifts was shown with theoretical estimates, provided they account for both the kinetic trapping effects, as well as for fluid-like contributions related to harmonic generation. Inspired by the results from the fully kinetic multi-species (electrons + ions) IAW simulations, a reduced kinetic model for electrons has been suggested, derived by invoking the adiabatic invariant related to the bounce motion of electrons trapped in the troughs of the slowly evolving IAWs. Implementation and preliminary testing of this reduced electron model is currently underway and may have the potential of significantly reducing the computational cost of multi-species kinetic simulations. The study of the nonlinear evolution of IAWs in multi-ion species plasmas, leading to slow and fast wave modes, is also being pursued.

Making use of the recently developed 2+2 Vlasov-Maxwell code LOKI (developed at LLNL), based on a novel fourth order accurate compact finite volume scheme, as well as of the PIC code BEPS (developed at UCLA by V. Decyk), the nonlinear evolution and stability of Electron Plasma Waves (EPWs) has been studied. In particular, the stability of large amplitude EPWs to so-called sideband (or modulational) instabilities, involving both longitudinal and transverse sidebands, has been studied. The stability of EPWs to transverse sidebands, leading to filamentation of the wave, has only recently been recognized as a relevant process in LPI and a sound theoretical description has been lacking. A novel reduced model, based on a generalization of the Trapped Particle Instability (TPI) model by Kruer, has shown good agreement with the numerical results.

Furthermore, LOKI and BEPS simulations of the nonlinear evolution of 2-dim EPW packets with a finite transverse width have been carried out. The competition between linear diffraction effects, leading to a negative bowing of the wave fronts, and nonlinear frequency shifts, leading to positive bowing and thus potentially to self-focusing, has been studied in detail. In addition, in sufficiently nonlinear regimes, filamentation of the wave packet may interfere with self-focusing. An envelope equation, based on a relatively

[*] Work not belonging to the Swiss Euratom Association

simple fluid-like model, has enabled to reproduce the kinetic simulation results to a surprising level of detail.

2.3 Operation of a specialised basic plasma physics device, TORPEX

In magnetically confined plasmas for fusion, turbulence causes large particle and energy transport, reducing the effectiveness of the plasma confinement system, hence that of fusion reactors. The Basic Plasma Physics Group at CRPP contributes to advancing the understanding of turbulence in magnetized plasmas of direct relevance for fusion devices.

The experiments are performed in the TORPEX device, which is characterized by low plasma densities (n_e~10^{16}-$10^{17}m^{-3}$) and temperatures (T_e~5-20eV). TORPEX is equipped with an extensive set of diagnostics allowing high-resolution measurements of plasma parameters and wave fields throughout the plasma cross-section. Plasmas of different gases are created by microwaves at 2.45GHz and are confined by a toroidal magnetic field up to B_T=0.1T, and a smaller vertical component, B_Z≤50mT. This magnetic geometry, known as simple magnetized torus (SMT), incorporates the main ingredients for drift and interchange instabilities and turbulence, namely pressure gradients and magnetic field line curvature. Although it does not possess a rotational transform of the magnetic field lines, the SMT mimics the crucial external region of magnetically confined plasmas for fusion, referred to as the Scrape-Off-Layer (SOL), where magnetic field lines intersect the vessel wall.

In 2012, the operation of TORPEX has been characterized by a large number of experimental sessions (>10000 plasma discharges) performed by undergraduate and graduate students. Several short interventions were performed to install new diagnostic and ancillary systems, and a major shutdown phase of approximately 2 months took place. During this period, the TORPEX device was upgraded by installing an internal wire system that carries a toroidal current so that, in addition to the SMT configuration, a poloidal field can be generated. Such new configuration increases the relevance to magnetic fusion devices, by creating a region of closed magnetic surfaces (as in the tokamak configuration).
Significant progress was achieved along several research avenues, from the study of the interaction between supra-thermal ions and interchange waves and turbulence to the first successful operation of TORPEX in closed field line configurations. Such progress is detailed in the paragraphs here below.

2.3.1 Supra-thermal ion studies

In burning plasmas, supra-thermal ions will be generated by ion cyclotron resonance heating (ICRH), neutral beam injection (NBI) and fusion reactions. As they will be responsible for a significant fraction of plasma heating and, in some scenarios, non-inductive current drive, understanding their transport across the magnetic field is of fundamental importance.

In previous years, we started theoretical and experimental investigations of supra-thermal ion-turbulence interaction on TORPEX. A miniaturized source is used, which produces Li6+ ions with energies in the range 100eV-1keV. In 2012, a motorized system was developed, which moves toroidally the ion source continuously over a distance of 50cm. The supra-thermal ions are injected in TORPEX plasmas and are detected, further apart in the toroidal direction, by a double gridded energy analyzer (GEA) that utilizes

differential measurement between two collector signals to cancel plasma contributions to the signal. The GEA is mounted on a 2D motorized movable system which can position it at almost any point of the poloidal cross-section. This system, together with the toroidally movable source, is used to reconstruct the three-dimensional profile of the supra-thermal ion beam, which can then be compared with numerical simulations.

We used a plasma scenario dominated by an ideal interchange mode, localized around the position of maximum pressure gradient. The time average electron density at the injection location is $n_e=5x10^{15}m^{-3}$ and the standard deviation of the floating potential time series, indicating the level of fluctuations, is ~1V. These plasmas, similar to those extensively studied in REFS using electrostatic probes, are characterized by the presence of a region on the low-field side, where blobs are observed to propagate radially outward resulting in intermittent transport of particles, heat, momentum and current.

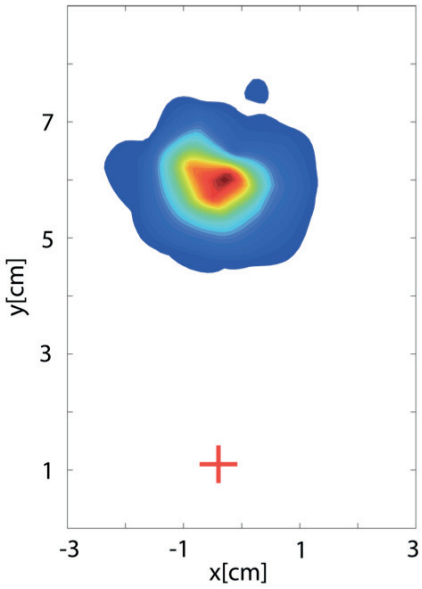

Fig. 2.3.1 *Poloidal profile of the fast ion current [a.u.] at a toroidal distance of 54cm from the source. The red cross indicates the poloidal position of the injection. Ion energy is 70eV.*

Supra-thermal ions are injected in the blob region with energy of 70 eV and horizontally. The source is moved toroidally between each discharge over a total distance of 50cm, in steps of 5cm. Poloidal profiles of the fast ion current are reconstructed at each toroidal position. Fig. 2.3.1 shows an example of a fast ion current profile at a toroidal distance of 54cm from the source. The red cross indicates the position of the injection, showing the displacement of the beam spot due to the vertical drift. Measurements are made with and without plasma, in the presence of magnetic fields. The radial and vertical spatial variances of the fast ion current profiles are shown as a function of the toroidal angle ϕ in Fig. 2.3.2.

To interpret the experimental data, we follow fast ion tracer trajectories using the full Lorentz force, with E and B-fields specified by a numerical model of drift-reduced Braginskii equations (GBS) in two dimensions. This model was previously validated to describe interchange turbulence on TORPEX. Comparisons with the simulations are possible using a synthetic diagnostic of the poloidal cross section of the fast ion current density.

Simulations are performed with source parameters based on measurements done without magnetic field. 10000 particles are launched with initial parameters modeled with Gaussian distributions. The energy is 70eV with a standard deviation of 10%. The initial position is X0=0.4cm and Y0=1.1cm with standard deviation of 1.2mm.

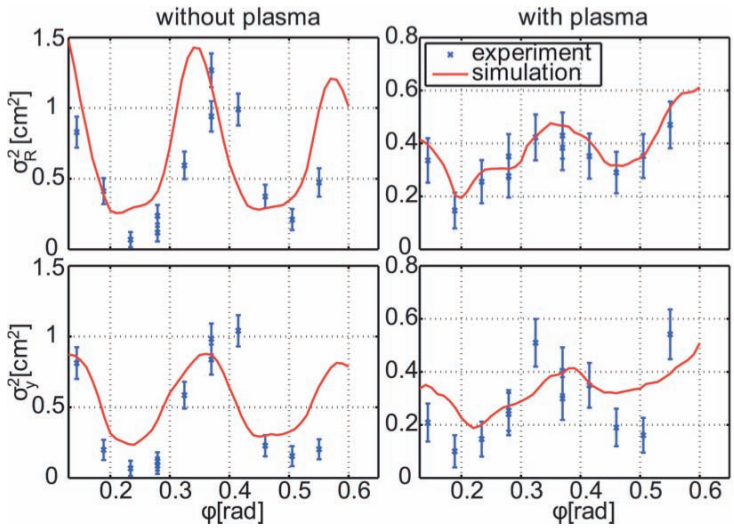

Fig. 2.3.2 *Radial (top) and vertical (bottom) variances of the beam profile at several toroidal positions.*

Simulations of the turbulence are performed with different values of the particle and heat sources to match the experimental time average density and temperature profiles. At the injection point, the fluctuation level of the floating potential is larger in the simulation than in the experiment. To match the potential fluctuations, the simulated plasma potential fluctuations are multiplied by a factor of 0.3. Figure 2.3.2 displays along the toroidal direction the variance of the beam profiles obtained with the synthetic diagnostic, from the simulations, and from experimental measurements. A remarkable agreement is obtained. For the case without plasma in Fig. 2.3.2(left), this also provides a benchmark for the particle tracer solver. The oscillations of the variance of the beam due to the Larmor motion of the particles are clearly evident, although a small mismatch in the phase of the oscillations between experiment and simulation is observed. This is not observed in the presence of plasma, although the absolute value of the variance is decreased. Indeed, the spreading on the initial angle, in the simulations, had to be decreased by a half to match the experiment. Those differences could be explained by the fact that the functioning of the source is affected by the surrounding plasma. In Fig 2.3.2, the turbulent broadening of the beam is clearly revealed by the radial variance of the beam, which increases as a function of the distance from the source. Numerical simulations at later times indicate that, in these conditions, fast ions undergo a sub-diffusive transport.

The experimental setup is now ready to explore the different fast ion transport regimes that are predicted by theory. The fast ion energy can easily be changed and the turbulent fluctuations amplitude can be varied by injecting at different locations, in the mode or in the blob region.

2.3.2 TORPEX Upgrade

TORPEX simple magnetized configurations represent a useful test-bed to perform fusion relevant studies of magnetically confined plasmas, since it includes some of the main features of a tokamak SOL, namely pressure gradients, magnetic field curvature and gradients. In the last years, a comprehensive study of electrostatic fluctuations and turbulence has been performed on TORPEX in the SMT configuration. This configuration, however, does possess neither a rotational transform nor a magnetic topology change between regions with open field lines and closed field surfaces, typical of tokamak SOLs.

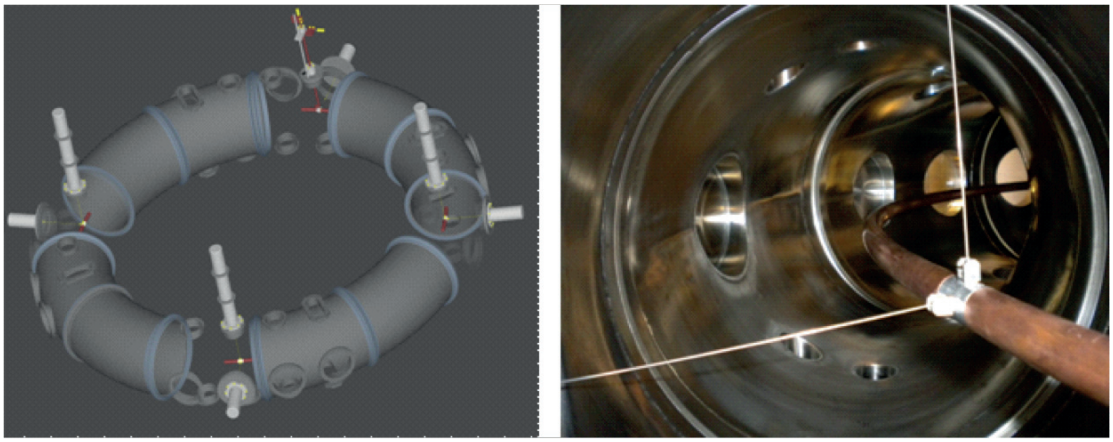

Fig. 2.3.3 *Left – CAD drawing of the new internal wire system. Right – A picture of the copper wire togethe with stainless steel supports installed in the TORPEX vessel.*

To better mimic the SOL-edge magnetic geometry in tokamak, we have developed and installed in the first half of 2012 a new system that will create twisted field line configurations. The new system consists of a toroidal copper wire suspended inside the vacuum vessel by an electrical coaxial feed-through, to minimize the magnetic field perturbations, and three vertical stainless steel wires (1mm diameter). In Figure 2.3.3, the three-dimensional CAD model of the system and a picture of the toroidal copper wire installed in TORPEX are shown. Four further horizontal supports are used to stabilize the wire during a TORPEX discharge. This set of supports allows for different vertical positions of the toroidal wire, so that previous SMT configurations can be recovered by pulling the wire up to the top of the vacuum vessel. A dedicated external power supply, already available at CRPP, provides the current up to 1kA that flows in the wire. The output dynamics of the power supplies is limited to a maximum slew rate of ~1400A/sec. This allows reaching a maximum flat top current in approximately 700ms. For simplicity, we do not use water cooling of the wire, but only of the feed through. The flat top current duration is limited by the Ohmic heating of the wire with almost pure radiative cooling in vacuum. This new system opens the possibility of investigating plasma fluctuations in the presence of a rotational transform in either confined regions with closed magnetic flux-surfaces, or SOL regions with open field lines.

After the successful installation of the system in the first half of 2012, we developed the electronic system and the graphical user interface for the remote control of the dedicated power supply. During the second half of 2012, several tests have been done to complete the commissioning of the system, such as proving the reproducibility of the current time-traces in the toroidal wire for different values of flat-top current in the range of values we are interested in (up to 1kA). Measurements of the generated poloidal magnetic field have been performed using a single-axis Hall probe to verify the reliability of the magnetic field simulations as a reference for the following experimental campaigns. Moreover, the very first experimental studies aimed at characterizing TORPEX plasmas in the new magnetic configurations have been conducted. We focused on the simplest case of concentric flux surfaces resulting from the sum of the poloidal magnetic field and a proper vertical field component. For this purpose Langmuir probes (LPs) have been mainly used (both the fixed HEXagonal Turbulence Imaging Probe – HEXTIP and movable LPs of different geometries), as well as a Fast Imaging Camera to obtain qualitative and quantitative information on plasma turbulent structures from the visible light of the plasma. In Figure 2.3.4, an example of HEXTIP signal is shown (top) together the time evolution of the current in the wire, reaching a flat top value of approximately 620A. In Figure 2.3.4(bottom), we show the HEXTIP ion saturation profles during the time-windows highlighted in color in the HEXTIP time trace. A preliminary analysis of these data

suggests the presence of coherent structures mainly localized on the LFS with a frequency in the range 10-25kHz.

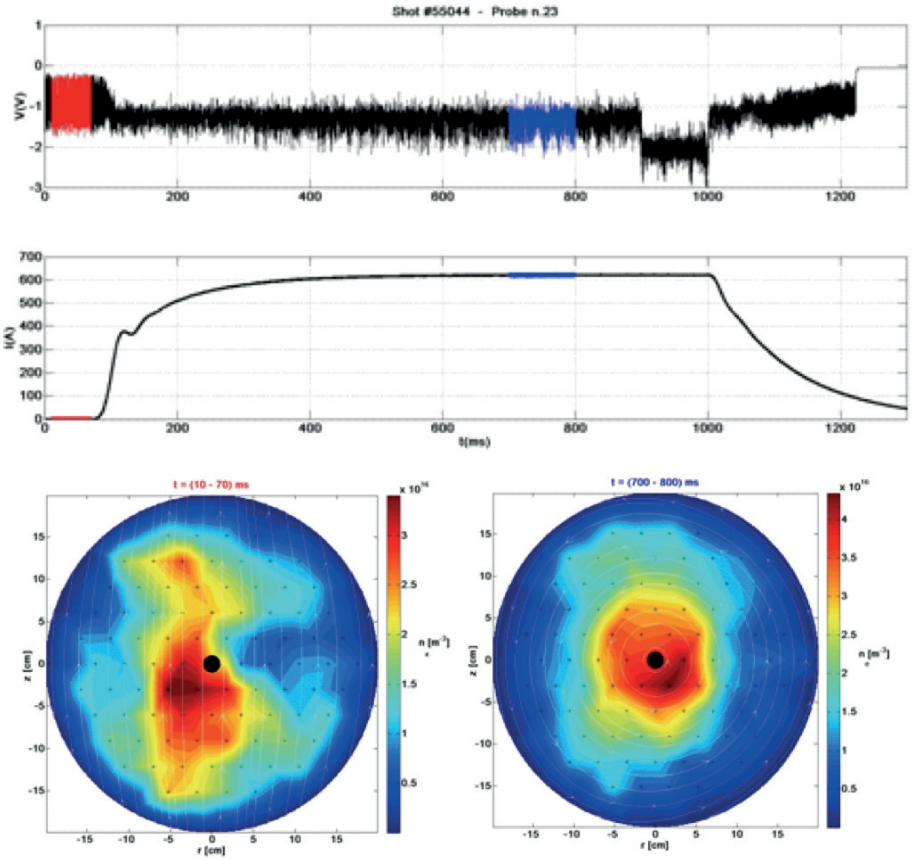

Fig. 2.3.4 *Top - Time evolution of the toroidal current in the wire and of a signal from HEXTIP. Bottom – Time-avergaed profiles of ion saturation signals from HEXTIP during the two time windows highlighted in color in panel (a).*

2.3.3 Specialized diagnostics development

In previous years, facilitated by the full diagnostics access of the TORPEX device with adequate spatial and temporal resolutions, we have undertaken a thorough investigation of blob physics. To further advance our understanding, internal measurements of the parallel current associated with blobs is needed. To this aim, we have developed in 2012 a dedicated miniaturized current probe diagnostics in the context of a student project. A picture and a CAD drawing of the probe are shown in Fig. 2.3.5. The probe consists of a Rogowski coil manually wound around a ferrite core to increase the magnetic flux. Electrical and thermal insulation from the plasma is obtained by placing the detecting coil inside a Peek cylindrical housing, machined as two halves of a container. The ratio of the area of detection (~1cm^2) to the area of obstruction of the probe is limited by the technical difficulty in machining thinner walls. The toroidal detecting coil consists of a single layer helical winding with an inside return loop to cancel the net single turn formed by the solenoid windings. Thus the output signal is generated only by the turns circling the toroidal magnetic flux created by parallel currents associated with blobs. The probe is operated in current mode, which provides a direct measurement of the total current flowing inside the detection area. The construction, assembly, and calibration of the probe have been recently terminated. The probe has been installed on a two-dimensional movable system, and preliminary tests are presently ongoing on TORPEX.

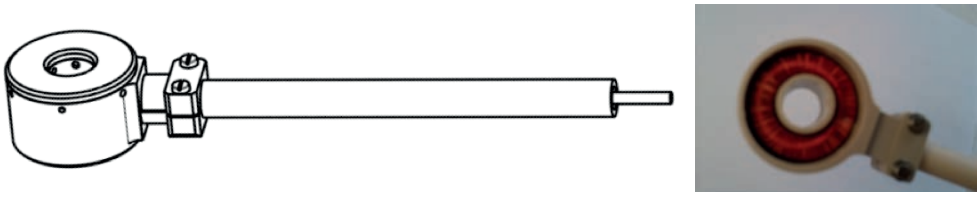

Fig. 2.3.5 *Left – CAD drawing of the miniaturized current probe. Right – A picture of the Rogowski coil wound around the ferrite core and assembled inside the Peek housing.*

2.4 Materials research

2.4.1 Emerging technologies

Development of material science and advanced materials for DEMO

Development of ODS ferritics steels

WP12-MAT-ODSFS-01-01/Swiss-Confederation/BS: Production and characterization of laboratory-scale batches of nanostructured ODSFS

The first stage of the powder metallurgy route for Oxyde Dispersion-Strengthened (ODS) steel production consists of preparing powders mixtures with the proportions corresponding to the final composition in a glove-box with Ar atmosphere, then transferring the powder mixtures into the attritor in container filled with Ar, milling of powders in a gas tight chamber and its discharging afterwards in a protective atmosphere. Our previous results indicated that the use of hydrogen as milling atmosphere can lead to improved plasticity of the steel by reducing powders oxidation and preventing trapping of Ar gas in the steel particles during mechanical alloying. In this work the powders were milled in attritor at controlled H2 pressure using the following parameters: cycles of 1min at 750 and 1min at 380rpm for total time of 80h in the case of the elemental powder and 8h for the mixtures of pre-alloyed powder and reinforcement particles. The optimum milling times were selected by Scanning Electron Microscopy (SEM) observations and X-Ray Diffraction (XRD) tests. Dissolution of the alloying elements was observed in the first case and an uniform distribution of oxide nano-particles in the second. The contamination of powders with oxygen and nitrogen was characterized by an inert gas fusion method for two types of ODS powders mixtures at various milling times (see Table 2.4.1). Much lower oxygen and nitrogen levels can be noticed in the case of the pre-alloyed Ar-atomised powder than in the elemental powders with addition of 0.3wt.% yttria particles.

	As mixed E+0.3Y_2O_3	E+0.3Y_2O_3 40h	E+0.3Y_2O_3 80h	As-mixed P+0.3Y_2O_3	P+0.3Y_2O_3 8 h
wt. % O_2	0.44	0.53	0.65	0.15	0.27
wt. % N_2	0.04	0.06	0.06	0.01	0.06

Table 2.4.1 *Concentration of oxygen and nitrogen in the powders - Criterion for selection of substrates and milling time. E – elemental; P – pre-alloyed Fe14Cr2W0.3Ti base alloy.*

The Hot Cross Rolling (HCR) was carried out at the CSM Center (ENEA) after Hot Isostatic Pressing (HIP) and stress-relieving heat treatment at 800°C. The highest achieved degree of deformation applied to ingots of ca. 300g was of 80% reduction of thickness (ROT). A single preheating at 1100°C was followed by rolling steps at deformation degree of 5% alternately in two perpendicular directions in the rolling plane at 800°C – and reheated to this temperature before every rolling step. The two-directional rolling was implemented to avoid non-uniformities in the microstructure, including an excessive texture in the rolling plane.

Optical microscopy was employed for low-magnification microstructure analysis of two ODS steels based on the elemental powders in the as-consolidated state - after HIP and after HCR at 65% ROT. In the case of the HIP sample there are quite large oxides and pores as black dots along the pre-particle boundaries (Fig. 2.4.1a) while in the case of the hot rolled sample these features are much finer (Fig. 2.4.1b). The micro-pores are the reason of weakening the pre-powder boundaries and thus cause of the brittle behavior of the steel after HIP.

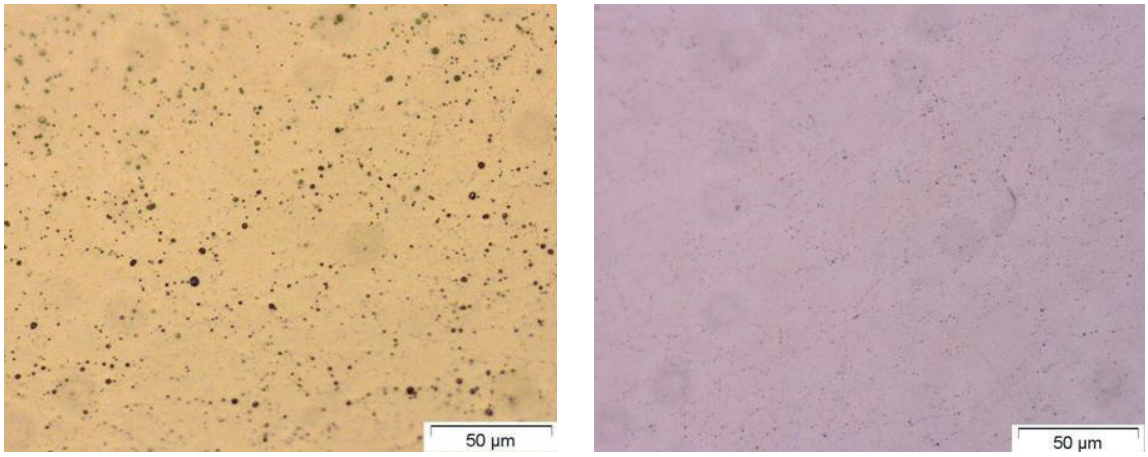

Fig. 2.4.1 *Optical microscope images of electro-polished surfaces of metallographic samples of ODS FS with Y2O3 particles after (a) HIP, (b) HIP and HC-rolling.*

Transmission Electron Microscopy (TEM) observations of the steels after HIP and after HCR showed large regions recovered from dislocations introduced by milling. The hot-cross rolling practically did not change the grain size and the average oxides particle diameter. The average grain size estimated by TEM was of 0.3 and 0.5 microns in the HIP and HCR-65% samples, respectively. The oxides particles diameter was estimated based on TEM bright field images at higher magnification (50k) of about 500 particles. The average diameter of the oxides slightly increased from 6nm after HIP to about 10nm after HCR in all degrees of deformation. This coarsening of oxides particles could be related to a preheating step at 1100°C close to the maximum HIPping temperature used to homogenize the composition before the rolling.

Effect of hot-cross rolling

Charpy impact tests were done for the v-notched ODS samples (3x4x27mm) before and after hot-cross rolling for the three deformation degrees: 50, 65 and 80% and for the HIP sample (see Fig. 2.4.2): for the HIP sample the upper shelf energy values are generally very low which could indicate a relatively low toughness in the plastic fracture regime,

which is characteristic for samples produced by powder metallurgy. It took about 1J to break the samples after HIPping and after HCR at 50% ROT. The hot-cross rolled ODS steels in which 65 and 80% ROT was achieved, show higher upper shelf energy (USE) and lower transition temperature (DBTT) in comparison with the as-HIPped sample and the rolled one at 50% ROT, whereas the 80% ROT has led to the lowest DBTT of about -50°C.

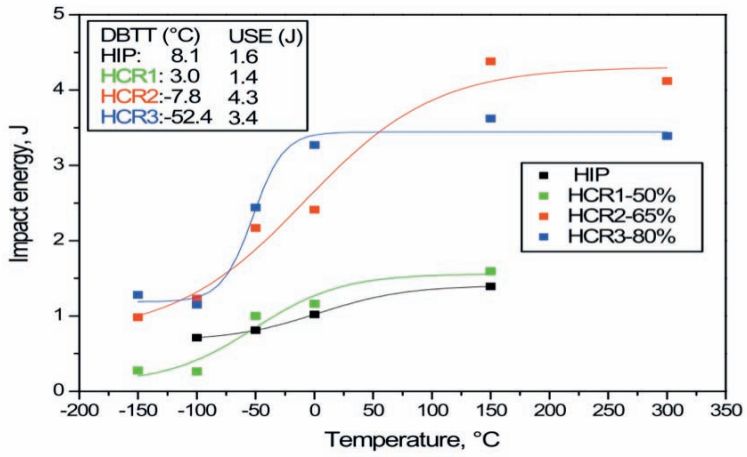

Fig. 2.4.2 *Charpy impact energy versus sample temperature for the as-consolidated (HIP) ODS steel samples and a series of samples having varying deformation degree (50-80%) after hot-cross rolling.*

Tensile test were done using flat samples with cross section of 0.75mm^2 and gauge length of 8 mm at test temperatures between 25 and 750°C. The results are summarized in Fig. 2.4.3. A significant reduction of tensile strength was observed in the case of samples in which 50% to 65% thickness reduction was obtained, while the elongation was gradually increasing with increase of applied deformation during rolling. A characteristic feature of the 50% and 65% - ROT samples was a smooth change of slope on the engineering strain-stress curves, compared with a rather abrupt change (strengthening degree) in HIP. The general tendency was a decrease of Ultimate Tensile Stress (UTS) and Yield Stress (YS) with test temperature in the non-rolled steels and at 50% reduction of thickness, whereas at 65% and 80% much lower UTS values at RT were observed, being comparable with the ones obtained at 450 C. Samples tested at 750°C had typically UTS of about 200MPa. Thus the effect of HCR causing the UTS and stiffness reduction is getting pronounced at above a thickness reduction of 50%, therefore the effect on improvement of Charpy impact behaviour is expected in that case. The tensile curves obtained for the steels produced using the pre-alloyed powder showed an opposite tendency compared with the ones made using the elemental powder that is: an increase in strength and decrease in total elongation at RT after hot rolling. In the HCR4 rolled to 65% ROT, the UTS at 450°C almost doubled while at 750°C it did not change after rolling. The total elongation of the RT-tested samples made of the pre-alloyed, higher quality material was larger by about 30% than in the case of the elemental material. This indicates a much better plasticity of the ODS containing less oxygen. Interestingly, the tensile strength and plasticity of the PA4 material are very similar to those obtained for HCR3 – so rolling resulting in 80% thickness reduction leads to a similar response like when using a higher purity powder. This could mean that in the series of samples HCR1-3 which have the same substrate powder with higher oxygen concentration, the present larger oxides and nitrides are probably getting refined and so do the pre-austenite grains, which substantially improves the plasticity of the steel.

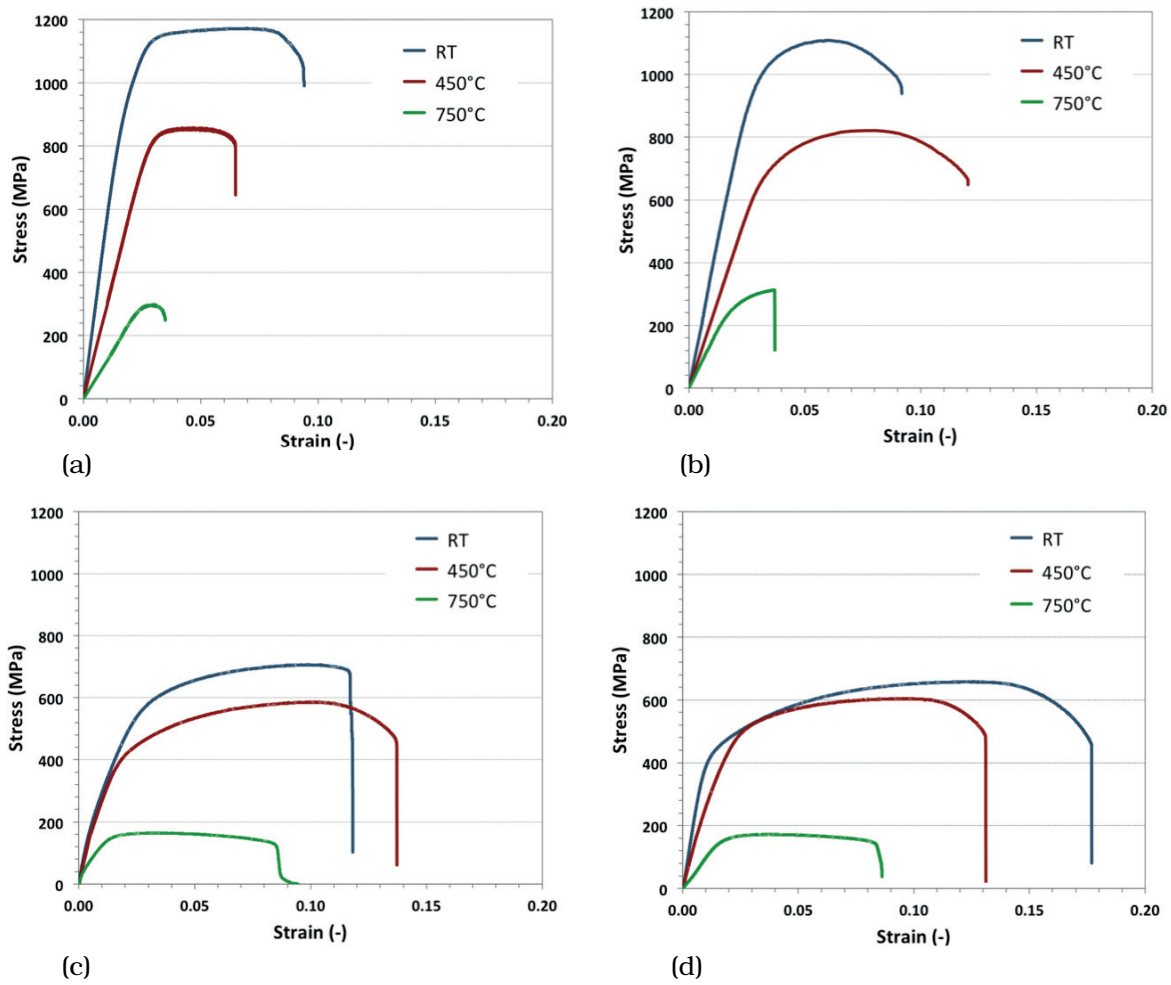

Fig. 2.4.3 *Stress-strain curves (engineering strain) at temperatures from room temperature to 750°C obtained by tensile tests of the ODS FS made using elemental powders with Y2O3 particles; (a) after HIP (b) HIP followed by HCR at 50% (c) 65% (d) 80% reduction of thickness.*

	ROT: 0%			**ROT: 50%**			**ROT: 65%**			**ROT: 80%**		
Test T (C)	25	450	750	25	450	750	25	450	750	25	450	750
R_m (MPa)	1173	858	299	1109	821	313	707	587	165	659	606	173
$R_{p0.2}$ (MPa)	1053	801	281	937	673	250	330	420	146	393	399	154
	0.095	0.065	0.043	0.092	0.12	0.037	0.118	0.137	0.095	0.161	0.131	0.086
u	0.02	0.028	0.024	0.027	0.033	0.019	0.012	0.021	0.014	0.011	0.019	0.017

Table 2.4.2 *Results of tensile test of the as-HIPped and hot-cross rolled ODS samples at various thickness reductions made of elemental base alloy.*

Effect of substrate powder purity

Charpy test were also carried out for the as-HIPped and for HC-rolled ODS samples made of the prealloyed powder (i.e. less oxygen contamination) (see Fig. 2.4.4). The hot rolled samples showed a higher USE and lower DBTT (-24°C) values than their elemental counterparts (-8°C), whereas although the USE also improvement in the case of the pre-alloyed as-HIPped samples, the DBTT was in that case worse (+59°C) than for the elemental ones (+8°C).

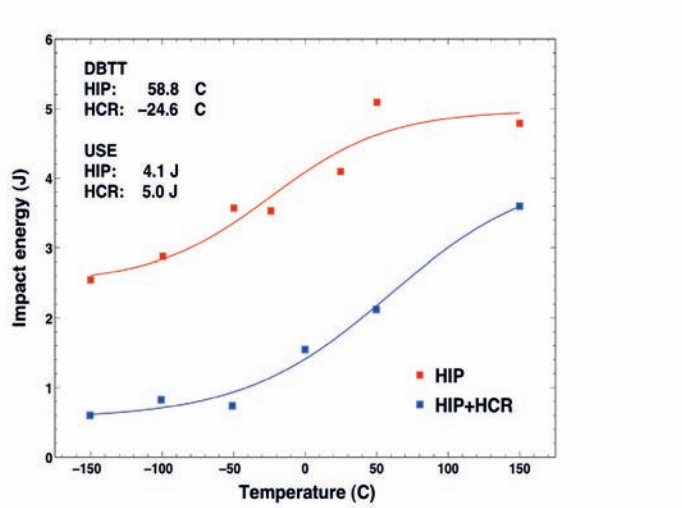

Fig. 2.4.4 *Results of Charpy impact tests of v-notched samples of the prealloyed ODS ferritic steels (a) after HIP and (b) HIP followed by HCR at 65% ROT.*

	ROT: 0%			**ROT: 65%**		
Test T (°C)	25	450	750	25	450	750
R_m (MPa)	1085	792	260	718	384	203
$R_{p0.2}$ (MPa)	848	712	233	412	329	168
	0.097	0.081	0.050	0.16	0.095	0.04
u	0.018	0.029	0.022	0.011	0.021	0.013

Table 2.4.3 *Results of tensile test of the as-HIPped and hot-cross rolled ODS samples made of prealloyed base alloy.*

The use of elemental powders required relatively long milling time for dissolution of elements and Y_2O_3 in order to produce fine dispersion of Y-Ti-O nanoclusters. On the other hand, this has led to a significant contamination with elements from atmosphere but also from the mill debris (EDS of the steel after MA for 80h showing presence of Si in the precipitates, most likely from the steel of the drum and the balls). As a way to avoid prolonged milling time, the elemental powders mixtures were substituted by an Ar-atomised, pre-alloyed powder (Fe-14Cr-2W-0.3Ti), which allowed using shorter milling time (between 8 and 40h instead of 80h). This has led to lowering the oxygen content in the as-mechanically alloyed powder but at the same time a sufficiently uniform distribution of oxides was achieved.

Precipitation strengthening by addition of fine oxide particles and transformation (HIP) induced stress are the main cause of high tensile strength and stiffness of the as-HIPped ODS ferritic steels. On the other hand, weak cohesion forces between the pre-particle grains due to either non-homogeneous distribution of alloying elements but mainly because of larger oxides and nitrides at the pre-particle boundaries lead to lower fracture toughness and in consequence, to a brittle fracture mode in these composites. In order to avoid typical for the ODS steels brittle fracturing, a thermal-mechanical treatment was applied in the current work, which allowed enhancement of the plasticity of these alloys. The multiple hot cross rolling allowed achieving desired deformation steps and rolling the samples in two perpendicular directions, which minimized the structure anisotropy in the rolling plane. The improvement of plastic yield in the hot rolled samples was related most probably to a decrease of the remnant porosity but also due to an extensive structure recovery which was evident from the microscopic observations which revealed:

smaller micro-porosity and much smaller dislocation density especially in the case of 65% deformation. The TEM observations also brought about grain elongation in the plane perpendicular to the rolling plane at 80% deformation, insignificant changes in grain size and some coarsening of the oxides nanoparticles with increasing degree of deformation.

The Charpy test showed a significant reduction of DBTT transition temperature and an increase of the upper shelf energy when the deformation was 65% of thickness or higher. The tensile test in all hot rolled steel samples showed a decrease in tensile strength and yield stress along with increase of plastic strain. An additional improvement of plasticity was achieved by using the pre-alloyed powder instead of a mixture of elemental powders.

WP12-MAT-ODSFS-02-01/Swiss-Confederation/PS: Production and characterization of industrial batches of nano-structured ODSFS

Production a 10kg batch of Fe-14Cr-2W-0.3Ti-0.3Y2O3 based on the prealloyed powders is an on-going task. All 10 of the 1kg batches of prealloyed powder supplied from Alpha Aesar were milled in attritor using BPR of 10:1, speed of 380-750rpm and dynamic hydrogen atmosphere. The canning and HIPping of the powders was intended to be done at Kennametal AMSG GmbH, Biel, with whom a contact and discussion were done. In order to perform the HIPping, Kennametal requires a powder density of about 70% while our powder after mechanical alloying was only 50%. Thus a cold-isostatic pressing has to be carried out before realizing the HIPping. The cold isostatic pressing could not be done yet. At this stage, it is intended to deliver the 10kg of powder to EFDA to proceed with the project. Hot pressing or hot rolling followed by annealing should be subsequently applied.

WP12-MAT-ODSFS-03-01/Swiss Confederation/BS: Irradiation and post-irradiation characterization of produced nano-structured ODSFS

Ion irradiations took place at JANNuS Saclay, France, in 2010 on two types of ODS steels: Fe-14Cr-2W-0.3Ti-0.3Y_2O_3 and Fe-14Cr-2W-0.3Ti-0.5Fe_2Y in the shape of 3 mm transmission electron microscopy (TEM) disks. The irradiation was performed with 24MeV Fe^{3+} and 2 MeV He^{+} ions at 300 and 700°C. The dose reached a value of 5dpa and 15appm/dpa He. For TEM observations, focused ion beam (FIB) lamellas have been extracted from the irradiated specimens. The irradiation to 5dpa with He implantation seemed not affect the microstructure too strongly, regardless the irradiation temperature, as illustrated in Fig. 2.4.5 in the case of Fe-14Cr-2W-0.3Ti-0.3Y_2O_3. Irradiations are higher doses would have been necessary and have been planned for 2011. Unfortunately, due to technical issues, until present, we did not get beam time and it is foreseen that this irradiation will be performed at the beginning of 2013, as agreed with EFDA.

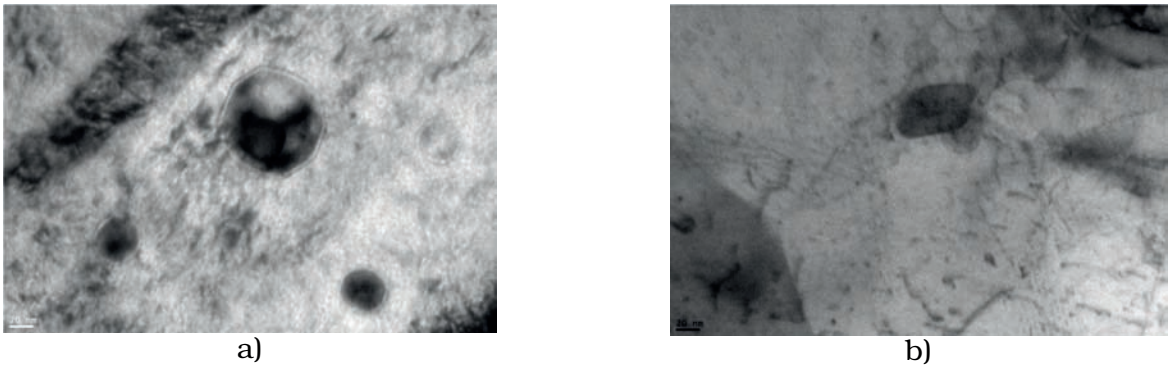

a) b)

Fig. 2.4.5 *TEM microstructure of Fe-14Cr-2W-0.3Ti-0.3Y_2O_3 irradiated up to 5dpa and 15appm/dpa He at a) 300°C and b) 700°C.*

WP12-MAT-ODSFS-04-01/Swiss Confederation/BS: State of the art of nano-structured ODSFS: Literature review

This activity is performed on a continuous basis by gathering as much as possible of published work on ODS steels especially developed for nuclear applications, by analyzing and assessing the data.

Materials modelling

WP12-MAT-IREMEV-02-01/Swiss-Confederation/PS: Evolution of microstructure

Although austenitic stainless steels with their fcc structure are widely used for internal components in the existing nuclear power plants and their physical behaviour and microstructure following irradiation is fairly established, the formation of nanometric stacking fault tetrahedra (SFT) induced by irradiation is still controversial. The presence of SFT after irradiation is important due to the fact that their interaction with mobile dislocations causes changes in the mechanical properties of the material, such as strengthening, hardening and plastic instability during deformation. In pure fcc materials with low stacking fault energy (SFE), such as Cu and Au, the predominant irradiation induced defects are SFT. Austenitic stainless steels, with a composition of about Fe-10Ni-18Cr, have a low SFE of 10 to 50mJ/m^2 and a high shear modulus of about 76GPa that should promote the formation of SFT, but this is not always the case. In order to assess the formation of SFT in fcc materials following irradiation, ion implantation experiments have been performed at JANNuS facility in Orsay between 22nd and 24th Mai 2012 on different austenitic stainless steels. The chemical composition of materials has been chosen to account for the influence of carbon content and other alloying elements on the formation of stacking fault tetrahedra from displacement cascades. A stainless steel with SFE was among the studied materials. The irradiation has been performed with 500keV Fe ions, at room temperature up to a dose of 0.1dpa for all specimens. It is found that the irradiation-induced defects formed at such low doses are too small to be identified by conventional TEM. No SFT could be identified unambiguously. A typical microstructure following the irradiation is exemplified in Fig. 2.4.6. Irradiation experiments at a higher dose are necessary for a more detailed characterisation of irradiation-induced defects in austenitic stainless steels. The defects are being quantified with respect to size and density number. The defect accumulation following ion irradiation up to 0.1dpa in this type of fcc structure materials will be compared to FeCr bcc alloys irradiated at JANNuS in same conditions.

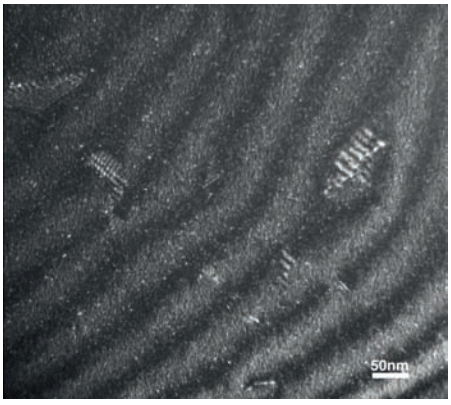

Fig. 2.4.6 *Weak beam dark field g(5g), g (200) of the austenitic stainless steel with reference stacking fault energy irradiated with 500keV Fe ions at room temperature up to 0.1dpa.*

Modelling oriented irradiation experiments in Ultra High Purity (UHP) Fe(Cr) model alloys are performed at the JANNUS ion irradiation platform to understand radiation damage in ferritic steels. Two irradiation campaigns we performed in 2012, the irradiation conditions are summarized in Table 2.4.4.

Specimen	Temperature	Ion	Energy, [keV]	Dose, [At/cm^2]	Flux, [At/s cm^2]	Actual dose [dpa]/ He content [appm]
UHP Fe	RT	Fe^+ He^+	500 10	$2.0\ 10^{14}$ $8.5\ 10^{14}$	$1.2\ 10^{10}$ $4.7\ 10^{10}$	1 dpa 1000 appm
UHP Fe	RT	Fe^+	500	$2.0\ 10^{14}$	$1.2\ 10^{10}$	1 dpa
UHP Fe	RT	Fe^+ He^+	500 10	$2.0\ 10^{14}$ $8.5\ 10^{14}$	$1.2\ 10^{11}$ $4.7\ 10^{11}$	1 dpa 1000 appm
UHP Fe	RT	Fe^+	500	$2.0\ 10^{14}$	$1.2\ 10^{11}$	1 dpa
UHP Fe	LN2	Fe^+ He^+	500 10	$1.0\ 10^{13}$ $4.25\ 10^{13}$	$1.2\ 10^{10}$ $5.1\ 10^{10}$	0.05 dpa 50 appm
UHP Fe	RT	Fe^+ He^+	500 10	$1.0\ 10^{13}$ $4.25\ 10^{13}$	$1.2\ 10^{10}$ $5.1\ 10^{10}$	0.05 dpa 50 appm
UHP Fe	LN2	Fe^+	500	$1.0\ 10^{13}$	$1.2\ 10^{10}$	0.05 dpa
Fe-5Cr	RT	Fe^+ He^+	500 10	$1.0\ 10^{13}$ $4.25\ 10^{13}$	$1.2\ 10^{10}$ $5.1\ 10^{10}$	0.05 dpa 50 appm
Fe-5Cr	RT	Fe^+	500	$1.0\ 10^{13}$	$1.2\ 10^{10}$	0.05 dpa
Fe-10Cr	RT	Fe^+ He^+	500 10	$1.0\ 10^{13}$ $4.25\ 10^{13}$	$1.2\ 10^{10}$ $5.1\ 10^{10}$	0.05 dpa 50 appm
Fe-10Cr	RT	Fe^+	500	$1.0\ 10^{13}$	$1.2\ 10^{10}$	0.05 dpa
Fe-10Cr	LN2	Fe^+	500	$1.0\ 10^{13}$	$1.2\ 10^{10}$	0.05 dpa
Fe-14Cr	LN2	Fe^+	500	$1.0\ 10^{13}$	$1.2\ 10^{10}$	0.05 dpa
Fe-14Cr	RT	Fe^+	500	$1.0\ 10^{13}$	$1.2\ 10^{10}$	0.05 dpa

Table 2.4.4 *Irradiation conditions of the two irradiation campaigns performed in 2012. (RT = room temperature; LN2 = liquid nitrogen)*

In the first campaign effect of irradiation dose rate in UHP Fe was studied. TEM thin foils were irradiated at RT with 500keV Fe^+ ions or simultaneously implanted with 10keV He^+ ions to the dose of 1dpa and 1000appm He content at two dose rates. Investigations, carried out at PSI, Villigen, revealed that density of the produced defects in the single beam case does not depend strongly on the dose rate, however fraction of ½ a_0<111> type loops increases at low dose rate (Fig. 2.4.7). Character of produced damage depends strongly on the dose rate in the presence of He. Defect number density is lower at the low dose rate and mixed population of ½ a_0<111> and a_0<100> loops is observed compared to high dose rate case where only ½ a_0<111> loops were detected Fig. 2.4.7 and 2.4.8. In the second campaign UHP Fe and Fe -5, -10, -14Cr samples were irradiated at room and liquid nitrogen temperature to the dose of 0.05dpa and 1000appm/dpa He content at the dose rate of $5 \cdot 10^{-5}$dpa/s. Given conditions are chosen in order to maximize the chances of observing the very first clusters stemming from displacement cascades, before thermal evolution of the irradiation-induced damage microstructure. Damage threshold, when defects start to appear in TEM, for the irradiated samples was established to be at the dose of about 0.002dpa. Detailed analysis of the Burgers vectors and total density of the produced defects is currently in progress.

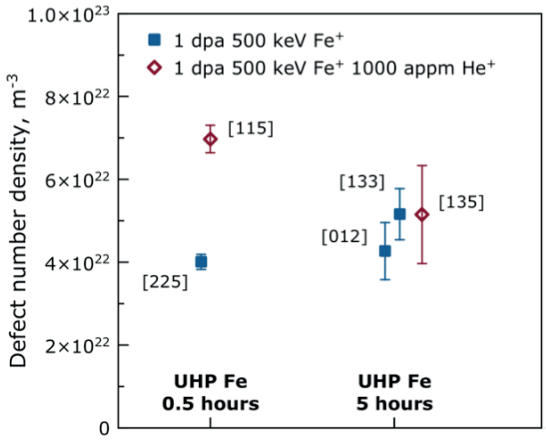

Fig. 2.4.7 *Number densities of the observed defects. Orientations of the thin foils are given in square brackets*

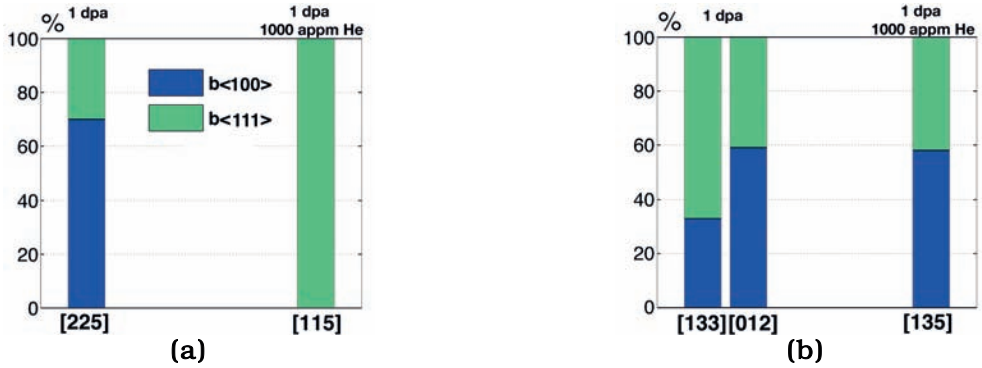

Fig. 2.4.8 *Relative proportions of Burgers vectors of two types in samples irradiated up to 1dpa with and without 1000appm He at RT with (a) 5 10^{-4}dpa/s and (b) 5 10^{-5}dpa/s. Foil normal is given below each bar.*

WP12-MAT-IREMEV-03-01/Swiss-Confederation/PS: Deformation and plasticity

Simulations are needed to better understand the experimental results of WP12-MAT-IREMEV-02. In fact, we simulate 14MeV neutron damage in iron using charged Fe ions irradiation. The problem is, that the Fe ions do not penetrate very deep in iron, see Fig. 2.4.9. The proximity of the free surface may influence the number of created interstitials and interstitial loops and thus it can make the comparison between neuron and ion irradiation more difficult.

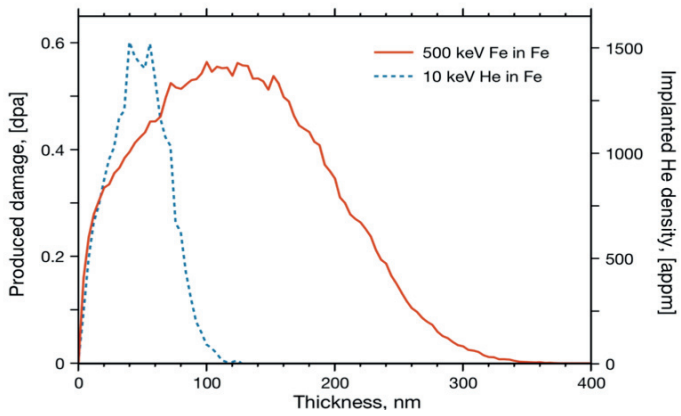

Fig. 2.4.9 *Implantation profile of 500keV Fe and 10keV He in pure Fe.*

The molecular dynamics simulations are divided into several stages. In the first stage we are interested in the escape of the single Self-Interstitial Atom (SIA) via the free surface. In the second stage we will investigate the escape of interstitial dislocation loops via the free surface. Both the decrease of the number of SIAs and dislocation loops directly influences the comparison of the thin foil sample with the bulk sample, i.e. the ion implantation with the neutron irradiation. In the first stage, before any dislocation loops are visible in in-situ TEM irradiation, we estimate that the SIAs concentration is around 50-100ppm. This corresponds to the dose of 0.001dpa and to the distances between SIAs of around 6.5nm. To speed up the calculation time, just one single SIA is introduced in a box with lateral dimensions corresponding to 6.5nm and the vertical length corresponding to the thickness of the TEM in-situ sample of 25, 50, 100 and 200nm and containing two free surfaces in the middle (see Fig. 2.4.10).

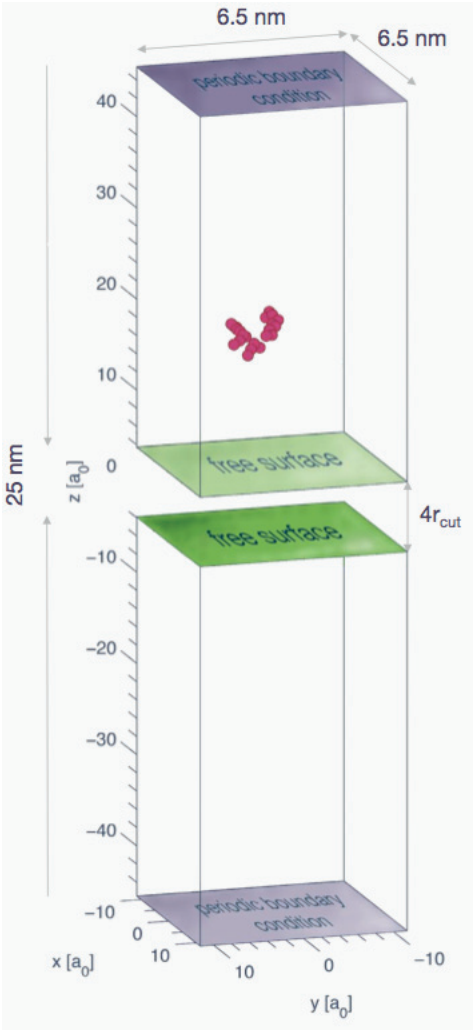

Fig. 2.4.10 *MD sample containing one moving 110SIA.*

As we want to study the number of escaped SIAs by the free surface as a function of the free surface orientation, we need to rotate the simulation boxes so, that the z axis is always perpendicular to the free surface. Otherwise the periodic boundary conditions in x and y will create unwanted steps. Total of 22 different orientations were investigated. We have used the Mendelev03 (2003) alpha iron potential.

The interesting side result is the dependence of free surface energy on the orientation of the free surface. It looks like the free surface orientation 110 has the lowest energy, then

is the 100 orientation, then all the other 19 orientations and finally 111 has the highest free surface energy (see Fig. 2.4.11).

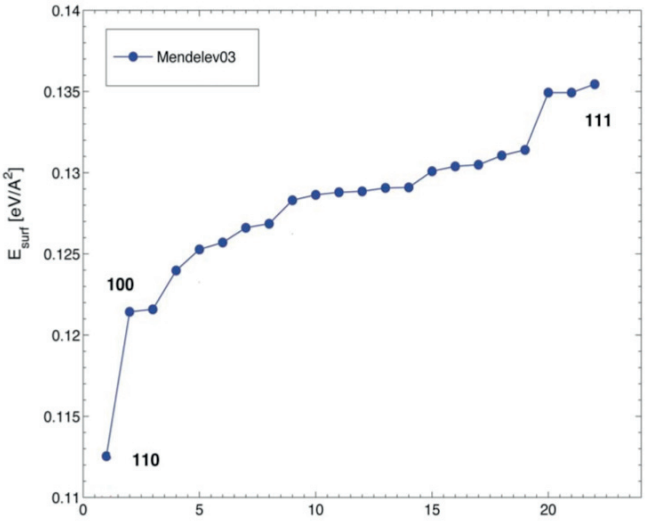

Fig. 2.4.11 *Dependence of free surface energy on the free surface orientation.*

To speed up the calculation time, the simulations were done at 500K. It was observed, that the diffusion mechanism at RT and at 500K are identical. The coordinates and orientations of the SIA are recorded every 10000 time steps and then the diffusion coefficients and the probability to jump towards the free surface are calculated as a function of the depth, i.e. the distance of the SIA from the free surface (see Fig. 2.4.12).

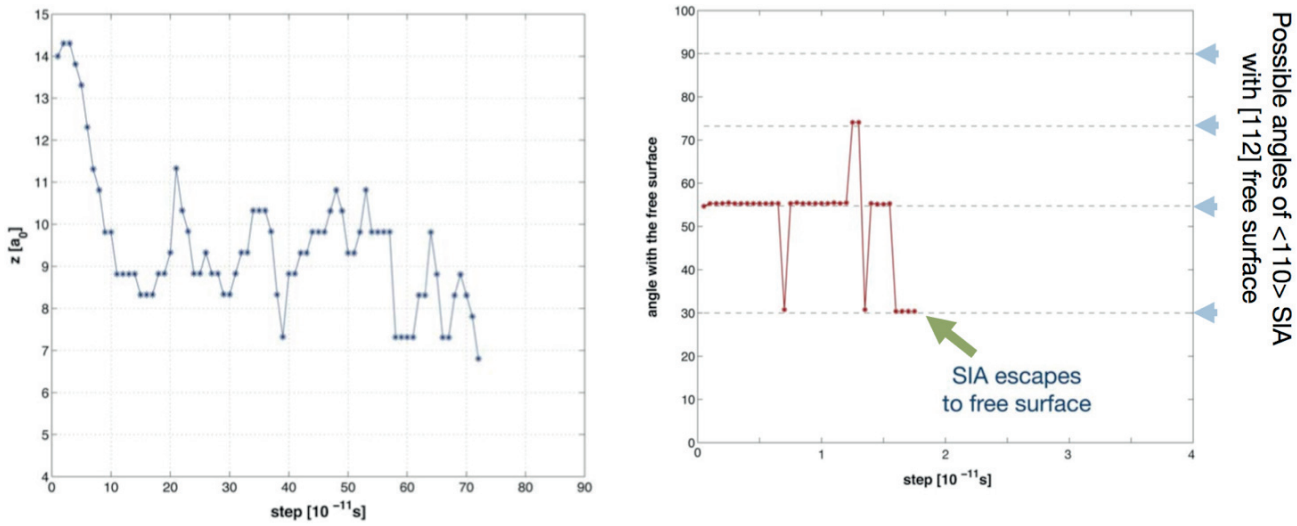

(a) (b)

Fig. 2.4.12 *The evolution of depth (a) and orientation (b) of a 110 SIA in the presence of a 112 free surface.*

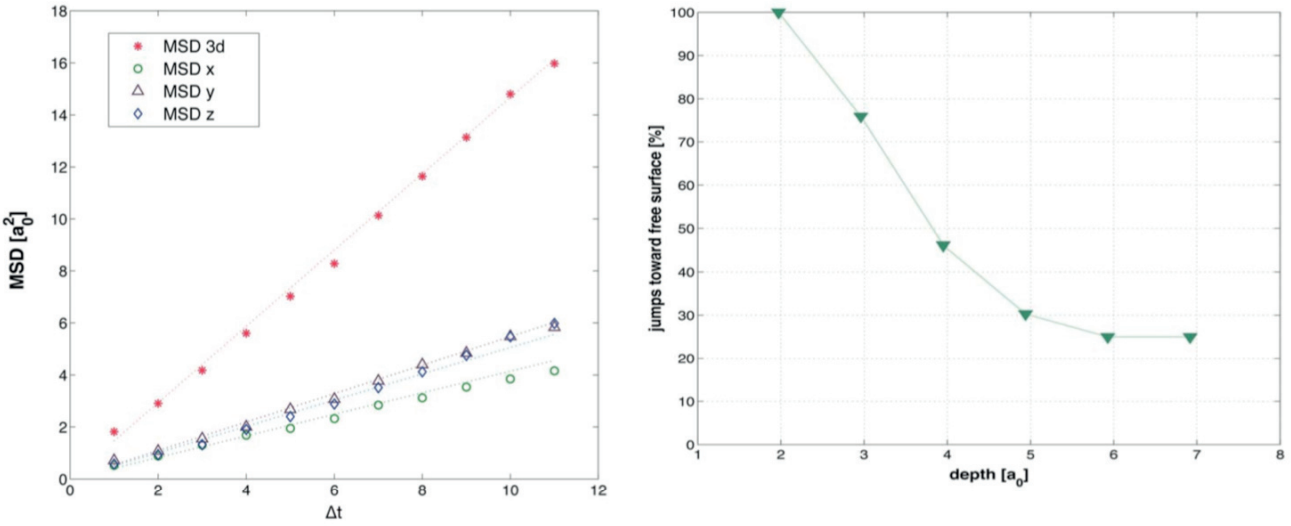

(a) (b)

Fig. 2.4.13 *The mean square displacement of SIA in 3D and in x, y and z (a) and the probability to jump towards the free surface as a function of the SIA's depth (b).*

The results show lower diffusion coefficient in the z direction in the presence of the free surface and the increase of the probability to jump in z direction towards the free surface with decreasing depth of the SIA (see Fig. 2.4.13).

WP12-MAT-IREMEV-04-01 / Swiss-Confederation/BS/PS: Experimental validation of models

The irradiation campaign scheduled in 2011 was started in March 2012 but due to a failure of the acquisition system it was interrupted. The irradiation planned in 2012 has not taken place yet.

Goal oriented training programme

WP10-GOT-FabriCharMe

A first work visit at CRPP of a trainee, Dr. Lorelei Commin hired at KIT, for a period of 6 weeks took place from the 30th of January until the 9th of March 2012. While a second work visit should have taken place in fall, this second visit had not been scheduled. However, the work initiated by Dr. Commin was continued. Experiments and finite element simulations have been carried out to assess the warm pre-stressing effects on the effective fracture toughness of the high-chromium reduced activation tempered martensitic steel Eurofer97. The experiments have been conducted on sub-sized compact tension specimens in the low ductile to brittle transition region. The specimens have been pre-loaded at room temperature before being tested at low temperature. A clear increase of fracture toughness measured after warm pre-stressing has been found that is discussed in the light of the finite element calculations. In particular, a discussion of the role of the residual compressive stress field, triaxiality level and accumulated equivalent plastic strain respectively on the fracture toughness increase after warm pre-stressing is analyzed. It is shown that a change of the local criterion for fast-fracture has to be considered, which results from the pre-deformation.

*2.4.2 Broader Approach activities**

International Fusion Materials Irradiation Facility – Engineering Validation Engineering Design Activities (IFMIF-EVEDA): Design of a test module for in-situ creep-fatigue tests to be performed in the IFMIF facility and construction of a mock-up of the test module

The mock up of the creep fatigue test moducle (CFTM) designed and built in previous years underwent extensive life time test in 2012. Some improvements were performed to the original apparatus. The life time tests were successfully performed and the specifications of the CFTM were shown to be met. The final report was submitted to F4E at the beginning of 2013 and the project was closed.

International Fusion Energy Research Center (IFERC): Contribution to the definition of irradiation matrices for IFMIF by means of development of new methods for testing and analyzing subsized specimens

Two series of tensile tests on irradiated Eurofer97 steel have been carried out. These series correspond to two different irradiations conditions; T_{irr}=150°C at 0.33dpa and T_{irr}=350°C at 0.37dpa. These tests have been conducted to supplement the fracture tests realized in 2011 on Eurofer97 irradiated in the same conditions. They have been done over the same temperature range as that of the fracture tests to characterize the irradiation-hardening (increase of the flow stress) and the evolution of the strain-hardening. The determination of theses quantities is necessary to model the irradiation-induced degradation of the fracture properties using finite element simulations as well as the micro-hardness change. The tensile curves for the 150°C and 350°C irradiations are presented in Fig. 2.4.14. Two important observations can be done from the curves plotted in these Figures. First, the overall shape of the 150°C irradiation curves is significantly different from that of the 350°C irradiation curves in the sense that there is practically no uniform elongation, indicating clearly that the specimens neck right after the onset of plasticity. On the contrary, the uniform elongation after 350°C remains large. Second, in both cases the temperature does not affect much the strain-hardening. We stress here that the 350°C irradiation engineering stress curves can be directly converted in true stress-strain curves that are used as input in finite element code. On the contrary, extracting the true stress-strain curves from the 150°C engineering stress curves is not straightforward but can be done by first analyzing by finite element simulations and by using an inverse methodology to fit the true stress-strain curve that reproduces the reproduces the engineering stress-strain curves.

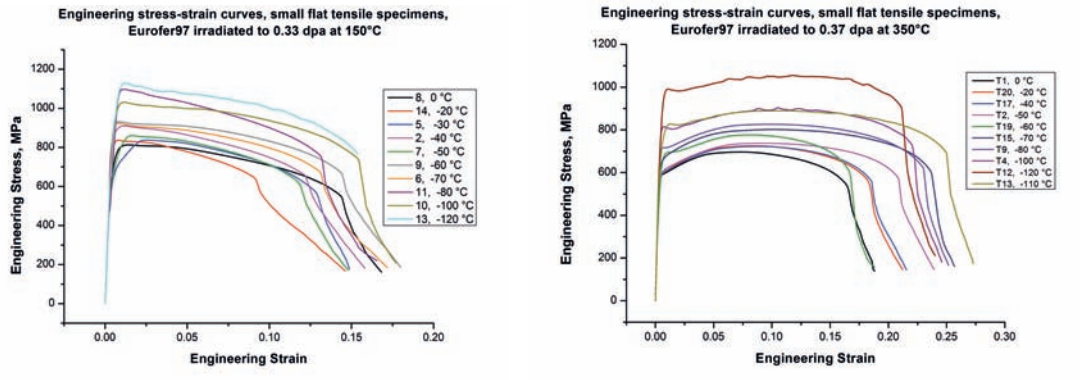

Fig. 2.4.14 *Engineering tensile stress of irradiated Eurofer97 after T_{irr}=150°C–0.33dpa and T_{irr}=350°Cdpa–0.37dpa*

* Work not belonging to the EURATOM Association workprogramme.

A series of a micro-hardness experiments on unirradiated and irradiated Eurofer97 have been done in 2012 to complement the macro-hardness data we gathered in 2011. The micro-hardness experiments have been performed with a fully instrumented G200 MTS nano-indenter equipped with a high-load module to do micro-hardness. The tests were done up to a maximum load of 5N with a Berkovich and Vickers tip. The load versus penetration depth was recorded and compared to finite element simulations. The main goal of the simulations was to determine the contact height H_c (between the tip and the specimen) as a function of the penetration depth H_p. Knowing the contact height is of primary importance as the hardness is defined by the load divided by the contact area. However, we had previously shown by simulations that H_c is strongly dependent on the constitutive behaviour. The data of the irradiated Eurofer97 confirms the importance of determining the contact area before calculating the micro-hardness. In Figure 2.4.15, we plot the ratio H_c/H_p versus the applied load. Above 1N, there is no significant difference between the Berkovich and Vickers tip. We stress that H_c/H_p is larger after the 150°C irradiation (low strain-hardening promoting plastic flow) than for the unirradiated material; on the contrary after the 350°C the strain-hardening capacity is not much altered by irradiation the ratio is lower that the unirradiated material due to the increase of the yield stress.

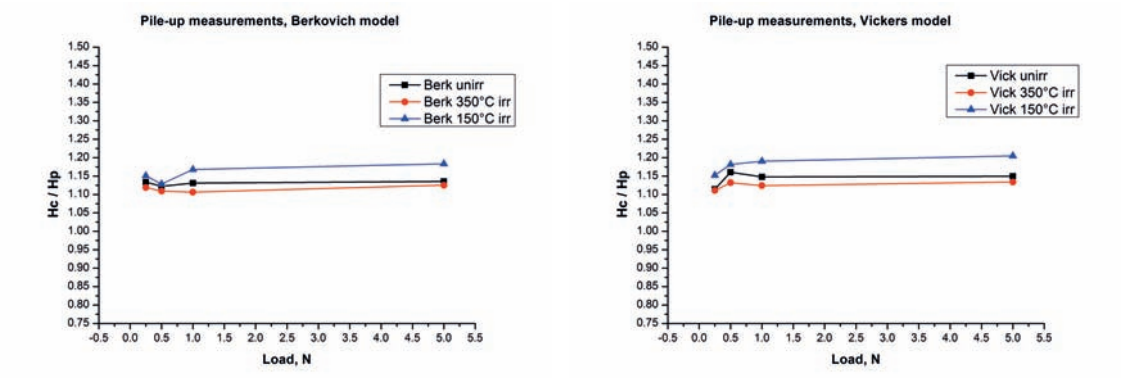

Fig. 2.4.15 *Contact height to penetration depth ratio for Berkovich and Vickers micro-indentation after T_{irr}=150°C–0.33dpa and T_{irr}=350°Cdpa–0.37dpa*

Finite element simulations were used to investigate the plastic flow in the contact region between the tip and the specimen. The simulations were validated by experimental tests carried out on the tempered martensitic steel Eurofer97 using a simple constitutive equation of Ludwik type:

$$\sigma = \sigma_y + A\ \varepsilon_p^{0.5}$$

A series of simulations using different constitutive behaviours representative of possible irradiation-induced changes were run. σ_y was varied from 530 to 800MPa and the strain-hardening coefficient A was comprised between 50 and 680 while the strain-hardening exponent n was kept at 0.5. In total, fourteen different constitutive behaviours were considered. In all cases, a pile-up of materials against the indenter tip was observed that is strongly dependent on the constitutive law. The effects of the constitutive behaviour on the relation $h_c(h_p)$ is illustrated in Fig. 2.4.16 where the α coefficient ($\alpha = h_c/h_p$) is plotted against the hardness. Clearly, the height of the pile-up is not a simple function of hardness but depends on the strain-hardening capacity as well as on the yield stress. In Figure 2.4.16, the data linked by the solid lines have the same strain-hardening

coefficients (A and n) but different yield stresses, while those linked by the dotted lines correspond to identical yield stress but different strain-hardening coefficients. Decreasing both σ_y and the strain-hardening capacity promotes the formation of the pile-up but again knowing the hardness only is not sufficient to predict the height of the pile-up. The information lying in Fig. 2.4.16 is sufficient to determine the constitutive behaviour. Indeed, both the height of the pile-up and the hardness can be determined experimentally, and from these two quantities (which actually correspond to the coordinates of a single point (H-α) in the plot) one can obtain the constitutive behaviour as defined by Ludwik. We recall that with this approach only two parameters are used to describe the constitutive behaviour: σ_y and A. In other words, the knowledge of the pair (H-α) defines the pair (σ_y-A). For practical purposes, a better precision in the determination of the pair (σ_y-A) from Fig. 2.4.16 can be obtained by drawing more lines separated by smaller increments $\Delta\sigma_y$ and ΔA than what was done in this study. In principle, the smaller the increments are, the smaller the domains defined by the intersections of the lines are and the better is the resolution.

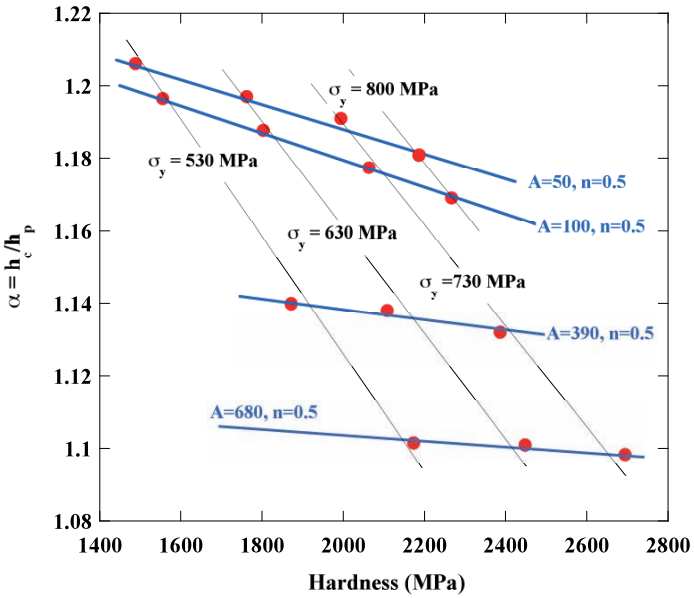

Fig. 2.4.16 *α coefficient (=h_c/h_p) versus hardness.*

Finally, the effect of the pre-loading fracture specimens of Eurfoer97 at a given temperature T_1 on fracture toughness measured at temperature T_2 such that $T_2<T_1$. This effect called *warm pre-stressing* can be of great importance in safety assessment where temperature transient are involved and should be taken into account when evaluating *embrittlement*. In this work, the residual stresses are introduced at the crack tip of fracture specimens, following a loading – unloading sequence. Fracture tests have been carried out on pre-cracked sub-sized compact tension 0.18T C(T) specimens. The pre-loading sequence consisted in loading the specimens at room up to a K_a value (K_a is the applied stress intensity factor), which was chosen to be about 60-70MPam$^{1/2}$. This corresponds to a point on the loading curve that slightly deviates from the elastic regime. Then the pre-loaded specimens were tested in the lower transition region, in the range -196 to -100°C. It was found that there is a clear increase of toughness with respect to the as-received Eurofer97 (see Fig. 2.4.17). In Figure 2.4.17, one can see the fracture data of Eurofer97 in the as-received condition and those obtained after the pre-loading sequence. In addition, a local approach of brittle fracture was applied on the 1% lower of the as-received Eurofer97 data. The criterion of is based on the attainment of a critical stress σ* over a critical area A* at the crack tip. In Figure 2.4.17, the predicted values of K based on the σ*-A* criterion, with σ*=1950MPa and A*=1100μm^2, show that the lower bound of the as-received Eurofer97 can be properly reconstructed with this criterion.

However, using these calibrated values of σ* - A* for the finite element simulations of the WPS specimens underestimates the measured fracture toughness. Indeed, as can be seen in Fig 2.4.17, when the same local criterion is used for the WPS-Eurofer97, the predicted fracture toughness, represented by the open black circles, cannot constitute the lower bound of WPS fracture data. In fact, keeping the fracture load at 1950MPa but increasing the critical area up to 15000μm^2 provides a much better description of a possible lower bound of the WPS fracture toughness data. Thus, changing the values of σ*-A* indicates that the plastic deformation accumulated during the loading and unloading on the microstructure at the crack tip may be sufficient to modify the local criterion of fracture. We emphasize here that active plastic deformation takes place during the loading (in traction) as well as during the unloading (in compression).

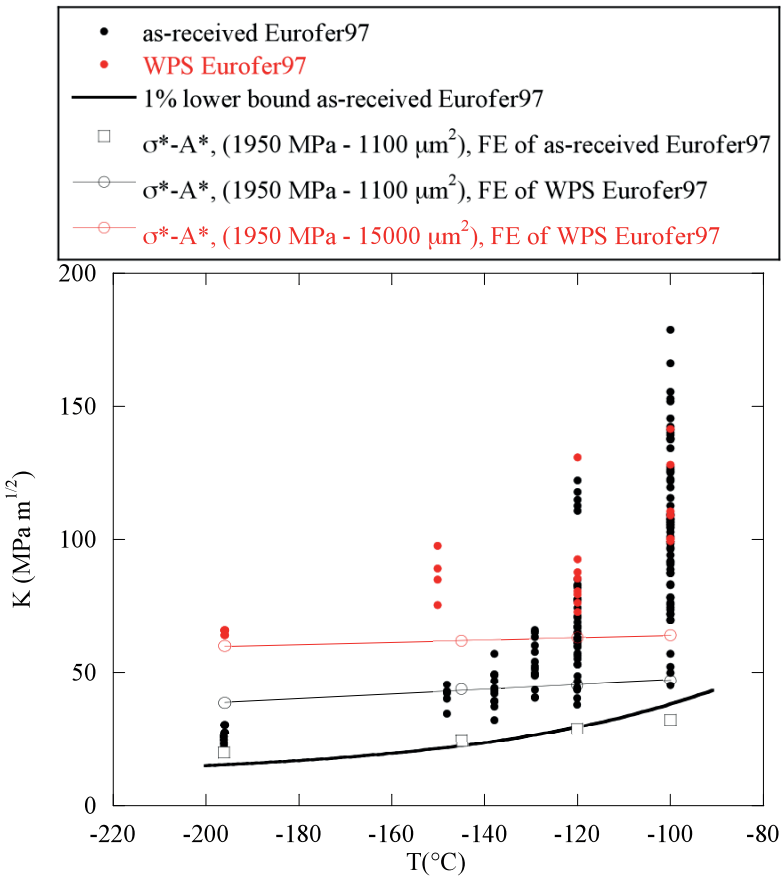

Fig. 2.4.17 *Effect of warm pre-stressing on 0.18T C(T) specimens of Eurofer97.*

2.4.3 Supporting research

The quest for radiation resistant materials
Swiss National Fund – Marie Heim-Vögtlin Programme

The project is structured in two parts. One part refers to the study of radiation damage in body centred cubic (bcc) materials. The second part proposes to solve the dilemma of stacking fault tetrahedra formation following irradiation in austenitic stainless steels with face centeed cubic (fcc) structure.

The existing data on the formation of stacking fault tetrahedra (SFTs) in austenitic stainless steels following irradiation are contradictory. It appears that SFTs do form in such fcc metals, as expected from elastic and energy considerations, but the conditions

of their formation remain unclear. They were observed in high purity and model austenitic stainless steels, irradiated at both very low and high doses. In commercial purity steels they are either scarce, absent or present in high densities. It seems that there is a gap in the formation of SFTs at irradiation temperatures around 400°C.

The approach of the present study is to perform molecular dynamics simulations and a systematic experimental study, consisting in transmission electron microscopy (TEM) in-situ ion irradiation and post mortem TEM observations of a variety of stainless steels.

Simulations: Molecular dynamics calculations

Molecular dynamics (MD) simulations were conducted on the Fe-Ni system. The equilibrium potentials for the Fe-Ni system were developed by Bonny et al. These potentials were implemented in the MOLDY-CRPP program in collaboration with Maria Jose Caturla from the University of Alicante, Spain. Calculations were applied for different Ni contents: 45, 50, 55, 60, 65, 70, 75, 80, 100%. The followings were observed:

- Pure Ni forms perfect SFT at all annealing temperatures and sizes of 21 and 66 vacancies. In the case of 15 vacancies, only at 10K the platelet remains without transformations. At all other temperatures perfect SFTs are formed. The 6 vacancies platelet collapses into a perfect SFT only at 300K, while all the others are imperfect.
- In the case of the alloys, things are not so straightforward. At low Ni contents of 45 and 50%, the structure is partly bcc and the platelets undergo no transformation, regardless their size or annealing temperature.
- In the alloys containing 55, 60, 65 and 70% Ni, the platelet remains in its initial state for all sizes and annealing temperatures, but for the cases of the alloys containing 65 and 70% Ni. In those cases the 66 vacancies platelet collapsed into an SFT, though imperfect at a temperature of 800K. At lower temperatures no SFT appeared.
- In the case of the Fe-80%Ni alloy, the platelets collapse to imperfect SFTs starting from 300K.
- The Fe-75Ni alloy was studied in more detail, as it shows the highest rate of SFT formation for all conditions. Calculations were performed also on structures with different random arrangements of the Fe atoms in the Ni lattice. 11 different structures were constructed. Platelets of 21 and 66 vacancies were formed. It appears that temperature is more important than local chemical order, as more SFT form at 800K as compared to 400K. However, local chemical order seems to have an impact. In few cases SFTs appear at 400K for both sizes. At 800K, the probability of SFT formation increases with its size. Also SFTs are more perfect at 800K than at 400K. At 400K the probability of SFT formation is lower for both sizes.

Besides, we observe that the addition of bcc Fe to the fcc Ni causes distortions in the structure, which could explain why the platelets remain untransformed after relaxation and anneal for the low Ni contents. It appears thus that below a Ni content of 70 % this potential set is unsuitable to reproduce the behaviour of a real austenitic stainless steel, where the Ni content is much lower, of the order of 8 to 15%.

Experimental: Ion irradiation and transmission electron microscopy observations

Ion irradiations were performed at JANNuS Orsay, France in Mai 2012.
Irradiation conditions:

- Single beam, 500 keV Fe^{+}
- Irradiation temperature: room temperature
- Fluence: 1 x 10^{10} ion/cm^2s

- Irradiation dose: ≈ 1.0 dpa

The material matrix is described in Table 2.4.5.

All the materials have been irradiated in the same conditions. An example of the microstructure is shown in Fig. 2.4.18. Figure 2.4.18a shows a microstructure in TEM typical of austenitic stainless steels, here the low stacking fault energy (SFE) material, with few dislocations and stacking faults. At the end of irradiation (Fig. 2.4.18b and c) the structure contains a fine dispersion of nanometric irradiation-induced defects.

Material	C, %	Cr, %	Ni, %	Cu, ppm	Mn, %	Mo, %	Ni, %	N, ppm	P, ppm	Si, ppm	S, ppm
316L	0.019	16.42	10.2	1800	1.39	2.14	10.2	260	250	5200	20
316	<0.12	16.5-20.0	8.0-14.0		< 2	2.0-3.5	8.0-14.0				
304LCP	0.013	18.32	10.42		1.16	-	10.42	0.027	0.021	0.13	0.011
304	<0.07	17.5-20	8-11		<2				<0.045	<1	<0.03
LSFE	0.04	18.04	8.75		1.52		8.75	0.06	0.033	1.07	0.02
Ref SFE	0.05	17.64	8.6		1.56		8.6	0.023	0.033	0.44	0.02

Table 2.4.5 *Material matrix for ion irradiations at JANNuS Orsay.*
316: commercial purity stainless steel with a different carbon content (316L and 316)
304: commercial purity stainless steel again with different low carbon content (304LCP and 304)
'SFE': low (LSFE) (11mJ/m^2) and reference (Ref SFE) (31mJ/m^2) stacking fault energy stainless steels

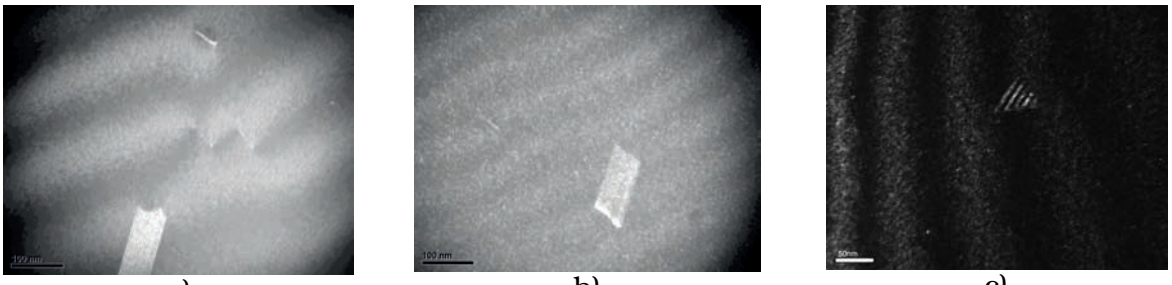

a) b) c)

Fig. 2.4.18 *Weak-beam dark-field transmission electron microscopy observations in the case of low stacking fault energy stainless steel: a) at the beginning of irradiation; b) at the end of irradiation; c) observation performed after irradiation. Notice the appearance of the white dots, the trace of radiation induced point defect clusters.*

2.5 Superconductivity

The milestones achieved in 2012 are the start of the EDIPO commissioning and of the three years framework contract for ITER conductor tests in SULTAN. In terms of personnel, the superconductivity group had 2.5 retirements and three new hiring. The high dedication of the employees and the lack of major technical failures contributed to a very productive year. The DEMO studies in the scope of EFDA PPPT are established as a steady activity for CRPP, with expected growth in the coming years.

2.5.1 High Temperature Superconductors for DEMO (Work programme 4.4)

In the framework of the EFDA PPPT WP12, CRPP carried out the following tasks:

- WP12-DAS01-T08 Study of the performance of HTS twisted stacked cable
- WP12-DAS01-T09 Study on the effect of transverse loads on RE-123 Roebel cables

For the magnets of future fusion reactors, superconducting cables with a current carrying capacity of the order of 50kA are required. In the scope of EFDA PPPT the possibility to use RE-123 tapes for the magnet conductors is studied. One of the challenges is the manufacture of high current conductors starting from tape-shaped strands. Three concepts have been proposed for the manufacture of RE-123 high current conductors:

- Roebel-Rutherford cable using small Roebel cables as sub-elements for the Rutherford cable
- Twisted stack cable
- Co-axial cable (tapes are wound around a copper core)

Twisted stack cables of around 500mm length consisting of 8 RE-123 tapes of 3mm width, which are embedded between two semi-circular copper profiles, have been prepared at CRPP. The twisted stack cables have been manufactured in two different ways. In the first manufacturing route, the RE-123 tapes and the copper profiles are soldered together before twisting, whereas in the second route the conductor is twisted before soldering. The performance of cables soldered with BiSn, InSn and PbSn has been compared.

For the non-twisted cables, the critical current reaches values between 420A and 440A at 77K in self-field. In cables soldered with BiSn, twisting and bending led to a continuous degradation of the critical current, which seems to be caused by crack formation in the BiSn solder. On the other hand, critical currents above 400A (77K, sf) have been achieved in cables soldered with InSn and PbSn even for twist pitches down to 300mm and 280mm respectively. A bending strain of 0.6% reduces the critical current of cables soldered with InSn by 7%, whereas this reduction is only 2% for soldering with PbSn. The degradation has been found to be reversible for the PbSn solder, while it is irreversible for the InSn solder. The performance of cables made by the “solder & twist” and “twist & solder” routes, are not significantly different. The achieved results seem to be very promising for the development of RE-123 fusion conductors.

For the investigation of the effects of transverse loads on the performance of RE-123 Roebel cables, industrially fabricated cables (5 × 2 tapes of 2mm width) have been procured from Industrial Research Limited in New Zealand. The apparatus for the measurements has been set up at CRPP. Forces up to 10kN can be applied by means of a piezo-electric load cell. On one side of the cable under test one current lead for each tape will be used to enable the study of the damage of individual tapes. It is expected that first results will be available in the near future.

2.5.2 Nb_3Sn TF Coil-Conductor for DEMO (WP12-DAS-Magnets)

In the scope of the EFDA PPPT WP12, CRPP carried out the following tasks:

- WP12-DAS01-T01 LTS Activity Coordination
- WP12-DAS01-T02 Define magnet and conductor system requirements in conjunction with WP12-SIP01 activity
- WP12-DAS01-T03 Select and define candidate conductor designs and define design criteria for assessment/evaluation
- WP12-DAS01-T02 Produce models and perform analysis of candidate designs

The main challenges for the TF coil/conductor design of DEMO, following the output of the PROCESS code, are the very large stored energy (11.5GJ/coil), the long dump constant (23s) and the very large size and weight (20m x 12m, > 1000 t/coil). The key design choices in the layout proposed by CRPP are the use of react&wind method (opposite to ITER wind&react&insulate), a layer wound winding pack (opposite to ITER pancake/radial plates), hybrid winding pack made of NbTi and Nb_3Sn layers, graded conductors. A sketch of the high grade Nb_3Sn conductor is shown in Fig. 2.5.1

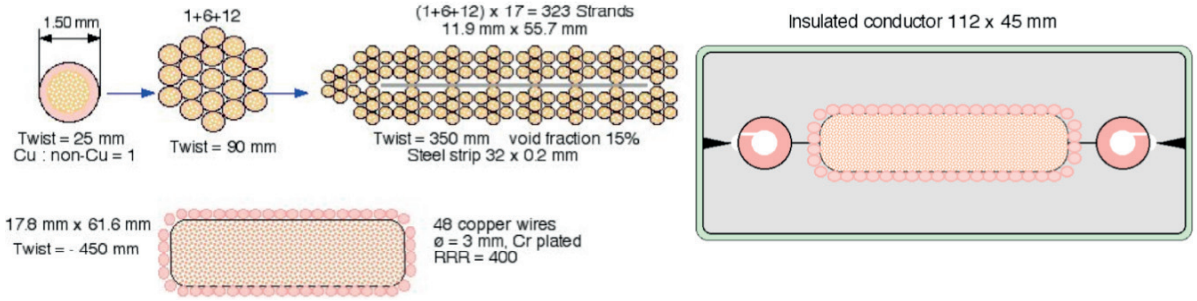

Fig. 2.5.1 *Schematic layout of the force flow, react&wind Nb_3Sn high grade conductor*

The assessment of the conductor/coil layout is carried out by electro-magnetic, thermal-hydraulic and mechanical analyses shared among CRPP, ENEA and Un. West Pomerania (PL). The first results larely confirm the soundness of the design.

2.5.3 The Preparation of EDIPO Test Facility (EFDA Task 5.1a)

At the end of 2011, a further extension of the EDFA task was granted by the Commission. The new deadline is June 30th 2013.

Because of the priority for the preparation and test of the ITER conductors, the access to EDIPO in the SULTAN hall was severely restricted and the manpower availability limited. The installation work for EDIPO progressed very slowly after November 2011. The days of non-operation of SULTAN because of sample change and compressor maintenance were intensively used for EDIPO installation. On April 26th the coil assembly was removed from the cryostat after the fitting checks to complete the electrical insulation, instrumentation and application of super-insulation. On June 6th the coil assembly was back, for good, in the cryostat. On June 8th the top flange was closed and leak tight checked. The final electrical and hydraulic connections, the wiring to the feed-through, the sensor checks, the application of the tilting sensors, the installation of the vacuum chamber for the sample environment, etc. were completed in the following months. The final closure of the cryostat was done on October 26th.

In the meantime the control system was installed and the static checks were carried out. The quench detection electronic and the sensor transmitters were installed and checked. The whole wiring from the cryostat to the electronic cabinets was completed in June by the PSI technicians.

An overtime scheme, funded by F4E, was used for the SULTAN tests in August-October, see section 4.5, to gain six weeks window for EDIPO commissioning. On October 29th the first three weeks window started as initial phase of the commissioning of EDIPO, with the main target of debugging the control system and start the cool-down. A similar overtime scheme will be placed in 2013 to gain an additional six weeks. The target date to carry out the most crucial phase of the commissioning (acceptance of the coil assembly from BNG) is May 2013.

*2.6 Industrial process plasmas**

Some of the ongoing projects concern the development of new plasma sources for high rate deposition processes. The present situation in industry shows that high deposition rate plasma sources and plasma reactors must be developed for new performant plasma processes waiting introduction in industry. These important topics are investigated in the frame of several CTI projects in collaboration with TetraPak and Helyssen. In addition, the group worked intensively on a CTI project in collaboration with OC Oerlikon Solar concerning the development of a novel capacitively coupled RF plasma reactor particularly designed for the specific demands of the amorphous/microcrystalline deposition for thin film solar cell production. Furthermore, the CTI project investigating the properties of RF and DC plasma sources for the deposition of semiconductor GaN layers for the production of LEDs, in collaboration with Sulzer-Metco was on going.

Discharge physics still remains a key issue in the world of industrial plasmas. One of the main problems in high deposition rate plasma sources in which high AC/DC powers are applied is the occurrence of arcing and parasitic discharges. This problem has been investigated in previous years. At present, in collaboration with RUAG Aerospace funded by ESA, the origin and consequences of arcing occurring in so-called slip-rings used in spacecrafts was studied.

The industrial plasma group collaborates with the Group de Thermique Appliquée et de Turbomachines (GTT) and the Laboratoire d'Ingénierie Numérique (LIN) of the Energy Institute (ISE) from the Faculty of Engineering (STI) of EPFL in the European FP7 PLASMAERO project aiming at application of plasmas in aerodynamics.

During the year several new projcts and mandates have been initiated. A new CTI project shall develop a very large area resonant network RF antenna for the industrial deposition of barrier coatings in packaging industry. This project is a follow-up project of the previous very successful CTI project with TetraPak. Projects concerning large area application of resonant network antennas for solar cell production are under discussion, as well as a basic project on the production of pure pyrolite for solar cell applications. Discussions about a FNS project concerning the plasma deposition of pure pyrite for solar cell application are presently under way with HE-Arc in Le Locle and the CSEM in Neuchâtel.

To summarize, our activities are focused in particular on discharge physics, arcing under various conditions and the development of novel high deposition rate plasma source and new materials for solar cells. During the year, meetings and discussions with various industries on other new plasma processing issues have been made and will give interesting future R&D topics and stimulating science for the industrial plasma group of the CRPP.

* Work not belonging to the EURATOM Association work programme.

2.6.1 A new low ion energy bombardment PECVD reactor for the deposition of thin film silicon for solar cell applications

A novel electrode configuration is currently being studied for improved plasma-enhanced chemical vapour deposition of thin films such as amorphous silicon and micro-crystalline silicon. The new electrodes are designed to protect the growing film from damages by plasma ion bombardment which is crucial for the manufacture of high-performance photovoltaic material. The new plasma reactor concept was optimised in laboratory tests and in a R&D industrial reactor. Experiments in the laboratory reactors at CRPP include a newly designed retarded-field ion energy analyser to measure the ion flux and ion bombardment energy on the substrate.

A plasma reactor using localized remote plasmas in a grid electrode is investigated for this purpose. The aim is to reduce the ion bombardment energy inherent to RF capacitively-coupled parallel plate reactors used to deposit large area thin film silicon solar cells. High ion bombardment energy is supposed to cause defects in silicon layers and deteriorate electrical interfaces, therefore by reducing the ion bombardment energy, films with lower defect density might be obtained. In this CTI project, the low ion bombardment energy results from the particular reactor design. By inserting a grounded grid close to the RF electrode of a parallel plate reactor, the electrode area asymmetry is increased while retaining the lateral uniformity required for large area deposition. The grounded area in contact with the plasma is much larger than the RF electrode area. This asymmetry causes a strong negative self-bias voltage that reduces the time-averaged plasma potential and thus lowers the ion bombardment energy (Fig. 2.6.1).

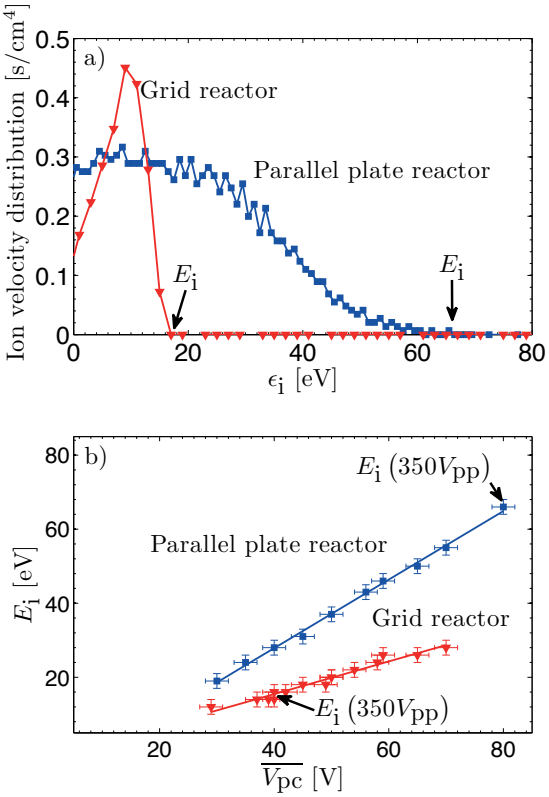

Fig. 2.6.1 *(a) Ion velocity distribution measured with the RFA in parallel plate and grid reactors, (b) The ion bombardment energy as a function of the estimated time-averaged plasma potential assuming capacitive sheaths.*

The second mechanism reducing the ion bombardment was revealed by differences in the temporal evolution of the light emission and plasma potential waveform between the grid reactor and a parallel plate reactor. The plasma potential waveform in the grid reactor is non sinusoidal and is similar to a plasma with resistive sheaths. The measured time-averaged plasma potential with this particular waveform is lower than for the sinusoidal waveform plasma found in parallel plate reactor thereby further reducing ion bombardment energy in the grid reactor.

Hence, the low ion bombardment energy in the grid reactor is due to a reduction of the time-averaged plasma potential, a consequence of the grid reactor configuration design rather than from VHF, high pressure or injected harmonics in the RF electrode.

2.6.2 Development of resonant network antennas as plasma sources

This project is performed in close collaboration with Helyssen Sarl. During the last years Helyssen Sarl and the industrial plasma group investigated together the applicability of resonant network antennas as plasmas sources.

Resonant network RF antennas have many advantages compared with the popular capacitive and inductively coupled devices. Resonant network antennas can be up-graded without too many difficulties to run as large area plasma sources with much less effort then the often-used plasma sources. Due to the real impedances of the resonant network an easier RF power matching is obtained than for the complex impedances in the conventional plasma devices leading to high RF currents or very high RF voltages.

We showed that resonant RF networks can be arranged to form large area or large volume plasma sources. Closed and open configurations of the coil for plasma production are both possible and can be described with the same theoretical formulation. The plane antenna is well suited for applications such as surface treatment of large flat areas, whereas the cylindrical version can be used as a volume source for large number piece processing or large substrate treatment. It was shown that it is possible to construct complex RF antennas out of the basic network that can be adapted to application and are therefore very user-friendly. Resonant RF network antennas can be used for large area applications such as coating of films and also for large volume applications such as plasma sources for neutral injectors.

In the frame of the present work two different resonant RF network assemblies have been investigated: a plane and a cylindrical antenna. The first antenna studied is a plane RF network antenna where the elementary meshes are composed of long copper rods and capacitors similar to the one used in previous works. The whole plane antenna is composed of 23 copper rods spaced by 2.5cm. The antenna is placed inside the vacuum vessel. In order to avoid parasitic discharges the antenna is entirely embedded in a metallic box filled with silicon and covered on one side by a thin glass plate acting as plasma-facing surface. Since the antenna is placed within the vacuum the antenna–plasma surface (glass plate) distance is only 5mm, shorter than in ICP devices. The RF power is fed in the middle of the antenna whereas four points of the antenna are grounded, thus favouring the mode m=6. The maximum RF power to be handled by the plane antenna was restricted to 200W due to the maximum RF current allowed in the capacitors or by the antenna heating in the absence of any cooling scheme. The plane antenna was placed in a large vacuum vessel with a diameter of 0.5m with a vacuum base pressure of about a few 10^{-7}mbar. The experiments are performed in Argon at a gas pressure of 10^{-3} to 10^{-1}mbar.

The cylindrical RF antenna was built following the concept of a high-pass birdcage coil. The antenna was fixed outside of a Pirex glass tube with a diameter of 35cm cm and of a

length of 30cm. The RF antenna consists of 16 copper legs equally spaced and interconnected with capacitors. The uncooled antenna was feed in the mid-point and mostly run with the opposite point grounded. The operating pressure range of the cylindrical RF network antenna was 10^{-1} to 10^{-3}mbar. The working gas used was Argon. The RF power operation range for this antenna assembly was limited to a maximum of 300-500W.

The theoretical background of the discussed plane and cylindrical network RF antennas was investigated. The calculation of the electrical circuit for the open and closed antennas is only distinguished by the boundary condition inherent to their structure. In this work the physics of the dissipative coil was also discussed in detail. It has been shown that in the neighbourhood of a mode resonance a simple resonant RLC electrical circuit can describe the overall behaviour of the complex antenna. This general result applies for both plane (open) and cylindrical (closed) antennas and is confirmed by the experiments. The simultaneous measurement of RF current and voltage and their phase relation gives the impedance of the antenna and with this the different components such as R, L and C. The measurements of the impedance during plasma operation show changes, which can be interpreted in terms of the plasma–antenna coupling mechanism and properties of the produced plasma.

Resonant RF network antennas can be used in different configurations, RF operating regimes and plasma parameters. Furthermore, the same resonant RF network antennas can be used for direct plasma production by antenna potentials and currents and also as a wave-excited plasma source in the presence of a background magnetic field.

2.6.3 Very fast SiOx barrier deposition on polymers by plasma-enhanced chemical vapour (PECVD) process with a helicon plasma source

The objective of the CTI project was to increase the deposition rate in the PECVD process producing SiO_x barrier coatings by using the novel high density Helyssen source described in Section 2.6.2.

High deposition rates of SiO_x for barrier application are achieved if the monomer is dissociated as much as possible. To achieve high dissociation degrees new more powerful plasma sources must be applied. The main goal of this project was to design and to test the resonant network antenna as developed by Helyssen S.a.r.l. as plasma source. A large part of the physical concepts and capabilities of this source is still only theoretical and has still to be concretized by basic experiments at the CRPP. A first version of a planar resonant network RF plasma antenna (Fig. 2.6.2) has been designed and finally constructed at the CRPP. The planar antenna was installed in a vacuum vessel in order to perform electrical tests and plasma diagnostics. As plasma diagnostics in particular Langmuir probes, optical emission spectroscopy and visualisation using a CCD camera are used, whereas the plasma wave diagnostics are mainly performed using 2D-B-dot probes. First characterisations were performed on the behaviour of the planar RF antenna and plasma which was then tested in view of the applications in a semi-industrial coater at TetraPak at Romont. With this coater at TetraPak the coating performances of the planar antenna have been evaluated in view of specific packaging applications. The plasma sources were used to deposit thin barrier layers on polymer foils in order to create a barrier mainly against oxygen and water. With the Helyssen planar antenna a higher line speed of the film than with the conventional plasma was obtained while keeping excellent barrier properties. The polymer foils processed with the Helyssen source have also been tested from the adhesion point of view, and it has been shown that the deposited layer sticks very well on its substrate. Finally, several thousand meters of processed polymer foil have been produced at high line speed and utilized to produce TetraPak packaging material. This one was used in an industrial

filling machine that produces the well known packages, which were filled with water for this test purpose. The obtained bricks show good barrier properties, which indicates that the layer deposited with the Helyssen source resists to the whole production process.

Beside packaging applications, the CTI project was rich in academic achievements concerning the understanding of resonant network RF antennas. The study of the Helyssen planar source at the EPFL shows that the antenna is highly efficient (up to 90%) and produces dense plasmas (10^{11}-10^{12}cm^{-3}) with a reasonable uniformity of the plasma density. At present, the application of resonant networks for plasma production seems to be a very rich field for future academic investigations. A follow-up CTI projct initiated during the year is presently underway. A larger planar antenna for industrial application shall be designed, constructed and be tested.

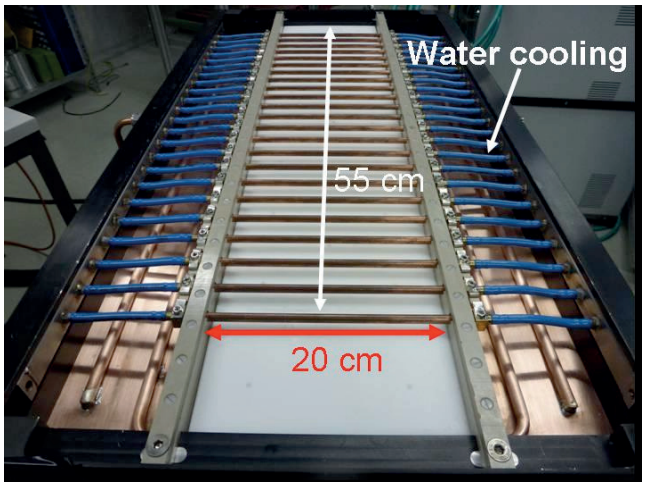

Fig. 2.6.2 *Water-cooled planar resonant network antenna as used for basic plasma research*

2.6.4 Development of industrial gas-metal plasma sources for the deposition of nanostructured GaN semiconductor layers for lighting applications

Epitaxial coating processes using low-energy gas-metal plasmas offer a promising path to cost-effective manufacturing of highly energy-efficient LED's for power-saving lighting applications and high-efficient third-generation solar cells. The goal of the present CTI project is to move this innovative coating technology a step closer to industrial application and commercial exploitation by developing and optimizing the plasma-processing equipment. In addition better understanding and controlling of the fundamentals of the GaN deposition process will be obtained.

In the frame of the project a commerecial RF source and a LEP-DC (low energy plasma source) shall be compared in view of the deposition of GaN semiconductor layers.

The RF GaN deposition device, transfered from Sulzer Metco, using a commercial RF source was installed at the CRPP and first nitrogen (and nitrogen-argon/and hydrogen) plasmas have been produced. In addition, different plasma diagnostics such as Langmuir probes, a Faraday cup and optical emission spectroscopy have been installed on the device. Injection of Gallium into the nitrogen plasma using an effusion cell has also been performed and the device performed the first GaN depositions. First characterization of the nitrogen(-Argon/Gallium) plasma using the existing diagnostics have been started. These results for emission spectroscopy are interpreted using available software such as Specair in order to simulate the spectra and to determine the population densities and

different species temperatures within the plasma and further investigate the influence of the injection of the neutral Gallium beam. These results were correlated with results obtained by GaN deposition characterisation. The characterisation of the obtained semiconductor layers shall be made at the LASPE (Laboratoire of advanced semiconductors for photonics and electronics) at the EPFL.

The DC plasma equipment already existing at the CRPP had been modified so that the Nitrogen(-Argon /and Hydrogen) plasma could be produced using either a point electrode or a ring electrode as necessary in view of GaN depositions. The DC device was used to obtain a detailed characterization of the DC plasma and its composition and in particular also of the stability of the plasma in the presence of a ring electrode. For these experiments optical emission spectroscopy and a moveable Langmuir probe have been applied and the results indicate an interesting difference between the RF nitrogen plasma and the DC nitrogen plasma.

In the running year GaN depositions in the RF reactor began and, after an initial period of process baseline runs and basic hardware characterization, first experiments aiming at correlating results from the plasma diagnostics to film properties could be started. Supporting the continuous experimental work in the laboratory, the development of theoretical and numerical models of relevant processes in the plasma represents another important task, often motivating new or additional experiments to align theory and experiments which in turn help to constantly improve the models. The goal of this work is to develop a tool which allows a maximum of insight into the process with unfortunately relatively limited information from in-situ analytics (in particular optical emission spectroscopy, which can eventually be used under industrial production cconditions). As one fundamental result, these theoretical works revealed the high significance of interactions between the plasma and reactor surfaces. This might have a direct impact on future equipment design.

In parallel to the tasks described above, various steps have already been taken towards the upcoming conversion of the deposition equipment to DC plasma. These modifications will be implemented as soon as the RF deposition study is concluded. Thanks to the detailed plasma diagnostics and modelling work already done based on the current DC reactor, a solid basis is available for selecting the relevant deposition experiments towards the development of the envisioned nanostructured GaN layers. As a further support, significant efforts have been undertaken to consolidate and integrate experimental results from previous projects with the results from the current project into a common research database, which can be accessed by all project partners. This tool facilitates correlation of new and old experiments and helps to make optimum use of knowledge acquired in the past.

2.6.5 European FP7 project: PLASMAERO

The consortium of the FP7 project PLASMAERO is composed of 12 partners from 8 countries (Arttic (F), ONERA (F), CNRS(F), EPFL(CH), CIRA(I), Technische Universitaet Darmstadt(D), University of Nottingham(GB), NLR(NL), University of Southampton(GB),, SNECMA(F) IMP(PL)). It gathers the key players from the plasma and aerodynamic scientific community in Europe. The PLASMAERO project ended in December 2012.

The CRPP participates together with the Group of Thermal Turbomachinery (GTT) and the Laboratoire d'Ingénierie Numérique (LIN) of the Energy Institute (ISE) from the Faculty of Engineering (STI) in this project. In addition the CRPP is work-package 1 leader ("Plasma devices, investigation, development and improvement) and task leader 3.5 (Shock/Boundary layer interaction).

The different partners from the EPFL performed experiments at transonic flow speed in their existing research wind tunnel facilities on several basic configurations of a flat surface dielectric discharge barrier (DBD) and on 2D profiles with curved DBD in order to obtain results on the modifications of flow and plasma characteristics. One part of the wind tunnel testing shall be performed at CIRA which possesses a large wind tunnel.

At the CRPP a simple design using existing power electronics was chosen and successfully applied to build a high voltage nanosecond pulsed generator (Fig. 2.6.3). The main component of the EPFL design of the power supply is a MOSFET switch triggered by a TTL pulse delivered from a function generator allowing changes in pulse width, pulse duration and duty cycle of the HV pulse. Rise time of a few 10's of nanosecond and discharge currents of up to 30-50A at frequencies up to 10-20kHz (or even higher) can be obtained. In addition fast high voltage and current measurements have been developed and incorporated into a compact design. Several power supplies have been constructed in particular also in view of the experiments in the frame of Plasmaero. In addition a power supply was constructed for the plasma group at the ETHZ (Prof Ph Rudolf von Rohr) for fast SiOx deposition. A lot of precautions and electrostatic shielding have been applied to reduce electromagnetic disturbances of the power supply. The observed disturbances were strongly reduced and allowed without problems wind tunnel experiments including operation of pressure tap in the vicinity of the actuator.

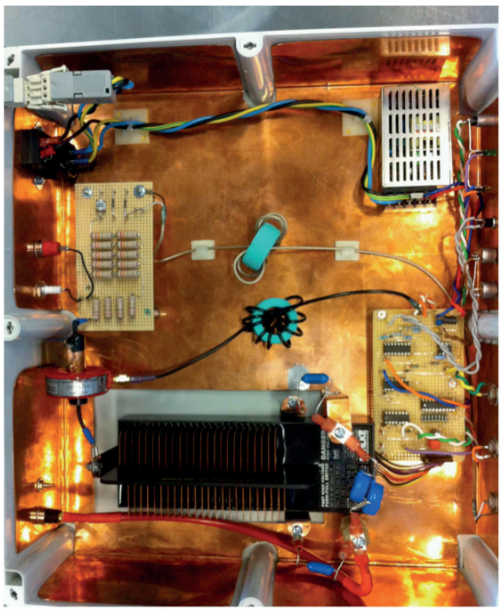

Fig. 2.6.3 *MOSFET high voltage nanosecond pulsed power supply including voltage and current measurements, frequency generator and protection circuit.*

Extensive plasma diagnostic techniques from the CRPP to evaluate scientifically and technologically the different plasma actuators has been used. Electrical measurements of the discharge parameters, various imaging techniques and some optical emission spectroscopy have been the main instruments to describe the plasma actuator and discharge parameters.

A diagnostic of great value and therefore often used within the Plasmaero project is imaging. Different fast cameras using different acquisitions have been used. First a CCD

camera with vary fast shutter time was used for repetitive phenomena in particular also for nanosecond pulsed DBD's. Recently also the camera with a very fast frame frequency up to 50kHz has been applied to detect moving shock fronts in transonic airflow.

From the acquired film sequence the shock front position versus time has been obtained and signal processing could be applied. FFT and coherence calculation allowed us to obtain insight into the physics of the interaction between the DBD plasma and the transonic airflow. Imaging of Schlieren visualization showed that in all nanosecond pulsed DBD a pressure wave was induced by the discharge, which confirmed numerical simulations.

First experiments with fast DBD's in transonic conditions have been started using a NACA 3506 airfoil and experiments in the larger wind tunnel at CIRA using a BAC1-11 profile have been started.

2.6.6 Arc Phenomena in Space Environment and Equipment

Arcing is a key issue in the application of plasma in industry and also, as in the present case, in space environment and space equipment. Modern satellites, in particular transmission satellites, are being equipped with larger and larger power systems. Since the weight aspect is very important the dimensions of the conducting paths for instance, in slide rings, are small. Therefore arcing is considered to be a limiting factor in several other applications of plasmas, thus triggering intense research and development on this topic.

In the present work for the European Space Agency (ESA) in collaboration with RUAG Aerospace in Nyon and the Haute Ecole d'Ingénierie et de Gestion du Canton de Vaud (HEIG/VD-IESE) laboratory, the necessary fundamentals of the arcing shall be established and be applied to the space equipment in order to reduce or suppress arcing in space environment and equipment.

The aim of the work at CRPP is to perfrom arc ignition, propagation and stability experiments in space environment and to define and conduct elementary experiments. Electrical simulations of the whole solar cell circuit of a spacecraft will be made by the HEIG/VD-IESE laboratory at Yverdon.

The first series of foreseen tests evaluated the extreme limits of a small test ring assembly as a function of the environment gas pressure and different gases. To simulate a slip-ring a model arrangement consisting of high voltage metal rings or grounded wires are investigated. The main discharge phenomena occurring when a DC high voltage of up to 30kV has been applied were vacuum arcs, corona and glow. Two different zones depending on the applied high voltage are observed. Optical emission spectroscopy with different gases confirmed two main discharge zones for a simplified ring assembly: metal lines for vacuum arc zone (low pressure) ignited by field emission and gas lines for gas discharge zone (high pressure) determined by Paschen law. On the high pressure side the breakdown voltage is clearly dominated by gas effect, whereas on the low pressure side breakdown leads to vacuum arcing. The DC breakdown voltage and leakage current can be measured under vacuum conditions with a commercial insulation tester. The tests were also carried out as a function of gas pressure (air, nitrogen, argon, helium) to measure to what extent the DC breakdown voltage is degraded by arc and plasma generation in the surrounding gas. In this way, the extreme limits of the test piece operation could be defined with respect to voltage and gas pressure. The most critical elements of the test pieces could be constructed as representative model samples by RUAG for further tests at EPFL-CRPP. The aim is that an iterative series of tests and redesigns of the model elements would eliminate weak points and design faults, finally leading to a more robust electrical transfer system. Various parameters under

investigation are, for example, isolator height, insulation of the brushes, track and brush dimensions, shape and dimensions of the enclosure, the sequence of connection polarities, and the configuration of the track and brushes adjacent to the enclosure at the ends of the test piece.

Numerical simulations were started of a parallel plate configuration based on the simple Paschen law. Once the simple model was corrected according to the analytic solution, the model was stepwise extended to the complex ring assembly. Preliminary results show similarities with experimental results as illustrated in Fig. 2.6.4.

Actually, simulations present higher breakdown voltages than experimental values, in particular for lower pressures. To reduce the breakdown voltage electron production needs to be increased. This is possible by including so far neglected phenomena like photoionization.

Moreover, simulations can help analyzing particular discharges by looking at electron and ion densities. An example of an external breakdown and an internal breakdown is shown in Fig. 2.6.5. This transition is also observed in experiment.

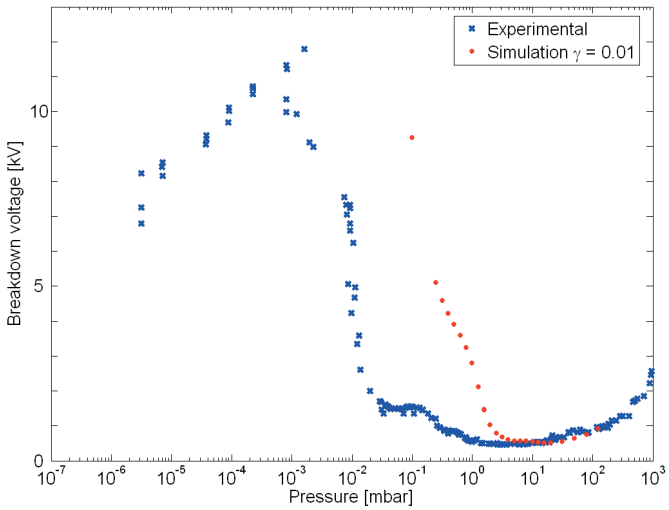

Fig. 2.6.4 *Simulation results and comparison with experimental breakdown voltage vs pressure*

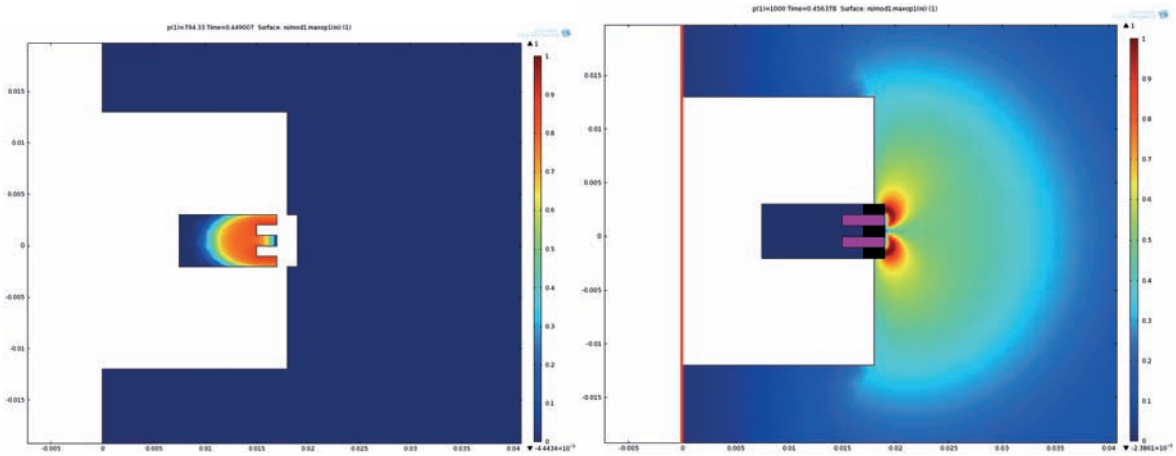

Fig. 2.6.5 *Ion density for 10mbar (left) and 7mbar (right) after breakdown in a ring assembly. The central ring (black) is charged whereas the top and bottom rings (black) are grounded. The conducting rings are separated by insulating rings (purple).*

2.6.7 Collaboration with Helyssen Sàrl, a start-up company

Helyssen SARL (www.helyssen.com), a start-up company, has for several years used a part of the laboratories of the industrial plasma group to evaluate the performances of different novel antennae for high deposition rate sources.

In collaboration with different Swiss industries and the CRPP the industrial application of resonant network RF antennas has been developed. The underlying plasma physics and chemistry of this network antennas have been investigated.

2.6.8 Additional R&D and future projects

During the year several mandates from Comadur (Swatch group) have been performed. In the frame of these mandates, processing up to production level of ceramic functionalisation was made.

A CTI project on the development of large area plane RF antennas for deposition of barrier coatings in packaging industry was accepted and should last over the date of retirement of the group leader. Furthermore different projects are presently under discussion with various interested industries such as Oerlikon Solar and HE-Arc/CSEM.

The future of the industrial plasma group after October 2013 is not yet clear due to the retirement of its leader, but some activities are supposed to be running for the next 2-3 years at least.

2.7 Gyrotron physics and simulations of mm-wave RF systems

The development of the gyrotron simulation code TWANG which has been intensively pursued in 2011, has turned out to be crucial in predicting novel operational regimes in gyrotron oscillators characterized by nanosecond pulses in the frame of the DNP-gyrotron developed for NMR spectroscopy applications (see Section 3.7). The experimental investigation and validation of this regime was essentially motivated by the findings based on the numerical simulations.

The modelling with TWANG of spurious interactions such as beam duct instabilities or the after cavity interaction (ACI) has been continued. By revisiting the interaction properties in the TCV 118GHz gyrotron cavity it was possible to show that this design is suffering of static ACI in which 10% of the RF power generated in the cavity is reconverted in electron beam kinetic energy. For the modelling of beam-duct instabilities and/or dynamic ACI, the underlying assumptions on which TWANG is based are violated and a particle-in-cell (PIC) numerical approach will be necessary.

The simulation of overmoded mm-wave system using finite elements codes such as COMSOL-multiphysics has been pursued. Quasi-optical matching components (MOU) between the gyrotron output and the overmoded HE_{11} transmission line are being completely designed using these simulation tools. Within the gyrotron DNP research programme, a Requip funding from SNSF and EPFL has been granted for the purchase of a Vector Network Analyser (VNA) with capabilities up to the THz frequency. Among a wide variety of applications, this facility will also be a key system for validating the simulation tools for mm-wave RF systems.

The spin-off activity of the gyrotron R&D programme, resulting in the foundation of the start-up company Swissto12, is receiving a very positive echo both via the numerous awards received by the company in 2012, but also the interest in their products by industry as well as by research laboratories in academic institutions.

2.7.1 Gyrotron physics and simulations

TWANG code

As mentioned above, the development of the time-dependent self-consistent monomode code TWANG has been intensively pursued in 2012. In view of writing a PIC version of this code, a parallelization of the code has been successfully performed using MPI. It is planned to pass to a PIC version in two steps. In the first step the PIC approach will be implemented on the linearized set of self-consistent equations governing the wave-particle dynamics. In a second step, one will extend it to the full nonlinear set of equations.

After Cavity Instabilities (ACI)

Using TWANG it has been shown that the TCV 118GHz-gyrotron suffers of static-ACI in which a spurious interaction remains in the launcher section placed after the extraction cavity and depletes the RF power by 10% corresponding to an absolute decrease of the available RF power in excess of 60kW. This effect is shown in Fig. 2.7.1 below.

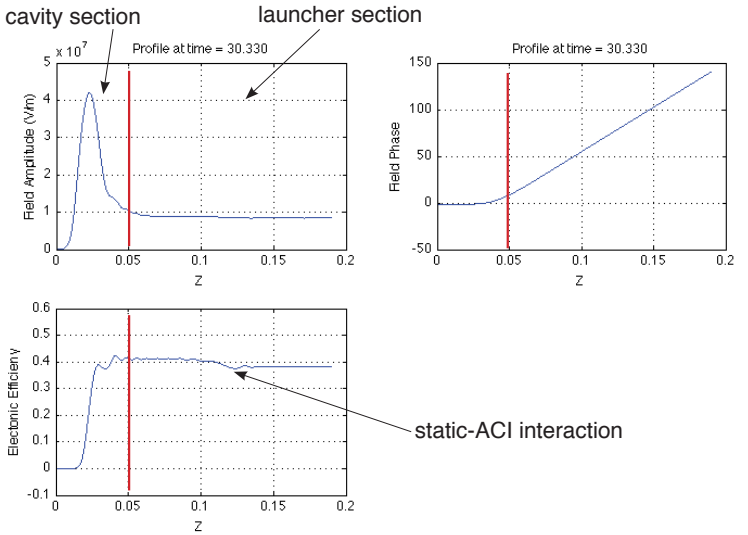

Fig. 2.7.1 *Simulated longitudinal profiles of: RF electric field amplitude (top-left), electric field phase (top-right) and electronic efficiency (bottom-left).*

For the study of dynamic ACI, a preliminary important step has been achieved by solving the issue related to the frequency dependent radiation boundary condition to be satisfied at the cavity exit. A numerical procedure to implement non-reflecting boundary conditions, based on the Laplace Transform, has been implemented and tested successfully in TWANG. These results are illustrated in Fig. 2.7.2 on a test case considering the 118GHz gyrotron cavity and imposing a constant magnetic field in the entire interaction region.

A thorough study of this ACI problem shows however that the time steps required are too small, invalidating thus the usual model assumption of separation of time scales between the RF field evolution and electron cavity traversal. This has motivated the development of the PIC version of TWANG in which no assumptions are made on the above mentioned time scale separation.

As previously mentioned a linear version of the PIC code will first be implemented. This PIC version is going to be benchmarked against a linearized self-consistent version of TWANG presently being studied and based on the above mentioned assumption on the time scale separation (slowtime scale model). The linear growth rate of the instability calculated with either linearized codes (PIC and slowtimescale) will be compared to the experimental data taken on the DNP-gyrotron experiment.

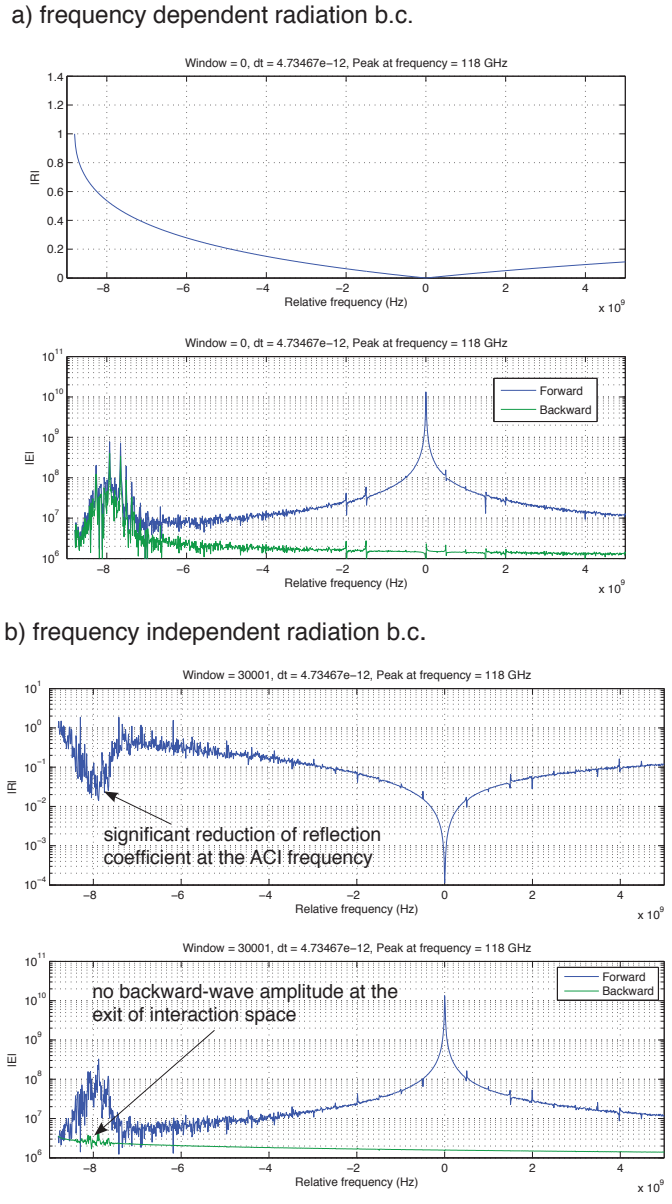

Fig. 2.7.2 *Reflection coefficient, |R|, and electric field amplitude, |E|, of the forward and backward propagating waves calculated at the output of the interaction space. The top two figures, a), are the results with the usual frequency-dependent radiation boundary condition. The bottom two figures, b), consider the newly implemented frequency-independent radiation boundary condition.*

Beam-duct instabilities

The linear version of TWANG either in the slowtimescale model or the PIC version will allow to study the conditions for the onset of instabilities in the beam duct. The time-dependent and self-consistent nature of the linear-TWANG simplifies the methodology for determining under which conditions (dielectric loading, geometry and/or magnetic field inhomogeneities) a positive growth rate of the instability is obtained.

Experimental studies on spurious instabilities

An experimental campaign dedicated to the study of spurious instabilities (beam-duct and/or ACI) is presently being carried out on the repaired 118GHz gyrotron part of the X3 ECH system of TCV.

3 TECHNICAL ACHIEVEMENTS

3.1 TCV operation

The TCV tokamak facility was operated intensively until the end of 2011 but was shut down for major maintenance and installation work from January to October 2012.

3.2 TCV ECH systems

The long maintenance of TCV during 2012 has allowed remedial work on the ECH system so to have it functional with the maximum X2 and X3 injected power at the restart of TCV operation in November 2012.

The 6 gyrotrons of the X2 system are presently ready for operation. The repaired gyrotron magnet has been fully commissioned and the gyrotron has been successfully tested in the repaired magnet. Significant damage was observed on one of the low field side X2 launchers during the TCV opening. The initiating source of the damage is under investigation, but it was certainly exacerbated by the RF beam: the launcher must be replaced. The manufacturing time exceeds the opening period. This dictates that only 5 X2 gyrotrons will be used at the beginning of the TCV campaign. Repairs are continuing on the damaged launcher.

The repaired X3 gyrotron has been successfully commissioned at CRPP. The existing X3 launching antenna has been redesigned with the aim of maximising the absorbed fraction under the constraint of minimizing the stray radiation effects associated with diffraction, refraction and/or reflection of gyrotron power which, with the existing launcher, have been identified to be a possible limitation on the tokamak operation. Geometric and quasi-optical calculations completed with linear ray-tracing/absorption simulations have been used to design and optimize the new top-launch mirror. Cold tests on the redesigned launcher have been made and the new launcher functions as expected.

The preparation of the upgrade of the X3 electron cyclotron heating system with three additional 1MW gyrotrons, in top-launch configuration, has been continued focusing more on technological aspects. This is described in this report in the section devoted to the TCV upgrades.

3.2.1 ECH security

The previous EC protection system constrained EC current drive operation to small toroidal launch angles since it had only limited machine coverage.

The new EC protection system will allow a more flexible operation of the EC installation and in particular operation with a large toroidal injection angle. This system has automatic detection of high stray power and automatically stops gyrotron operation when there is a risk of compromising TCV machine integrity. Observers exist on all TCV ports that have windows. The new protection system is complemented with “EC stray” shots each morning to confirm the integrity of the protection chain.

A new density security is also operational, tripping the gyrotrons if the measured density exceeds programmed “in-specs” limits (both below and above) on the density reference trace.

3.2.2 ECH real-time control

The new distributed real-time control system has been successfully integrated and commissioned including the EC system. It is routinely, extensively and very successfully exploited for the scientific programme of TCV. The results obtained with this system are described in section 2.1 of this report.

3.3 TCV Diagnostics

3.3.1 TCV Thomson scattering diagnostic

The development of novel and advanced scenarios of tokamak operation sets new requirements for plasma diagnostics. This is the case for the Thomson scattering system on TCV, which has been intensively used since the start of operation in 1992. In its present state, the system provides spatial profiles of electron temperature (T_e) and density (n_e) at repetition rates up to 60Hz. It comprises a cluster of 3 repetitively pulsed Nd:YAG lasers and filter spectrometers permitting measurements in the T_e range from 50eV to 20keV. The use of fibre optic components to collect the scattered radiation in the image plane of 3 wide-angle lens assemblies offers flexibility for the arrangement of the observation volumes along the laser beam (intersecting the plasma in vertical direction). At present, 23 spatial points are available for measurements in the plasma core region. A sub-system, comprising 9 spectrometers with adapted filter sets, is dedicated to measurements with higher spatial resolution in the so-called “pedestal” region near the plasma edge.

An extraordinary financial allocation from EPFL is being used to upgrade this system by adding more spatial channels to improve the coverage of the plasma cross section and obtain better accuracy in the strong gradient regions of the profiles, in particular at the plasma edge pedestal.

For this purpose a series of 20 new filter spectrometers is being constructed. The design is based on a spectrometer unit developed at CCFE-Culham, UK, for the same type of application. The spectrometers will be equipped with sets of 4 or 5 interference filters with Si avalanche photodiode detectors. Two filter sets were chosen to match the width of the spectrum of scattered radiation for the T_e range of interest. The filter pass bands are shown schematically in Fig. 3.3.1(a,b). The performance of the spectrometers over a range of plasma parameters has been simulated and representative results are shown in Fig. 3.3.2(a,b). The version (a) is designed for plasma core measurements, with a T_e range from 20eV to >15eV, and version (b) for the edge region with a T_e range from 10eV to >2keV.

For the new spectrometers, electronic circuits for signal processing are being designed at CRPP. These will comprise amplifiers with remotely selectable gains and a circuit for stabilisation of the detector response that is sensitive to variations of the surrounding temperature. Each spectrometer will include a test circuit sending short light pulses from a LED to all detectors in the unit for monitoring and calibration purposes.

In the TCV Thomson scattering system, an individual spectrometer is attributed to each observation chord. The spatial sampling intervals and spatial resolution are defined by the arrangement of fibre bundles in the image plane of the camera lens and by the size of their front ends. Aiming at improved spatial resolution, whilst making use of existing fibre bundles (made from several large-core fibres), we have decided to split the fibre bundles at the rear (spectrometer) end and sort the fibres to feed 2 (or 3) spectrometers per bundle. With the upgraded system, we plan a total number of 40 to 42 spatial channels with a spatial resolution of 16mm and 12mm for observation in the plasma core and near the edge, respectively.

Most components like detectors, filters and optics required for the new set of spectrometers are already ordered and will be delivered by early 2013. It is planned to install the new equipment on TCV during the second half of 2013.

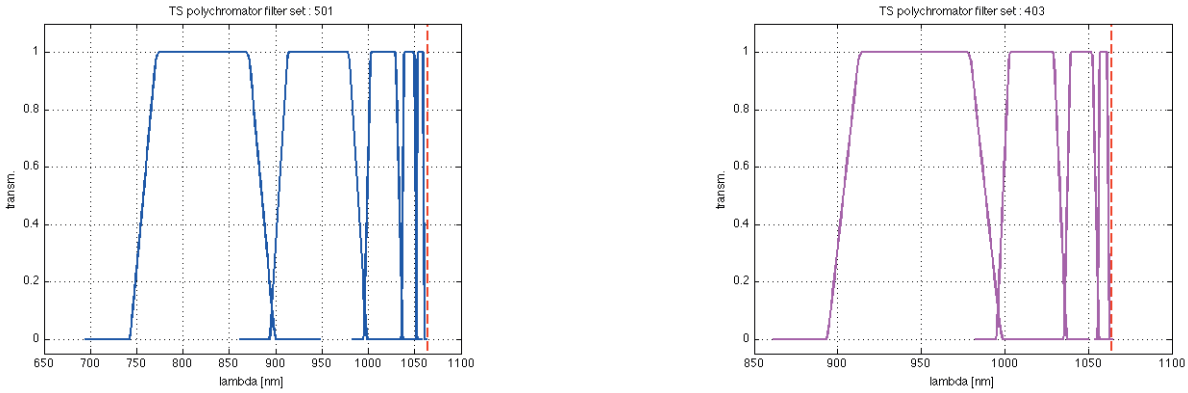

Fig. 3.3.1 *(a,b) Transmission curves of the interference filters in the new spectrometers (dashed line marks Nd:YAG laser wavelength) a) configuration with 5 channels for observation in the plasma core region b) configuration with 4 channels for observation near the plasma edge*

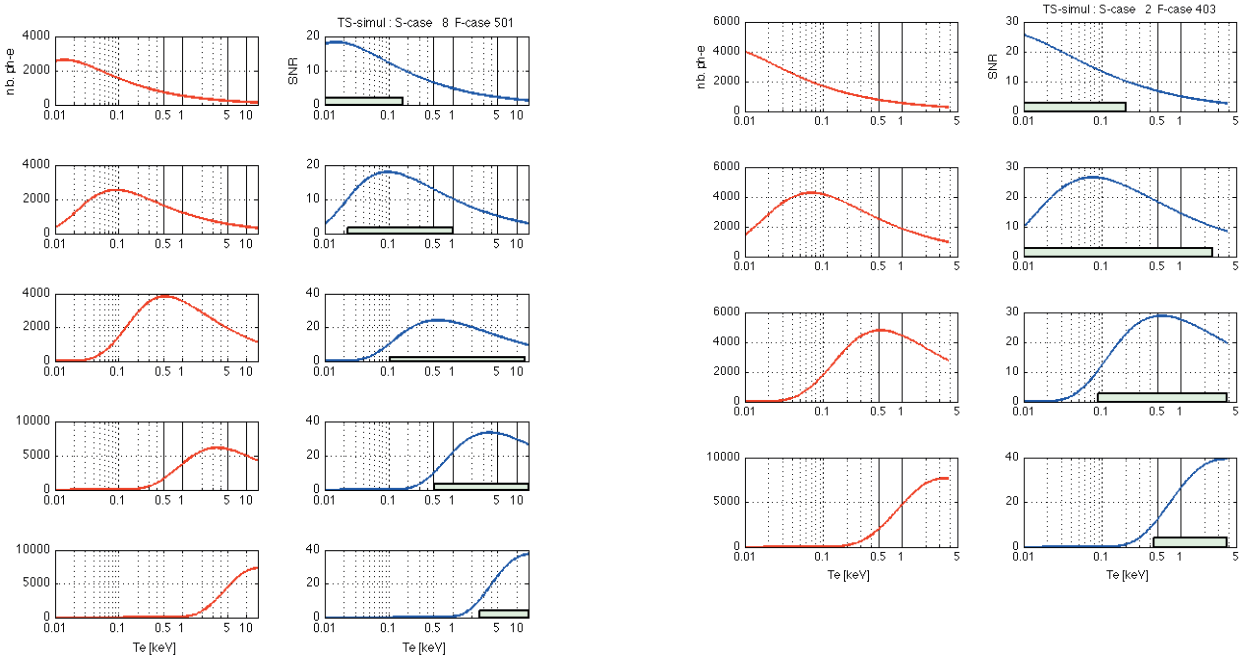

Fig. 3.3.2 *(a,b) Number of photoelectrons per spectral channel and signal-to-noise-ratio (SNR) as function of electron temperature T_e. For a representative set of system parameters and electron density n_e=1.10^{19}m^{-3} (a) 5-channel version (core) (b) 4-channel version (edge)*

3.3.2 Edge diagnostics upgrade

During the 2012 shutdown, a new array of Langmuir probes was installed in the lower part of the of the TCV outer wall. It consists of 17 flush-mounted graphite tips with a spatial resolution of 16mm (Fig. 3.3.3 left). This new probe array will increase the coverage of regions where plasma-wall interactions occur. In particular, for the snowflake diverted plasma configuration, simultaneous heat load measurements around all four strike points will become possible (Fig. 3.3.3 right). This new array of probes will be also be beneficial in the characterisation of diverted plasma at negative triangularity.

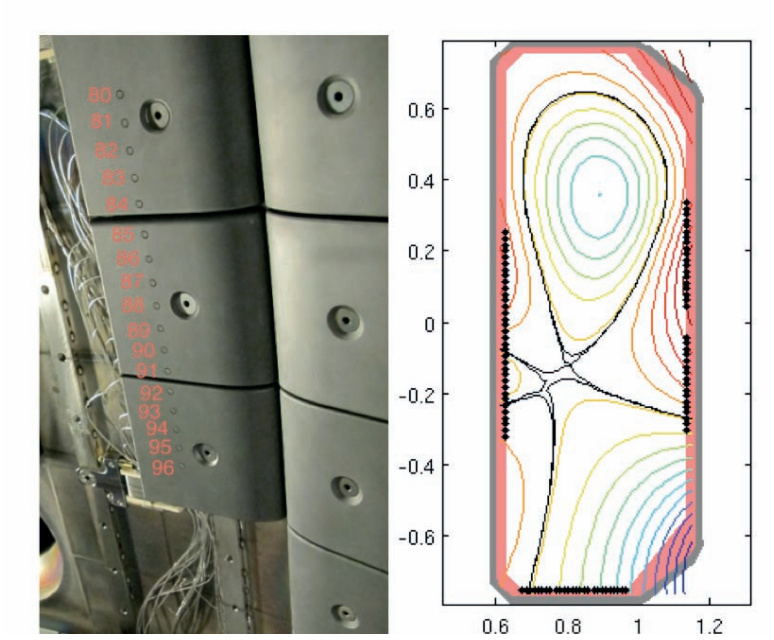

Fig. 3.3.3 *New Langmuir probe array being installed inside TCV (left). Reconstructed plasma equilibrium for a snowflake divertor plasma (right) showing that LPs (black dots) are covering the four strike points of this configuration.*

To better characterize the plasma scrape-off layer, a reciprocating probe with several Langmuir probes and magnetic sensors will be installed during the next year through collaboration with colleagues from the University of California San Diego (UCSD).

3.3.3 Infrared Camera System

The infrared camera system of TCV consists of a Thermosensorik camera CMT256M HS, which uses a CMT (Cadmium Mercury Telluride) detector with sensitivity in the infrared range 1.5-5.1μm, and two relay optics for imaging the central column and floor carbon tiles. This diagnostic provides measurements of the tile surface temperature, which is used to estimate the power deposition onto the wall. The camera can operate on slow timescales, to provide information about steady-state divertor behaviour, and on fast timescales (up to 25kHz), enabling ELM and disruption-related studies. In order to improve the calibration of the horizontal system, a heated tile with six thermocouples was installed on the central column (Fig. 3.3.4). It will be used to improve the estimation of the carbon tile IR emissivity, as well the transmission of the optical components in the

relay optics. The transmission of the optical components in the relay optics is obtained by comparing the measured intensity with a previous, *in situ,* calibration in which a black body source was placed inside TCV. The tile emissivity can be obtained by comparing the measured intensity with that expected from a black body. Since the estimate of the heat power deposition from surface temperature measurements relies on the thermal properties of a thin layer on the tile surface, the thermocouples are used to constrain the IR measurements of the total amount of energy stored in the tile during a discharge.

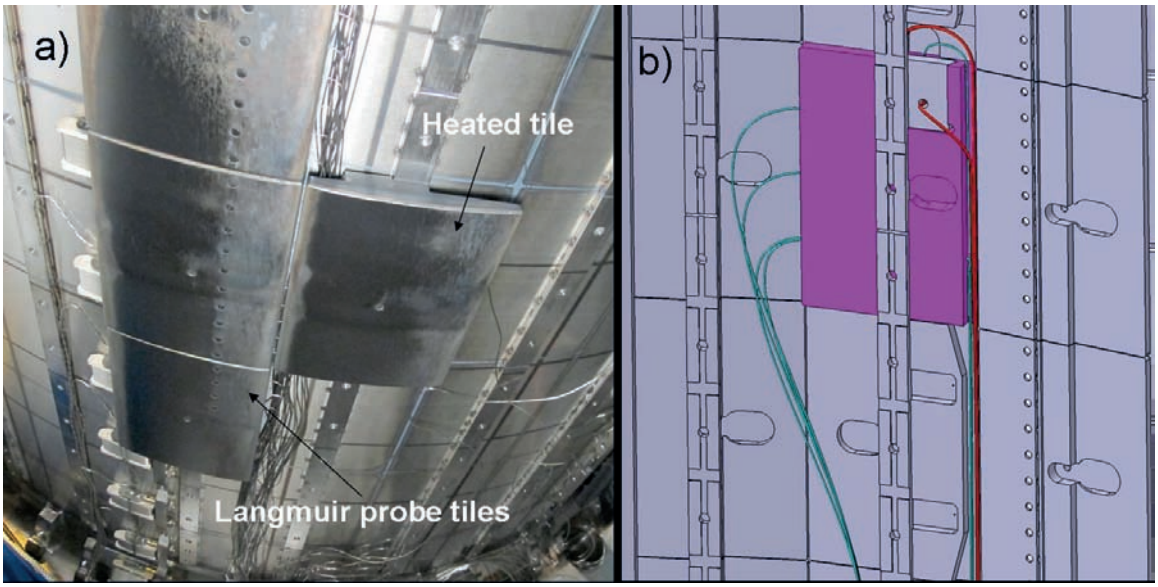

Fig. 3.3.4 *(a) Central column tiles housing the Langmuir probes and heated tile with six thermocouples installed. (b) Mechanical drawing of the heated tile with six thermocouples and heating element.*

3.3.4 Hard X-ray tomography

Progress has continued in the development of a new spectroscopic hard X-ray tomography diagnostic. The complete system will include four cameras, each with 24 CdTe detectors, plus an additional "blind" monitoring detector situated behind heavy tungsten shielding to discriminate against non-collimated γ rays. The primary goal of the diagnostic is to study for the first time the full 2D distribution of bremsstrahlung emission from suprathermal electrons, and compare its poloidal dependence with theoretical predictions. The first camera has been in operation since 2011 and has fully delivered the design specifications, resulting in a host of new high-quality results.

New developments in 2012 included: the construction of the entire second camera, which is now ready for installation on TCV; a large fraction of the mechanical design of the third camera, which should be completed by the end of 2012; and the installation of the primary vacuum interface for the fourth camera. The latter implies that all the remaining installations on TCV will not require a break in the primary vacuum.

3.3.5 Tangential X-ray detector array

This diagnostic, comprising 7 detectors and used to detect the total flux of hard X-ray radiation emitted by high-energy electrons along the magnetic field lines, has been

equipped with a new set of amplifiers built in-house, to replace the original ones supplied with the system, which had proved unsatisfactory.

3.3.6 Reflectometry

A number of reflectometers are installed on TCV, sharing a single port among them as well as with an electron cyclotron emission diagnostic. These instruments are all extremely vulnerable to stray radiation from the powerful microwave sources that are operated on TCV, and indeed several components have been damaged or destroyed in the past. A stripline notch filter at 82.7GHz (the frequency of the microwave sources) proved insufficient to avoid this problem as it was itself severely damaged by radiation and then failed to protect the equipment behind it. A lowpass filter based on a reflective metal mesh was then considered as a primary line of defence. We tested destructively a similar filter using an 82.7GHz gyrotron, and, based on this test, procured a dedicated filter for TCV. In conjunction with a thermal detector observing the back of the filter and interlocked to the microwave power supplies, it is believed that this filter will protect the equipment sufficiently, although it provides an attenuation of only 23 dB. The stripline filter, which has a depth of 70dB, has been repaired and will still be used as the final line of defence.

3.3.7 Tangential phase contrast imaging

This diagnostic consists of a laser imaging apparatus to study core density fluctuations with high spatial localisation (down to 1% of the minor radius), thanks to a tangential arrangement. The system produced first data in December 2011. Two primary flaws were discovered during the initial tests. Firstly, the beam displayed severe aberrations after passing through the vessel; the primary aberration was astigmatism, with smaller contributions from higher-order components. Secondly, the beam shifts caused by mechanical vibrations of optics mounted on the vacuum vessel were significantly larger and at higher frequency than expected. As a result, the feedback stabilisation system that had been included in the diagnostic to damp these vibrations on the focal plane was not optimised for the nature of the vibrations and did not prove fully adequate. Both of these problems have the primary consequence of a significant increase in the minimum fluctuation wave number that can be resolved. While the astigmatism was temporarily compensated with the addition of two cylindrical lenses, the performance degradation remained significant. Nonetheless, the initial experiments have yielded valuable results, including the discovery of a coherent oscillation mode never before observed on TCV and believed to play a significant role in transport.

During an extended vessel opening in 2012, a back-calibration was performed in order to validate these results, using ultrasonic waves in air. Subsequently, the in-vessel optics were removed and analysed with the aim of resolving the problems observed. A design flaw in the way the five vessel mirrors were mounted was identified, leading to a (primarily cylindrical) deformation of each mirror, consistent with the observed aberrations. The mounting concept was changed drastically, ensuring that each plane mirror surface is constrained at exactly three points. To tackle the vibration problem, the mirror mounts were rebuilt using titanium instead of stainless steel to reduce weight and conductivity, and with appropriate slits to significantly reduce the paths for current loops, under the assumption that inductive forces are primarily responsible for the vibrations. After reinstallation, we have already been able to determine that the aberrations have disappeared. Vibration measurements will be performed in 2013.

3.3.8 Electron Cyclotron Emission Radiometers

TCV has been equipped with a suite of heterodyne radiometers since 2001 for ECE electron temperature measurements. The first radiometer covers the radio frequency (RF) range 83GHz to 114GHz and was installed with the intention of measuring electron cyclotron emission (ECE) from the high field side (HFS) of the machine. This unit is referred to as the HFS radiometer. The second radiometer covers the RF range 65GHz to 87GHz and measures the ECE spectrum from the low field side (LFS) of TCV. It is known as the LFS radiometer. Both the LFS and HFS radiometers are ageing and, indeed, their respective intermediate frequency (IF) and video stages contain failing and failed components. Using financial support offered by the EPFL it was decided to refurbish both radiometers' IF and video sections. A procurement package was put in place to replace the entire IF and video sections of both radiometers. The IF equipment has been purchased and delivered to the CRPP. Initial tests produced satisfactory results. Video stage amplifiers, designed by the electronics department of the CRPP, are under construction. It is expected that the refurbished radiometers will come on-line in early 2013.

3.3.9 Correlation Electron cyclotron Emission

A new six-channel correlation electron cyclotron emission (CECE) radiometer has been installed on TCV. It comprises six, independently controlled, tuneable YIG filters. It is planned to use the six-channel CECE radiometer taking signal from the high frequency side of the LFS ECE radiometer. The additional channels will enable radial scans of electron temperature fluctuation measurements to be made in one plasma discharge where previously at least four discharges were required. The new CECE radiometer is operational and ready for service following the long 2012 TCV shutdown.

In addition a new RF front end has been procured for the CECE radiometer allowing it to use all of available signal thus improving its signal to noise. In addition, its frequency coverage has been increased permitting HFS measurements. It is expected to be able to use the upgraded CECE radiometer to make meaningful measurements for negative triangularity discharges that were previously impossible due to lack of signal and radial coverage.

3.3.10 300GHz interferometer (1mm)

The existing, unreliable 280GHz interferometer will be replaced by a homodyne 300GHz interferometer. RF components for probe beam and receiver have been purchased and a new optical diplexer ordered. The latter allows simple control of the power levels in the local oscillator and signal arms of the interferometer. A new electronics suite for demodulation and phase tracking will be designed and built in-house.

3.3.11 CXRS

With access to the TCV vessel available during the TCV 2012 opening, it was decided to perform a complete CXRS chord alignment verification. Furthermore, following renewed interest in using the high field side (HFS) chord array as a method to extract the poloidal rotation, particular care was taken to calibrate the position of the HFS CXRS observation camera.

The absolute CXRS sensitivity (from which the impurity content is calculated) requires a measurement of the whole detector chain from fibre optic collection optics through the spectrometers to the CCD detectors. A “lab sphere” was placed in the TCV torus vessel (Fig. 3.3.5) so as to optically fill the CXRS viewing camera. It was thus possible to measure the light flux that finally arrived on the CCD detector of the whole system which can only be estimated without access to the torus. Similarly, by retro-illuminating the observation fibres with a solid state diode laser, the position of the LFS and HFS camera chords was registered using a target placed in the same position as the diagnostic neutral beam path (Fig. 3.4.6).

By removing the target and locating the retro-light illuminated circle from the fibres onto the TCV vessel wall, position markers were assessed so that, during 2013 with the vacuum vessel closed, it will be possible to verify that the CXRS lines of sight have not moved.

Fig. 3.3.5 *Picture showing the absolute calibration sphere placed inside the TCV vessel during the TCV 2012 vacuum opening.*

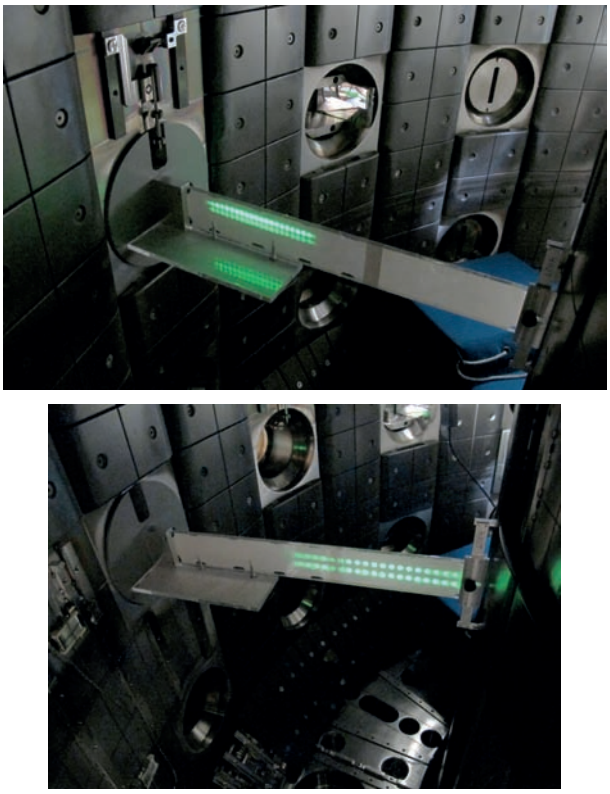

Fig. 3.3.6 *Retrolit target for the LFS (top) and HFS (bottom) showing the CXRS observation chord array.*

Third Andor CXRS CCD camera

Following a successful bid for internal funding from the EPFL School of Basic Sciences, a third high gain CCD camera was purchased for the CXRS system. This camera is slightly upgraded from those purchased in 2010 and is capable of providing data to a remote PC using a “CamLink” connection offering the possibility of real-time ion temperature parameter measurements. Initially, it is intended to use the device to replace the HFS toroidal rotation camera that should facilitate CXRS measurements in a region where, by plasma attenuation, the signal is relatively small.

3.3.12 Oblique ECE

The fast polarizers used in the Oblique ECE system were tested for the first time during TCV operations. The variation of coupling to a low power broadband receiver was roughly consistent with modelling predictions. More information is found in the results section on 2-pass EC transmission measurements and quasi-linear effects of EC absorption.

3.4 TCV control

3.4.1 Specific computer node for real time equilibrium reconstruction

The computer node 3 (CPU only node) of the TCV digital control system was replaced by a more powerful PC dedicated to running real-time (RT) plasma flux surface reconstruction codes (RTLIUQE code). This new computer node features an "unlocked" Intel Core i7 processor that, with additional cooling, is able to reliably overclock at 5GHz. Together with strong code development, this system is expected to provide RTLIUQE results in less than 1ms, the cycle time identified for TCV operations. The RTLIUQE algorithm is programmed in the Simulink/Matlab language and has been tested in the RT cycle (without plasma to date). In this workflow, the Simulink model is translated into C language, and then compiled, linked and the resulting executable code uploaded to the RT node. Using the reflective memory network between the RT computers, the RTLIUQE executable code was able to use shared, acquired and calculated data, which are posted by the other computer nodes, and then post its results back through the reflective memory. The fastest performance achieved to date for the Grad-Shafranov solver was 0.3ms. The RTLIUQE will provide a real-time estimation of the last closed flux surface, which offers the possibilities to control the plasma shape. This system is expected to have a strong influence on many aspects of TCV physics research, providing information that was previously only available after the plasma discharge.

3.4.2 New computer node for XTOMO acquisition

RT computer node 3 was modified to become data acquisition node (RT node 5). This computer node now controls the three XTOMO acquisition cards via an Adlink pci-bus extender so that the XTOMO diagnostic now can be used in two modes. "Acquisition mode" offers high frequency continuous acquisition, preferred for post shot analysis, but the data are not available in real time. In "Real time mode", the XTOMO measurements are continuously acquired and posted to the shared reflective memory network. Easy remote switching between these operational modes permits legacy data acquisition and analysis together with RT XTOMO data calculations.

3.4.3 Project FPGA

The TCV real time control system has been designed to be readily extendable to include newer technologies. The recently rapid evolution of high power dedicated calculation computer chip FPGAs offer a performance improvement for plasma fusion engineering both for diagnostic and RT control. The hardware configurable FPGAs offer the possibilities of low latency control. Using a low-cost evaluation board system, only few microseconds were required for a complete cycle: acquiring data from ADCs, performing a simple calculation on the FPGAs, and sending the result to the DACs. A prototype

system using this FPGA board combining 4 analogue inputs and 4 analogue outputs is directly applicable for real applications in TCV, such as robust control of density diagnostics and plasma control such as fast vertical stabilization control. FPGAs can also be used to pre-treat diagnostic data for the TCV digital control system. By generalising the digital control system paradigm, data are acquired directly from the diagnostic and complex calculations performed prior to their usage in the main Plasma Control System eg: an FPGA-based subsystem could take the raw data from a pickup coil at high rates, perform a Fast Fourier Transform filter, and send only the requested coefficients to the control system.

3.4.4 Graphical user interface for TCV real time control system

TCV's digital control system (DCS) is increasingly used for everyday TCV experimental operation. The graphical user interface was revised and upgraded so that it can be accessed by non-control experts. Via the graphical interface, the user can observe the evolution of the DCS's state machine during TCV discharge, supervise the messages and errors and monitor the network connection of the computer nodes and acquisition cards. In normal operations, the digital control system is initiated and run automatically by TCV's plant and discharge control systems. However, in case of problems, the graphical interface displays them and performs a limited range of automatic actions to resolve the problem. In continuation of this theme, work is progressing to store the Simulink model of control algorithms on a SVN server for better version traceability over the coming years.

3.5 TCV upgrades

3.5.1 Introduction

To extend TCV operational domain towards the burning plasma regime and enhance the reactor relevance of its results, some hardware upgrades will need to be implemented. The main goal will be to make it possible on TCV to heat high-density plasmas with variable ion and electron temperature ratio, and explore new plasma shapes in the presence of high performance plasmas.

Although financial support for the upgrades still needs to be secured, feasibility studies and preparation work have already started a few years ago. The preliminary design of the ELM control coil system was previously completed.

Activities in 2012 were dedicated to the preparation of the minimal set of upgrades that was endorsed in the 2010 CRPP audit, encompassing the installation of a ~1MW neutral beam heating system and an increase of the microwave plasma heating power at the third harmonic (2MW). These, together with the modifications of in-vessel components (low-field-side tiles) necessary to combine shape capabilities with increased heating power, will put TCV in a unique position to contribute to ITER and DEMO physics basis. TCV will become able to disentangle effects of electron-ion coupling, rotation, q_{95}, edge density control and shape, in L- and H-modes and study heat, particle and momentum transport in dominantly electron heated discharges with varying T_e/T_i and keeping shape flexibility.

3.5.2 Low field side modifications

In plasma scenarios of interest for the TCV scientific missions, which were recently developed and are planned for optimizing tokamak operation, such as additionally heated H-modes with negative triangularity or snowflake divertors, the configuration includes separatrix legs connected to the low field side (LFS) wall. However, the present set of tiles on the LFS of the vessel is not designed for high power handling. Thus, in order to preserve the TCV shaping flexibility in the presence of strong additional heating, an upgrade of the internal LFS wall is investigated.

The LFS high purity graphite protection tiles were installed in TCV between 1996 and 1998 and completely cleaned by abrasive removal of deposits with boron carbide powder projection in 2007. The basic geometric shape featuring elliptical edges in the toroidal direction was optimized for the large gaps at the port apertures to avoid exposing metallic or sharp edges to excessive plasma particle flux and radiation.

Since the joint installation of an array of low field side coils (LFSC) and an upgrade of the LFS graphite tiles has for the moment been abandoned, the following local modifications to the LFS tiles were performed during the 2012 opening of TCV. For the tangential phase contrast imaging (TPCI) diagnostic system, 8 newly designed graphite tiles were added around the two ports used by the optical mirror systems to protect the reflectors from excessive impurity deposition and absorption of scattered mm-waves. The *in situ* spot welding of additional rails was required to support these new tiles. The LFS Langmuir probe arrays were extended with the addition of 17 probe tips in 3 graphite tiles of the lower half of the torus. Some adjacent tiles were modified on their backside to accommodate the new routing of the Thermocoax cables carrying the signals to the feed-throughs located at the bottom of the torus.

In preparation for the installation of a neutral beam heating system (NBH), calculations have been performed to estimate the heat loads at the LFS wall in the absence of plasma or with only partial absorption by the plasma. Results indicate a 6.3kW/cm^2 on-axis peak power density, a value requiring a local redesign of the intercepting tiles and possibly the substitution of graphite with a refractory metal, such as tungsten, to withstand the temperature rise and transient thermo-mechanical stresses.

3.5.3 Neutral beam heating

In the frame of preparation for the installation on the Neutral Beam Heating (NBH) system on the TCV, the earlier analysis of the plasma scenarios of relevance for NBH, preliminary design of the neutral beam injector and structural analysis of vacuum vessel (VV) deformation with installation of the new ports for NBI were accomplished in 2012 by engineering and feasibility study of the TCV VV modification as well as by modelling of the beam propagation in the beam duct with scrapers and power load on limiters, tokamak central column and beam dump. The installation of two low divergence injectors in tangential double path alignment with energy below 20-35keV, neutral beam power of 1MW per injector is recently the base option.

To implement the tangential NB alignment on the TCV, a modification of the tokamak vacuum vessel to create new ports, specially designed for NBIs and fitted between magnetic field coils is considered. The analysis of the possibility of the *in situ* modifications of the TCV vacuum vessel to provide access for neutral beams has been completed by the De Pretto Industrie S.r.l., Schio, Italy (manufacturer of the original TCV vessel). The contract on the technological feasibility of the *in situ* vacuum vessel

modification was aiming at defining the sequence of activities and the technical boundary conditions for the installation of the two new tangential NBI ports on the TCV. The work comprised on-site inspection of the TCV vacuum vessel by De Pretto specialists, the design and identification of tools for vessel modification, 3D modelling of the modified area, definition of operational planning and risk analysis for the modification.

The propagation of the NB in the TCV has been analyzed to estimate beam losses and heat load on different elements along the beam path. The initial beam is generated by an ion emitter (IOS) with a slit apertures geometry. This emitter has intrinsically anisotropic angular divergence along and across slits (8x18mrad). The beam is geometrically focused at 3.6m from the emitter. The grid diameter of 200mm has been chosen for NBI-TCV. The total current of the initial deuterium ion beam is 40A, ion energy –35kV. The ion beam is converted into the neutral beam in a neutralizer with efficiency η=82% for deuterium. Thus, the 1.4MW of ion power is converted in 1.148MW in neutrals. The mean ion power density on the IOS is 4.46kW/cm^2. The beam duct is modelled by a set of plane scrapers (diaphragms) with different shapes (circle, ellipse, rectangle) placed perpendicularly to the beam. The geometry and position limiters are chosen according to the preliminary injector design (done by Budker INP, RF), the geometry of existing TCV vacuum vessel and the proposed design of the new TCV port with maximal aperture of 240x200mm. Limiters in the beam duct incorporate the neutralization tube, limiter on the exit from injector vacuum tank, NBI-TCV gate valve, DC break, bellow and the TCV port (Fig. 3.5.1(A)). The edge of the beam intersects with the TCV central column, the shine-trough beam power is deposited on the low field side (LFS) of the tokamak vessel. The maximal power load in the beam duct of about 30W/cm^2 is estimated on the wall of the port extension near the entrance in the tokamak; it is compatible with the use of stainless steel (316LN, wall thickness ≥5mm) as a material of the beam duct. The power loss in the beam duct is less than 2% of the injector neutral beam power.

The power load on the TCV central column without beam attenuation by the plasma does not exceed 2.5MW/m^2 (Fig.3.5.1(C)) and is well below the design operational limit for CC graphite tiles (25MW/m^2 during 2sec plasma ELMy H-mode discharge). On the other hand, the maximal power load on the beam dump (LFS wall) without attenuation in plasma is expected to be 50MW/m^2. It is thus not compatible for 1-2s beam pulse with the existing LFS first wall and even with any feasible design of the beam dump fitted in the TCV vessel. The beam dump power load reduces to about 18MW/m^2 by attenuation in plasma with on-axis density of 10^{19}m^{-3} and parabolic profile. The design of the beam dump with graphite tiles similar to the central column should permit to use the NBI at most of the TCV scenarios with vertically centred plasma. It is considered to incorporate the design of the beam dump in the incoming activity with the modification of in-vessel component (LFS tiles) aimed at extending the TCV shape capability with increased heating power. The design of an interlock system to avoid NB injection without sufficient plasma density along the beam path with a time response better than 100ms is critical for the implementation of NBI on the TCV.

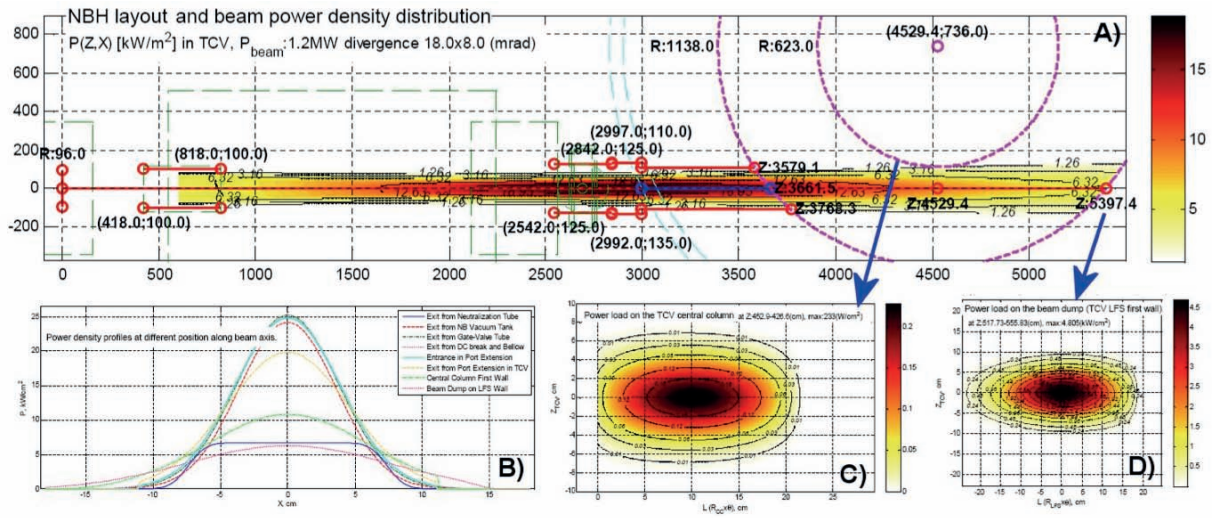

Fig.3.5.1 *Modelling of the neutral-beam propagation in a duct with scrapers:*
A) geometrical layout and beam power density distribution;
B) power density distribution across beam at different positions;
C) power load on the central column (without plasma);
D) power load on the beam dump (without plasma).

3.5.4 TCV/EC-system upgrade

X3-1MW/2s gyrotrons

The change of paradigm for the European ITER gyrotron has somehow modified the strategy for developing the X3 gyrotrons for the upgrade of the TCV/EC-system. In 2012, Fusion for Energy (F4E) has decided to reorient the ITER gyrotron development programme from the coaxial cavity 2MW/170GHz gyrotron to the conventional cavity 1MW/170GHz version. An initial design of this ITER gyrotron has been completed in 2010, in the frame of GRT-08 activities. This design includes many state-of-the-art features in the domain of high-power gyrotrons for fusion applications. In conjunction to the gyrotron design, the specifications of a He-free superconducting magnet (SCM) for operating the gyrotron have been defined and the Call for Tender documents have been prepared at CRPP. This R&D programme is consistent with the ITER requirements and is carried out within the European Gyrotron Consortium (EGYC) and supervised by F4E. The details of this activity will be found in the present report under section 4.2: *ITER 170GHz gyrotron.*

For taking advantage of this reorientation and stimulate the synergy with the ongoing ITER programme, CRPP has decided to carry out a predesign of the gyrotron for the TCV-upgrade based on the 1MW/170GHz ITER gyrotron. Moreover, the He-free superconducting magnet specifications and tendering documents will eventually be used for purchasing the SCM's for the TCV/EC-system upgrade. The preliminary activities of the reoriented programme for the TCV upgrade will be carried out in 2013.

X3 top-launcher

As mentioned earlier under section 3.2: *TCV ECH system,* the optics of X3 launching antenna has been completely redesigned. The new mirror design will be tested and validated during the coming TCV experimental campaign

A preliminary thermal calculation has shown that the top-launch mirror design is compatible with an operation considering an incident power of 3MW. In the frame of the TCV upgrade project, it remains to perform a quantitative analysis of the thermo-mechanical properties of the X3 top-launch mirror where also the mirror deformation is considered with the possible perturbation of the optical properties. This activity will be carried out in 2013

3.6 Superconductivity

3.6.1 Faster cyclic loading operation for SULTAN samples

A major object of the test of the ITER conductors in SULTAN is the "cyclic loading", consisting of ramping up and down the current in the sample. The rate of cyclic loading is a limiting factor for the test of the CS conductors, which should be tested up to 30 000 load cycles. Until 2009, the duration of one cycle was about 2 minutes, limited by the voltage of the power supply of the primary coil of the superconducting transformer (±10V). With a new power supply procured in 2009 the rate of cyclic loading could be doubled, but the full voltage of the power supply (±40V) could not be exploited, as the electronic of the quench detection was saturated by the large inductive voltages.

Under contract with IO, a new quench detection system for the primary coil of the transformer was designed, built and installed in August 2012. The new features include a faster sampling rate (up to 3kHz compared to previous 100Hz), an online visualization of the signals, and larger allowed input voltages. The new system was commissioned in August. Now the full voltage of the power supply is accessible for faster cyclic loading: one load cycle of CS conductor lasts 30s, i.e. the cyclic loading rate is doubled.

3.7 Gyrotron for Dynamic Nuclear Polarization (DNP) enhanced Nuclear Magnetic Resonance (NMR) Spectroscopy*

The DNP gyrotron has been delivered in December 2011 and integrated in the complete DNP gyrotron setup in January 2012. The system integration and the commissioning of the protection and control system was completed by March 1st 2012. A very significant effort has been devoted to the design and realization of the gyrotron control and protection system. This activity has been carried out within a joint effort between CRPP and LPMN of EPFL. One essential goal for this control/protection system is related to the fact that eventually the gyrotron will be used by scientific personnel specialized in NMR spectroscopy, but with very little knowledge of the physics and technology associated to the gyrotron. It is therefore essential that the control and protection system allows non-expert personnel to safely and efficiently operate this scientific equipment. The formal contractual gyrotron acceptance test has been succesfully carried out in the presence of Thales representatives on March 8-9, 2012. In Figure 3.7.1, the layout of the entire system is shown.

* Work not belonging to the EURATOM Association's work programme, supported by Requip (no. 206021-121303/1), Sinergia (no. CRSI20-122708/1) and (no: 200020-120503/1) grants of the Swiss National Science Foundation, by the EPFL and by the Faculty of Basic Sciences of EPFL.

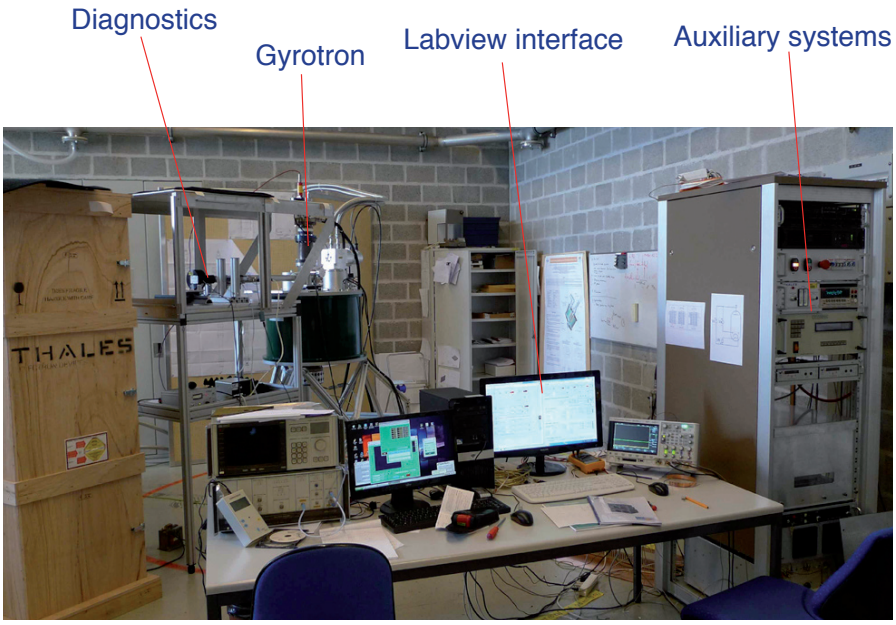

Fig. 3.7.1 *Overview of the gyrotron, diagnostics devices in place, power supplies, protection and control system.*

Very extensive experimental studies of this gyrotron have been carried out and are presently ongoing at CRPP. After these studies the gyrotron will be moved to LPMN and integrated into the DNP/NMR experimental set-up. From the operational point of view, the gyrotron operation is extremely reliable and flexible. It has to be stressed that this is a first prototype gyrotron and it has met both the operational criteria (thanks to the know-how of Thales in manufacturing this complex device) and the scientific criteria far beyond expectations.

As compared to gyrotrons presently used in DNP/NMR experiments, we have demonstrated that this specific gyrotron design allows us to significantly extend the experimental capabilities in the domain of DNP/NMR spectroscopy. These features are for example : continuous frequency tuning over 1GHz bandwidth, short-pulse (10μs) to CW regime with arbitrary duty-cycle, fast frequency tuning (1ms) over 80-100MHz.

This system has revealed to be an ideal experimental set-up for studying basic wave-particle interaction dynamics in the domain of coherent radiation by intense electron beams. It has been shown that a variety of operational domains starting from linear theory up to chaotic regimes can be experimentally investigated. These novel operational domains are hardly accessible with high-power gyrotrons for magnetic fusion applications. The accessibility to non-stationary operating points, characterized by the excitation of side-bands, allows us to explore novel regimes such as nanosecond pulsed modes. The development of a numerical code, TWANG, has been shown to be essential in predicting these new operational regimes and is presently used for analysing and interpreting the experimental data. The gyrotron R&D programme for fusion applications will also largely benefit from this code development.

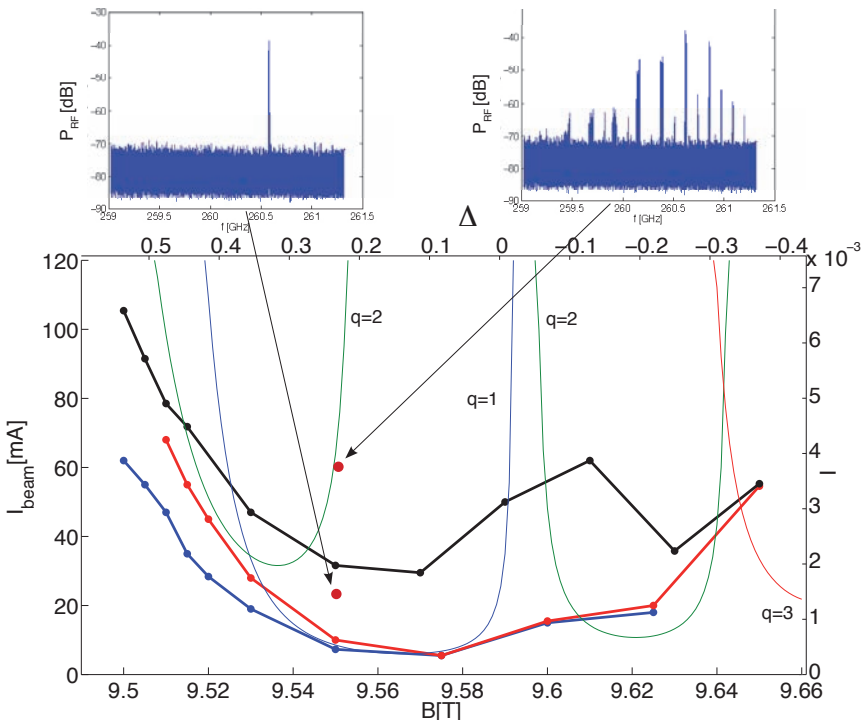

Fig. 3.7.2 *Experimentally observed operating regimes in the magnetic field, B, beam-current, I_{beam}, space. The red thick-line represents the starting current curve. The blue thick-line, the no-oscillation region. The black thick-line the starting current curve for nonstationary operating points characterized by the sudden appearance of side-bands. The two insets show the frequency spectra for a monomode regime (top left) and a multimode regime (top right) with side-bands. The thin continuous lines are the linear starting current curves for different longitudinal modes based on a fixed-field, cold-cavity profile.*

A research activity has recently started as a PhD project to investigate the physics of gyrotrons in short-pulse nanosecond operation regimes. From the educational point of view this gyrotron experiment is also well suited for Semester and Master projects.

4 ACTIVITIES IN SUPPORT OF ITER

4.1 Introduction

This chapter describes activities which are aimed directly towards ITER construction. They encompass the main fields of expertise of the CRPP, namely the technology of ECW systems, supraconductivity, and plasma control.

4.2 ITER 170GHZ gyrotron and its test facility

4.2.1 Coaxial Cavity Gyrotron refurbished First Prototype tests

Summary of the activities

Due to unexpected events during the manufacture, the refurbished first prototype of 2MW coaxial gyrotron for ITER was delivered end of September 2011, with almost one year of delay. A leak developed during the transport and the tube was untight upon arrival. The vacuum leak could nevertheless be fixed and it was decided to start experiments, in spite of the reduced expectable maximal pulse length.

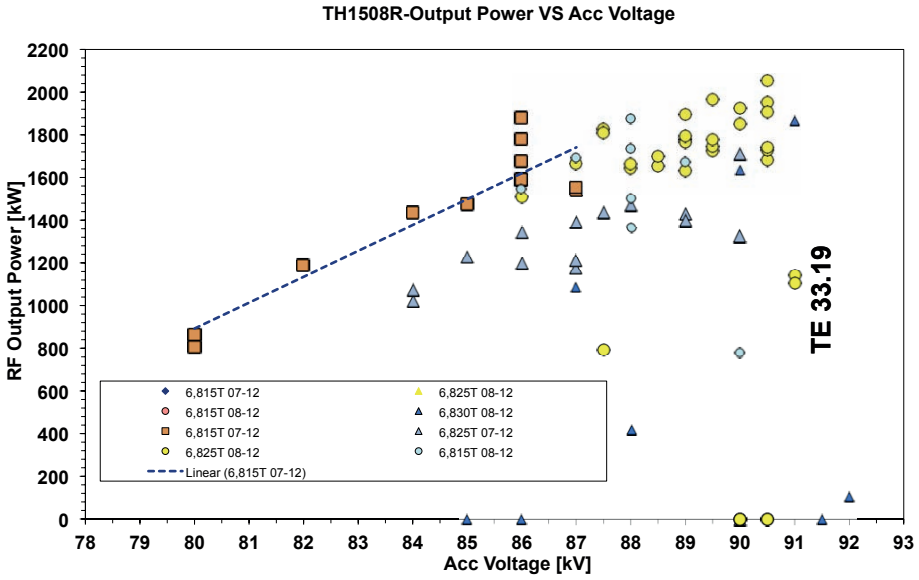

Fig. 4.2.1 RF output power versus accelerating voltage for different magnetic fields

The operation of the test stand including upgrades and improvements was covered by Grant GRT-054 (managed by CRPP, single beneficiary), whereas the scientific interpretation of the results was covered by Grant GRT-049 (managed by KIT, beneficiaries among the European GYrotron Consonsortium EGYC).

- The voltage stand-off of the tube was excellent with and without magnetic field, bringing a validation of the gun design principles improvements.

- Within a record time, it was possible to reach 2MW of output power at 170GHz single mode, with pulses in the ms range (see Fig. 4.2.1).
- The efficiency was close to 45%, and no sign of saturation was observed.
- Radiation on a wrong rotation mode was intermittently observed. The trace was a loud noise caused by a shockwave in cooling circuits. This lead to the failure of an internal load metal-ceramic interface. The tube was then irremediably flooded, putting an abrupt end to the experimental period. These events took place in December 2011.
- The reason for oscillation on a wrong rotation mode is not known yet.

The gyrotron was opened and inspected in 2012, confirming the diagnostic of the metal-ceramic interface failure.

Following the project plan, F4E decided to switch to the development of a conventional (i.e without coaxial insert) 1MW/CW/170GHz tube, making benefit of the 1MW/CW/140GHz W7-X experience.

The signature of a contract between F4E and TED for the manufacture of a prototype is expected by June 2013, with a foreseen delivery in December 2014.

4.2.2 On-going activities

Development activities related to the ITER gyrotron were continued under the following F4E Grants and supply contracts:

- The Grant GRT-049 (Design and Development of the European Gyrotron ("CCGDS7"), managed by KIT) continued.
- The Grant GRT-054 (Tests with the refurbished 2MW First Prototype Gyrotron, Managed by CRPP) is closed and has been finalized.
- A new Grant covering the EGYC development activities is at an advanced phase of discussions (GRT-432, Design And Development Of The European Gyrotron, coordinated by CRPP). This grant will cover the continuation of the theoretical development activities, the follow-up of the manufacture of the future 1MW/CW/170GHz prototype, the design and tests of a short pulse prototype to be tested at KIT, and further modifications/improvements of the CRPP test stand to host a 1MW/CW gyrotron tube.

4.3 The ITER Upper Launcher for Electron Cyclotron Waves

4.3.1 F4E-GRT-161

The ECHUL-CA (electron cyclotron heating upper launcher - consortium of associates) is working, in close collaboration with both F4E and IO, towards the final design of first confinement system (FCS) components and subsystems in preparation for the Final Design Review (FDR) at ITER, planned for spring of 2014. New plasma scenarios, new first wall configurations, inclusion of space for ITER's internal coils, and simplifications of assembly vis-a-vis remote handling led to a redesign of the Quasi-optical (QO) layout of the launcher. A decision to definitively fix the location of the tritium boundary interface of the launcher closure plate allows us to effectively decouple the ex-vessel work related to the FCS from the in-vessel design of the QO system. This also allows us to

recuperate delays in the schedule resulting from the late arrival of some critical information from IO; the latter resulting from the multiparty nature of the ITER project. A preliminary design review (PDR) of the overall EC system was carried out in November with the participation of one CRPP expert panel member. Collaboration within ECHUL pointed to the necessity of clearly defined sign conventions to deal with the various codes used in ray-tracing; a paper describing the conventions was written to this end (within the EU integrated tokamak model task force (ITM-TF)).

4.4 Superconductivity ITER studies

Test in SULTAN

The activities in support of ITER are focused on the test in SULTAN of the ITER conductors. Until the end of April 2012, the tests were carried out under bilateral contracts with the ITER Domestic Agencies and the ITER Organization. Starting May 2012, all the SULTAN test activities and the preparation of Nb_3Sn sample are gathered under one single contract with IO, flanked by six agreements with the ITER DAs. The duration of the contract is thee years and gives full priority access to SULTAN for the test of the superconductors delivered by the ITER Domestic Agencies.

In 2012, following samples have been tested:

- Two extended test campaigns for CSIO1 and CSIO2 samples, developmental samples for CS, respectively seven and six weeks long, in January, February and April, under bilateral contract with IO.
- TFEU6, three weeks long test campaign, European qualification sample for the toroidal field conductor, under bilateral contract with F4E, in March.
- Framework contract IO from May 2012:
  - TFRF3, Russian TF conductor qualification sample (bronze strand).
  - TFKO4, Korean TF process qualification sample (int Sn strand).
  - TFCS2, JT60 NbTi conductor from F4E (U-bend sample)
  - TFJS2, JT60 NbTi conductor from F4E (sample with bottom joint)
  - TFCN4, Chinese TF process qualification sample (int Sn strand).
  - TFEU8, European TF conductor qualification sample (bronze strand).
  - TFEU7, European TF conductor qualification sample (int Sn strand).
  - CBCN1, Chinese conductor qualification sample for NbTi busbar for correction coils.
  - CCCN3, Chinese process qualification sample for NbTi correction coils.
  - TFRF4, Russian TF process qualification sample (bronze strand).
  - TFJA8, Japanese TF conductor qualification sample (bronze strand).

For each test in SULTAN, as well as for each sample assembly, a detailed report is handed to IO and the respective Domestic Agency.
As the SULTAN facility is fully booked by the framework contract, an overtime scheme, funded by F4E, was introduced in August-October to compress the schedule of the ITER conductor tests and gain six weeks window for the start of the EDIPO commissioning. The first window of three weeks is exploited in November. Next three weeks are planned in March 2013.
From November 19th to the end of the year, the ITER conductor test in SULTAN resumes with CSJA3, a critical qualification sample for the CS conductor.

4.5 ITER discharge simulation

The DINA-CH and CRONOS combined simulators have been used to develop free boundary simulations of hybrid mode simulations and steady state simulations. Although these were achieved as planned, achieving a good steady q-profile remains very challenging given the available actuators. This work was presented at IAEA, EPS and is being prepared for publication. The activity was extended to a collaboration with LeHigh University (US) to develop q-profile control as part of an ongoing PhD thesis and the DINA-CH&CRONOS tool proved to be very useful for such studies. This experience has also allowed us to contribute to the ongoing work at CEA to develop two free boundary codes to compete with DINA-CH&CRONOS and CORSICA, using different numerical approaches in FREEBIE and CEDRES++. Both these codes are starting to function and in the process of being tested.

4.6 Support for Plasma Control and CODAC

CRPP continues to provide "voluntary" support to ITER avoiding the administrative burden of contracts where small amounts of work are considered to be useful. We have provided support for the ITER Data Archiving, assistance with various Design Reviews and have written first versions of a concept of operations overview.

4.7 ITERIS

The contract for contributing to the development of the Integrated Modelling Analysis Suite (IMAS) has been confirmed for 2012-2013, after the successful completion of the first year contract. The data model has been further developed and a "rapid prototype" has been implemented in Matlab at the CRPP to verify the main functionalities and to test the generic ideas introduced with the new concepts. The interaction between the IMAS and a plasma control system simulator has been further tested as well. In this case, the simulations are driven from the Simulink GUI. It was demonstrated, using a RZIP model, that each framework could be paused, for debugging or for changing a parameter, and that "events" could be triggered to test the PCS through a modification of the plasma behaviour.

The status of the conceptual design has been discussed in detail at the IMEG meeting in September. The experts have confirmed that the choices being made by the team are appropriate and have been impressed by the amount of work that has been performed so far. The EU-ITM infrastructure is being modified to match the new data model and requirements. A prototype should be ready by the end of 2012, to be able to start coupling various codes and an interface with CORSICA.

5 INTERNATIONAL AND NATIONAL COLLABORATIONS

5.1 Exploitation of the JET facilities

5.1.1 Non-diffusive Momentum Transport in JET H-modes

A broad survey of the experimental database of neutral beam heated baseline H-modes and hybrid scenarios in the JET tokamak has established the ubiquity of non-diffusive momentum transport mechanisms in rotating plasmas. The analysis procedure consists in assessing if the local plasma parameters in stationary conditions obey a steady-state diffusive-convective transport equation, written in dimensionless form, such as to provide experimental values of the ratio of momentum to ion heat diffusivity (Prandtl number) χ_ϕ/χ_i, the pinch number RV/χ_ϕ, where V is the pinch velocity and, if possible, the stress number $\tau_{rs}^* = \tau_{rs}/(m_i n_i v_i \chi_\phi)$,where τ_{rs} is the momentum flux resulting from residual stresses, n_i the ion density and v_i the ion thermal velocity. The torque resulting from momentum deposition by the neutral beams was calculated using the Monte Carlo orbit code ASCOT. Radial profiles of χ_ϕ/χ_i and of the overall convection number (pinch and residual stress combined), expressed as a function of ε=r/R is shown in the figure. The contribution by residual stresses could not be assessed directly by regression. An upper bound for the typical residual stress contribution to R/L_{v_ϕ} shown in blue was estimated by assessing the scaling with the residual stress ordering parameter $O_{rs}=\rho_i^*/(R/L_{Ti})^2/u$, where u is the Mach number and ρi* the normalised Larmor radius. As $O_{rs}<0.2$ in the majority of cases, the Coriolis pinch is clearly the dominant non-diffusive momentum transport mechanism in these strongly rotating plasmas (u>0.1). The experimental non-diffusive transport is in fair agreement with linear calculations of the Coriolis pinch using the gyrokinetic code GKW and have similar scalings with R/L_n, q and ε. The evaluation of the theoretical contribution of residual stresses is still ongoing.

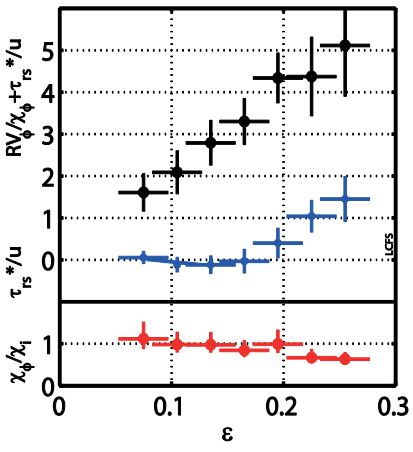

Fig. 5.1.1 *Experimental profiles of typical momentum transport coefficients in JET H-modes.*

5.1.2 JET TAE upgrade project

Since 2011, CRPP has lead the JET Toroidal Alfvén Eigenmode (TAE) diagnostic upgrade project involving international collaborations with the São Paulo University (IFUSP-Brasil), the MIT (US) and EFDA. This work is supported by the EFDA Task Agreement JW11-TA-SED-TAU-03 and is especially important for the future JET D-T campaign. The

main aims of this enhancement are to develop and install a new generation of amplifiers, one for each in-vessel antennas, and to control them with a new digital control system to strongly enhance the reliability of this diagnostic, to allow independent phase control between antennas, to increase the antenna currents thus enhancing the TAE excitation, and to prepare the system for future frequency range of operation up to 1MHz. In 2012, a prototype D-band power switching amplifier was developed, manufactured and successfully tested allowing the production of final units. A solution for the digital control system has been identified and is under test before procurements can start for delivery early 2013. On the JET-Operator side, substantial design activities were performed to interface the new diagnostic components and installation, tests and commissioning of the upgraded diagnostic will take place throughout 2013.

5.1.3 ITER relevant Sawtooth Control in JET

Up until recently sawteeth and NTM instabilities have been controlled using ion cyclotron resonance heating (ICRH) with resonance on the high field side of JET. Those experiments were very successful, and in particular a regime was found for the first time where ICRH could control sawteeth in high confinement mode. Those experiments were ITER-relevant in many new respects except that high field side resonance in ITER will not be technically possible unless the antenna design is modified. Consequently, sawtooth control experiments during the C30 campaign of the summer of 2012 employed, for the first time in JET, low minority concentration ICRH with resonance on the low field side tangent to the q=1 rational surface. Unfortunately ITER-relevant minority He3 was not available, and consequently the minority gas was chosen to be hydrogen. Due to a number of challenging technical problems, only several auxiliary heated pulses were achieved during four allocated sessions. Nevertheless, these pulses indicated evidence of sawtooth control using this scheme, and this in turn has enabled the CRPP lead team to be allocated 4 sessions in the C31 JET campaign (2013) in order to execute low field side sawtooth control the real time actuators.

5.1.4 Collaboration on Alfvén Waves and Fast Particle Studies: Studies of Alfvén Eigenmodes

Following the shutdown for the installation of the ITER Like Wall (ILW) that concluded in early 2011, our activities have mainly focused on the analysis of the data collected during the C20-C27 experimental campaigns, as dedicated Alfvén Eigenmodes (AEs) experiments have not yet been run on JET with the new ILW. Building up from the work initiated in 2011, the main focus of our work has been the analysis of the dependence of the damping rate of Toroidal Alfvén Eigenmodes (TAEs) with intermediate toroidal mode numbers in the range $|n|<16$ as a function of the plasma effective isotope ratio A_{EFF}, which was varied throughout a dedicated D-H-He4 gas scan in C27. With respect to the work initially carried out in 2011 on this topic, we have enlarged the database of the discharges considered in our studies (from 15 in 2011 to 47 in 2012), and improved the accuracy of our results by including a more detailed error analysis, including specifically the contribution of ion impurities, and by developing a more precise procedure for combining together the data for similar values of A_{EFF} that were in discharges with a nominally different background isotope composition. The work carried out in 2012 has therefore led to a refinement of the initial analysis started in 2011, removing the issue of uncertainties.

5.1.5 *Analysis of the "Anomalous" Ion Heating During the JET DTE1 Experiment*

With respect to the work initially carried out in 2011 on this topic, we have improved our GENE simulations using a refined numerical grid, and the analysis of the turbulence measurements by using a different approach to combine the magnetics, reflectometry and electron cyclotron emission measurements. We have also used different modelling of the background plasma parameters for the simulations we have carried out for the ITER reference scenarios. The work carried out in 2012 has led to a confirmation of the main findings of the initial analysis started in 2011.

5.2 *Plasma surface interactions in collaboration with the University of Basel**

A laser ablation system has been constructed and used to determine the damage threshold of stainless steel, rhodium and single-, poly- and nanocrystalline molybdenum in vacuum, at a number of wavelengths between 220 and 1064nm. All materials show an increase of the damage threshold with decreasing wavelength below 400nm. Tests in a nitrogen atmosphere showed a decrease of the damage threshold by a factor of two. Cleaning tests have been performed in vacuum on stainless steel samples after applying mixed Al/W/C/D coatings using magnetron sputtering. In situ XPS analysis during the cleaning process as well ex situ reflectivity measurements demonstrate near complete removal of the coating and a substantial recovery of the reflectivity. The first results also show that the reflectivity obtained through cleaning at 532nm may be further increased by additional exposure to UV light, in this case 230nm.

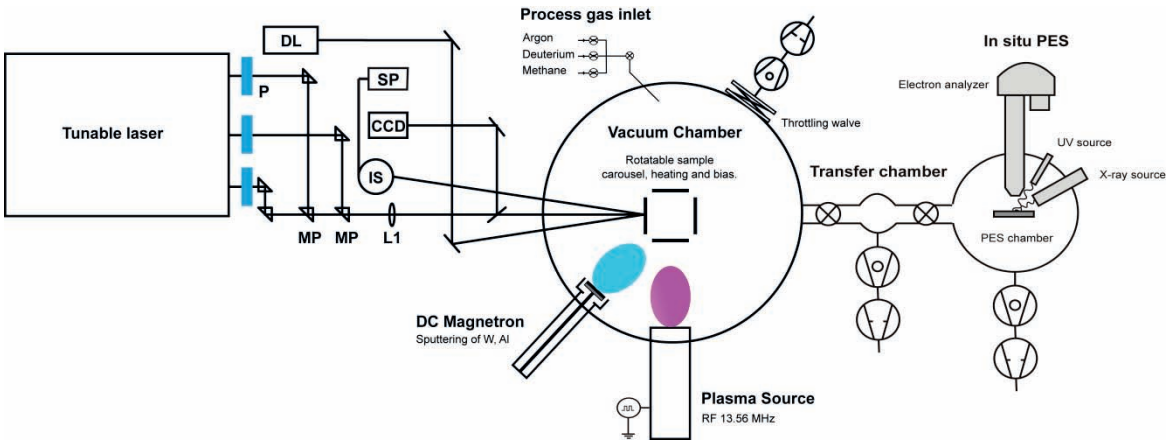

Fig.5.3.1 *Schematic of the plasma exposure facility with added laser ablation system and in situ photo-electron spectrometer. Tuneable pulsed laser radiation (210-2300nm, 20Hz, 5ns pulses) is emitted from one of three ports and attenuated by filters and/or polarisers (P), guided along the same beam path by moveable prisms (MP) and focused onto the sample with a plano-convex lens (L1). A diode laser (DL) beam is coupled into the chamber to monitor the evolution of the reflectivity as well as to keep track of the position of the main laser beam. The reflected beam is captured by an integrating sphere (IS) coupled to a USB spectrometer (SP)*

* Work performed in the frame of the Association. For information.

EFDA Technology Tasks

WP12-IPH-A01-3-12: Influence of mixed surface layers on fuel retention and release
WP12-IPH-A11-1-13: Qualification of tungsten as plasma-facing material for the ITER divertor

JET Fusion technology

JW12-FT-4.25: Feasibility of plasma cleaning mirror in BeHf
JW12-FT-4.26: Laser cleaning mirror

ITER IO

Development of a Concept Design for a Plasma Sputtering Cleaning System for ITER Diagnostic First Mirrors (Contract number: ITER/CT/12/4300000557)

5.3 Collaborations with other EURATOM Associations

J-F. Artaud, V. Basiuk, Association EURATOM-CEA, France, *"Coupling of the DINA-CH and CRONOS codes to simulate the ITER hybrid scenario"*

K. Avramides, Association Euratom Hellenic Republic, Greece, *"Studies of high-power gyrotrons for ITER"*

A. Bottino, IPP-Garching, Germany, *"Global PIC gyrokinetic simulations of turbulence and code development"*

S. Bremond, Tore Supra, CEA-Cadarache, F, *"Real-time control of TCV and Tore Supra"*

I.T. Chapman, CCFE, UKAEA, U.K., "*Collaboration with MAST on the accessibility of bifurcated helical core equilibrium states in the presence of external perturbed n=3 coils used for ELM control"*

C. Cianfarani, O. Tudisco, ENEA, Frascati, *Italy, "Collaboration on high-frequency magnetic sensors based on the Low-Temperature Co-fired Ceramic technology for FTU*"

A. dellaCorte, Association EURATOM-ENEA, Italy, *"Development of superconductors for DEMO"*

G. Conway, IPP-Garching, Germany, *"Turbulence and flow measurements on TCV"*

N. Cruz, A. Rodrigues, C. Varandas, CFN Lisbon, Portugal, *"Vertical position control using Advanced plasma control system"*

G. Cunningham, CCFE, U.K., *"Experiments on H-modes and transformerless tokamak operation in TCV"*

J. Decker, Y. Peysson, CEA-Cadarache, France, "*Quasilinear Fokker-Planck simulations and modelling of hard X-ray emission in TCV*"

V. Erckmann, H.P. Laqua, IPP-Greifswald, Germany, **M. Thumm, G. Gantenbein,** KIT, Karlsruhe, Germany, *"Collaboration with W-7X"*

F. Felici, FOM and Technische Univ. Eindhoven, NL, *"Real-time control of tokamaks and plasma simulator development"*

I. Fernandez , CIEMAT, Spain, *"Design integration of DEMO magnets"*

W. Fietz, KIT Karlsruhe, Germany, *"DC test of High Temperature Superconducting cables for DEMO"*

X. Garbet, Ph. Ghendrih, V. Grandgirard, G. Falchetto. Y. Sarrazin, Association EURATOM-CEA, France, *"Gyrokinetic global turbulence simulations"*

G. Granucci, A. Tuccillo and F. Crisanti, ENEA, Frascati, Italy, *"Collaboration on EC systems with FAST and FTU"*

T. Hellsten, Euratom-VR, KTH Stockholm, Sweden, *"Ion cyclotron heating and current drive"*

P. Hennequin, L. Vermare, Ecole Polytechnique Palaiseau and CEA-Cadarache, France, "*Measurements of edge turbulence and flows in TCV by reflectometry"*

P. Hill, **S. Saarelma**, CCFE-Culham, UK, *"Global PIC gyrokinetic simulations of turbulence with flows"*

M. Hirsch, IPP-Greifswald and **E. Holzhauer**, University of Stuttgart, Germany, *"Loan of a reflectometer and participation in data analysis and interpretation*"

G. Hommen, FOM and Technische Univ. Eindhoven, NL, *"RT-camera image reconstruction"*

F. Jenko, T. Goerler, F. Merz, IPP-Garching, Germany, *"Development and application of the gyrokinetic code GENE"*

T. Johnson, EURATOM-VR Association, Stockholm Univ., Sweden *"Ion cyclotron current drive, heating, and sawteeth"*

A. Koenies, V. Kornilov, A. Mishchenko, S. Sorge, IPP Greifswald, Germany, **A. Bottino, A. Peeters**, IPP Garching, Germany, **R. Hatzky**, Rechenzentrum MPG Garching, Germany *"Linear and nonlinear gyrokinetic code developments and simulations"*

A. Krämer-Flecken, FZJ, Jülich, Germany, "*Measurements of edge turbulence and flows in TEXTOR and TCV by reflectometry"*

P. Lauber, IPP-Garching, Germany, *"Damping rates of Alfvén Eigenmodes: theory-experiment comparison"*

E. Lazzaro, S. Nowak, CNR-Milano, I, *"Study of the rôle of rotation on the onset of triggerless NTM/TMs"*

M. Lewandowska, EURATOM-Poland Association, Univ. of Stectin, *"Hydraulic experiments and modeling of DEMO conductors"*

Y. Liu, CCFE, UKAEA, U.K., "*Resistive wall modes and interaction with energetic ions"*

T. Lunt, Max-Planck-Institut für Plasmaphysik, EURATOM Association, Garching, Germany, *"EMC3-Eirene simulations of the TCV snowflake configuration"*

N. Mellet, Association EURATOM-CEA, Cadarache, France, *"Application of the LEMAN code for heating and stability"*

P. McDermott, IPP-Garching, Germany, *"Intrinsic rotation measurement comparison AUG & TCV"*

C. Michael, CCFE, U.K., *"Collaboration on the design of a phase contrast imaging diagnostic for MAST"*

F. Nave, JET/IST Abingdon, UK, *"Plasma rotation measurement comparison between JET and TCV plasmas"*

A. Nijhuis, Un. Twente, The Netherlands, *"AC loss characterization of HTS cables"*

R. Scannell, CCFE-Culham, UK, *"New filter polychromators for the TCV Thomson scattering system"*

M. Spolaore, N. Vianello, Consorzio RFX, Padova, Italy *"Collaboration on the investigation of current filaments in magnetized plasmas"*

D. Ricci, G. Granucci, D. Iraji and M. Lontano, CNR-Milano, Italy, *"Collaboration with the linear basic plasma device GyM"*

J. Romero, CIEMAT and **M.G.S. Berasategui, I. Garrido,** EHU, Spain, *"Real-time control of the current profile in TCV"*

O. Schmitz, KFZ Juelich and the DIII-D team, *"Collaboration with DIII-D, General Atomics, USA on bifurcated helical equilibria and ELM control coils"*

G. Temmerman, FOM, the Netherlands, *"Inner-outer divertor power assymetries on TCV"*

D. Terranova, P. Martin, L. Marrelli, M. Gobbin, EURATOM-ENEA-CNR Association, Italy, "RFX-Mod Shax equilibrium and MHD stability"

I. Tigelis, G. Latsas, Association Euratom Hellenic Republic, Greece, *"Instability calculations in the 170GHz coaxial-cavity-gyrotron beam-duct"*

M. Valisa, L. Carraro, A. Scaggion, Consorzio RFX, Padova, Italy, *"H-mode studies in TCV"*

G. Veres, B. Tal, S. Zoletnik, D. Nagy, Association EURATOM-HAS, KFKI Reasearch Inst. For Particle & Nuclear Physics, Budapest, Hungary, *"Plasma imaging and tomography" and "Mitigation disruption studies, particle transport studies in the SOL, high temporal resolution radiation measurements for ELMs"*

L. Vermare, P. Hennequin, Ecole Polytechnique, Palaiseau + CEA, France, *"Reflectrometry measurements on TCV"*

C. Wahlberg, EURATOM-VR Association, Uppsala University, Sweden, *"MHD aspects of the sawtooth instability, Kelvin Helmholz and infernal modes"*

H. Wilson, York, University, UK, *"Physics and diagnostics of snowflake divertor configurations"*

W. Witrant, Univ. Joseph Fourier, GAPSI-Lab, Grenoble, F, *"Real time current profile control"*

C. Zignani , Association EURATOM-ENEA, Italy, *"Test of 20 kA HTS current leads"*

Collaboration with IPP-Garching, FZJ-Jülich, IGVP-Stuttgart, TUM-München, LPP-Palaiseau in the frame of the Helmholtz Society Virtual Institute on Advanced Microwave Diagnostics

Collaboration with KIT, NTUA and CNR in the frame of the gyrotron consortium EGYC

Collaboration with KIT, FOM, CNR, IPP, NTUA in the frame of the Upper Launcher Consortium ECHUL

Collaboration with CEA and RFX in the frame of the Magnetic Diagnostics Consortium

5.4 Other international collaborations

G. Annino, Istituto per i Processi Chimico-Fisici, CNR, via G. Moruzzi 1, 56124 Pisa, Italy, *"Development of THz-waves Instrumentation for DNP-NMR spectroscopy"*

J. Boedo, UCSD, USA, *"Reciprocating probe for edge measurements on TCV"*

A. Bortolon, PPPL, Princeton, USA, *"Rotation comparison between NSTX and TCV"*

R. Buttery, L. Lao, A.D. Turnbull, General Atomics, San Diego, USA, *"Quasiaxisymmetric field in DIII-D for enhanced élongation"*

Y. Camenen, Univ. Marseille, France, *"Modelling of plasma rotation and momentum transport on the TCV tokamak"*

H. Carfantan, Laboratoire d'Astrophysique de Toulouse - Tarbes, Université de Toulouse - CNRS, Toulouse, FR, *"Development of the Sparse Signal Representation method for real-time and post-pulse decomposition and analysis of a frequency-degenerate spectrum"*

W. Choe, Korea Advanced Institute of Science and Technology, Daejeon, Korea, "*Collaboration on multi-wire soft X-ray diagnostics*"

B. Décamps, Centre de Spectrométrie Nucléaire et de Spectrométrie de Masse, Université Paris-Sud, "*In-situ irradiations with JANNUS facility at Orsay*".

R. Galvao, Univ. of Sao Paulo, Brazil, *"Upgrade of the TAE Alfvén Eigenmode Exciter"*

R. Ganesh, J. Chowdury, Inst. For Plasma Research, Bhat, Gandhinagar, India, *"Effects of non-adiabatic electron dynamics in gyrokinetic simulations of microinstabilities"*

G. Giunchi, EDISON, Italy, *"Characterization of MgB2 superconductors"*

R. Gruber, EPF-Lausanne, Switzerland, **S.P. Hirshman**, **Y. Suzuki**, **Y. Asahi, S. Ohdachi, R. Seki**, ORNL, USA, **K.Y. Watanabe, H. Yamada, S. Okamura, Y. Narushima**, NIFS, Japan, **K. Yamazaki**, Nagoya Univ., Japan, *"3D anisotropic pressure equilibrium and fluid magnetohydrodynamic stability"*

E. Gusakov, A. Popov, A. Saveliev, Ioffe Institute, St. Petersburg, Russian Federation, *"Modelling of parametric decay from EC wave in TCV"*

R.W. Harvey, A.P. Smirnov, Comp-X, San Diego, CA, USA, *"Modelling of electron cyclotron heating and emission in TCV"*

W. Heidbrink, H. Boehmer, UC Irvine, USA, *"Sources for energetic ions for a simple magnetized torus"*

S.P. Hirshman, Oak Ridge National Laboratory, USA, *"Three-dimensional anisotropic pressure free boundary equilibria: the ANIMEC code"*

J. Hittinger, R. Berger, Lawrence Livermore National Laboratory, USA, **E. Valeo**, Princeton University, USA, and *"Development of numerical methods for Vlasov simulations"*

Y. Idomura, JAEA, Japan, *"Global gyrokinetic simulations of turbulence with grid-based and particle-based methods"*

ITER Organization, F4E, ASIIP, KODA, JADA, USIPO. ITER RF, *"Test of ITER conductors in SULTAN"*

M.Yu. Isaev, Russian Research Centre Kurchatov Institute, Moscow, Russia, **A. Konies**, IPP-Greifswald, D, *"Development of the VENUS-df Code for Bootstrap Current and Neoclassical Transport and Alfvén mode stability in Stellarators"*

JT60-SA research team, JAEA, Japan, "*Participation to the definition of the JT60-SA research project"*

N. Kirneva, RRC Kurchatov Institute, Moscow, Russia, *"Investigation of turbulent tokamak plasma self-organization and influence of the tokamak cross-section geometry on the plasma-pressure self-consistent radial profile"*

T. Kruml, Institute of Physics of Materials, Brno. Czech Republic, *"Low-cycle fatigue of ODS-steels"*

M. Lanctot, General Atomics and the TBM task force on DIII-D, San Diego, Ca, USA, *"Collaboration on the effect of test blanket modules (TBMs) in ITER on H-mode energy, particle and momentum confinement"*

L. Lao, A.D. Turnbull, T.E. Evans, Genaral Atomics, San Diego, USA, *"Torkil Jensers Award experiment on Helical core structures in DIII-D"*

V.E. Lukash, Kurchatov Inst. Moscow, Russia, **R.R. Khayrutdinov**, TRINITI, Russia, *"Development of the DINA-CH simulator"*

B. McMillan, Univ. of Warwick, UK, *"Global gyrokinteic simulations of turbulent flows and momentum transport"*

A. Marinoni, C. Rost, M. Porkolab, PSFC, MIT, MA, USA, *"Turbulence measurements by phase contrast imaging in TCV, C-Mod, DIII-D"*

S.Yu. Medvedev, A.A. Martynov, A.A. Ivanov, Yu.Yu. Poshekhonov, Keldysh Institute of Applied Mathematics, Moscow, Russia, **M.Yu. Isaev, V.D.Shafranov, A.A. Subbotin**, RRC Kurchatov Institute, Moscow, Russia, *"Equilibrium and Stability of 2D and 3D plasma configurations"*

M. Mikhailov, V.D. Shafranov, M.Yu. Isaev, M. Samitov, Russian Research Centre Kurchatov Institute, Moscow, Russia; J. **Nuehrenberg**, Max Planck Institut fuer Plasma Physik, Greifswald *"Optimisation of Advanced Stellarator Systems"*

G.R. Odette, Univ. California Santa Barbara (UCSB), Santa Barbara, CA, USA, *"Fracture mechanics and small specimen test technology"*

M. Porkolab, P. Woskov, PFSC, MIT, USA, *"Fast particle physics, Alfven waves, and active MHD mode excitation on the Alcator C-Mod tokamak plasma"*

J. Rice, C-MOD, Boston, USA, *"Intrinsic rotation comparison between CMOD & TCV"*

B. Rogers, Dartmouth College, USA, *"Theoretical characterization of turbulence in TORPEX plasmas"*.

D. Ryutov, **T. Rognlien, M. Umansky**, LLNL, USA, *"Snowflake divertor generation and characterization in TCV"*

P. Savrukhin, A. Sushkov, RRC Kurchatov Institute, Russian Federation, *"Suprathermal electron physics on T-10 and TCV"* (SC)

P. Smeibidl, HZB, Berlin, Germany, *"Design and construction of a SC Cable-in-Conduit coil for a horizontal series-connected hybrid magnet system within the framework of the high field magnet project (HFM) at HZB"*

A.D. Turnbull, General Atomics, San Diego, USA, *"Stability studies of ARIES stellarator configurations"*

K.Y. Watanabe, NIFS, Japan, *"Collaboration on LHD MHD equilibrium and stability"*

A. White, MIT, USA, *"Correlation ECE measurements on TCV and Alcator C-mod"*

5.4.1 International Tokamak Physics Activity (ITPA)

The following staff members were involved in ITPA activities in 2012:

ITPA Diagnostics Topical Group: H. Weisen (member), R. Behn (expert), L. Marot (expert)

ITPA Energetic Particle Physics Topical Group: A. Fasoli (member), D. Testa (expert)

ITPA MHD, Disruptions & Control Topical Group: O. Sauter (member), J.B. Lister (expert), A. Fasoli (expert)

ITPA Pedestal & Edge Physics Topical Group: Y. Martin (member)

ITPA Transport & Confinement Topical Group: Y. Martin (expert), H. Weisen (expert), O. Sauter (expert)

ITPA MHD 3D Equilibrium distortions working group: J. Graves (expert), W.A. Cooper (expert)

5.5 Other collaborations within Switzerland

J.-Ph. Ansermet, EPFL/SB/LPMN; **A. Comment**, EPFL/SB/IPSB/LIFMET; **G. Bodenhausen**, EPFL/SB/ISIC/LRMB, **G. Boero**, EPFL/STI/IMT/LMIS1, *"Development of THz-waves Instrumentation for DNP-NMR spectroscopy"*

E. Cadoni, University of Applied Sciences of Southern Switzerland, Canobbio, *"High strain rate tensile testing of the EUROFER 97 RAFM steel"*

C. Hébert, CIME-EPFL, *"TEM analysis of He bubbles in steels"*

F. Holdener, WEKA, Bäretswil, *"Technology transfer for HTS current leads manufacture"*

G. Lucas, CIME-EPFL, *"Advanced statistical analysis methods in TEM spectroscopy"*

A. Macor, E. de Rijk, Swissto12, *"Development of passive THz-waves components"*

L. Marot, Department of Physics of University of Basel, *"Thin films used as coating materials"*

R. Wepf, EMEZ-ETHZ, *"Advanced TEM techniques and TAP for ODS steels and Fe(Cr)"*

R. Spolenak, LNM-ETHZ, *"Radiation induced mechanisms of selective grain growth in metals"*

Besides the activities in the field of plasma wall interaction with the University of Basel, the CRPP also collaborates with the PSI in the field of materials under irradiation.

6 THE EDUCATIONAL ROLE OF THE CRPP

The CRPP plays a role in the education of undergraduate and postgraduate students, particularly in the Faculté des Sciences de Base (FSB) of the EPFL. Advanced education and training in fusion physics and technology and plasma physics topics is carried out as part of the research activities of the Association. Section 6.1 presents the 9 courses given to physics undergraduates and to engineering undergraduates. In their fourth and final year, physics undergraduates spend time with a research group at the EPFL, typically 12 hours per week for the whole year. During this period, they perform experimental or theoretical studies alongside research staff, discovering the differences between formal laboratory experiments and the "real" world of research. After successful completion of the first year of the Master Programme (4^{th} year of studies), physics students are required to complete a "master project" with a research group, lasting a full semester. This master project is written up and defended in front of external experts. The CRPP plays a role in all of these phases of an undergraduate's education, detailed in Sections 6.2 and 6.3.

As an academic institution, the CRPP supervises many Ph.D. theses, also in the frame of the Physics Section of the EPFL. 2 PhDs were awarded in 2012. At the end of 2012 we had 31 PhD students supervised by CRPP members of staff, in Lausanne and at the PSI site in Villigen. Their work is summarised in Section 6.4.

6.1 Undergraduate courses given by CRPP staff

S. Alberti, Maître d'Enseignement et Recherche – *"Plasma Physics I"*
This course is an introduction to plasma physics aimed at giving an overall view of the essential properties of a plasma and at presenting the approaches commonly used to describe its behaviour. We study single particle motion, the fluid description and the kinetic model. The relation between plasma physics and developing a thermonuclear reactor is presented and illustrated with examples.

P. Spätig - Maître d'Enseignement et Recherche and **J. Fikar:** *"Fundamentals of radiation damage and effects"*
This 28-hours course is part of the EPFL's Minor in Space Technologies. The objective of this course is to provide a detailed description of fundamental interaction mechanisms between particles and matter, radiation damage and its characterization methods, and radiation effects with emphasis on the relationships between microstructure and mechanical properties. Various types of materials are being considered as well as various examples of applications related to nuclear, semi-conductor and aerospace industries.

P. Ricci, Assistant Professor – *"Plasma physics II"*
One semester option course presented to 4th year Physics students, introducing the theory of hot plasmas via the foundations of kinetic and magnetohydrodynamic theories and using them to describe simple collective phenomena. Coulomb collisions and elementary transport theory are also treated. The students also learn to use various theoretical techniques like perturbation theory, complex analysis, integral transforms and solutions of differential equations.

A. Fasoli, Professor – *"General Physics II"*
This course completes the introduction to mechanics provided in the first semester with the basic concepts of statics, oscillations and special relativity. It also covers the whole of thermodynamics, from the introduction to heat, temperature and kinetic theory to the

first and second principles, including entropy and thermal engines, ending with a treatment of transport and non-equilibrium phenomena in open systems.

A. Fasoli, Professor and **M.Q. Tran**, Professor - *"Nuclear fusion and plasma physics"*
The aim of this course is to provide a basic understanding of plasma physics concepts of fusion energy, and of the basic principles of fusion reactors, including the main technological aspects. This course was given within the frame of the Master in Nuclear Engineering.

J.B. Lister, *Maître d'Enseignement et Recherche (MER) – "Plasma Physics III"*
An introduction to controlled fusion, presented as a one semester option to 4th year Physics students. The course covers the basics of controlled fusion energy research. Inertial confinement is summarily treated and the course concentrates on magnetic confinement from the earliest linear experiments through to tokamaks and stellarators, leading to the open questions related to future large scale fusion experiments.

M.Q. Tran, *Professor - "General Physics II and III"*
This course, given to the Mathematics Section, covers mechanics and thermodynamics (General Physics II) and hydrostatic, hydrodynamics waves and electromagnetism (General Physics III).

L. Villard, *Professeur Titulaire – "Computational Physics I-II"*
Full year course given to students in their 2nd year in Physics. The course covers various time and space integration techniques for ordinary and partial differential equations, and is applied to various physics problems ranging from particle dynamics, hydrodynamical equilibrium, electromagnetism, waves and quantum mechanics. It includes a strong practical work aspect.

6.2 Undergraduate work performed at the CRPP

EPFL Master students (4th year)

During the Spring semester of 2011, CRPP staff members have supervised 6 students performing their Advanced Physics Laboratory work. During the Automn and Spring semester of 2011, we had 4 students.

6.3 EPFL Master degrees awarded in 2012

J. Dominski, *"Study of non-adiabatic response of passing electrons in ITG and TEM microturbulence"*
F. Margairaz, *"Synthetic diagnostics of CECE and PCI based on non-linear gyrokinetic flux-tube simulations relevant to the TCV tokamak"*
G. Oberli, *"Characterisation of a new RF plasma source producing large volume plasmas"*
V. Vuille, *"Spectral and spatial analysis of micro-turbulence by correlation ECE radiometry on the tokamak TCV"*

6.4 Postgraduate studies

Postgraduate courses given in 2012

W.A. Cooper, J.-M. Moret, D. Testa, M.Q. Tran, O. Sauter, P. Ricci, A. Fasoli, P. Angelino, W. Vijvers, *"Magnetic confinement"*, Doctoral School, EPFL

I. Furno, H. Reimerdes, B. Labit, *"Plasma diagnostics in basic plasma physics devices and tokamaks: from principles to practice",* Doctoral School, EPFL

R. Behn, S. Coda, I. Furno, H. Weisen, *"Diagnostics of fusion plasmas",* Doctoral School, EPFL

J.B. Lister, J.-M. Moret, H.B. Lè, B.P. Duval, W. Vijvers, *"Tokamak plasma control",* Doctoral School, EPFL

P. Spätig, *"Seminar on Nuclear Materials"*, Doctoral School, EPFL

Doctorate degrees awarded during 2012

Janos MARKI: *"Infrared thermography of divertor ELM heat loads on TCV"* (EPFL thesis 5021(2012))
Edge Localised Mode (ELM)-induced heat loads, in particular divertor heat loads present one of the main challenges in adopting nuclear fusion as an industrial-scale energy source. At present, the type-I ELMy plasma regime is chosen as the most suitable operational scenario because of its energy confinement and steady-state capabilities, however, with the understanding that the enormous quasi-periodic heat loads deposited by the ELMs will need to be controlled in order to avoid intolerable damage to heatbearing elements. At present, a detailed theoretical understanding, and in particular, a sufficiently reliable way of predicting ELM behaviour based on basic discharge parameters is missing. The fusion community has been expending a great deal of effort in order to improve this situation by gathering as much experimental data as possible from a range of different-sized tokamaks, in order to develop empirical scalings and refine theoretical models, with the ultimate aim of mitigating their destructive power below thresholds where they won't affect continuous scientific exploitation of the reactors.
This experimental thesis joins into this effort via the installation and commissioning of a fast infrared camera on TCV viewing the outer divertor. Near the end of the thesis, an effort of similar magnitude has been carried out with a camera on temporary loan from the MAST group, in order to image the inner divertor region as well. The cameras possess a sub-array recording capability, enabling acquisition frequencies up to 25 kHz. Both cameras were calibrated with the combination of a lowand high-temperature blackbody source with large and small radiation surfaces, respectively. By estimating the surface emissivity as 0.85 and employing a gray-body model, target surface temperatures could be inferred. The resulting images were processed to produce 1D poloidal temperature profiles serving as an input to the THEODOR (THermal Energy Onto DivertOR) 2D finite-element code, with the goal of calculating the heat fluxes impinging on plasma facing components.
The VIR (Vertical InfraRed) outer divertor system images a flat, horizontal surface covered by relatively large tiles from a perpendicular viewing angle. Deposited layers, microscopic surface changes and very small dust particles cause the appearance of microscopic hot-spots in the field-of-view (FOV), leading to a substantial deviation from

the assumed model of a single-temperature (the tile bulk graphite) gray body radiator. Near the middle of the thesis, nearly all tiles inside TCV have been removed for cleaning via sandblasting. With 3 of the tiles having been left untouched, this presented a good opportunity to contrast the behaviour of the cleaned and uncleaned (~12 years of operation) surfaces. It has been found that already after 10 days of operation, the temperature signal significantly exceeds what could be expected from a pure graphite surface. This, though increasing error bars of the final heat flux figures, is also beneficial in the sense that it serves as a signal amplifier – e.g. most observed ELM filaments near the main divertors carry very little energy, and were it not for this effect, they would not be visible at all.

In contrast to the outer divertor, the inner divertor geometry is more complicated, as the tiles' shape causes a gradual toroidal change in the magnetic field line attack angle from ~20 to 0 degrees, excluding toroidal averaging. Sequences recorded by this system also require a correction for mechanical vibrations, which, though also present for the vertical system, are much more pronounced, affecting the outcome of heat flux calculations to a great degree. Best results have been achieved with a method based on cross-correlations. Apart from eliminating the effects of the horizontal shaking, as the global vertical movement of the strike point leg on the target needed to be retained, the vertical shaking was either left uncorrected or parametrized in a way to remove the oscillations about the obtained vertical displacement trendline.

In the process of calculating the heat flux from the temperature spatio-temporal evolution, the surfaces' deviation from a one-temperature blackbody radiator manifests as an overshooting during transients, in both the positive and negative directions. This leads to the appearance of unphysical results (heat fluxes conducted outwards from the tiles, whilst plasma is still depositing heat on it). By introducing a simple boundary condition in THEODOR, a crude correction for this effect could be applied. The resulting tile deposited energies were cross-checked with rudimentary heat capacity calculations based on tile-installed thermocouples, yielding ~25% agreement.

Two discharges, one in FWD-, the other in REV-B configuration, were selected for detailed analysis of ELM divertor heat loads. Both were heated by 3rd harmonic ECRH heating, the former exhibiting large- and the latter type-III ELMs. A dataset of various parameters such as maximum heat flux, profile width, total divertor deposited powers, ELM deposited energies and in-out power balance during and in between the ELMs, as well as the fraction of ELM energy recovered at the divertors, the rise-to-peak times and integral energy-to-peak was built up and evaluated in detail.

The TCV outer divertor power loads dominate those of the inner under all circumstances – a finding that contradicts empirically established ELM characteristics from other tokamaks. The observed power imbalance is larger during the ELMs, and smaller in between. The ratio of ELM deposited energies at the inner- and outer divertors is 1:3, always in favour of the outer divertor. ELM profile broadening of a factor in the range ~1-2 has been found to occur consistently in both field directions, at both divertors. The total fraction of ELM energy recovered at the divertors (E_{IR}/DW_{ELM}) has been found to decrease with growing ELM size. The ELM pedestal energy fraction versus collisionality, the rise-to-peak time versus parallel convection time and integral rise-topeak energy versus collisionality were compared to values from other tokamaks. With the exception of the ELM pedestal energy fraction of the "giant" ELMs in FWD-B discharge #38014, all values are in agreement with what would be extrapolated from other devices.

In line with the target of predicting ELM heat loads, comparisons with 1D kinetic PIC simulations and the so-called free-streaming particle (FSP) approach (an analytical expression for the power density based on a relatively simple model) were performed. With the exception of the early rise phase, PIC simulations of type-III ELMs reproduce the experimental time evolution well. They give insight into finer details of ELM heat transport: a very fast electron heat pulse (carrying about 5% of total ELM energy), is followed by the main pulse on a slower time-scale. About 3/4 of the total energy is carried by the ions, of which 0.3-0.4 is deposited in the rise phase. The FSP expression, based on a collisionless approximation, provides a reasonable fit to the temporal evolution of divertor-deposited power for TCV ELMs of various sizes. In most cases, both the riseand decay phases can be described by the single time parameter within the

expression. This parameter is at least twice as large as the parallel transport time based on pedestal parameters, implying a delaying of particles near the X-point region.
In contrast to other tokamaks, filamentary ELM heat deposition patterns are only occasionally recorded at the outer divertor. The observed spatial structure is consistent with a plasma release at discrete toroidal locations in the outer midplane vicinity, but as very few are visible on the IR (when compared to the Langmuir probes), the determination of quasi-mode numbers was deemed unfeasible. A crude estimation of the energy content of individual filament spirals yielded 1% of the total ELM energy in each, consistent with existing non-divertor ELM heat load predictions.
Finally, a new divertor configuration, the snowflake, was recently demonstrated in TCV experimentally, and, subsequently, the creation of H-modes in it. This configuration presents many advantages, most prominently the possibility of distributing the divertor heat load to 4 (as opposed to 2 for standard single-null divertors) regions. Infrared measurements at one of these additional legs have confirmed substantial heat loading and a lack of ELM profile broadening.

Jonathan ROSSEL: *"Edge localized mode control in TCV"* (EPFL thesis 5311(2012)
The Tokamak concept, based on magnetic confinement of a hydrogen plasma, is one of today's most promising paths to energy production by nuclear fusion. The experimental scenarios leading to the largest fusion rate are based on a high confinement plasma regime, the H-mode, in which the energy and particle confinement are enhanced by a transport barrier located at the plasma edge and forming a pedestal in the plasma pressure profile. In standard axisymmetric magnetic configurations, stationary H-mode regimes suffer from instabilities of the plasma edge, the so-called edge localized modes (ELMs), leading to potentially damaging repetitive ejections of heat and particles toward the plasma facing components. In ITER, a Tokamak currently being built to demonstrate net power production from fusion, type I ELMs are expected to occur during high performance discharges. It is expected that the power flux released by these ELMs will cause an intolerable erosion and heat load on the plasma facing components. The control of ELMs, in terms of frequency and energy loss, is therefore of primary importance in the field of magnetic fusion and is subject to an intense research effort worldwide. This thesis, in line with this effort, focuses on two particular ELM control methods: local continuous or modulated heating of the plasma edge, and application of resonant magnetic perturbations (RMP). In this thesis, the effects of plasma edge heating on the ELM cycle have been investigated by applying electron cyclotron resonant heating (ECRH) to the edge of an H-mode plasma featuring type I ELMs in the Tokamak à Configuration Variable (TCV). As the power deposition location is shifted gradually toward the plasma pressure pedestal, an increase of the ELM frequency by a factor 2 and a decrease of the energy loss per ELM by the same factor are observed, even though the power absorption efficiency is reduced. This unexpected and, as yet, unexplained phenomenon, observed for the first time, runs contrary to the intrinsic type I ELM power dependence and provides a new approach for ELM mitigation. The effects of heating power modulation on the ELM cycle have also been experimentally investigated. It showed that power modulation synchronized in real-time with the ELM cycle is able to pace the ELMs with low deviation from a given frequency. Experimental results also clearly indicate that the ELM frequency purely remains a function of the heating power averaged over the ELM cycle, so that power modulation itself is not able to drive the ELM frequency and only has a stabilization effect. These results are in qualitative agreement with a simple 0D finite confinement time integrator model of the ELM cycle. RMP consists in applying a magnetic field perpendicular to the plasma magnetohydrodynamic equilibrium flux surfaces with a spatial variation tuned to align with the equilibrium magnetic field lines. If each coil of an RMP coil system (i.e. a set of toroidally and poloidally distributed coils) is powered with an independent power supply, the coil current distribution can be tuned to optimize the RMP space spectrum. In the course of this thesis, a multi-mode Lagrange method, with no assumption on the coil geometry or spatial distribution, has been developed to determine this optimum, in the limit of the vacuum magnetic field approximation. This method appears to be an efficient way to

minimize the parasitic spatial modes of the magnetic perturbation, and the coil current requirements, while imposing the amplitude and phase of a set of target modes. A figure of merit measuring the quality of a perturbation spectrum with respect to RMP independently of the considered coil system or plasma equilibrium is also proposed. To facilitate the application of the Lagrange method, a spectral characterization of the coil system, based on a generalized discrete Fourier transform applied in current space, is performed to determine how spectral degeneracy and side-bands creation limit the number of simultaneously controllable target modes. Finally, this thesis sets the foundations of experimental research in the particular subject of RMP at CRPP by proposing a physics-based design for a multi-purpose saddle coil system (SCS) for TCV, a coil system located and powered such as to create a helical magnetic perturbation. Using independent power supplies, the toroidal periodicity of this perturbation is tunable, allowing simultaneously ELM control, error field correction and vertical control. Other experimental applications, like resistive wall mode and rotation control, are also in view. In this thesis, the adequacy of two SCS designs, an in-vessel one and an ex-vessel one, is assessed with respect to the desired experimental applications. The current requirements and the system performances are also characterized. The conducting vessel wall is accounted for in a model used to determine the coupled response functions of the SCS, the screening of the magnetic perturbation by the wall, the induced voltages and currents during a plasma disruption and the maximal magnetic forces exerted on the SCS. A scaling of the SCS parameters with the number of coil turns is presented and the issue of coil heating and cooling is discussed.

Ph.D. Theses supervised by CRPP staff at the end of 2012

Himank ANAND: *"Real time control of plasma shape using poloidal flux measurements"*
This thesis plans to implement a real time control of different plasma shapes on TCV by controlling the poloidal flux at the prescribed boundary points, which would result in an accurate control of plasma shape with high β values. These shapes are to be precisely controlled for optimization of the coupling with the additional heating systems, avoidance of wall interactions and divertor shape optimization for pumping.
An initial effort was devoted to developing a triangularity observer in the context of the existing analogue plasma control system. More recent work has focused on developing a digital, generalized plasma shape control algorithm with the help of poloidal flux estimators at prescribed boundary points. The algorithm calculates the flux using the output of the equilibrium reconstruction code Liuqe. It then calculates the perturbation of currents needed in all the coils in order to make the flux errors at the prescribed boundary points equal to zero and attain the prescribed shape. The algorithm also contains an optimization function which helps to minimize the power dissipation and dipole terms in adjacent coils. It uses Lagrangian Multipliers with a linear constraint and a non linear optimization function.

Fabio AVINO: *"Turbulence at the boundary of toroidal plasmas with open and closed magnetic flux surfaces"*
The work I have carried out in 2012 has followed the same path started in the previous year, focusing on the in-vessel toroidal wire project on TORPEX. We have completed the development of the experimental set-up which can be considered as an effective upgrade of the TORPEX machine.
The final design of the system was achieved during the first months of 2012. A toroidal copper wire is suspended inside the TORPEX vacuum vessel by an electrical coaxial feed through, to minimize the magnetic field perturbations, and three vertical stainless steel wires (1mm diameter). A dedicated power supply provides a current up to 1kA that flows in the wire. The output dynamics of the power supply is limited to a maximum slew rate of 1400A/sec.

The manufacturing of the system components has been commissioned and finished during the summer of 2012. The remote control of the dedicated power supply was developed at the same time, both from the hardware side (the electronic system built at the CRPP electronic workshop) and from the software one (GUI interface for the TORPEX control developed by me). The installation of the experimental set-up was performed during the month of August, so that the second half of the year was spent to complete the commissioning of the system, such as proving the reproducibility of the wire current time-traces for different values of flat-top current in the range we are interested in, up to 1kA. Measurements of the generated poloidal magnetic field have been done as well using a single-axis Hall probe to verify the reliability of the magnetic field simulations as a reference for the following experimental campaigns.
Furthermore, the first experimental studies aimed at characterizing TORPEX plasmas in the new magnetic field configurations have been conducted. We focused on the simplest case of concentric flux surfaces, using both Langmuir probes and a Fast Imaging Camera. A preliminary analysis of these data suggests the presence of coherent structures mainly localized on the Low-Files Side with a frequency in the range 10-25kHz.

Karim BESSEGHIR: *"ITER hybrid and steady-state scenario simulations using DINA-CH"*
Advanced scenarios are of high interest to the long-term goal of using fusion in an energetically and economically viable manner because they provide high neutron fluence per plasma pulse by taking advantage of the heating and current drive systems. Hybrid scenarios consist of plasma pulses of medium duration and medium fusion gain with respect to basic inductive scenarios. Steady-state scenarios consist of long plasma pulses with low fusion gain, and are characterized by the achievement of a steady-state.
Although hybrid and steady-state scenarios have been performed on presently-operated tokamaks, ITER raises new challenges that have not been faced in existing tokamaks. Namely, the presence of a higher self-heating fraction via -particle, the foreseen higher density profile peaking and the resulting increase in bootstrap current density fraction, the uncertainties regarding the achievable pedestal pressure and confinement enhancement factor, and the specific technical constraints in ITER in terms of Poloidal Field (PF) coils power supplies, heating and current drive power supplies, and currents, fields, and vertical forces that the PF coils can sustain. For these reasons, simulations of the ITER hybrid and steady-state scenarios are necessary in order to assess their feasibility given the present ITER design.
This work started in December 2010 in the framework of a Fusion for Energy grant and was completed in April 2012. The hybrid and steady-state scenarios were simulated using the full tokamak simulator DINA-CH coupled with the CRONOS suite of codes. The outcome of this study demonstrated the feasibility of the hybrid and steady-state scenarios using the present ITER design, with the caveat that several physical assumptions were made, especially regarding transport modelling. These results were reported in the 2012 ITPA Integrated Operation Scenario meeting in Madrid, Spain.
This work, although successful, was not mature for publication due to several weaknesses in the control scheme. Additional work was required in order to tackle the remaining challenges and was carried out since May 2012.

Alexandre BOVET: *" Investigation of fast ion transport in the TORPEX experiment"*
Basic aspects of fast ion transport in ideal interchange turbulent plasmas are investigated in the simple toroidal plasma device TORPEX. Fast ions are injected in the plasma by a miniaturized lithium 6+ ion source with energies up to 1keV, and are detected using a double-gridded energy analyzer (GEA) mounted on a two-dimensional movable system. A motorized system was developed, which moves toroidally the ion source continuously over a distance of 50cm.
A first set of experiments with the toroidally moving system was conducted in 2012. We used a plasma scenario dominated by an ideal interchange mode, localized around the

position of maximum pressure gradient. Supra-thermal ions are injected in the blob region with energy of 70eV and horizontal orientation. The source is moved toroidally between each discharge over a total distance of 50cm, in steps of 5cm. Poloidal profiles of the fast ion current are reconstructed at each toroidal position.
To interpret the experimental data, fast ion tracer trajectories are followed using the full Lorentz force, with turbulent electric fields, which are numerical computed by solving the drift-reduced Braginskii equations in two dimensions. Comparisons with simulations are performed using a synthetic diagnostic, allowing the poloidal cross section of the fast ion current density to be reconstructed.
Simulations are performed with source parameters based on measurements done without magnetic field. 10000 particles are launched with initial parameters modeled with Gaussian distributions.
Agreement between experiments and simulations is remarkable and the turbulent broadening of the fast ion beam is revealed.

Falk BRAUNMUELLER: "*"Nonstationary operating regimes in Gyrotron oscillators"*
For the purpose of Dynamic Nuclear Polarization (DNP) Nuclear Magnetic Resonance (NMR) spectroscopy a gyrotron prototype has been developed over the last years at CRPP. This gyrotron was made available for experimental studies at CRPP during 2012. In the course of this year I took part in the characterization of this device. It could be shown that the gyrotron meets and in some aspects exceeds the specifications given for the use in NMR-spectroscopy. Part of this work was devoted on measuring the starting-current conditions, output power, frequency tunability, RF-beam profile and spectral characteristics of the microwave output for different operational regimes over a wide range of system control parameters. This activity included the optimization for maximum gyrotron performance. From the point of view of fundamental gyrotron physics our device gave us the possibility to perform extensive studies on the nonstationary operation regime of gyrotrons with astonishing and novel results. By scanning the cavity magnetic field and the beam-current a transition from stationary monomode regime (single-frequency) to chaotic behavior (broad frequency spectrum) and back to stationary regime could be shown in experiment. In nonstationary operation a regime with very strong variation of output power was observed, resulting in microwave pulses of the order of a nanosecond (FWHM). Furthermore, experiments on the start-up conditions for the nonstationary regime were performed and the spectral width of the RF could be related to the temporal fluctuation of the external parameter of the anode-voltage. The analysis of the acquired data is presently ongoing and will still consume some time in the future.
For understanding the experimental results, also and in particular for the case of nonstationary behaviour, the monomode time-dependent code TWANG has proven to be an essential tool for predicting novel operational regimes and for interpreting the experimental data. Most of the features seen in experiment could be reproduced in simulations and scans have given a deeper insight on various phenomena. For better performance of the code, I've parallelized TWANG using MPI in the frame of a project for a course of the doctoral school. For next year the development of a linearized version of TWANG is planned.

Danielle BRUNETTI: *"MHD properties in the core of ITER-like hybrid scenarios"*
This work was devoted to the study of instabilities (both ideal and resistive) in hybrid tokamak scenarios. A numerical study of an ITER like hybrid scenario in the ideal MHD frame has been performed, showing that when $q_{min}>1$ equilibrium calculations almost agree with nonlinear simulations and analytic prediction, giving a saturated internal kink-like helical distorsion. However for $q_{min}<1$ such helical distorsion is not found in the equilibrium calculation, in contrast with theory and nonlinear results. From the analytical point of view, the quasiinterchange mode model has been extended in order to include perpendicular viscosity, plasma diamagnetism and equilibrium E×B flows (~10KHz). Since the self adjointness of the MHD operator is lost, the equation describing

the perturbed fluxes were derived directly from the equation of motion rather than performing a δW minimization. Under an appropriate choice of the rotational transform, an exact analytic treatment of the magnetic perturbation has been possible; three dispersion relations, corresponding to three different regimes which consider one at a time the plasma diamagnetism, the viscosity and the equilibrium toroidal flows, have been derived showing the possibility of fast growing resistive modes close to the MHD stability boundary. Comparison of the model with numerical simulations and possibly with experimental data, with application to to post-sawtooth scenarios and fast growing NTMs will be carried out as part of the future work.

Ciro CALZOLAIO: *"Irreversible degradation in Nb_3Sn CICC"*
The understanding of the behaviour of the Nb_3Sn cable in conduit conductor (CICC) requires the knowledge of the strain of the superconducting strands inside the CICC. An indirect technique to measure the strain state in a large CICC has been developed. This technique is based on the inductive measurement of the magnetic susceptibility of both a CICC and of the filaments etched from the strands used for the cable manufacture. Thanks to these measurements it is possible to compare the critical temperature (T_c) of the CICC with the one of the corresponding filaments. The aforementioned comparison, in conjunction with the usage of appropriate scaling laws able to describe the behaviour of the Nb_3Sn T_c as a function of temperature, magnetic field and strain provides at first the T_c distribution and then the strain distribution in the CICC cross section. For the calculation of the strain distribution from the T_c one it is necessary to make the hypothesis of Gaussian distribution due to the non-monotonic behaviour of T_c with the strain. This analysis was applied to several toroidal field (TF) and central solenoid (CS) samples tested in the SULTAN test facility. The measurements were carried on during the cyclic loading test in SULTAN to study the CICC performance degradation with the number of electromagnetic (EM) cycles. The results show a broadening of the strain distribution with the EM cycles. For the samples that show an increase of the current sharing temperature (T_{cs}) with the number of EM cycles, it is possible to observe a shift of mean value of the strain distribution toward the lower compressive region. For the sample with opposite T_{cs} behaviour the mean value either shifts toward the higher compressive region or remains constant (inside the error bar). The analysis of the strain distribution provides information about the predominance of reversible or irreversible (filaments damage) effects responsible of the CICC performance degradation with the EM cycles.

Gustavo CANAL: *"Sawtooth Generated Magnetic Islands and properties of New Divertor Configurations"*
Neoclassical Tearing Modes (NTMs) are one of the most critical limiting plasma instabilities for the baseline scenario in ITER. This work has shown that the seeding process of both 3/2 and 2/1 sawtooth triggered NTMs is found to occur in less than one toroidal mode revolution (tens of microseconds) in TCV. This time scale is too short to react to it and, therefore, a strategy based on a pre-knowledge of the triggering mechanism is needed to avoid the NTM seeding. Hence, the work has focused on experiments in which a sawtooth-pacing technique has been used to precisely control the time of an individual sawteeth. The knowledge of the time of the next sawtooth allows for a detailed study of the effect of preemptive ECRH on the triggering of NTMs by sawtooth crashes.
Fusion reactors based on tokamaks will have to deal with very high heat loads on the divertor plates. One of the approaches to solve the heat load problem is the so called "snowflake" divertor. In order to evaluate the potential of the snowflake divertor to reduce the wall loading, the snowflake topology has been implemented into the 3D plasma edge Monte Carlo code EMC3, which solves Braginskii's equations and is self-consistently coupled to Eirene, which solves the kinetic equation for the neutrals. The particle and power deposition profiles on strike points obtained from the first EMC3 simulations are

found to be in qualitative agreement with the experimental observations, as well as the amount of power which arrives on them.

Michael CHESAUX: *"A grid reactor with low ion bombardment energy for large area PECVD of thin film silicon solar cells"*
A Phase Resolved Optical Emission Spectroscopy (PROES) diagnostic was installed on the grid reactor. Measurements showed that the time evolution of the grounded sheath in this reactor differs from the sinusoidal evolution observed in parallel-plate reactors. This evolution was analysed in more detail with a capacitive probe by measuring the plasma potential waveform. It showed that the plasma potential is non-sinusoidal in the grid reactor and that the potential waveform contributes to reducing the ion bombardment energy in this reactor. Therefore the principal mechanisms reducing the ion bombardment energy in the grid reactor have been identified. The stronger mechanism is the self-bias caused by the electrode asymmetry. The second mechanism is the non-sinusoidal plasma potential waveform.
In parallel to the plasma diagnostics, silicon thin films were deposited using a semi industrial version of the grid reactor. The analysis showed that the layer defect densities and the best solar cells obtained with this grid reactor are approaching the quality of the reference cells obtained with other low energy ion bombardment reactors.

Cornelis DE MEIJERE: *" An experimental study of plasma fluctuations in the TCV and TEXTOR tokamaks"*
In December 2011 the first measurements of electron density fluctuations with a new tangential phase-contrast imaging diagnostic (TPCI) had been performed in TCV. Suspicions that the diagnostic still suffered from substantial optical aberrations were confirmed by extensive testing during the first months of the TCV opening in 2012. These limitations notwithstanding, analysis of the December 2011 data clearly demonstrated the existence of the geodesic acoustic mode (GAM) in TCV. The observed radial mode structure was found to be in good agreement with gyrokinetic simulations with the ORB5 code. In confirmation of recent theoretical work, the GAM was found to have a weak, axisymmetric magnetic component. After the restart of TCV, followup experiments in December 2012 have additionally yielded measurements of the fluctuating electric field (through Doppler reflectometry) and electron temperature (correlation ECE) associated with the GAM. These findings, some of which are novel, are presently being prepared for publication.
Secondly, the experimental results that had previously been obtained on beam-driven modes and ELMs in the TEXTOR tokamak were published in the October 2012 issue of Plasma Physics and Controlled Fusion (http://stacks.iop.org/0741-3335/54/i=10/a=105024).

Julien DOMINSKI:
1) "Role of non-adiabatic passing electrons response in ITG/TEM microturbulence"
The non-adiabatic response of passing electrons has been studied in ITG and TEM microturbulence using the flux-tube version of the gyrokinetic code GENE. This non-adiabatic electron response has a destabilizing effect, as shown thanks to a reduced (local) model, and leads to the developpement of fine radial structures in the vicinity of low order mode rationnal surfaces. These structures have first been studied and characterized in the linear regime. In a second stage, non-linear simulations were carried out to understand to which extent the radial structures survive in the turbulent regime and how they may affect the associated transport levels of particle and electron/ion heat fluxes. Results were presented at the 2012 Varenna Conference, Italy.
2) "Implementation of an integral field solver in ORB5"
The implementation of a quasi-neutrality equation valid to all orders in $k_{||}\ \rho_L$ (~ Larmor radius / wavelength perpendicular to magnetic field) has been initiated, and shall provide an essential improvement upon the currently used field solver in ORB5, which is only valid to second order in $k_{||}\ \rho_L$. The new field equation, in the form of an integral

equation for the electrostatic field phi, is discretized using finite elements. To this end, the implementation makes use of the B-spline module Bsplines developed by Trach-Minh Tran.

Lucia FEDERSPIEL: *"Rotation studies in eITBs plasmas and CXRS diagnostic"*
During the first part of the year a complete alignment and a simultaneous absolute calibration for all three CXRS systems was performed inside the TCV vessel. The alignment inside the TCV vessel has permitted to derive the positions of the CXRS-DNBI crossing points for all the three systems in TCV spatial coordinates. The absolute calibration is essential to derive reliable density profiles and was performed inside TCV using an integrating sphere.
The formation and sustainment of eITBs with the help of toroidal and poloidal rotation measurements was the main study during this year. The aim was to assess the role of rotation and E×B shearing rate in TCV's eITBs using the present CXRS cameras set up allowing measurement of stationary and pre-barrier formation rotation profiles. Two eITBs targets at z=3 cm were developed with difficulty during the December 2011 TCV campaign by applying on axis counter-ECCD (cnt-CD) giving a central eITB or off-axis co-CD to obtain a stronger eITB.
The effect of central EC power on the barrier strength, rotation and E_r profiles was examined by applying 730kW co-CD or counter-CD (giving a central eITB). When applying a central cnt-CD power the peaked counter current rotation sustained in the core and the p_e profiles have doubled values compared to the co-CD case, indicating a confinement improvement in the central region. Even though the inward E_r profile is slightly deeper for the co-CD case, the E×B shearing rate remains similar for both heating cases. This confirms, for the first time experimentally, that the E×B shearing rate is not the cause of eletron transport improvement in TCV. Moreover the E×B shearing rate remains well of an order smaller than the γ of TEM modes, which is consistent with the negligible effect of E×B shearing rate on TEM in TCV reverse shear.
The poloidal rotations were determined using an indirect method based on the asymmetry of the toroidal rotation on a flux surface and compared with the measured profiles. In TCV, it is now possible to obtain the poloidal rotation and the E_r profiles by using directly the CXRS diagnostics or exploiting this indirect method without needing to run neoclassical simulations.

Jonathan FAUSTIN: *"A 3D equilibrium formulation for implementation of the effects of RMP and magnetic islands"*
The aim of this thesis is to write an equilibrium code for describing the effects of the RMPs in tokamaks. The computation will use a finite element method to compute the equilibrium quantities in both radial and poloidal direction. Fourier elements will be used in the toroidal direction. Equilibrium codes used so far are based on equilibrium formulations that prescribe nested flux surfaces. This hypothesis forbids the description of magnetic islands. A new formulation without this hypothesis is investigated and should be able to describe magnetic islands in addition to the effect of RMPs. This formulation is now tested with respect to the axisymmetric Solov'ev equilibrium. This test should indicate whether or not the formulation is suitable for a 2D equilibrium code in a first step, and then to be extended to 3D.

Natalia GLOWA: *"Quench characterization and protection of the HTS insert coil"*
Due to extremely high upper critical fields B_{c2}, high temperature superconductors (HTS) have the potential to be used as high field insert coils in magnet systems where the background field is provided by low temperature superconductors (LTS).
However, the quench propagation velocity (QPV) in HTS wires is low in comparison with LTS. In LTS magnets operating at 4.2K the QPV may reach several meters per second, in HTS the normal zone spreads much slower, typically few centimeters per second. This

may lead to developing a hot spot, where most of the stored electromagnetic energy of the coil will be dissipated. Because of slow propagation of the normal zone it is extremely challenging to detect hot spot formation and subsequent overheating of an HTS insert by means of a voltage measurement. As a result of large temperature gradients, large thermal strains will be developed within the coil, which may eventually damage the whole magnet. Therefore, it is of great importance to provide fast and reliable quench detection and protection scheme in order to provide a stable operation for an HTS insert coil.
After the quench is initiated, the normal zone is not confined in the direction only along the conductor, instead it will propagate three-dimensionally. In a non-insulated coil, it is expected that the radial heat transfer between adjacent tapes is enhanced. Operating such coils would also allow for a re-distribution of current among the turns. This would ensure that the stored energy can be better dissipated throughout the whole winding and the normal zone could dissipate over larger volume, thus reducing the risk of local burnout.
The first measurements of the heat propagation in the non-insulated and insulated coils have indeed shown the radial dissipation of heat is increased when no insulation is present between the adjacent tapes resulting in a lower hot spot temperature.

Zhouji HUANG: *"Experimental study of turbulence in TCV plasmas"*
The tangential phase contrast imaging (TPCI) diagnostic has been installed and operated on TCV for measuring line-integrated density fluctuations. The tangential geometry allows localization of the measurement with a spatial filter. In the past year the mounting systems of the vessel mirrors were redesigned to prevent vibrations and aberrations. The problem of astigmatism was solved, whereas the vibrations appear at present to remaina problem.
The first TPCI measurement in December 2011 revealed the presence of the geodesic acoustic mode (GAM) in TCV. The magnetic component of the GAM was detected from the analysis of magnetic probe measurements on TCV in past shots; this component appears to have a m=2/n=0 standing wave structure as expected from theory. In December 2012, experiments were performed to characterize the GAM in TCV using TPCI, supplemented with Doppler backscattering, magnetic probe and correlation ECE measurements.
Previously performed Doppler backscattering measurements in snowflake shots with the 78 GHz homodyne reflectometer and CEA V-band heterodyne reflectometer were also analyzed in the past year.

Nazar ILCHUK: *"Characterization and modeling of neutron irradiation, pre-deformation and warm prestressing effects on the fracture behavior of the tempered martensitic steel Eurofer97"*
Experimental activities were undertaken to investigate the hardness behavior of Eurofer97 after irradiations to 0.35dpa at two different temperatures, 150°C and 350°C, respectively. The Vickers and Berkovich hardness tests were carried out using a Nanoindenter G200 in the hotlab at Paul Scherrer Institute. The constitutive behaviors of the irradiated Eurofer97 were determined from small flat tensile specimens as well as from Vickers and Berkovich 3D finite element (FE) models that were developed and successfully validated with the experimental data. The development of the pile-up around the indenter tip for irradiated material was studied in detail since it is an issue for the mechanical characterization by instrumented nanoindentation of the materials which exhibit plasticity. The series of tensile tests of two above mentioned irradiations of Eurofer97 were performed in the hotlab at low temperatures varying from -120°C to 0°C necessary to get the constitutive behaviors for the further use in the FE modeling of the fracture toughness tests. To study the warm prestressing (WPS) effect on Eurofer97 the material was forged to 9-12% and the flat tensile specimens as well as the notched pre-cracked sub-sized CT specimens were machined out of it. In order to obtain the constitutive behaviors of prestressed material in the fracture toughness transition region

of the Eurofer97 the tensile tests were done at low temperatures from -150°C to -50°C. Fracture toughness tests of pre-cracked sub-sized CT specimens were carried out revealing the expected shift towards lower temperatures in median fracture toughness-temperature curve. The modification of the stress field structure at the crack tip was analyzed utilizing FE modeling in an attempt to better understand the underlying micro-mechanisms of fracture responsible for the variation in fracture toughness after WPS. The results lead to conclusion that the plastic deformation occurring during the initial loading and subsequent unloading of the CT specimens induces a change in the micro-mechanism of fracture.

Josef KAMLEITNER: *"Suprathermal electron studies in Tokamak plasmas by means of diagnostic measurements and modeling"*

The main objective of this work is to improve the current understanding and develop new insight into the physics involving electrons at suprathermal energies in tokamak plasmas.

The tokamak à configuration variable (TCV) features a preeminent, real-time controlled electron cyclotron resonance heating and current drive (ECRH/ECCD) system with surpassing power density. It is therefore optimal for ECRH/ECCD physics studies. Additionally, instabilities like sawteeth can be studied in a wide plasma parameter range.

Suprathermal electrons are observed indirectly through the hard X-ray bremsstrahlung radiation in the range of several to hundreds of keV, emitted by the electrons during collisions. The measured data is analyzed in conjunction with quasilinear Fokker-Planck codes to determine the electron distribution function.

Hard X-ray measurements are primarily performed using the novel hard X-ray tomographic spectrometer (HXRS) diagnostic. The first two of its four cameras, comprising 25 CdTe detectors and a digital data acquisition system, were fabricated, tested and calibrated. The first camera has already been successfully operated on TCV for several months, and the second camera is currently being installed.

The HXRS digital pulse processing was optimized through a thorough study of pulse processing algorithms.

Other TCV diagnostics were also improved and integrated.

Several data analysis codes have been developed, including the general tomographic inversion (GTI). The new “snapshot” framework offers a quick overview of TCV discharges. Advanced sawtooth and edge localized mode (ELM) detection is used for conditional averaging.

Several physics results were also obtained.

A fully relativistic study of the Thomson Scattering diagnostic showed that the electron temperature measurement deviation due to non-thermal electron distributions is usually negligible.

With the first HXRS camera turned by 90 to provide toroidal coverage in the co- and counter-current directions, the enhanced bremsstrahlung emission in the forward cone due to relativistic effects was observed and quantified for the first time, agreeing well with Fokker-Plank modeling.

To analyze the suprathermal electron dynamics, the response to an ECCD power step was studied using coherent averaging. The fast rise of the suprathermal electron temperature can be determined and its flat radial profile confirms previous observations.

Conditional averaging around sawtooth crashes allows studies of the suprathermal electron dynamics associated with these MHD events in the sub-ms timescale. At medium density with ECCD the emission profiles in the low energy range correspond to the typical soft x-ray signal with a fast decay at the crash while a sharp high energy photon peak is observed directly after the crash.

Doohyun KIM: *"Experimental analysis and simulation of the pacing and locking of sawteeth in the TCV tokamak"*

In this year, the main focus of my research was preparation of predictive sawtooth simulation and to refine sawtooth pacing and locking simulations. For the predictive

sawtooth simulation, we set a new electron heat transport coefficient χ_e as a function of safety factor q. In addition, we defined an effective H-factor, H_{eff}, which incorporates an additional effect of the heating position on the scaling factor. By comparing the electron temperature profile, the stored electron energy, and the electron confinement time, we tested these predictive χ_e and H_{eff}, reproducing pacing and locking experimental results. Furthermore, this year we scrutinised how the modulation of EC power affects the magnetic shear and critical shear at q=1 surface. We investigated the time evolution of shear and critical shear and at the same time examined profiles of temperature, safety factor, current density and magnetic shear. We now understand why shear shows different evolution depending on EC modulation period, how critical shear changes when EC power is turned down, and which term affects the change of critical shear. Finally, we analysed the reason that there were fully stabilised sawteeth during experiment. We did sawtooth simulations with real-time controlled heating deposition position and high power density with narrow EC beam width. With very narrow beam (width ~ 0.05 in ρ) and keeping ρ_{dep} just inside of q=1 surface (ρ_{dep} - $\rho_{q=1}$ ~ -0.01 in ρ), magnetic shear and critical shear became parallel and thus do not meet resulting in fully stabilised sawteeth. This simulation result can be one of explanations how sawteeth are fully stabilised in the experiment. Based on this simulation result, we will propose another experiment and test the effect of power density and fixed relative heating position on sawtooth period.
We presented all of this work at the EPS that was held in Stockholm, July 2012. Based on simulation result conducted on the TCV experiment, we are trying to apply pacing and locking simulation to KSTAR. In order to experimentally validate the simulation results, we visited KSTAR for two weeks and further experiments will be proposed for the next KSTAR campaign.

Joaquim LOIZU: *"Simulation of plasma turbulence in the TORPEX basic plasma physics experiment"*
An effort was put in the improvement of the GBS code, focusing on the physics of the magnetized plasma-wall transition (PWT). In fact, any drift-reduced fluid model aiming to describe the dynamics of a magnetized plasma in an open magnetic field line configuration, as it is the case for GBS, requires boundary conditions at the magnetic presheath entrance, namely the region where the assumptions of the model breakdown. Their importance can be appreciated by noting that the plasma losses at the vessel, which are determined by the boundary conditions, strongly affecting the steady state profiles. A combined fluid and kinetic description of the plasma was used to derive an analytical set of boundary conditions for each GBS field (plasma density, temperature, potential, vorticity, and parallel ion and electron velocities) at the magnetic presheath entrance. Those boundary condtions were verified by performing particle simulations of the magnetized PWT using the ODISEE (One-Dimensional Sheath Edge Explorer) code. Then the implementation of these boundary conditions in the GBS was carried out. Simulations of the tokamak SOL region were performed and showed for the first time a smooth transition between the plasma bulk and the limiters, indicating that the presence of the sheath was indeed well described. Also, the spectrum pollution of all quantities in both the parallel and perpendicular directions appeared to be almost completely removed. The effect of the new boundary conditions on the steady satet profiles and global plasma ciruclation is being studied. In particular, spontaneous plasma rotation arises from the sheath condition. This may provide for the first time a quantitative understanding of the SOL plasma rotation.

Claudio MARINI: *"Poloidal passive CX plasma rotation diagnostic in TCV"*
The CXRS system installed on TCV provides valuable impurity velocity, temperature and density measurements. The aim of the new diagnostic system is to extend the poloidal rotation measurements to the region of the LCFS and possibly beyond, in order to verify the correlations between core and edge rotation and to study the momentum flux. Reliable rotation measurements are also needed to compute the edge radial electric field,

through the radial force balance equation, which is commonly accepted as responsible for the suppression of edge turbulence and therefore involved in improving the confinement. During the last year my work has been focused on the design of this new system, in particular on modelling the passive CX emission, using the ADAS database for the necessary atomic data, and on optimizing the spectrometer parameters and input optics in order to reach the target spacial and time resolution of 1-2mm and 1-3ms respectively. I started the characterization of the high throughput Kaiser f/1.8 spectrometer and of the new camera Andor iXon Ultra. I have also improved some routines used in the CXRS data analysis, for example the function correcting the effects due to the line multiplet structure for both CVI and BV.

David MARTINET: *"Development of industrial gas-metal plasma sources for the deposition of nanostructured GaN semiconductor layers for lighting applications"*
This CTI project (No. 11548.1 PFIW-IW), in collaboration with Sulzer METCO and the Laboratory of Advanced Semiconductors for Photonics and Electronics (LASPE) at the EPFL, will try to modify the existing RF and DC plasma sources in order to grow GaN films on SiC or sapphire substrates, by evaporating Ga in nitrogen plasma.
The DC plasma source has been studied in different configurations using OES and Langmuir probe measurements: without anode, different circular anode positions, anode with grid, confinement tube. The emission spectra showed that the plasma composition does not change drastically with the experimental set-up. The densities can vary in a range of one order of magnitude depending on the configuration. The Langmuir characteristics showed that the electron energy distribution function is a cold Maxwell distribution with a hot electron beam superimposed on it.
Unfortunately some problems with the effusion cell occurred, especially regarding the temperature stability, leading to the non reproducibility of the results. A new effusion cell has been ordered, but the delivery time was extremely long (7 months), making the growths impossible up to November 2012. During the meantime a new DC plasma source has been installed in the deposition reactor, to compare the future deposited layers with the RF source used until now.
Beside the plasma experiments in the laboratory, a plasma model based on the reactions occurring in the chamber has been developed. The low pressure regime permits to reduce considerably the number of possible reactions, keeping only the electron impact reactions and diffusion. Particle balance equations are solved to obtain the different states densities. The ionization coefficient found with the model is then compared to the experimental one, to validate the reactions and the electron energy distribution. Densities time evolution is made to test the stability of the plasma. Further modelling will be gallium interaction with the different nitrogen species.

Gabrielle MERLO: *"Local and global gyrokinetic simulations of plasma shaping effects on microinstabilities and turbulence"*
Microturbulence and microinstabilities can be approached using the gyrokinetic equation which, thanks to its ordering, allows to average out the fast gyromotion. This procedure reduces the description of the dynamics of each particle distribution function from a 6-dimensional phase space to a 5D problem. For this work we use the Eulerian code GENE, which solves the gyrokinetic equation in both local-flux tube and global-full torus simulations.
Plasma shaping effects are known to play a crucial role in determining the plasma behaviour and improving the confinement. However from a theoretical point of view the role of the shape is not totally clear, and local simulations are not able to fully predict the experimental measurements. Thus the main goal is to investigate the effects of plasma shaping using the global version of GENE interfaced with the MHD equilibrium code CHEASE, to understand and overcome the limits of flux tube simulations.
The first step was to study in the local limit how different shapes, corresponding to a set of realistic and self consistent parameters, influence microinstabilities and turbulence.

This exercise allowed also to benchmark GENE against other codes, namely GKW and GS2.
Then the study of the global effects was initiated, with reference to two TCV shots having same parameters but opposite triangularity, firstly by local simulations which helped to define the numerical parameters, and then with global simulations.

Annamaria MOSETTO: *"Linear and non-linear modelling of scrape off layer instabilities"*
The goal of my work has been to provide a framework to identify the fastest growing instabilities as a function of the parameters characterizing the tokamak SOL region. The focus has been put on ballooning modes and drift wave instabilities, more precisely on their resistive, inertial and ideal branches. In order to determine the instability regions in the SOL, I isolated the most important contributions to the development of each instability and I built a set of simplified linear codes capable of describing them separately. The system behaviour has been analized first in the electrostatic limit, identifying four main instabilities: the resistive and inertial branches of the drift wave and of the ballooning mode instabilities. The transition between each couple of instabilities has been investigated as a function of the SOL parameters. I also included electromagnetic effects in the linear model: drift waves are suppressed at a finite plasma β, and, when the threshold for ideal instability is overcome, the ideal ballooning mode branch develops. Finally I applied the parameters space study to the analysis of results obtained from the linear code, and I identified the main instability governing the system in each chosen scenario. With non-linear simulations I have verified the validity of the linear framework previously described. I performed a first set of non-linear simulations in order to assess the influence of the shear on the instability regime. As expected by the linear analysis, the gradient length is reduced by the presence of the shear, i.e. for the same set of parameters, the system stabilizes on a steeper gradient and the instability is suppressed. Further on, I considered a second set of non-linear simulations aimed at reproducing each instability identified through the linear parameters space study, in the electrostatic limit. I chose four sets of parameters, each one falling in a different instability region, according to the linear framework. My objective is to demonstate that the linear simulations can predict the main characteristics of the non-linear scenarios, such as gradient length and poloidal mode number. A detailed analysis is ongoing.

Federico NESPOLI: *"Study of the edge plasma physics in TCV"*
Radiative processes occurring at the plasma edge are the main energy loss mechanism during a typical discharge in the TCV tokamak. The amount of total radiated power is needed for a proper power balance estimate.
The radiation emitted in the region outside the core plasma (from UV to soft X-rays) is measured on TCV with 8 bolometer cameras with a total of 64 lines of sight at the same toroidal location. This system allows for tomographic reconstruction of the emitted power.
During the last year, my work has been focused on operating the bolometer cameras, starting from the understanding of the basic operating principles, to the manual calibration of the cameras and the balancing of the electronic circuitry. Different tomographic inversion methods, previously implemented in the GTI package, have been compared. This has allowed selecting the "minimum Fisher information method" as the one providing better results for this particular diagnostic. Furthermore, I have implemented a method to automatically discard data showing non-physical behavior due to problems in the electronic acquisition.

David PFEFFERLE: *"Exploitation of a general-coordinate guiding-centre code for the redistribution of fast ions in deformed hybrid Tokamak equilibria"*
A collaboration with scientists at MAST was initiated to investigate the transport of fast ions in long-lived modes (LLM). Experimentally looking at neutron emissivity, there is

evidence that these particles are ejected from the core region when these m=n=1 helical structures develop. By providing 3D ANIMEC equilibrium to VENUS-LEVIS orbit solver, slowing-down distributions were obtained and compared in both the axisymmetric and the helical core cases. Our simulations clearly show a depletion of hot particles in the core region of the plasma, proportionally to the displacement of the helical axis. Our results are currently being pedantically verified and benchmarked for publication.
A second collaboration with the developers of MHD code MINERVA was started with the long-term goal to interface MINERVA and VENUS-LEVIS to model fast ions and plasma rotation in a self-consistent kinetic-MHD framework. Focus was given on the formulation of the linear problem in terms of equilibrium quantities. VENUS-LEVIS was adapted to follow orbits in MINERVA generated equilibrium without perturbations. Benchmarks are still in progress.

Anna PROKHODTSEVA: *"Primary Radiation Damage in Ultra High Purity Iron and Model Iron Cromium Alloys"*
Modelling oriented irradiation experiments in ultra high purity Fe(Cr) model alloys were performed at the JANNUS ion irradiation platform to understand radiation damage in ferritic steels envisaged for the future fusion reactor. Two irradiation campaigns we performed in 2012.
In the first campaign effect of irradiation dose rate in UHP Fe was studied. TEM thin foils were irradiated at RT with 500keV Fe^+ ions or simultaneously implanted with 10keV He^+ ions to the dose of 1dpa and 1000appm He content at two dose rates. Investigations, carried out at PSI, Villigen, revealed that density of the produced defects in the single beam case does not depend strongly on the dose rate, however fraction of ½ a_0 <111> type loops increases at low dose rate. Character of produced damage depends strongly on the dose rate in the presence of He. Defect number density is lower at the low dose rate and mixed population of ½ a_0 <111> and a_0 <100> loops is observed compared to high dose rate case where only ½ a_0 <111> loops were detected.
In the second campaign UHP Fe and Fe -5, -10, -14Cr samples were irradiated at room and liquid nitrogen temperature to the dose of 0.05dpa and 1000appm/dpa He content at the dose rate of 5 10^{-5}dpa/s. Given conditions are chosen in order to maximize the chances of observing the very first clusters stemming from displacement cascades, before thermal evolution of the irradiation-induced damage microstructure. Damage threshold, when defects start to appear in TEM, for the irradiated samples was established to be at the dose of about 0.0015dpa. Up to 0.05dpa linear growth of defect density was observed. Detailed analysis of the Burgers vectors and total density of the produced defects is currently in progress.

Ralf SCHNYDER: *"Discharge ignition phenomena in a complex electrode configuration for space applications"*
Arcing is again a key issue in the application of plasma in industry and also, as in the present work, in space environment and space equipment. Modern satellites, in particular transmission satellites are being equipped with larger and larger power systems. Since also the weight aspect is very important the dimensions of the conducting paths for instance, in slide rings are small. Moreover arcing is also considered to be a limiting factor in several other applications of plasmas, thus triggering intense research and development on this topic.
In the present work for ESA (European Space Agency), the collaboration with RUAG Aerospace led to an understanding of fundamentals of the arcing and this knowledge should to be applied to reduce or suppress arcing in space environment and equipment.
This year was mostly focus on simulation. The numerical results for a multi gap geometry showed the importance of the biggest and smallest gap respectively the intermediate available paths which explain the left and right threshold respectively the flat part in the breakdown voltage versus pressure curve for the ring assembly geometry.

Joyeeta SINHA: *"Breakdown Studies on TCV"*
This thesis seeks to improve the reliability of the plasma initiation in TCV and should ultimately yield the conditions required for a simultaneous breakdown and plasma start up at two locations inside the vacuum vessel, which is thought to be the most promising strategy for the creation of doublet plasmas in TCV.
In Tokamaks, gas breakdown is the process that leads to the creation of the plasma. There are two possible plasma start-up scenarios:

1. Inductive: free electrons are accelerated by an electric field and ionize the neutral gas molecules. The Physics involved in this process can be explained on the basis of the Townsend's theory.
2. ECH assisted: electrons are accelerated by electromagnetic waves.

The work has so far focused on the inductive start-up scenario, which mainly depends on the neutral gas pressure, the poloidal magnetic field configuration, the impurity content and the toroidal electric field. In order to obtain successful and reproducible breakdown, these parameters have to be well controlled. The magnetic configuration at the time of breakdown has been characterized by the size of the magnetic null defined as the distance of the 1mT contour from the null-point. During the analysis of various breakdown scenarios in TCV, it was found that there is a difference between the programmed and actual position and time of the breakdown. The main parameters that could be causing this discrepancy are:

1. Improper OH and vessel back-off.
2. Differences between the programmed and actual vessel and coil currents.

The effectiveness of the OH and vessel back-off has been checked for breakdown positions at z=0, +23 and -23 cm. It was observed that for the z=0cm breakdown position the back-off was not done correctly and a new set of back-off co-efficients has been proposed. The difference between the programmed and the measured OH currents was of the order of 2-3 kA, resulting in changes of the poloidal magnetic field configuration. This problem has been solved by using the OH feedback control system. However, there also exists a difference for the PF coil currents, which also contributes to the changes of the magnetic field configuration. The offsets in the reference waveforms have been identified as a possible reason for this difference.

Thibaud VERNAY: *"Collision operators in the gyrokinetic code ORB5: neoclassical transport and turbulence studies"*
The year 2012 was mainly dedicated to the study of Trapped-Electron-Mode (TEM) turbulence in tokamak plasmas through global gyrokinetic simulations using the ORB5/NEMORB code. This particularly challenging task involving a kinetic electron response has allowed the gyrokinetic group at CRPP to obtain important scientific results regarding the effects of finite plasma size or zonal flow shearing on TEM turbulence levels. Electron collisions have been shown to reduce the turbulence drive in TEM-dominated regime, both in linear and non-linear simulations. A successful benchmark accounting for a fully kinetic electron response has been carried out against the global GENE code. A realistic gyrokinetic simulation based on a TCV tokamak magnetic equilibrium has demonstrated the ability of the ORB5 code to provide reliable results related to realistic tokamak shots. The frequencies and wavelengths associated to Geodesic Acoustic Mode (GAM) oscillations have indeed been successfully compared to experimental measurements from the Phase Contrast Imaging (PCI) diagnostics. Furthermore, the experimental density and temperature profiles have been accounted for, leading to an experimentally relevant TEM-dominated regime. The mentioned results have been presented through an invited talk at the Varenna Workshop (Theory of Fusion Plasmas, August 2012).

Vincent VUILLE: *"CECE diagnostic update"*
PhD started on the 1st of september 2012. The correlation electron cyclotron diagnostic has been entirely updated during the year 2012. In particular, four new correlation channels have been added in order to increase the efficiency of the measurements. It has

been succesfully installed on TCV and the minor hardware and acqusition problems have been solved. Some interesting data have already been obtained, such as GAM measurement (both amplitude and phase have been observed) and nice turbulence spectra. The analysis code, CECE_vv.m, has also been updated in order to use the 6 channels.
In its final state, the CECE should be separated from the standard ECE. Then, the construction of a dedicated RF-part has started. The possibility of manufacturing two notch-filters with the CRPP ressources has been studied and found to be too expensive.
Also, the starting points of a collaboration with the theory group in order to create a simple linear synthetic diagnostic for CECE and turbulence studies has been fixed.

David WAGNER: *"Experimental and theoretical study of Impurity Transport in TCV"*
In the 2011 TCV experimental campaign a series of impurity transport experiments was conducted resulting an extensive dataset of argon and neon puff experiments. The numerical code STRAHL was used to solve the direct transport problem, that is to obtain impurity density evolution given some transport coefficients. The expected radiation pattern of the injected impurities can be computed and compared to the experiments when the impurity density evolution is known.
A more difficult problem is the inverse one, that is to obtain the transport coefficients from the observed radiation pattern. Two numerical methods proposed recently for solving the inverse problem were implemented and applied to the impurity injection experiment dataset. The transport coefficients reconstructed from the soft x-ray radiation of argon and neon show a weaker variation as a function of the plasma parameters such as plasma current, shape etc. than it was reported previously. The solution of the inverse problem with different methods provides a better insight into the nature and limitation of these transport investigations.

7 PUBLIC RELATION ACTIVITIES IN 2012

Visits of CRPP laboratories still represent a large fraction of the communication effort of the CRPP. Almost 2000 persons from whole over Europe visited the CRPP in 2012. The research section of the web site was improved and animations were developed to explain basic plasma concepts. In addition, news were regularly posted on the public web site.

8 FUSION & INDUSTRY RELATION

The Swiss industry benefits from the services of an Industry Liaison Officer to support procurement opportunities that are arising from the construction of the ITER Experimental Fusion Reactor. Official submissions to which the Swiss industry is invited to apply are issued either from the European Domestic Agency (Fusion for Energy, in short F4E) seated in Barcelona either directly from ITER Organization, located in Cadarache, France.

In 2012 two events in particular were coordinated to increase the visibility of the ITER tender activity to the Swiss industry:

- June 20-21, 2012: Swiss Industry Day on the ITER site in Cadarache. 15 Swiss enterprises participated to the event. Speakers from ITER Organization were selected from different technical fields and according to Swiss Industry main competences and expectations. Presentations from Swiss companies already involved in ITER contracts were given to stimulate new business development actions and prepare for possible national cooperation.

- September 24-28 2012: SOFT (Symposium On Fusion Technologies) Conference in Liège bringing together the entire Fusion Engineering Community (researchers and industry). In total 19 Swiss companies participated and presented product/marketing material at the ITER Switzerland exhibition booth.

Being known that the industrial landscape in Switzerland is rather composed of SMEs, attendance to future international events in Europe can only be encouraged in order for Swiss firms to build up transnational partnerships. In this approach two dedicated meetings with component provider companies were organized in the UK and Hungary in 2012.

The potential of Swiss Industry to contribute to ITER is not negligible, even if not immediate due mostly to the usual large size of the contracts - not compatible with the financial risk management of SMEs. Upcoming calls more oriented towards specialized, high-precision mechanical components and mid-size weighted contracts may favour the positioning of Swiss technology towards the ITER demand.

APPENDICES

APPENDIX A Members of the Steering committee

Members of the Steering Committee of the Association Euratom – Confédération Suisse are:

June 2012

Present for the Associate:
Members: A. Fasoli, G. Margaritondo, M.Q. Tran (Chair) - EPFL

Present for the EU Commission:
Members: M. Cosyns, V. Marchese, S. Webster

Experts: P. Bruzzone, A. Iorizzo, Y. Martin, K. Mieusset, P. Ricci, F. Romanelli, C. Schlatter, L. Villard

Apologies: A. Werthmueller - SER

November 2012

Present for the Associate:
Members: B. Deveaud-Plédran, A. Fasoli, M.Q. Tran (Chair), A. Werthmueller

Present for the EU Commission:
Members: M. Cosyns, V. Marchese

Experts: D. Borba, P. Bruzzone, Y. Martin, K. Mieusset, G. Sonnino, P. Ricci, C.Schlatter, L. Villard

Apologies: S. Webster (E.U. Commission)

APPENDIX B Articles published in Refereed Scientific Reviews during 2012

(see CRPP archives at http://crppwww.epfl.ch/archives)

M. Albergante, A. Fasoli, J.P. Graves, S. Brunner and W.A. Cooper. *Assessment of turbulent beam ion redistribution in tokamaks through velocity space-dependent gyrokinetic analyses*, Nuclear Fusion, vol. 52, num. 9, p. 094016, (2012).

S. Alberti, J.P. Ansermet, K.A. Avramidis, F. Braunmueller, P. Cuanillon, J. Dubray, D. Fasel, J.P. Hogge, A. Macor, E. De Rijk, M. Da Silva, M.Q. Tran, T.M. Tran, Q. Vuillemin, *Experimental Study from Linear to Chaotic Regimes on a Terahertz-Frequency Gyrotron Oscillator,* Physics of Plasmas **19**, 123102 (2012).

D. Barmaz, W.A. Cooper, B.F. McMillan, R.L. Dewar, *Diamagnetic Drift Stabilized Ballooning Modes in a 3D Heliotron,* Plasma Physics and Controlled Fusion **54**, 014006 (2012).

M. Battabyal, R. Schaeublin, P. Spaetig, N. Baluc, *W-2 Wt.%Y2o3 Composite: Microstructure and Mechanical Properties,* Materials Science And Engineering A Structural Materials Properties Microstructure And Processing **538**, 53-57 (2012).

A. Bortolon, Y. Camenen, A.N. Karpushov, B.P. Duval, Y. Andrebe, L. Federspiel, O. Sauter, The TCV Team, *Measurement of Neoclassical Poloidal Rotation Using Inboard-Outboard Asymmetry of Toroidal Rotation,* Nuclear Fusion **53**, 023002 (2012).

A. Bovet, I. Furno, A. Fasoli, K. Gustafson, P. Ricci, *Investigation of Fast Ion Transport in TORPEX,* Nuclear Fusion **52**, 094017 (2012).

V. Bratanov, F. Jenko, D. Hatch, S. Brunner, *Aspects of Linear Landau Damping in Discretized Systems,* Physics of Plasmas **20**, 022108 (2012).

M. Breschi, A. Devred, M. Casali, D. Bessette, M.C. Jewell, N. Mitchell, I. Pong, A. Vostner, P. Bruzzone, B. Stepanov, T. Boutboul, N.Martovetsky, K. Kim, Y. Takahashi, V. Tronza, W. Yu, *Results of the TF Conductor Performance Qualification Samples for the ITER Project,* Superconductor Science and Technology **25**, 095004 (2012).

P. Bruns, M.Q. Tran, D. Kunz, H. Mueller, C. Soltmann, *Spillover Benefits from Controlled Nuclear Fusion Technology - a Patent Analysis,* World Patent Information **34**, 271-278 (2012).

P. Bruzzone, B. Stepanov, R. Wesche, M. Calvi, *Test Results of a 100kA NbTi CICC,* IEEE Transactions on Applied Superconductivity **22**, 4805304-4805304 (2012).

P. Bruzzone, B. Stepanov, R. Wesche, C. Calzolaio, S. March, M. Vogel, *Operation and Test Results from the Sultan Test Facility,* IEEE Transactions on Applied Superconductivity **22**, 9501704-9501704 (2012).

C. Calzolaio, P. Bruzzone, D. Uglietti, *Measurement of Tc Distribution in NbSn CICC,* Superconductor Science and Technology **25**, 054007 (2012).

C. Calzolaio, P. Bruzzone, D. Uglietti, B. Stepanov, D. Bessette, M. Jewell, *In Situ Tc Measurements of Cable in Conduit Conductors Via an Inductive Method,* IEEE Transactions on Applied Superconductivity **22**, (2012).

I.T. Chapman, W.A. Cooper, A. Kirk, C.J. Ham, J.R. Harrison, A. Patel, S.D. Pinches, R. Scannell, A.J.M.T. Thornton, *Three-Dimensional Corrugation of the Plasma Edge When Magnetic Perturbations Are Applied for Edge-Localized Mode Control in MAST,* Plasma Physics and Controlled Fusion **54**, 105103 (2012).

I.T. Chapman, Y.Q. Liu, O. Asunta, J.P. Graves, T. Johnson, M. Jucker, *Kinetic Damping of Resistive Wall Modes in ITER,* Physics of Plasmas **19**, 052502 (2012).

J. Chowdhury, S. Brunner, R. Ganesh, X. Lapillonne, L. Villard, F. Jenko, *Short Wavelength Ion Temperature Gradient Turbulence,* Physics of Plasmas **19**, (2012).

W.A. Cooper, J.P. Graves, H. Reimerdes, O. Sauter, M. Albergante, D. Brunetti, F. Halpern, D. Pfefferlé, J. Rossel, A. Pochelon, S. Coda, B.P. Duval, B. Labit, I.T. Chapman, A.D. Turnbull, T.E. Evans, L. Lao, R. Buttery, J.R. Ferron, E. Hollman, C. Petty, M. Van Zeeland, E.A. Lazarus, F. Turco, J. Hanson, M.E. Fernstermacher, M.J. Lanctot, A.J. Cole, S.C. Jardin, B.J. Tobias, *Bifurcated Helical Core Equilibrium States in Tokamaks,* Proceedings of the 24th IAEA Fusion Energy Conference (2012).

G. Croari, P. Bruzzone, C. Marinucci, S.A. March, R. Felder, *EDIPO Quench Detection System: Concept and Development,* IEEE Transactions on Applied Superconductivity **22**, (2012).

M. De, C. Adrianus, S. Coda, A. Krämer-Flecken, S. Soldatov, M. Albergante, TCV Team, *Observations on Turbulence and Beam-Ion Driven Modes in TEXTOR,* Plasma Physics and Controlled Fusion **54**, 105024 (2012).

J. Dominski, S. Brunner, S.K. Agdham, T. Görler, F. Jenko, D. Told, *Identifying the Role of Non-Adiabatic Passing Electrons in Itg/TEM Microturbulence by Comparing Fully Kinetic and Hybrid Electron Simulations,* Joint Varenna Lausanne International Workshop 2012 **401**, 012006 (2012).

F. Felici, T.P. Goodman, O. Sauter, G. Canal, S. Coda, B.P. Duval, J.X. Rossel, *Integrated Real-Time Control of MHD Instabilities Using Multi-Beam ECRH/ECCD Systems on TCV,* Nuclear Fusion **52**, 074001 (2012).

F. Felici, O. Sauter, *Non-Linear Model-Based Optimization of Actuator Trajectories for Tokamak Plasma Profile Control,* Plasma Physics and Controlled Fusion **54**, 025002 (2012).

S. Gnesin, J. Decker, S. Coda, T.P. Goodman, Y. Peysson, D. Mazon, *3rd Harmonic ECRH Absorption Enhancement by 2nd Harmonic Heating at the Same Frequency in a Tokamak,* Plasma Physics and Controlled Fusion **54**, 035002 (2012).

J.P. Graves, I.T. Chapman, S. Coda, M. Lennholm, M. Albergante, M. Jucker, *Control of Magnetohydrodynamic Stability by Phase Space Engineering of Energetic Ions in Tokamak Plasmas,* Nature Communications **3**, 624 (2012).

P. Guittienne, D. Grange, C. Hollenstein, M. Gindrat, *Plasma Jet-Substrate Interaction in Low Pressure Plasma Spray-CVD Processes,* Journal Of Thermal Spray Technology **21**, 202-210 (2012).

P. Guittienne, S. Lecoultre, P. Fayet, J. Larrieu, A.A. Howling, C. Hollenstein, *Resonant Planar Antenna as an Inductive Plasma Source,* Journal of Applied Physics **111**, 083305 (2012).

K. Gustafson, P. Ricci, *Lévy Walk Description of Suprathermal Ion Transport,* Physics of Plasmas **19**, 032304 (2012).

K. Gustafson, P. Ricci, A. Bovet, I. Furno, A. Fasoli, *Suprathermal Ion Transport in Simple Magnetized Torus Configurations,* Physics of Plasmas **19**, 062306 (2012).

J. Hanson, H. Reimerdes, M. Lanctot, Y. In, R. La Haye, G. Jackson, G. Navratil, M. Okabayashi, P. Sieck, E. Strait, *Feedback Control of the Proximity to Marginal Rwm Stability Using Active MHD Spectroscopy,* Nuclear Fusion **52**, 013003 (2012).

W.W. Heidbrink, H. Boehmer, R. Mcwilliams, A. Preiwisch, Y. Zhang, L. Zhao, S. Zhou, A. Bovet, A. Fasoli, I. Furno, K. Gustafson, P. Ricci, T. Carter, D. Leneman, S.K.P. Tripathi, S. Vincena, *Measurements of*

Interactions between Waves and Energetic Ions in Basic Plasma Experiments, Plasma Physics and Controlled Fusion **54**, 124007 (2012).

T. Hemmi, Y. Nunoya, Y. Nabara, M. Yoshikawa, K. Matsui, H. Kajitani, K. Hamada, T. Isono, Y. Takahashi, N. Koizumi, H. Nakajima, B. Stepanov, P. Bruzzone, *Test Results and Investigation of Tcs Degradation in Japanese ITER CS Conductor Samples,* IEEE Transactions on Applied Superconductivity **22**, (2012).

A.A. Howling, B. Legradic, M. Chesaux, C. Hollenstein, *Plasma Deposition in an Ideal Showerhead Reactor: A Two-Dimensional Analytical Solution,* Plasma Sources Science & Technology **21**, 015005 (2012).

D. Iraji, D. Ricci, G. Granucci, S. Garavaglia, I. Furno, A. Cremona, D. Minelli, *Imaging of Turbulent Structures and Tomographic Reconstruction of Gym Plasma Emissivity,* Fusion Science and Technology **62**, 428-435 (2012).

S. Jolliet, B.F. Mcmillan, L. Villard, T. Vernay, P. Angelino, T.M. Tran, S. Brunner, A. Bottino, Y. Idomura, *Parallel Filtering in Global Gyrokinetic Simulations,* Journal Of Computational Physics **231**, 745-758 (2012).

M. Jucker, W.A. Cooper, J.P. Graves, *Integrated Modelling of ICRH in a Quasi-Axisymmetric Stellarator,* Nuclear Fusion **52**, 013015 (2012).

S.H. Kim, J.B. Lister, *A New Approach to Plasma Profile Control in ITER,* Fusion Engineering and Design **87**, 1921-1925 (2012).

S.H. Kim, J.B. Lister, *A Potentially Robust Plasma Profile Control Approach for ITER Using Real-Time Estimation of Linearized Profile Response Models,* Nuclear Fusion **52**, 074002 (2012).

V.G. Kiptily, D. Van Eester, E. Lerche, T. Hellsten, J. Ongena, M.L. Mayoral, F.E. Cecil, D. Darrow, M.G. Johnson, V. Goloborod'ko, G. Gorini, C. Hellesen, T. Johnson, Y. Lin, M. Maslov, M. Nocente, M. Tardocchi, I. Voitsekhovitch, *Fast Ions in Mode Conversion Heating (He-3)-H Plasmas in JET,* Plasma Physics and Controlled Fusion **54**, 074010 (2012).

M. Lauret, F. Felici, G. Witvoet, T.P. Goodman, G. Vandersteen, O. Sauter, M.R. De Baar, *Demonstration of Sawtooth Period Locking with Power Modulation in TCV Plasmas,* Nuclear Fusion **52**, 062002 (2012).

S. Lecoultre, P. Guittienne, A.A. Howling, P. Fayet, C. Hollenstein, *Plasma Generation by Inductive Coupling with a Planar Resonant RF Network Antenna (Vol 45, 082001, 2012),* Journal of Physics D Applied Physics **45**, 409502 (2012).

S. Lecoultre, P. Guittienne, A.A. Howling, P. Fayet, C. Hollenstein, *Plasma Generation by Inductive Coupling with a Planar Resonant RF Network Antenna,* Journal Of Physics D Applied Physics **45**, 082001 (2012).

E. Lerche, D. Van Eester, J. Ongena, et al. M. Maslov, *Optimizing Ion-Cyclotron Resonance Frequency Heating for ITER: Dedicated JET Experiments (Vol 53, 124019, 2011),* Plasma Physics and Controlled Fusion **54**, 069601 (2012).

M. Lewandowska, M. Bagnasco, *Conceptual Design and Analysis of a Cryogenic System for a New Test Facility for High Temperature Superconductor Current Leads (Hts Cls),* Przeglad Elektrotechniczny **88**, 140-143 (2012).

H. Liu, Y. Wu, P. Bruzzone, F. Long, Y. Shi, J. Chen, Z. Ren, M. Yu, *Test Results of ITER Correction Coil Short Samples Cccn1 and Cccn2,* Fusion Science and Technology **62**, 311-315 (2012).

J. Loizu, P. Ricci, F.D. Halpern, S. Jolliet, *Boundary Conditions for Plasma Fluid Models at the Magnetic Presheath Entrance,* Physics of Plasmas **19**, 122307 (2012).

F. Long, Y. Wu, F. Liu, B. Liu, Y. Shi, L. Lei, J. Qin, P. Bruzzone, *Manufacture and Acceptance Test of the Full Size ITER Pf5 Conductor Sample,* IEEE Transactions on Applied Superconductivity **22**, (2012).

A. Macor, E. De Rijk, S. Alberti, T. Goodman, J.P. Ansermet, *Note: Three-Dimensional Stereolithography for Millimeter Wave and Terahertz Applications,* Review Of Scientific Instruments **83**, 046103 (2012).

L. Marot, T. De Los Arcos, A. B ºnzli, C. W §Ckerlin, R. Steiner, P. Oelhafen, E. Meyer, D. Mathys, P. Spaetig, G. Covarel, *Nanocomposites of Carbon Nanotubes Embedded in a (Ti,Al)N Coated Film,* Surface & Coatings Technology **212**, 223-228 (2012).

B.F. Mcmillan, P. Hill, S. Jolliet, T. Vernay, L. Villard, A. Bottino, *Gyrokinetic Transport Relations for Gyroscale Turbulence,* Journal of Physics: Conference Series **401**, 012014 (2012).

S. Mordijck, E.J. Doyle, G.R. Mckee, R.A. Moyer, T.L. Rhodes, L. Zeng, N. Commaux, M.E. Fenstermacher, K.W. Gentle, H. Reimerdes, O. Schmitz, W.M. Solomon, G.M. Staebler, G. Wang, *Changes in Particle Transport as a Result of Resonant Magnetic Perturbations in DIII-D,* Physics of Plasmas **19**, 056503 (2012).

Y. Nabara, Y. Nunoya, T. Isono, K. Hamada, Y. Takahashi, K. Matsui, T. Hemmi, K. Kawano, N. Koizumi, N. Ebisawa, M. Iguchi, H. Kajitani, M. Oshikiri, Y. Uno, F. Tsutsumi, M. Yoshikawa, H. Nakajima, K. Okuno, P. Bruzzone, B. Stepanov, *Examination of Japanese Mass-Produced Nb3Sn Conductors for ITER Toroidal Field Coils,* IEEE Transactions on Applied Superconductivity **22**, (2012).

G.A. Naylor, R. Scannell, M. Beurskens, M.J. Walsh, I. Pastor, A.J.H. Donne, B. Snijders, W. Biel, B. Meszaros, L. Giudicotti, R. Pasqualotto, L. Marot, *The ITER Thomson Scattering Core Lidar Diagnostic,* Journal Of Instrumentation **7**, - (2012).

T. Nishitani, P. Garin, M. Sugimoto, N. Nakajima, R. Heidinger, H. Kimura, K. Okano, K. Tobita, T. Yamanishi, G. Federici, N. Baluc, *Progress of Fusion Nuclear Technologies in the Broader Approach Framework,* Fusion Engineering and Design **87**, 535-542 (2012).

T. Nishitani, H. Tanigawa, T. Yamanishi, N. Baluc, *Overview of Materials Research and Ifmif/Eveda under the Broader Approach Framework,* Fusion Science and Technology **62**, 210-218 (2012).

M. Nocente, M. Tardocchi, V. Kiptily, P. Blanchard, *High-Resolution Gamma Ray Spectroscopy Measurements of the Fast Ion Energy Distribution in JET 4he Plasmas,* Nuclear Fusion Original Edition **52**, 063009 (2012).

S. Nowak, E. Lazzaro, B. Esposito, G. Granucci, M. Maraschek, O. Sauter, H. Zohm, D.a.U.T. Brunetti, *Interpretation of the Effects of Electron Cyclotron Power Absorption in Pre-Disruptive Tokamak Discharges in Asdex Upgrade,* Physics of Plasmas **19**, (2012).

Z. Oksiuta, M. Lewandowska, K.J. Kurzydlowski, N. Baluc, *Effect of Vanadium Addition on the Microstructure and Mechanical Properties of the ODS Ferritic Steels,* J. Nuclear Materials (2012).

I.G. Pagonakis, F. Li, S. Illy, B. Piosczyk, S. Alberti, J.-P. Hogge, S. Kern, M. Henderson, C. Darbos, *Study of the ITER Stray Magnetic Field Effect on the EU 170-Ghz2-MW Coaxial Cavity Gyrotron,* IEEE Transactions on Plasma Science **40**, 1945-1956 (2012).

T. Panis, A. Fasoli, D. Testa, *Analysis of Damping Rate Measurements of Toroidal Alfven Eigenmodes as a Function of N: Part I,* Nuclear Fusion **52**, 023013 (2012).

T. Panis, A. Fasoli, D. Testa, *Analysis of Damping Rate Measurements of Toroidal Alfven Eigenmodes as a Function of N: Part Ii (Vol 52, 023014, 2012),* Nuclear Fusion **52**, 039501 (2012).

S.-H. Park, S.P. Kwon, K. Kim, B. Stepanov, P. Bruzzone, *Conductor*

Performance Qualification of Tfko3 Sample for ITER TF Magnet, IEEE Transactions on Applied Superconductivity **22**, (2012).

D. Pfefferlé, J.P. Graves, W.A. Cooper, *Exploitation of a General-Coordinate Guiding Centre Code for the Redistribution of Fast Ions in Deformed Hybrid Tokamak Equilibria,* Journal of Physics: Conference Series **401**, 012020 (2012).

A. Pitzschke, R. Behn, O. Sauter, B.P. Duval, J. Marki, L. Porte, L. Villard, S. Yu Medvedev and TCV team, *Electron Temperature and Density Profile Evolution During the ELM Cycle in Ohmic and EC-Heated H-Mode Plasmas in TCV,* Plasma Physics and Controlled Fusion **54**, 015007 (2012).

A. Portone, J. Amend, W. Baker, P. Bruzzone, F. Cau, G. Croari, E. Fernandez-Cano, S. March, E. Salpietro, H. Scheller, B. Stepanov, E. Theisen, M. Vogel, R. Wesche, *The EDIPO Project: Status and Outlook,* IEEE Transactions on Applied Superconductivity **22**, (2012).

P. Ricci, F.D. Halpern, S. Jolliet, J. Loizu, A. Mosetto, A. Fasoli, I. Furno, C. Theiler, *Simulation of Plasma Turbulence in Scrape-Off Layer Conditions: The Gbs Code, Simulation Results and Code Validation,* Plasma Physics and Controlled Fusion **54**, 124047 (2012).

J.E. Rice, M.J. Greenwald, Y.A. Podpaly, M.L. Reinke, P.H. Diamond, J.W. Hughes, N.T. Howard, Y. Ma, I. Cziegler, B.P. Duval, P.C. Ennever, D. Ernst, C.L. Fiore, C. Gao, J.H. Irby, E.S. Marmar, M. Porkolab, N. Tsujii, S.M. Wolfe, *Ohmic Energy Confinement Saturation and Core Toroidal Rotation Reversal in Alcator C-Mod Plasmas,* Physics of Plasmas **19**, 056106 (2012).

J.A. Romero, J.M. Moret, S. Coda, F. Felici, I. Garrido, *Development and Validation of a Tokamak Skin Effect Transformer Model,* Nuclear Fusion **52**, 023019 (2012).

J.A. Romero, J. Svensson, *Optimisation of out-Vessel Magnetic Diagnostics for Plasma Boundary Reconstruction in Tokamaks,* Nuclear Fusion (2012).

J.X. Rossel, J.M. Moret, S. Coda, O. Sauter, T.P. Goodman, F. Felici, D. Testa, Y. Martin, *Edge-Localized Mode Control by Electron Cyclotron Waves in a Tokamak Plasma,* Nuclear Fusion **52**, 032004 (2012).

O. Schmitz, T.E. Evans, M.E. Fenstermacher, M. Lehnen, H. Stoschus, E.A. Unterberg, J.W. Coenen, H. Frerichs, M.W. Jakubowski, R. Laengner, C.L. Lasnier, S. Mordijck, R.A. Moyer, T.H. Osborne, H. Reimerdes, D. Reiter, U. Samm, B. Unterberg, *Resonant Features of Energy and Particle Transport During Application of Resonant Magnetic Perturbation Fields at TEXTOR and DIII-D,* Nuclear Fusion **52**, 043005 (2012).

J.A. Snipes, D. Beltran, T. Casper, Y. Gribov, A. Isayama, J. Lister, S. Simrock, G. Vayakis, A. Winter, Y. Yang, L. Zabeo, *Actuator and Diagnostic Requirements of the ITER Plasma Control System,* Fusion Engineering and Design **87**, 1900-1906 (2012).

W.M. Solomon, K.H. Burrell, A.M. Garofalo, R.J. Groebner, C.J. Lasnier, M.A. Makowski, T.H. Osborne, H. Reimerdes, J.S. Degrassie, E.J. Doyle, T.E. Evans, M.E. Fenstermacher, G.L. Jackson, M.J. Schaffer, *ELM Pacing Using Modulated Non-Axisymmetric Magnetic Fields on DIII-D,* Nuclear Fusion **52**, 033007 (2012).

B. Stepanov, P. Bruzzone, R. Wesche, S. Turtп, V. Corato, P. Decool, A. Devred, D. Bessette, A. Vostner, T. Boutboul, S. Lelekhov, W. Yu, *Test Results of Three Poloidal Field Superconducting Samples in Sultan,* IEEE Transactions on Applied Superconductivity **22**, (2012).

B. Teaca, A. Banon Navarro, F. Jenko, S. Brunner, L. Villard, *Locality and Universality in Gyrokinetic Turbulence,* Physical Review Letters **109**, 235003 (2012).

D. Testa, M. Albergante, *Evidence for a New Path to the Self-Sustainment of the Thermonuclear Fusion in Magnetically Confined Burning Plasma Experiments,* Europhysics Letters **97**, 35003 (2012).

D. Testa, M. Albergante, *A Phenomenological Explanation for the Anomalous Ion Heating Observed in the JET Alpha-Heating Experiment of 1997,* Nuclear Fusion **52**, 083010 (2012).

D. Testa, T. Panis, P. Blanchard, A. Fasoli, J.-E. Contributors, *Plasma Isotopic Effect on the Damping Rate of Toroidal Alfven Eigenmodes with Intermediate Toroidal Mode Numbers,* Nuclear Fusion **52**, 094006 (2012).

D. Testa, M. Toussaint, R. Chavan, A. Encheva, J.B. Lister, J.M. Moret, F. Sanchez, *Prototyping Conventional Wound High Frequency Magnetic Sensors for ITER,* Fusion Science and Technology **61**, 19 (2012).

C.G. Theiler, I. Furno, J. Loizu, A. Fasoli, *Convective Cells and Blob Control in a Simple Magnetized Plasma,* Physical Review Letters **108**, 065005 (2012).

D. Uglietti, C. Marinucci, *Design of a Quench Protection System for a Coated Conductor Insert Coil,* IEEE Transactions on Applied Superconductivity **22**, 4702704 (2012).

D. Uglietti, R. Wesche, B. Stepanov, P. Bruzzone, *Statistical Analysis of the Current-Sharing Temperature Evolution in Nb3Sn Cable-in-Conduit-Conductors for ITER,* IEEE Transactions on Applied Superconductivity **22**, 4802204 (2012).

P. Unifantowicz, R. Schaeublin, C. Hebert, T. Plocinski, G. Lucas, N. Baluc, *Statistical Analysis of Oxides Particles in ODS Ferritic Steel Using Advanced Electron Microscopy,* Journal Of Nuclear Materials **422**, 131-136 (2012).

D. Van Eester, E. Lerche, T.J. Johnson, T. Hellsten, J. Ongena, M.L. Mayoral, D. Frigione, C. Sozzi, G. Calabro, M. Lennholm, P. Beaumont, T. Blackman, D. Brennan, A. Brett, M. Cecconello, I. Coffey, A. Coyne, K. Crombe, A. Czarnecka, R. Felton, M.G. Johnson, C. Giroud, G. Gorini, C. Hellesen, P. Jacquet, Y. Kazakov, V. Kiptily, S. Knipe, A. Krasilnikov, Y. Lin, M. Maslov, I. Monakhov, C. Noble, M. Nocente, L. Pangioni, I. Proverbio, M. Stamp, W. Studholme, M. Tardocchi, T.W. Versloot, V. Vdovin, A. Whitehurst, E. Wooldridge, V. Zoita, *Minority and Mode Conversion Heating in (He-3)-H JET Plasmas,* Plasma Physics and Controlled Fusion **54**, 074009 (2012).

T. Vernay, S. Brunner, L. Villard, B.F. Mcmillan, S. Jolliet, T.M. Tran, A. Bottino, *Synergy between Ion Temperature Gradient Turbulence and Neoclassical Processes in Global Gyrokinetic Particle-in-Cell Simulations,* Physics of Plasmas **19**, 042301 (2012).

L. Villard, P. Angelino, A. Bottino, S. Brunner, S. Jolliet, B.F. Mcmillan, T.M. Tran, T. Vernay, *Global Gyrokinetic Itg Turbulence Simulations of ITER,* Plasma Phys. Control. Fusion (2012).

D. Wagner, E. Fable, A. Pitzschke, O. Sauter, H. Weisen, *Understanding the Core Density Profile in TCV H-Mode Plasmas,* Plasma Physics and Controlled Fusion **54,** 085018 (2012).

H. Weisen, Y. Camenen, A. Salmi, T.W. Versloot, P.C. De Vries, M. Maslov, T. Tala, M. Beurskens, C. Giroud, *Identification of the Ubiquitous Coriolis Momentum Pinch in JET Tokamak Plasmas,* Nuclear Fusion **52**, 042001 (2012).

H. Weisen, Y. Camenen, A. Salmi, T.W. Versloot, P.C. Devries, M. Maslov, T. Tala, M. Beurskens, C.J.E.T.E.C. Giroud, *Ubiquity of Non-Diffusive Momentum Transport in JET H-Modes,* Nuclear Fusion **52**, (2012).

R. Wesche, M. Boersch, P. Bruzzone, F. Holdener, E. Iten, N. Magginetti, S.A. March, D. Oertig, H. Quack, M. Vogel, *Development of Hts Current Leads for*

Industrial Fabrication, IEEE Transactions on Applied Superconductivity **22**, (2012).

R. Wesche, P. Bruzzone, S.A. March, M. Vogel, H. Ehmler, P. Smeibidl, *Design and Manufacture of 20 Ka Hts Current Leads for a Hybrid Magnet System,* Superconductivity Centennial Conference 2011 **36**, 927-930 (2012).

R. Wesche, D. Uglietti, P. Bruzzone, S.A. March, C. Marinucci, B. Stepanov, N.H. Glowa, *Development of Magnet Technologies for Hts Insert Coils,* Superconductivity Centennial Conference 2011 **36**, 1165-1168 (2012).

W. Wu, R. Schäublin, J.C. Chen, *General Dislocation Image Stress of Anisotropic Cubic Thin Film,* J. of Applied Physics **112**, 093522 (2012).

APPENDIX C Conferences and Seminars

(see CRPP archives at http://crppwww.epfl.ch/archives)

C.1 Conference and conference proceedings published in 2012

P. Angelino, A. Bottino, S. Brunner, Y. Camenen and A. Pochelon et al. *Improving energy confinement in fusion plasmas by plasma shaping and current profile tailoring in the TCV tokamak*, in Communications SPS, SPG Mitteilungen, Communications de la SSP, vol. 2012, num. Nr.36, January 2012, p. 12, Progress in Physics (26), 2012.

F. Avino, A. Bovet, A. Fasoli, I. Furno and K. Gustafson et al. *Review and perspectives of electrostatic turbulence and transport studies in the basic plasma physics device TORPEX*. 54th Annual Meeting of the APS Division of Plasma Physics, Providence, Rhode Island, USA`, October 29–November 2, 2012.

D. Barmaz, W.A. Cooper, B.F. McMillan, R.L. Dewar, *Diamagnetic Drift Stabilized Ballooning Modes in a 3d Heliotron,* Symposium on Celebrating Professor Robert Dewars Accomplishments in Plasma Physics, Atlanta, GA, Oct 31, 2009, Plasma Physics And Controlled Fusion **54**, 1 p.014006 (2012).

A. Bovet, A. Fasoli, I. Furno, K. Gustafson, P. Ricci, *Investigation of Suprathermal Ion Transport in TORPEX,* 39th EPS Conference & 16th Int. Congress on Plasma Physics, Stockholm, Sweden, 2 - 6 July 2012 (2012).

D. Brunetti, W.A. Cooper, J.P. Graves, F. Halpern, C. Wahlberg, H. Lütjens, J.F. Luciani, *MHD Properties in the Core of ITER-Like Hybrid Scenarios,* 13th Joint Varenna Lausanne International Workshop on the Theory of Fusion Plasmas, Varenna, ITALY, Aug 27-31, 2012, Journal of Physics: Conference Series **401**, 012003 (2012).

G.P. Canal, B.P. Duval, F. Felici, T.P. Goodman, J.P. Graves, A. Pochelon, H. Reimerdes, O. Sauter, D. Testa, *Fast Seeding of Neoclassical Tearing Modes by Sawtooth Crashes in TCV,* EPS/ICPP 2012, 39th EPS Conf. on Plasma Physics 16th Int. Congress on Plasma Physics, Stockholm, Sweden, 2-6 July 2012 (2012).

S. Coda, *Overview of Recent and Current Research on the TCV Tokamak*, 24th FEC 24th IAEA Fusion Energy Conference, San Diego CA (USA), 8-13 October 2012, 24th IAEA Fusion Energy Conference, OV/4-4 (2012).

J. Decker, Y. Peysson, S. Coda, *Effect of Density Fluctuations on ECCD in ITER and TCV,* 17th Joint Workshop on Electron Cyclotron Emission and Electron Cyclotron Resonance Heating (EC 17), Deurne, The Netherlands, EPJ Web of Conferences **32**, 01016 (2012).

B.P. Duval, *Charge Exchange Recombination Spectroscopy on Fusion Devices,* 17th International Conference on Atomic Processes in Plasmas (ICAPiP), Belfast, NORTH IRELAND, Jul 19-22, 2011, 17Th International Conference On Atomic Processes In Plasmas (Icapip) **1438**, 189-196 (2012).

W.W. Ehsetu, L. Porte, A. Fasoli, O. Sauter, S. Coda, T.P. Goodman, *Vertical Electron Cyclotron Emission Diagnostic for TCV Plasmas,* 17th Joint Workshop on Electron Cyclotron Emission and Electron Cyclotron Resonance Heating (EC 17), Deurne, The Netherlands, EPJ Web of Conferences **32**, 03011 (2012).

A. Fasoli, F. Avino, A. Bovet, I. Furno, K. Gustafson, J. Loizu, P. Ricci, C.G. Theiler, *Basic Investigations of Electrostatic Turbulence and Its Interaction with Plasma and Suprathermal Ions in a Simple Magnetized Toroidal Plasma,* IAEA, San Diego, USA, 2012 (2012).

F. Felici, J.X. Rossel, G. Canal, S. Coda, B.P. Duval, T.P. Goodman, Y. Martin, J.M. Moret, O. Sauter, D. Testa, *Real-Time Control of Multiple MHD Instabilities on TCV by ECRH/ECCD,* 17th Joint Workshop on Electron Cyclotron Emission and Electron Cyclotron Resonance Heating (EC 17), Deurne, The Netherlands, EPJ Web of Conferences **32**, 02005 (2012).

T. Hellsten, A. Hannan, T. Johnson, L.G. Eriksson, L.J. Hook, L. Villard, S. Ratynskaya, L. Blomberg, A. Fasoli, *Self-Consistent ICRH Modelling,* EPS/ICPP 2012, 39th EPS Conf. on Plasma Physics 16th Int. Congress on Plasma Physics, Stockholm, Sweden, 2-6 July 2012, 39th European Physical Society Conference on Plasma Physics **36F**, P4.002 (2012).

J. Kamleitner, S. Gnesin, S. Coda, P. Marmillod, J. Decker, *A New Hard X-Ray Spectrometer for Suprathermal Electron Studies in TCV,* EPS/ICPP 2012, 39th EPS Conf. on Plasma Physics 16th Int. Congress on Plasma Physics, Stockholm, Sweden, 2-6 July 2012, Europhys. Conf. Abstr. **36F**, P-1.010 (2012).

A. Karpushov, Y. Andrebe, B.P. Duval, L. Federspiel, *Charge Exchange Recombination Spectroscopy Measurement of Ion Temperature, Rotation and Impurity Density Profiles on the TCV Tokamak,* EPS/ICPP 2012, 39th EPS Conf. on Plasma Physics 16th Int. Congress on Plasma Physics, Stockholm, Sweden, 2-6 July 2012, 39th EPS Conference & 16th Int. Congress on Plasma Physics **36F**, O5.117 (2012).

S.A. March, P. Bruzzone, B. Stepanov, D. Bessette, M. Jewell, *Effect of Thermal Loading on Nb3Sn CICC Performance,* MT 22, International Conference on Magnet Technology, Marseille, France, September 11-16, 2011, Ieee Transactions On Applied Superconductivity **22** (3)(2012).

L. Porte, S. Coda, T.P. Goodman, A. Pochelon, V.S. Udintsev, V. Vuille, *Recent Results and Prospects for Correlation ECE Measurements on TCV,* 17th Joint Workshop on Electron Cyclotron Emission and Electron Cyclotron Resonance Heating (EC 17), Deurne, The Netherlands, EPJ Web of Conferences **32**, 03007 (2012).

A. Priebe, B. Dehning, M. Sapinski, M.Q. Tran, A. Verweij, *Investigations of Quench Limits of the Lhc Superconducting Magnets,*Applied Superconductivity Conference, Portland, USA, October 7-12, 2012 (2012).

S. Ratynskaya, L. Blomberg, A. Fasoli, A. Martynov, S.Y. Medvedev, L. Villard, *Ideal MHD Stability of Helically Symmetric Magnetic Islands,* EPS/ICPP 2012, 39th EPS Conf. on Plasma Physics 16th Int. Congress on Plasma Physics, Stockholm, Sweden, 2-6 July 2012, EPS/ICPP 2012, 39th EPS Conf. on Plasma Physics 16th Int. Congress on Plasma Physics **36F**, P1.082 (2012).

S. Ratynskaya, L. Blomberg, A. Fasoli, S.Y. Medvedev, A.A. Ivanov, A.A. Martynov, Y.Y. Poshekhonov, Y.R. Martin, J.M. Moret, F. Piras, A. Pochelon, H. Reimerdes, O. Sauter, L.T.C.V.T. Villard, *Optimization of the Snowflake Diverted Equilibria in the TCV Tokamak,* EPS/ICPP 2012, 39th EPS Conf. on Plasma Physics 16th Int. Congress on Plasma Physics, Stockholm, Sweden, 2-6 July 2012, 39th EPS Conference on Plasma Physics **35F**, P1.029 (2012).

J.A. Romero, S. Coda, F. Felici, J.M. Moret, J. Paley, G. Sevillano, I. Garrido, B.H. Le, *Sliding Mode Control of a Tokamak Transformer,* 51st IEEE Conference on Decision and Control, Maui, Hawaii, USA, 10-13 December 2012, 51st IEEE Conference on Decision and Control, 386 (2012).

B. Teaca, A.B. Navarro, F. Jenko, S. Brunner, L. Villard, *Locality of Non-Linear Interactions in Gyrokinetic Turbulence,* EPS/ICPP 2012, 39th EPS Conf. on Plasma Physics 16th Int. Congress on Plasma Physics, Stockholm, Sweden, 2-6 July 2012, EPS/ICPP 2012, 39th EPS Conf. on Plasma Physics 16th Int. Congress on Plasma Physics (2012).

B.2 Seminars presented at the CRPP in 2012

R. Wenninger, IPP-Garching, D, *"Solitary magnetic perturbatins at the ELM onset"*

G. Hommen, TUE Univ. of Technology, Eindhoven, NL, *"Optical boundary reconstruction of tokamak plasmas"*

Dr. W. Suttrop, IPP-Garching, D, *"ELM mitigation with magnetic perturbations in ASDEX Upgrade"*

Dr. D. Carralero, CIEMAT, Madrid, Espagne, *"Experimental Studies on Edge Filament Properties"*

Dr. T.P. Goodman, R. Chavan, CRPP-EPFL, *"ITER EC upper launcher design: towards the final design review"*

Prof. F. Paganucci, Associate Professor, University of Pisa, Pisa Vice President, Alta SpA, Pisa, *"An Overview of the State of the Art of Electric Propulsion for Space Applications"*

C. Marini, Università degli studi di Milano, I, *"Electron bunch Diagnostics based on Thomson backscattering in the ELTRAP machine"*

S. Jang, Dept. of Physics, Korea Advanced Inst. of Science & Technology (KAIST), Daejon, Korea, *"Tangential x-ray pinhole camera system with duplex MWPC for KSTAR plasma diagnostics"*

S.H. Lee, Dept. of Physics, Korea Advanced Inst. of Science & Technology (KAIST), Daejon, Korea, *"Development of soft X-ray array diagnostics on KSTAR and its results"*

J. Barton, Dept. of Mechanical Engineering and Mechanics, Lehigh University, USA, *"Toroidal Current Profile Control in Tokamaks via First Principles Driven Model-based Control Synthesis"*

J. Khamlichi, Univ. degli Studi di Padova, I, *"Mean field magnetization in harmonic traps"*

Dr. I. Joseph, Lawrence Livermore National Laboratory, USA, *"Using non-axisymmetric scrape-off layer perturbations to control the tokamak edge plasma"*

J. Faustin, External Contractor - Plasma Confinement, ITER Organization, Science Division, F, *"Pedestal conditions which can lead to small ELM losses in ITER"*

Dr. S. Alberti, CRPP-EPFL, *"Experimental study of basic gyrotron physics from linear to chaotic regimes"*

Dr. A.R. Sanderson, Scientific Computing and Imagining Institute, University of Utah, USA, *"Analysis and Visualization Tools for Assessing Fusion Simulations"*

Dr. J.A. Romero, CIEMAT, Madrid, Spain, *"Equilibrium reconstruction in tokamaks using out vessel, steady state magnetic field sensors"*

Prof. E. Witrant, University Joseph Fourier, Grenoble, France, *"Profiles Control and Stability in Thermonuclear Fusion: Some Issues for ITER"*

V. Vuille, EPFL, Department of Physics, *"Correlation ECE on TCV : present status and future plans"*

Dr. L.F. Delgado-Aparicio, Princeton Plasma Physics Laboratory, Princeton, USA, *"Characterization of formation and stability of impurity 'snakes' in tokamak plasmas"*

A. Merle, SCCP/GTTM, CEA/DSM/IRFM, CEA Cadarache, France, *"Stability of electron-driven fishbones"*

Dr. Ch. Watts, ITER Organisation, Cadarache, France, *"Electron Density Measurements in the ITER Fusion Plasma"*

Prof. M. Furukawa, Dept. of Advanced Energy, Division of Transdisciplinary Sciences, Graduate School of Fontier Sciences, The University of Tokyo, Japan, *"A new matching solution method for stability analysis of MHD mode with a singular layer including finite Larmor radius effects"*

Dr. N. Kirneva, NRC "Kurchatov Institute", Moscow, Russia, *"Analysis of TCV high density experiments"*

J. Wilson, School of Mathematical Sciences, University of Nottingham, UK, *"How Super Is The Superlens?"*

F. Nespoli, Università degli Studi di Milano, Italy, *"Acceleration mechanisms of ferromagnetic dust in tokamaks"*

Dr. N. Miyato, Rokkasho, JAEA, *"On the gyrokinetic model in the long wavelength régime"*

A. Gallice, Technisch-Wissenschaftlicher Transfer, TWT GmbH, Germany, *"Modeling the Ascent of Sounding Balloons: Derivation of the Vertical Air Motion"*

A. Döpp, Institute for Theory of Statistical Physics, RWTH Aachen University, Aachen, Germany, *"Betatron Radiation in Laser-driven Electron Accelerators"*

Dr. T. Stolzfus-Dueck, MPI-Greifswald, Germany, *"Transport-driven toroidal rotation in the tokamak edge"*

Dr. J.M.R. Barredo, Dept. of Physics UAF/ Carlos III de Madrid, Spain, *"Coherent Events in 2D Turbulence"*

M. Hübner, CRPP-EPFL, ITER Liaison Officer - Switzerland CRPP-EPFL *"ITER Opportunities for the Swiss Industry"*

Prof. M. Gilmore, Univ. of New Mexico, Albuquerque, New Mexico, USA, *"Measurements of Hypervelocity Plasma Jets for Plasma Liner-Driven Magneto-Inertial Fusion"*

Dr. D. Newman, Univ. Carlos III de Madrid / Univ. of Alaska Fairbanks - Physics Dept., *"The Multiple Impacts of Sheared Flows on Turbulence and Turbulent Transport"*

Dr. F. Anderegg, UCSD Physics Department, 9500 Gilman Drive, La Jolla CA USA, *"Measurement of Correlation-Enhanced Collision Rates"*

Dr. T. Shekar Goud, Inst. for plasma research, Gandhinagar, Gujarat, India, *"Intrinsic poloidal flow generation and its role in sustaining mean profiles in a simple toroidal plasma"*

M. Cavedon, Universitá degli studi di Padova, Italy, "NBI power loss mechanisms at ASDEX Upgrade under different plasma configurations"

Dr. J.M. Garcìa-Regaña, Max-Planck-Institute für Plasmaphysik, Greifswald, D, *"Neoclassical impurity transport in stellarator geometry"*

Dr. X. Sarasola, Dept. Of Applied Physics and Applied Mathermatics, Columbi Univ. New York, USA (Current address: Max-Planck-Institute für Plasmaphysik, Greifswald, D), *"First experimental studies of the physics of plasmas of arbitrary degree of neutrality"*

Dr. P. Hennequin, Lab. de Physique des Plasmas, Ecole Polytechnique de Palaiseau, F, *"Fluctuations des petites aux grandes échelles mesurées par retrodiffusion Doppler dans Tore Supra"*

Dr. D. Gates, Princeton Plasma Physics Laboratory, Princeton, USA, *"Origin of tokamak density limit scalings"*

Dr. L. Vermare, Ecole Polytechnique de Palaiseau, F et Tore Supra Team, CEA, F, *"Study of GAMs on Tore Supra using Doppler backscattering"*

Dr. D. Terranova, CNR – Istituto Gas Ionizzati, Consorzio RFX - ENEA Association, I, *"RFP helical equilibria reconstruction with V3FIT-VMEC"*

Dr. Th. Vernay, CRPP-EPFL, *"Collisions in Global Gyrokinetic Simulations of Tokamak Plasmas Using the Delta-f Particle-In-Cell Approach"*

APPENDIX D External activities of CRPP Staff during 2012

D.1 National and international committees and ad-hoc groups

MEMBERSHIP

P. Bruzzone	International Magnet Technology Conference Organizing Committee European Magnet Expert Group 23rd Magnet Technology Conference, Programme Committee EUCAS 2013 Conference, Program Committee SST-1 (India), Magnet Review Group Series Connected Hybrid Magnet, Project Review Group
W.A. Cooper	Visiting professor, National Institute for Fusion Science, Japan, 1st January 2012- 10 April 2012
B.P. Duval	TTG-rotation/transport working group chair, EU-TTG
A. Fasoli	Visiting Professor, MIT Physics Department EFDA Steering Committee ASDEX Upgrade Programme Committee, Germany International Tokamak Physics Activities: Energetic Particles Topical Group Scientific Committee, 13th IAEA Technical Meeting on Energetic Particles in Magnetic Confinement Systems, 2011 Expert for the Review of projects submitted to the French National Agency for Research (ANR) International Scientific Committee for the French Laboratory of Excellence in Plasma Science Chair of Programme Committee of the 39th European Physical Society Conference on Plasma Physics and 16th International Congress on Plasma Physics Chair of Fusenet Academic Council French National Research Agency review Scientific Council of PLAS@PAR, joint plasma initiative across all Universities in Paris, France PhD exam committee, Padova University, Italy Associate Editor of the Journal of Plasma Physics Scientific Board of the Helmotz Virtual Institute on Advanced Microwave Diagnostics
Ivo Furno	Member of the SPS Committee
Ch. Hollenstein	Editorial Board Plasma Chemistry and Plasma Processing Kluwer Academic/Plenum Publisher Member of the IUVSTA Plasma Division
J.B. Lister	Member of the European Physical Society Executive Committee
A. Pochelon	Member of the Committee of the SWISS NUCLEAR FORUM Secretary and Member of the Swiss Physical Society Committee Member of the FORATOM Committee, in particular of the "Research and Development Task Force (R&D.TF) Associate member of IUPAP (International Union of Physics and Applied Phyiscs), Commission C16: Commission on plasma physics
O. Sauter	International Tokamak Physics Activities: MHD, Disruption and Control Topical Group Co-chair Varenna-Lausanne International Theory Conference

P. Spätig	International Organization Committee of the 27th Symposium on Fusion Technology, Liège, Belgium, 2012. IEA Annex II Executive Committee. IEA Fusion Materials Agreement Executive Committee.
M.Q. Tran	Consultative Committee for the Euratom Specific Research and Training Programme in the field of Nuclear Energy, Fusion (CCE-FU) Swiss expert to the Governing Board of F4E Member of the Core Commission for nomination of Max-Planck for Plasma Physics Committee of the International Symposium on Fusion Nuclear Technology Vice-Chair and Swiss delegate at the Fusion Power Coordinating Committee Member of the Power Plant Physics and Technology Board Member of the Ad'hoc Group on Material for DEMO
L. Villard	Member, Board of the High Performance Computing for Fusion, EFDA Special working group 1 of the IFERC-CSC Member, Standing Committee of the IFERC CSC Member, Fachbeirat, Max-Planck-Institut für Plasmaphysik
H. Weisen	Seconded to EFDA-JET CSU, programme department Member of the Diagnostics Working Group within the ITPA Member of the expert panel for evaluating PhD and post-doc research proposals submitted to the Fonds National de la Recherche, Luxembourg

PARTICIPATION

S. Alberti	Expert panel member of PDR of the ITER EC system, Cadarache, France
Y.R. Martin	International Tokamak Physics Activity: "Transport and Confinement Modelling Topical Group" and "Edge and pedestal physics Topical Group"
D. Testa	Expert panel member of PDR got ITER HF system magnetics + Plasma Control working group

D.2 Editorial and society boards

S. Alberti	Editorial Board International Journal Infrared Millimeter and Terahertz Waves Editorial Board IEEE Transaction on THz Science and Technology (Topical editor: THz plasma science and instruments)
S. Coda	Editorial Board of Plasma Physics and Controlled Fusion
Ch. Hollenstein	Editorial Board Plasma Chemistry and Plasma Processing Kluwer Academic/Plenum Publisher
J.B. Lister	Member of the International Advisory Board of Plasma Physics and Controlled Fusion
Y.R. Martin	Member of the EFDA Public Information Network (PIN) Chairman of the Association Vaudoise des Chercheurs en Physique
Ph. Spaetig	Member of the Advisory Editorial Board of Journal of Nuclear Materials

D.3 EPFL committees and commissions

A. Fasoli	Président de la Commission Stratégique de la Physique, EPFL Direction de la Faculté FSB Comité de Coordination Joint Doctoral Initiative EPFL-IST Lisbon Conseiller d'études pour la Physique - Master
J-Ph. Hogge	Commission du Doctorat de la Section de Physique, FSB-EPFL
P. Ricci	Groupe de travail technique HPC (High Performance Computing) – EPFL
O. Sauter	Commission du Doctorat de la Section de Physique, FSB-EPFL
M.Q. Tran	Director of the Inst. of Physics of Energy and Particle, EPFL Commission du Doctorat de la Section de Physique, FSB-EPFL Commission stratégique de la Section de Physique, EPFL Membre du Comité de Sélection du Prix de la meilleure thèse EPFL "Core Group" of the Master in Nuclear Engineering Programme
T.M. Tran	Groupe de travail technique du Comité de Pilotage HPC/MPC, EPFL
L. Villard	Délégué à la mobilité, Section de physique, FSB-EPFL Commission d'Ethique, EPFL Commission d'Enseignement de la Section de Physique, FSB-EPFL Groupe de travail technique HPC (High Performance Computing) – EPFL Steering Committee, HPC (High Performance Computing) – EPFL

APPENDIX E The basis of controlled fusion

E.1 Fusion as a sustainable energy source

Research into controlled fusion aims to demonstrate that it is a valid option for generating power in the long term future in an environmentally, politically and economically acceptable way. Controlled fusion is a process in which light nuclei fuse together to form heavier ones: during this process a very large amount of energy is released. For a fusion reactor it is planned to use the two isotopes of hydrogen: deuterium (D) and tritium (T), which fuse together much more readily than any other combination of light nuclei according to the following reaction:

$$D^2 + T^3 \rightarrow He^4 + n + 17.6MeV$$

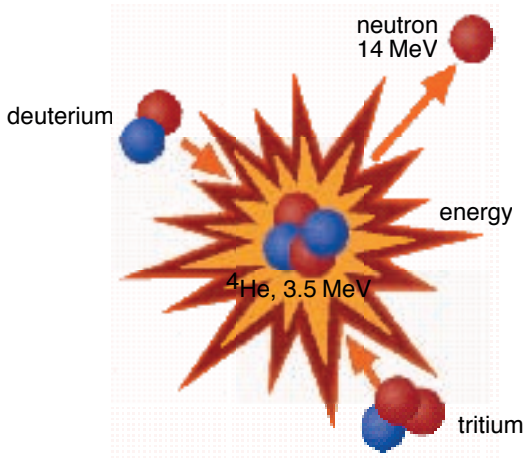

Fig. E.1 *Schematic of a fusion reaction between deuterium and tritium nuclei. The products are 3.5MeV ^4He, the common isotope of helium, and a 14MeV free neutron.*

The end products are helium and neutrons (n). The total energy liberated by fusing one gram of a 50:50% mixture of deuterium and tritium is 94000kWh, which is 10 million times more than from the same mass of oil. 80% of this energy is carried by the neutrons with an energy of 14MeV while the remaining 20% is carried by the helium nucleus. Most of this energy eventually becomes heat to be stored or converted by conventional means into electricity.

The temperature at which fusion reactions start to become significant are above a few tens of millions of degrees. For the D-T reaction, the optimal temperature is of the order of 70-200 million degrees. At such temperatures the D-T fuel is in the plasma state.

Deuterium is very abundant on the earth and can be extracted from water (0.034g/l). Tritium does not occur naturally, since its half-life is only 12.3 years, but it can be regenerated from lithium using the neutrons produced by the D-T fusion reactions. The two isotopes of natural lithium contribute to this breeding of tritium according to the reactions:

$$Li^6 + n \rightarrow He^4 + T^3 + 4.8MeV$$

$$Li^7 + n \rightarrow He^4 + T^3 + n - 2.5MeV$$

The relative abundance of the two lithium isotopes Li^6 and Li^7 are 7.4% and 92.6%, respectively. The known geological resources of lithium both in the earth and in the sea water are large enough to provide energy for an unlimited time.

E.2 Attractiveness of fusion as an energy source

The inherent advantages of fusion as an energy source are:

- The fuels are plentiful and their costs are negligible because of the enormous energy yield of the reaction;
- The end product of the reaction is helium, an inert, non-radioactive gas;
- No chain reaction is possible: the neutron emitted by the fusion process does not trigger subsequent reactions;
- Only a very small amount of fuel is present in the core of the reactor: the plasma weights a fraction of gram;
- Any malfunction would cause a quick drop of temperature and all fusion reactions would stop within seconds;
- No after-heat problem can lead to thermal runaway even if the case of a loss of coolant accident;
- None of the materials required by a fusion power plant are subject to the provisions of the non-proliferation treaties.

Its further potential advantages are:

- Radioactivity of the reactor structure, caused by neutrons, can be minimised by careful selection of low-activation materials resulting in a manageable quantity of long lived radioactive waste;
- The release of tritium in normal operation can be kept at a very low level. The inventory of tritium on the site can be sufficiently small so that even the worst possible accident could not lead to a harmful release to the environment requiring evacuation of the nearby population.

APPENDIX F Sources of Financial Support

In 2012, the work carried out at the CRPP and presented in this annual report was financed from several sources. The major financial support is provided by:

Swiss public institutions:

- the Ecole Polytechnique Fédérale de Lausanne (EPFL)
- the Conseil des Ecoles Polytechniques (CEPF)
- the Swiss National Science Foundation
- the Paul Scherrer Institute (PSI), which hosts the Supraconductivity and the Materials science activities
- the Swiss Secrétariat d'Etat à l'Education et à la Recherche (SER)
- the Swiss "Departement Fédéral de l'Intérieur" in the frame of the Broader Approach
- the Swiss "Commission pour la Technologie et l'Innovation" (CTI)

International public institutions:

- EURATOM
- ITER
  - ITER Organization
  - Domestic Agencies in China, Europe (F4E), Japan, Korea, Russia, USA
- Helmholtz-Zentrum Berlin, D

Private organisations

- Allper AG
- Atela SA
- Comadur SA
- Inspire AG
- OC Oerlikon Solar / TEL Solar
- Ruag AG
- Sulzer Innotec AG
- Sulzer Metco AG
- Tetra Pak SA.
- WEKA AG

APPENDIX G Glossary

A general purpose glossary for the field of controlled fusion and plasma physics is provided in the CRPP Annual Report every two years. Since it was part of the Annual Report 2009, it will not be provided here. (http://crpp.epfl.ch/page-48260-fr.html)